The behaviour of potassium feldspar at high water pressures

Pauline Thompson

PhD
University of Edinburgh
1995

ABSTRACT

Some natural potassium feldspars have been shown to contain traces of structural "water" which may have been incorporated into the structure at high partial pressures of water. At even higher partial pressures of water potassium feldspar is known to break down to form a hydrated phase (referred to as "sanidine hydrate") which is structurally comparable to cymrite which forms from barium feldspar (celsian) at high pressures. This study investigates the capacity for potassium feldspar and "sanidine hydrate" to act as reservoirs for hydrous fluids in the Earth's crust and upper mantle, and establishes the pressure-temperature range of stability of the hydrate phase.

Sanidine and "sanidine hydrate" have been synthesised from gels at a variety of pressures and temperatures in a piston cylinder apparatus and cold seal apparatus. These run products have been used to determine the equilibrium position of the reaction between sanidine and water to form "sanidine hydrate". The reaction was found to lie between four brackets of 2.35 and 2.5 GPa at 450°C, 2.4 and 2.59 GPa at 550°C, 2.67 and 2.74 GPa at 650°C and 2.70 and 2.72 GPa at 680°C. Infrared spectroscopy showed that the dominant water species in "sanidine hydrate" was structural H_2O. The quantity of this structural H_2O, measured by thermogravimetric analysis, was found to vary between 4.42 and 5.85 wt% over the pressure range of 2.7 to 3.2 GPa and the temperature range of 450 to 680°C. Systematic variation in water content over the experimental range studied was not clearly established. The samples were contaminated with platinum (up to 0.5 mg) from the capsule and the resultant thermogravimetric analyses would be too low. The maximum value was below 6.07 wt% which would be equivalent to 1 molecule of H_2O per formula unit. It was possible to remove the water entirely by heating at atmospheric pressure to produce anhydrous hexagonal $KAlSi_3O_8$ ("hexasanidine") implying that the structural "water" content of "sanidine hydrate" is variable, perhaps as a continuous solid solution between the end members where n = 1 and n = 0 in the formula $KAlSi_3O_8.nH_2O$. The unit cell parameters, measured by powder X-ray diffraction, for "sanidine hydrate" were a = 0.5337 (±0.0003) nm and c = 0.7714 (±0.0009) nm, and those for "hexasanidine" were a = 0.5288 (±0.001) nm and c = 0.7818 (±0.0005) nm. This change in the unit cell parameters on dehydration was of a similar magnitude and direction to those for cymrite and hexacelsian, which would also suggest a solid solution in the water content as was found in the barium analogue. The water content data was not of a sufficient quality to calculate the average enthalpy and entropy of the dehydration of "sanidine hydrate". If the structural "water" content of "sanidine hydrate" is presumed constant over the pressure-temperature range of the study the

average values for the enthalpy is 18000 (±5000)$Jmol^{-1}$ and for the entropy is 92.75 (±5.80) $JK^{-1}mol^{-1}$.

Synthetic sanidines and natural sanidines from the Klokken layered intrusion of South Greenland were examined using infrared spectroscopy to determine the type and relative proportions of structural "water" in order to see if there was any pressure-temperature control on the structural "water" content. Sanidines were synthesised at a variety of pressures and temperatures but showed no systematic variation in the water content when the relative proportions were calculated by normalisation of the infrared OH stretching peaks to a peak caused by vibrations of part of the silicate lattice. In fact this study showed a greater difference in the infrared spectra obtained when a different gel starting material was used. Laminated syenites from the Klokken intrusion, Greenland, show deuteric alteration which could be caused by exsolution of structural "water" incorporated into the feldspar at higher temperatures. This hypothesis presumes that water solubility in feldspars is greater at higher temperatures. Testing this hypothesis using feldspars from the Klokken intrusion might provide additional evidence for a pressure-temperature control on the structural "water" content. Hence the structural "water" content of the granular syenites roof-chill series was examined in order to see if its abundance increased with depth in the intrusion until a saturation level was achieved when fluid inclusion water began to exsolve. However, the normalised peak areas in the OH stretching region did not increase regularly, probably indicating that the method of analysis was not adequate rather than a lack of systematic increase of the water content with depth. Infrared spectra of the Klokken feldspars were not easily interpreted in terms of the structural "water" content, perhaps because the feldspars were perthites containing a mixture of microcline and low albite. The OH peaks present looked somewhat similar to microcline but lacked a peak at 3620 cm^{-1}. The variation in the size and position of the peaks present with orientation of the crystal was irregular. This irregular behaviour does not agree with previous work on the orientational effect on the infrared OH stretching peaks.

Thus the solubility of water in potassium feldspar could not be calculated and hence its capacity for storage of water in metamorphic and igneous rocks under various geological conditions was not evaluated. "Sanidine hydrate" can contain a large proportion of structural "water". Its occurrence is limited to high pressure but very low temperature conditions and could therefore act as a reservoir in cold subduction zones. However, the occurrence of "sanidine hydrate" would also be limited by the bulk composition of the rock and may only be common in granitic compositions at these pressures and temperatures.

ACKNOWLEDGEMENTS

This research project would not have been feasible without the assistance of many people. In the first instance thanks are due to my supervisors Prof. Ian Parsons, Prof. Colin Graham and Dr Steve Elphick for initiating the project and their subsequent supervision of the research. Much of my interest and curiosity for the work was maintained by the laughter and boundless enthusiasm of Prof. Ian Parsons. In the experimental laboratory Dr Steve Elphick taught me to use the equipment so successfully that I caused no major explosions and with the help of Dr Nic Odling and Dr Damian Carrington I overcame frequent experimental crises. Discussions with Nic were invaluable as a source of numerous ideas and I fear I may have exploited his preference for any work other than his own. Damian helped me to run experiments 96 and 97 in the gas bombs. Bob Brown provided all the technical assistance I could possibly need. Geoff Angel assisted me with X-ray diffraction but more importantly with frequently re-booting the computer every time it crashed. Prof. Ian Parsons, Prof. Colin Graham and especially my Mum (Dr A.P. Valintine) proof read everything such that little of the original remains.

The gel starting material was kindly provided by Dr D.L. Hamilton of Manchester University. The cell refinements programme used was written and supplied by Dr Pam Champness, also of Manchester University. Infrared spectroscopy was conducted at the National Museum of Scotland under the guidance of Dr Brian Jackson who did his utmost to help solve the problems I encountered. Thermogravimetric analysis was performed in St. Andrews University Chemistry Department with Dr John Irvine and John Smith.

Much gratitude for assistance is also due to Dr Alec Livingston of the National Museum of Scotland (cell parameters), Dr Mike Saunders (atomic absorption), Graham and Alistair of the University of Edinburgh Chemistry Department (first attempt at thermogravimetric analysis), Prof. Mike Henderson and Cathy of Manchester University (third attempt at thermogravimetric analysis) and Dr Bertrand Maillot (remedial mathematics and cubic equations).

This research was funded by the Natural Environment Research Council.

CONTENTS

Chapter 1
Introduction

Potassium feldspar is nominally an anhydrous mineral containing no stoichiometric water. However, natural examples of feldspar can contain traces of water held within defects in the structure. Gem quality microclines and adularia, studied by Hofmeister and Rossman (1985a), Aines and Rossman (1985) and Kronenberg et al. (in press), have been found to contain structural H_2O located in at least two different defect sites within the feldspar structure. Sanidines from the Eifel region of West Germany, studied by Hofmeister and Rossman (1985b), Beran (1986) and Behrens and Muller (1995), may contain more structural OH than H_2O although Beran considered H_2O to be the dominant species. The structural "water" content of these feldspars may have been acquired at high partial pressures of water. However, the variation of the solubility of water in potassium feldspar with pressure and temperature of crystallisation is not known. Feldspars frequently contain a large quantity of water as fluid inclusions in micropores (Burgess et al., 1992).

Potassium feldspar is an abundant mineral on the surface of the earth and may, in some lithologies, persist to depths of up to 100 km in the presence of water. At high partial pressures of water potassium feldspar reacts with water to form a hydrated phase, referred to as "sanidine hydrate" in the present study. This phase was first recorded by Seki and Kennedy in 1964. They determined the pressure and temperature required to synthesise the hydrated phase but did not attempt to determine the equilibrium position of the reaction. Graham et al. (1992) studied the stability of the barium feldspar hydrate analogue, cymrite, $BaAl_2Si_2O_8.nH_2O$ and the relationship of water content (nH_2O) to pressure and temperature. They discovered that cymrite could hold more structural "water" at higher pressures and lower temperatures and that cymrite had a composition that could vary between one molecule of H_2O per formula unit ($BaAl_2Si_2O_8.H_2O$) and anhydrous hexacelsian with a hexagonal structure and the formula $BaAl_2Si_2O_8$. Viswanathan et al. (1992) confirmed that this was a solid solution by showing that the cell parameters of intermediates between cymrite and hexacelsian, synthesised by dehydrating cymrite, varied continuously between the cell parameters for each end member.

The abundance of potassium feldspar could allow it to act as a large reservoir for water in the crust even though it only contains traces of water. Therefore knowledge of how this water content, both as structural "water" and as fluid inclusion water, varies with pressure and temperature conditions may explain some of the sources and sinks of fluids in metamorphic and igneous rocks. For example, pervasive feldspar-fluid interactions in cooling igneous rocks may reflect the exsolution of water incorporated into the feldspar at higher temperatures and pressures (Brown et al.,

1983). At higher pressures "sanidine hydrate" may be stable and therefore, as "sanidine hydrate" could contain a large proportion of structural "water". It may, in part, contribute to the storage of fluids in subducting slabs, the lower crust or the upper mantle.

In the study described here I addressed these questions by investigating the stability of "sanidine hydrate" under geological conditions. The properties of "sanidine hydrate" could follow a similar pattern to those of cymrite. Examining the solubility of water in potassium feldspar and "sanidine hydrate" may help to explain the occurrence and storage of geological fluids. I have therefore investigated the nature of structural "water" within these phases and attempted to quantify the structural "water" at a number of pressures and temperatures in order to see if any systematic behaviour can be identified.

The background work on the hydrated phase "sanidine hydrate" and the analogous barium feldspar hydrate, cymrite, is reviewed in Chapter 2. Chapter 3 summarises the experimental methods and analytical techniques used throughout the thesis. The reversal experiments on the reaction between sanidine and water to form "sanidine hydrate" are detailed in Chapter 4 showing the equilibrium position of the reaction to lie between four brackets of 2.35 and 2.5 GPa at 450°C, 2.4 and 2.59 GPa at 550°C, 2.67 and 2.74 GPa at 650°C and 2.70 and 2.72 GPa at 680°C. In Chapter 5 the structural "water" of "sanidine hydrate" is shown, from infrared spectroscopy, to be H_2O molecules held within a single site within the crystal structure. Any systematic variation of this water within "sanidine hydrate", with pressure and temperature of synthesis, was also sought from thermogravimetric analysis, but the data obtained were poor, perhaps because the samples were contaminated with platinum. The unit cell parameters may also show variation with structural "water" content as was seen in the work of Viswanathan et al. (1992). Chapter 6 contains the measurements of the cell parameters of "sanidine hydrate" for differing pressures and temperatures of synthesis. Again little variation was found but when the cell parameters of the fully dehydrated form of "sanidine hydrate", referred to henceforth as "hexasanidine", were measured they showed only small changes in unit cell parameters from the original hydrous "sanidine hydrate". Hence subtle changes in the water content of "sanidine hydrate" may not be detectable by measuring the unit cell parameters. Chapter 7 outlines calculations of some thermodynamic state functions, using the measured unit cell parameters, water contents and position of the reaction as determined in Chapter 4. The possible natural occurrences of "sanidine hydrate" are discussed in Chapter 8. Chapter 9 describes attempts to find evidence for the

variation in structural "water" content of potassium feldspar at high temperatures and partial pressures of "water" by looking at the water content of some synthetic sanidines with infrared spectroscopy. Similar work on a suite of feldspars from the Klokken layered syenite intrusion, which it was postulated could also show evidence for a greater capacity for water at higher temperatures, is described in Chapter 10. Finally Chapter 11 summarises the major conclusions of the thesis and includes suggestions for further work. A diagrammatic summary of the thesis is also shown in Appendix B.

Chapter 2

Previous work on the system $KAlSi_3O_8$-H_2O and its barium analogue at high pressures

2.1 Introduction

In the absence of other components all the common feldspars break down at pressures below 4 GPa. At high partial pressures of water albite breaks down to jadeite plus quartz or coesite (Holland 1980), anorthite transforms to zoisite + kyanite + quartz + vapour (Goldsmith, 1981), and celsian (Ba feldspar) to cymrite ($BaAl_2Si_2O_8.nH_2O$) (Seki and Kennedy 1964b). However, little is known about the transformations of potassium feldspar since they occur at such high water pressures that any high pressure phases close to $KAlSi_3O_8$ have never been found to exist in nature. In the absence of water Kinomura at al (1975) showed that potassium feldspar breaks down to form a wadeite type phase ($K_2Si_4O_9$) + kyanite + coesite. This breakdown occurs between 3 GPa at 700°C and 6 GPa at 1400°C. There has only been one major study to date on the potassium feldspar system in the presence of water (Seki and Kennedy 1964a). This work showed that sanidine transformed to a hydrate phase at high water pressure with a composition which was presumed to be $KAlSi_3O_8.nH_2O$. The position of the reaction was at slightly lower pressures than the anhydrous breakdown would be if extrapolated to lower temperatures. In this current work this hydrate phase is referred to as "sanidine hydrate". Several other authors have encountered a hydrate phase whilst studying the effects of pressure and temperature on natural orthoclases or studying melting systems involving sanidine but none of them have studied it in any further detail.

Graham et al (1992) studied the barium analogue, cymrite. Since the Ba and K ions have a similar ionic radius it was thought possible that "sanidine hydrate" ($KAlSi_3O_8.H_2O$) may behave in a similar manner to cymrite. Solid solutions between "sanidine hydrate" and cymrite were found in natural examples from Perthshire, known as hyalophanes, by Moles (1985). Therefore the current project was instigated in order to see if "sanidine hydrate" does behave in a similar manner to cymrite.

2.2 The $KAlSi_3O_8$-H_2O system.

Seki and Kennedy (1964a) discovered that potassium feldspar undergoes a reaction at water pressures in excess of 1.0 GPa which produced a new hydrous phase. Hence they conducted a series of experiments at high pressures and temperatures in order to investigate this reaction and then measured the X-ray diffraction pattern and calculated the unit cell dimensions, unit cell volume, optical properties and density of this new phase. Seki and Kennedy did not establish by direct analysis that the new phase was of the assumed composition of sanidine + water, $KAlSi_3O_8.nH_2O$. However, the physical properties of this phase were all strikingly similar to cymrite, the hydrated phase of barium feldspar, which they assumed to have the formula $BaAlSi_3O_8(OH)$ (Seki and Kennedy, 1964b) and hence they were not sure of the composition of their new phase. Anhydrous runs using sanidine alone, at 1300°C and 6.0 GPa, did not produce any reaction (unlike dry albite which under the same physical conditions breaks down to jadeite and quartz/coesite). Both these observations would indicate that this new phase was in fact a hydrate but the strongest evidence was the agreement between the measured and calculated densities (2.58 +/- 0.02 and 2.60 respectively), which was within 1% if there was one molecule of H_2O per formula unit. If the new phase had either 0 or 2 molecules of water in the formula the difference would have been about 8%. This hydrated phase was therefore called "sanidine hydrate".

The experiments of Seki and Kennedy were unreversed, synthesis experiments, and so the boundary they determined was not necessarily the equilibrium reaction position but merely the lowest temperature at which "sanidine hydrate" crystallised. "Sanidine hydrate" may have been metastable over part of this field. These high pressure runs were made in both a piston anvil device (as described by Griggs and Kennedy 1956) and a piston cylinder apparatus (similar to the apparatus described in Chapter 3). These two methods have been known to give different results but in Seki and Kennedy's study they produce almost identical results. The starting materials used were:

i) sanidine crystallised from pure $KAlSi_3O_8$ in a piston anvil device and water,
ii) a natural orthoclase, with Na_2O = 4.4% and K_2O = 11.7%, and water.

The products were characterised using powder X-ray diffraction techniques and a petrographic microscope. X-ray diffraction was used to position the phase boundaries as it showed the presence of "sanidine hydrate" more distinctly, with a large change in the proportions of the phases within 0.05 GPa of the boundary. Using sanidine as a

starting material, the results obtained by Seki and Kennedy in the piston anvil and the piston cylinder apparatus are shown in Figures 2.1a & b. Sanidine and water gave a hydrated phase with a hexagonal structure at high water pressures. The properties of this phase are given in Table 2.1. The refractive index was measured by the immersion method, the density of the phase by suspension with methylene iodide liquid and the unit cell dimensions from X-ray diffraction patterns. The measured value of density agreed with the unit cell dimensions and the chemical composition of $KAlSi_3O_8.H_2O$. If the chemical reaction is

$$KAlSi_3O_8 + H_2O = KAlSi_3O_8.H_2O$$

with only one H_2O molecule per formula unit then the total molar volume of the left hand side is 0.212 nm^3 and of the right hand side is 0.19 nm^3. This would therefore favour the formation of the hydrate at high water pressures, as observed.

Table 2.1 Properties of "sanidine hydrate" from Seki and Kennedy (1964a) compared with similar values for cymrite (Smith et al 1949)

"sanidine hydrate"	cymrite
a = 0.553(5) nm	a = 0.532 nm
c = 0.770(0) nm	c = 0.767 nm
Unit cell volume = 0.1898 nm^3	Unit cell volume = 0.188 nm^3
Hexagonal	Hexagonal
$\omega = 1.545 \pm 0.003$	$\omega = 1.6225 \pm 0.001$
$\varepsilon = 1.535 \pm 0.003$	$\varepsilon = 1.6125 \pm 0.001$
Uniaxial negative	Uniaxial negative
Elongation positive	
Calculated density = 2.6	
Measured density = 2.58 ± 0.02 gcm^{-3}	Measured density = 3.413 ± 0.005 gcm^{-3}

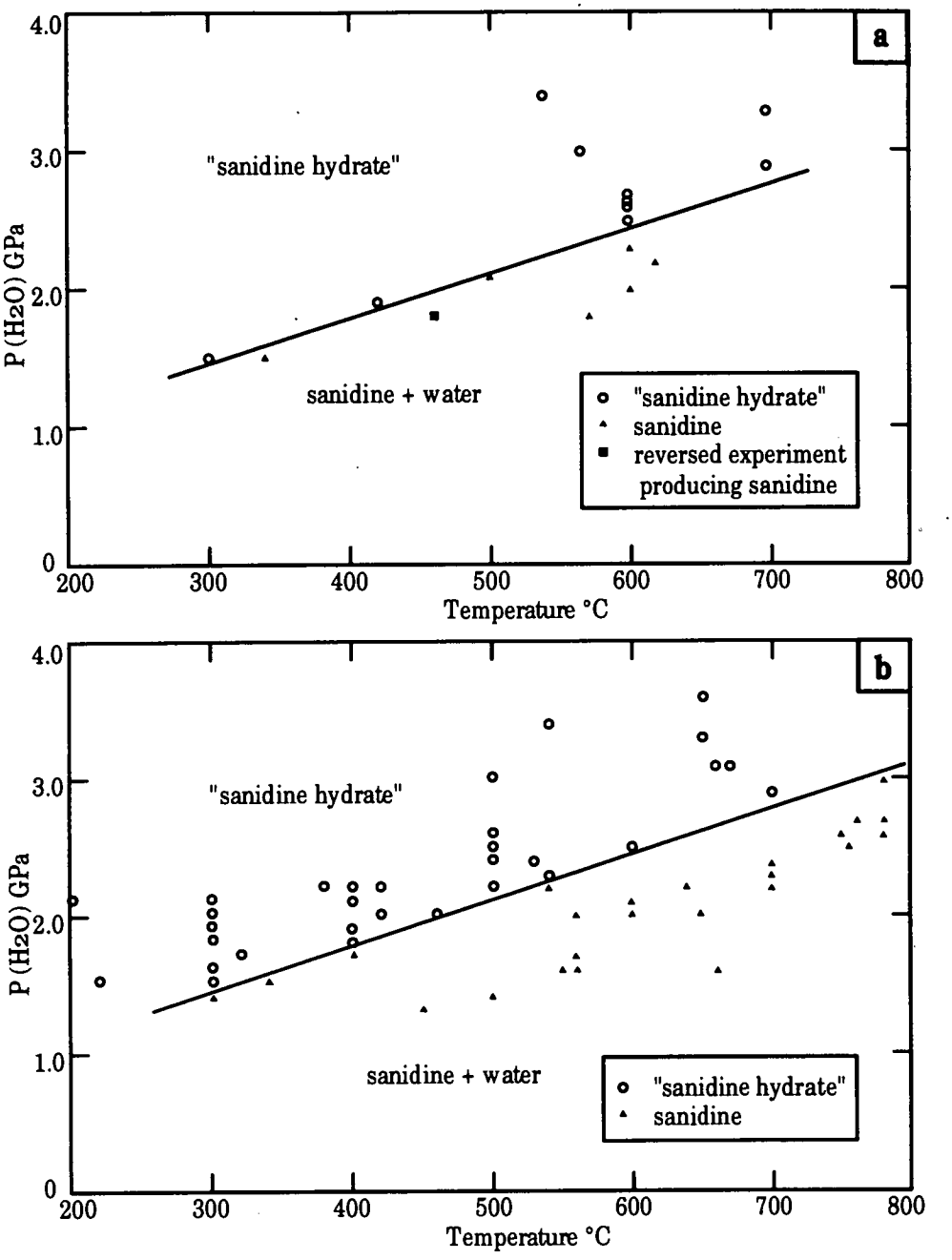

Fig. 2.1. a) Results of synthesis experiments in a piston cylinder apparatus of a similar design to the one described in Chapter 3 b) Results of synthesis experiments using a piston anvil device as described by Griggs and Kennedy (1956) (Seki and Kennedy 1964a)

Figure 2.2 shows the results of Seki and Kennedy's experiments conducted on natural orthoclase under similar conditions. In the presence of water this natural orthoclase broke down to sanidine + jadeite + quartz, followed by sanidine + jadeite + coesite and then "sanidine hydrate" + jadeite + coesite. Without water the third reaction did not occur. The jadeite produced in these experiments was very similar to natural jadeite in its X-ray diffraction pattern. The intensities of the jadeite reflections increased with distance into the jadeite field but their d-spacing remained the same, implying that there was no incorporation of potassium into the formula. The phase $KAlSi_2O_6$ with a pyroxene structure, i.e. pure potassium jadeite, did not occur even at 6.2 GPa and 1000°C.

Figure 2.3 shows a comparison of the results determined with the piston cylinder and piston anvil apparatus on synthetic samples with the experiments carried out on a natural sanidine.

Experiments on albite glass + water and albite crystals + water failed to synthesise a hexagonal phase, but produced jadeite + quartz/coesite.

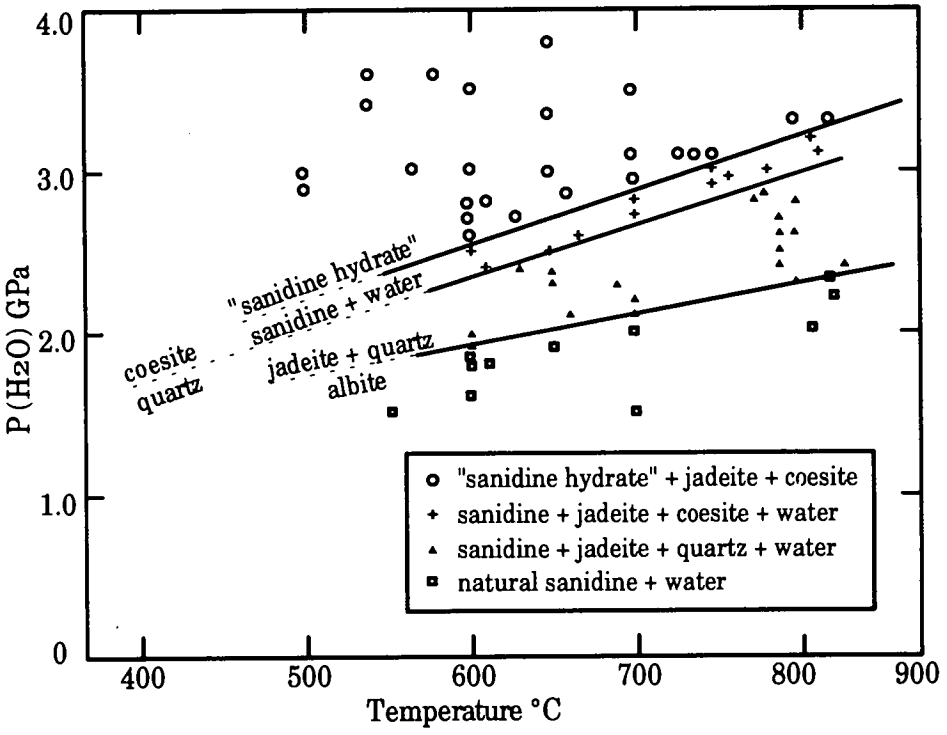

Fig. 2.2. Results of experiments using natural sanidine as a starting material (Seki and Kennedy 1964a)

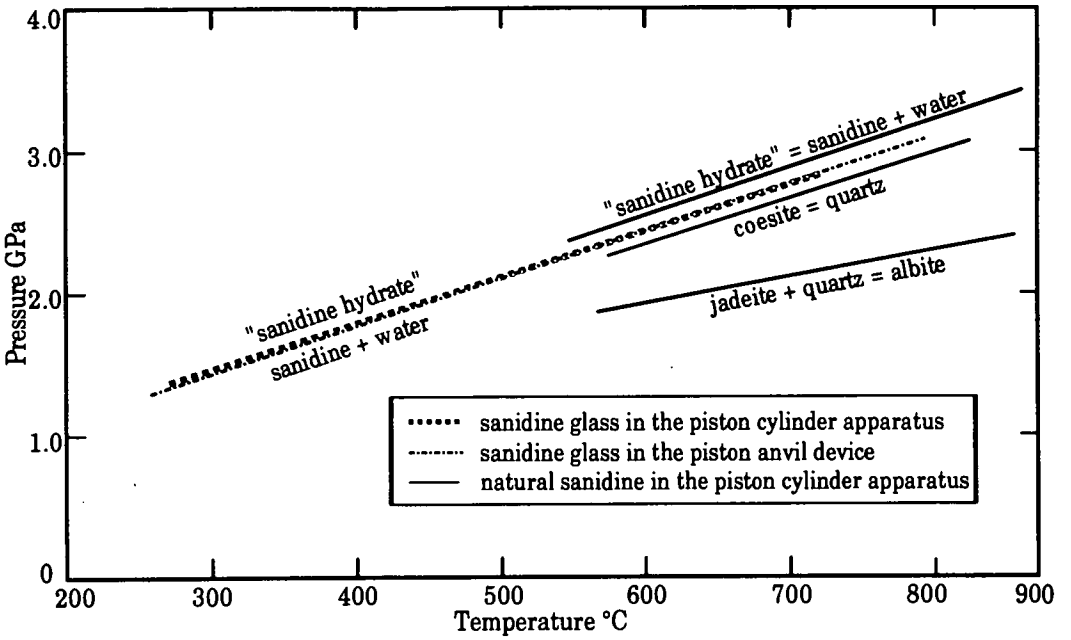

Fig. 2.3. A comparison of the results of Seki and Kennedy (1964a) shown in Figures 1a and b and 2. The piston cylinder apparatus (as described in Chapter 3) and the piston anvil device (as described by Griggs and Kennedy 1956) gave almost identical results using synthetic sanidine glass as a starting material. The same reaction, determined using natural sanidine as a starting material in the piston cylinder apparatus, was also in a similar position.

Ryabinin et al (1965) carried out a similar study of a moistened natural sanidine at high pressures and temperatures. They conducted their experiments in a graphite resistivity furnace, with $KHCO_3$-saturated solution as a flux, between pressures of 6.6 - 7.9 GPa and temperatures of 400 - 2300°C.

Several reactions occurred over the entire experimental range. Optically, two minerals could be seen; acicular crystals (phase A) that were surrounded by irregular grains (phase B). The densities of these two phases were 3.3 and 2.5 - 2.7 g/cm^3 respectively, measured by the immersion technique. The electron probe showed that the acicular crystals were virtually potassium free, (see Table 2.2 for characteristics of the phases in comparison with published data). Powder X-ray diffraction data showed not only jadeite lines and the hexagonal hydrate phase of sanidine but also the principal coesite lines. This would agree with the bulk chemical composition; the coesite may have been too fine to see optically.

Table 2.2. A comparison of the phases synthesised by Ryabinin et al (1965) with published data
N(m,ρ,g,ρ',g') = refractive indicies, ρ = density
** = Larsen and Berman (1965) * = Seki and Kennedy 1964a

Original sanidine	Phase A	Jadeite**	Phase B	"sanidine hydrate"*
SiO_2 = 65.03	Si/Al ≈ 1.96	Si/Al = 2	Si/Al ≈ 3.14	Si/Al = 3
Al_2O_3 = 19.32	K_2O ≈ 0.2%		Si/K ≈ 3.16	Si/K = 3
K_2O = 12.21			Al/K ≈ 1.1	Al/K = 1
Na_2O = 4.49				
$Na_{0.218}K_{0.764}AlSi_3O_8$		$NaAlSi_2O_6$		$KAlSi_3O_8.nH_2O$
Nm = 1.524	Nρ' = 1.660	Nρ = 1.654	Nρ' = 1.537	Nρ = 1.535
Nρ = 1.520	Ng' = 1.667	Nm = 1.659	Ng' = 1.546	Ng = 1.545
		Ng = 1.667		
ρ = 2.54-7 gcm^{-3}	ρ ≈ 3.3 gcm^{-3}	ρ = 3.3-4gcm^{-3}	ρ = 2.5-2.7 gcm^{-3}	ρ = 2.58 gcm^{-3}

Therefore the breakdown of natural sanidine in the presence of water resulted in the differentiation of potassium into a low density, hydrous mineral and sodium into a higher density, anhydrous mineral. "Sanidine hydrate" was stable over the entire pressure, temperature range studied by Ryabinin et al, up to 8.0 GPa and 2300°C, which corresponded to a depth of 250 - 300 km beneath the surface of the Earth. However, if such a material formed at that depth, it would be substantially less dense (ρ = 2.5 - 2.7 g/cm3) than the assumed density of the surrounding mantle (ρ = 3.2 - 3.4 g/cm3).

2.3 The $BaAl_2Si_2O_8$-H_2O system

The $BaAl_2Si_2O_8$-H_2O system possibly represents a low pressure analogue for the anticipated phase relations and thermodynamic properties of the $KAlSi_3O_8$-H_2O system at mantle pressures.

At high partial pressures of water barium feldspar, celsian, breaks down to form a hydrous phase known as cymrite. This mineral was first identified by Smith et al (1949) who assigned it a hexagonal symmetry and a composition of $BaAl_2Si_2O_8.OH$. Later work (Carron et al, 1964, and Essene, 1967) showed the true formula to be $BaAl_2Si_2O_8.nH_2O$. The first work on the reaction of celsian and water to form cymrite was carried out by Seki and Kennedy (1964b). Subsequent workers (Nitsch, 1980, Moles, 1985) attempted to find the equilibrium position of the reaction by reversal experiments.

Graham et al (1992) conducted a series of experiments on the synthesis and growth rates of cymrite and reversal experiments on the reaction

$$BaAl_2Si_2O_8 + nH_2O = BaAl_2Si_2O_8.nH_2O,$$

celsian + water = cymrite.

Graham et al used $BaAl_2Si_2O_8$ gel and water as starting materials in their experimental runs carried out within internally heated argon gas pressure vessels. The run products were characterised optically, by powder X-ray diffraction techniques and by the electron microprobe if the crystals produced were coarse enough. In order to investigate the possible metastable growth of cymrite they varied the length of their runs between 3 hrs and 3 days. At low pressures and temperatures, within the celsian stability field (at the point labelled "kinetic study" in Figure 2.5) after only 3 hours cymrite grew rapidly but metastably, being replaced by celsian in longer runs. Experimental studies by Nitsch (1980) and Moles (1985), prior to those performed by Graham et al, were conducted at lower pressures and temperatures below 600°C. Metastable growth of cymrite in the celsian stability field might explain the discrepancy between the position of the equilibrium boundary (see below) in these works and the work of Graham et al. The results of Nitsch (1980) and Moles (1985) may have shown metastable cymrite growth only (see Fig. 2.4) as equilibrium is hard to attain in realistic run times at these pressures and temperatures.

Graham et al then reversed the reaction using 50:50 mixtures of synthetic cymrite and celsian (Fig. 2.5). The direction of reaction was determined optically and with powder X-ray diffraction techniques. Only large shifts in the X-ray diffraction peaks

(>20%) were used as results, because of the possibility of rapid metastable cymrite growth in the stability field of celsian. The reaction was curved due to the varying equilibrium water content of cymrite, and therefore varying reaction stoichiometry, over this pressure-temperature field. The reversals gave tight brackets for the equilibrium position of the reaction at high temperatures (>600°C) of 10-15°C, but at lower temperatures the brackets were much larger (0.075-0.1 GPa) owing to the slow rates of reactions. These brackets, however, were thermodynamically consistent with the tighter brackets at higher temperatures.

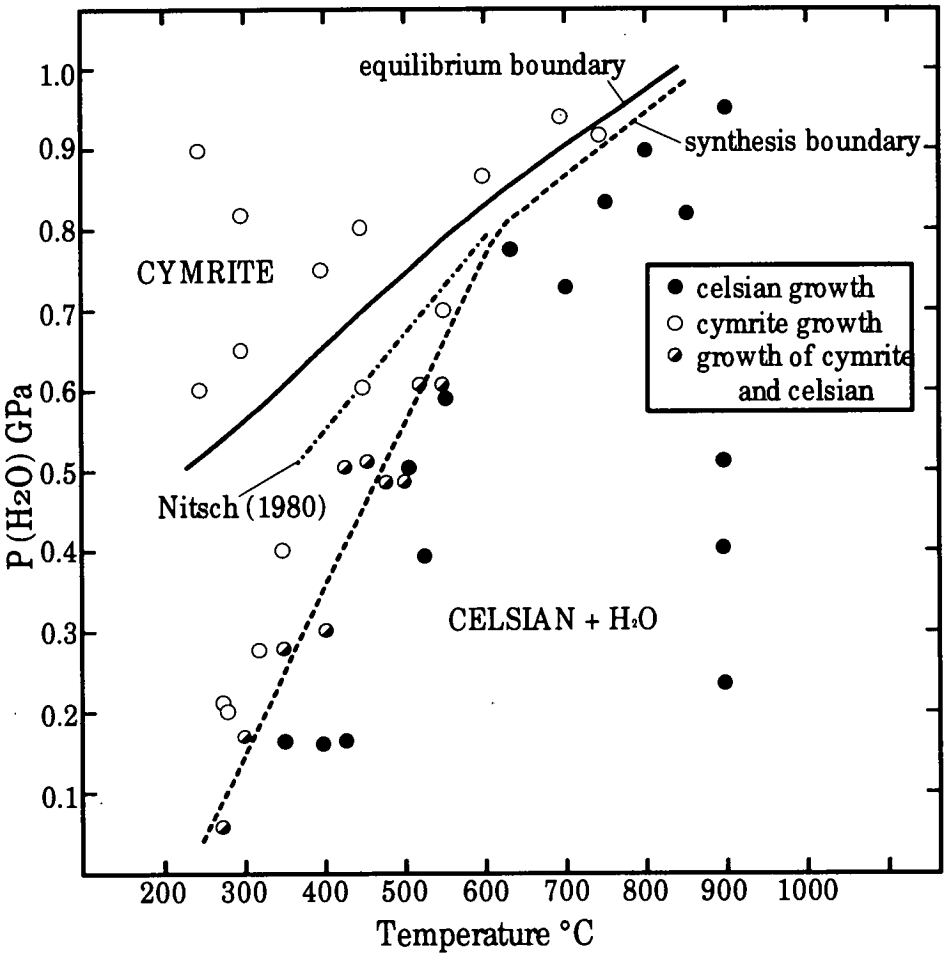

Fig. 2.4. Plot to show the phases which grew initially after only short duration runs (Graham et al 1992). The solid line shows the position of the equilibrium boundary found by reversal experiments (see Fig. 2.5). Therefore cymrite grew metastably beneath this equilibrium reaction in short duration runs. For comparison, the position of the reaction that was found by Nitsch (1980) is shown.

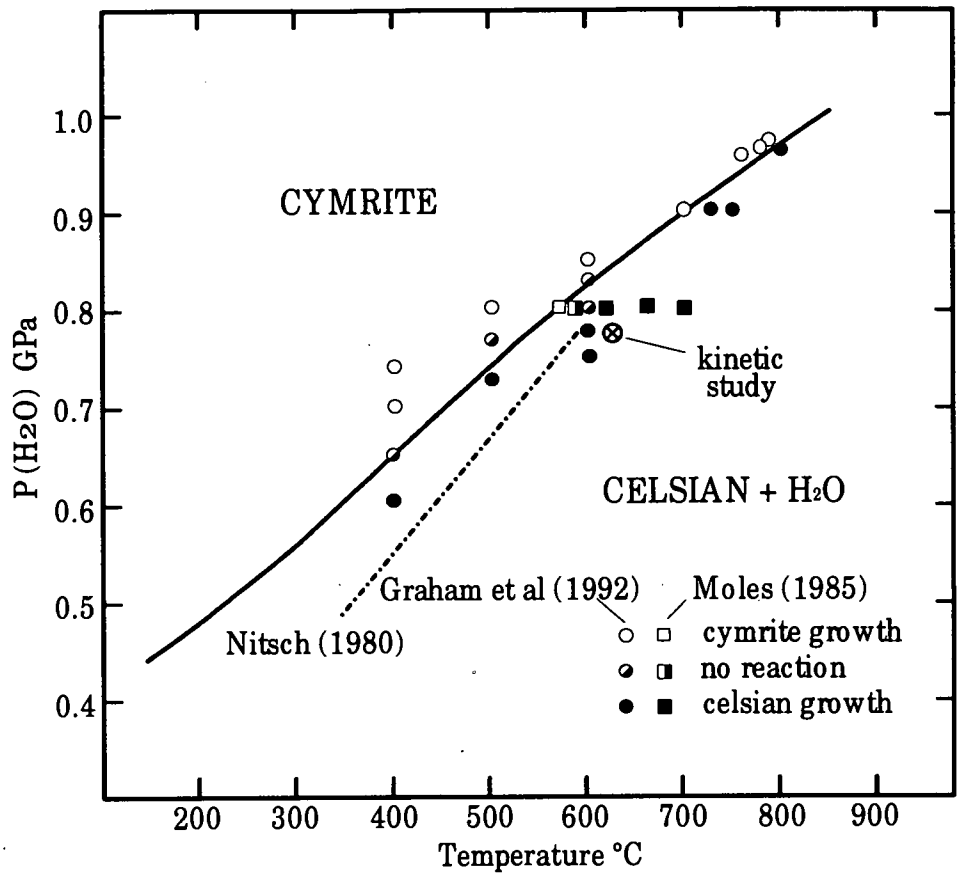

Fig. 2.5. Results of reversal experiments on the cymrite - celsian reaction. (Graham et al 1992). The results of Nitsch (1980) may have shown metastable growth only. The point labelled "kinetic study" produced cymrite in an experiment of only 3 hours duration but produced celsian in a longer experiment.

Results of thermogravimetric analyses (TGA) of cymrites, synthesised stably and metastably at various pressures and temperatures in the presence of excess water are shown in Figure 2.6. The weight loss to 300°C was thought to represent adsorbed water on the surface of poorly or finely crystalline samples and so for the purposes of calculating the formula of cymrite this was ignored. The principlal weight loss occurred between 300°C and 600°C which was thought to represent molecular water being lost from the structure. The largest amount of water lost in this temperature range was 4.7 wt% which corresponded to the theoretical molecular water content of 1 H_2O per formula unit. The weight loss varied according to the pressure and temperature of synthesis. Above 750°C a small but significant amount of weight was lost which was also dependent on the pressure and temperature of synthesis. This was interpreted as structurally bound OH which was more strongly bound into the cymrite structure.

The variation of the molecular water content with pressure and temperature was plotted by subtracting the water lost in the ranges below 300°C and above 600°C as shown in Figure 2.7. Thermodynamic analysis, as described below, supported the conclusion that these values of water loss varied systematically with $P(H_2O)$ and were the equilibrium water contents. However, reversal of the water content lines was not possible, probably because reduction of water was much faster than uptake, i.e. for some kind of kinetic reason. Alternatively, by raising the pressure and temperature of synthesis, water was being moved into the OH sites and hence gave a smaller value than expected between 300°C and 600°C on dehydration. When the pressure and temperature were lowered again the water was too firmly bound into the OH sites to readily re-equilibrate to the equilibrium molecular water value for those conditions, as shown in Figure 2.7.

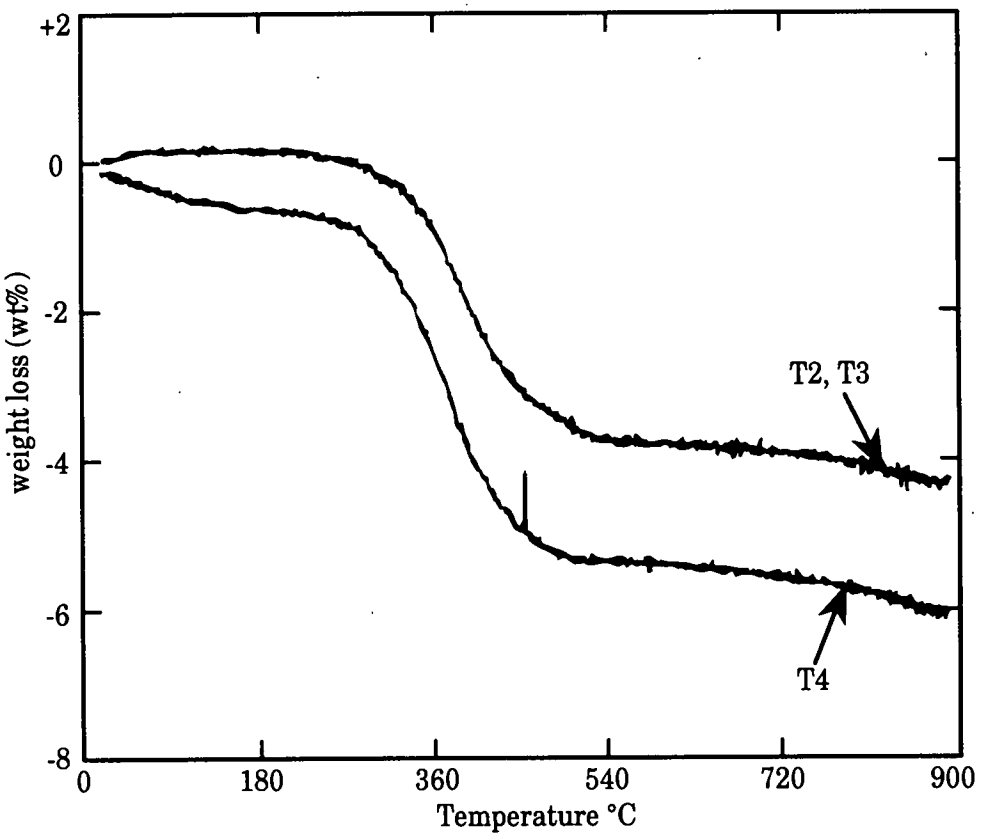

Fig. 2.6. Plot of weight loss versus temperature for three synthetic cymrite samples using a STA 780 series thermal analyser. (Graham et al 1992)

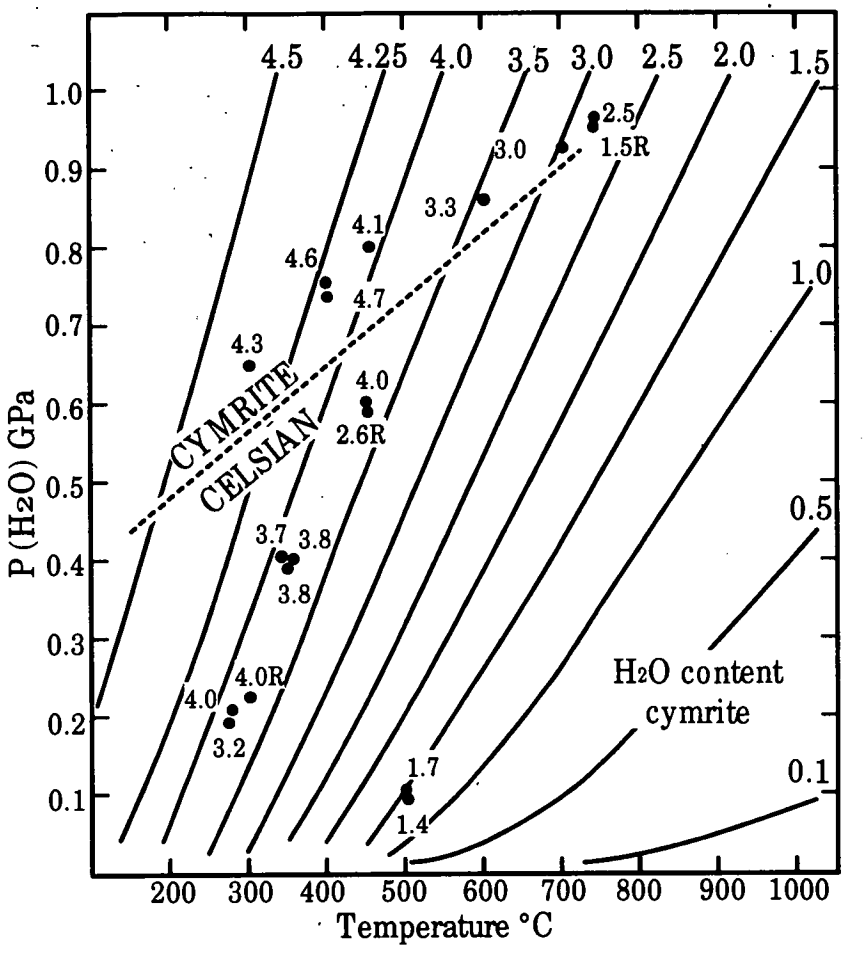

Fig. 2.7. The point values show the water contents of cymrites synthesised at various pressures and temperatures. The water content was measured by the loss in weight between 300 and 600°C during thermogravimetric analysis. Isopleths of constant water composition were calculated, as described in the text, and found to be in good agreement with the measured values. Therefore the measured values of water content in cymrite were probably equilibrium ones even in the region where the cymrite itself is metastable. (redrawn from Graham et al 1992)

Infrared and micro-Raman spectroscopic studies were performed on two of the cymrite samples. The micro-Raman study of the sample prepared at higher pressure and temperature showed stronger peaks in the HOH bending region than the lower pressure-temperature sample, implying that there was increased orientational ordering of the H_2O molecules. In the lower frequency region the low pressure sample showed broader peaks which could be related to some structural disorder. The infrared absorption spectra also showed increased orientational ordering of the H_2O molecules in the higher pressure-temperature sample by the sharper peaks for OH stretching and HOH bending. The infrared OH stretching peaks for cymrite occurred at a lower frequency than for H_2O in cordierite or beryl, which suggested that the degree of hydrogen bonding of water in the cymrite was greater, in good agreement

with thermodynamic data (see below). The intensity of the O-H stretching and HOH bending peaks in the lower pressure-temperature sample was greater, which fitted with the higher water content of the lower temperature sample.

Therefore, the water in the cymrite was shown to be mainly molecular H_2O with the quantity varying with pressure and temperature up to a maximum of one H_2O molecule per formula unit. The structure of cymrite was found to be pseudohexagonal with an overall monoclinic structure (Drits et al, 1975) and the varying amounts of water could lie in the large hexagonal channels. The hexagonal structure of cymrites could be supported by the water molecules forming hydrogen bonds to the adjacent oxygen atoms in the hexagonal channels and thus preventing the collapse of the structure and its subsequent transformation to monoclinic celsian.

Finally Graham et al investigated the thermodynamics of water in cymrite. They assumed that the composition of cymrite was an ideal solid solution between the hydrous (cymrite, $BaAl_2Si_2O_8.H_2O$) and the anhydrous (hexacelsian, $BaAl_2Si_2O_8$) end member. This assumption was supported by the unit cell data of Viswanathan et al (1992) (see Figures 2.9 and 2.10). It was shown experimentally that the quantity of water in the cymrite structure never exceeded one molecule per formula unit (equivalent to 4.58 wt%). Therefore the mole fraction of the hydrous end member (X_{cym}) could be calculated from the thermogravimetric molecular water loss data by the proportion of the measured weight percentage of water to the weight percentage of water in one molecule per formula unit. For the reaction

$$BaAl_2Si_2O_8 + nH_2O = BaAl_2Si_2O_8.nH_2O, \qquad (1)$$

$$\text{hexacelsian} + \text{water} = \text{cymrite},$$

at equilibrium

$$\Delta G^\circ_T = \Delta H^\circ_T - T\Delta S^\circ_T + RT\ln K + \Delta V_S P = 0. \qquad (2)$$

Cymrite and hexacelsian have a very similar structure, since they form a solid solution, and so the volume change of the solids in the reaction was presumed negligible. Hence

$$\frac{\Delta H^\circ_T}{T} - \Delta S^\circ_T = -R\ln K, \qquad (3)$$

where

$$K = \frac{a_{cym}}{a_{hexcel}\, a_{H_2O}} \approx \frac{X_{cym}}{(1 - X_{cym})\, f(H_2O)} \qquad (4)$$

assuming $a_{cym} = (X_{cym})^n$ in an ideal solid solution (where n = number of sites per formula unit on which mixing can take place - which, in this case, is one).

A plot of -RlnK against 1/T gave a linear correlation with a slope of ΔH_T^o of -59.03(3.0) kJmol^{-1} and an intercept at 1/T of ΔS_T^o of -133.47(3.2) JK^{-1}mol^{-1} for the reaction between hexacelsian and water to form cymrite.

The good fit of this data to equation (3) demonstrated its internal consistency, supporting the hypothesis that the measured water contents were equilibrium ones.

Calculated values of ΔH_T^o and ΔS_T^o could be put back into equation (3) to give the equation

$$\ln\left(\frac{X_{cym}}{1-X_{cym}}\right) - \ln f(H_2O) = \frac{7100.64}{T} - 16.054. \qquad (5)$$

ln$f$(H$_2$O) depends on pressure and temperature, as tabulated in the data of Burnham et al (1969), and thus values of the water content were used to calculate X_{cym} and solve equation (5) to give the isohydrons of Figure 2.7. It can be seen from Figure 2.7 that even where the cymrite itself is metastable the water contents still agree with the isohydrons are therefore probably equilibrium values.

After calculating a thermodynamic model for the equilibrium water contents, the location and curvature of the cymrite celsian equilibrium was calculated more accurately within the experimental brackets and then extrapolated to lower pressures and temperatures. To achieve this equation (2) was applied to the reaction

$$BaAl_2Si_2O_8.H_2O = BaAl_2Si_2O_8 + H_2O, \qquad (6)$$

cymrite = celsian + water.

In this reaction the volume change of the solids is not negligible and was calculated from the change in cell parameters using the data of Viswanathan et al (1992). If celsian and H$_2$O are pure then the equation can be rewritten as

$$\frac{\Delta V_S^o(P-1)}{RT} + \ln f(H_2O) - \ln X_{cym} = -\frac{\Delta H_T^o}{RT} + \frac{\Delta S_T^o}{R}. \qquad (7)$$

For the experimental conditions of the reversal experiments which bracket the cymrite-celsian equilibrium the left hand side of the equation was evaluated and plotted against 1/T. Thus the values for ΔH_T^o and ΔS_T^o for the reaction between

celsian and water to form cymrite were calculated to be 37,425(707) $Jmol^{-1}$ and 116.37(0.6) $JK^{-1}mol^{-1}$ respectively. By substituting these values back into equation (7) the position of the $P(H_2O)$-T locus was determined both within the experimental brackets and outside this pressure-temperature range. On extrapolating the reaction to lower pressures and temperatures Graham et al discovered that the curvature on the reaction was not sufficient to explain the occurrence of cymrite in low pressure and temperature conditions in near surface sedimentary and hydrothermal rocks. The cymrite found in these rocks is therefore metastable.

Hsu (1994) also investigated the equilibrium position of the reaction between celsian and water to form cymrite. He found that the position of the reaction lay in a different position to that determined by Graham et al. (1992). Figure 2.8 shows the results of Hsu's work in comparison to that of Graham et al. described above

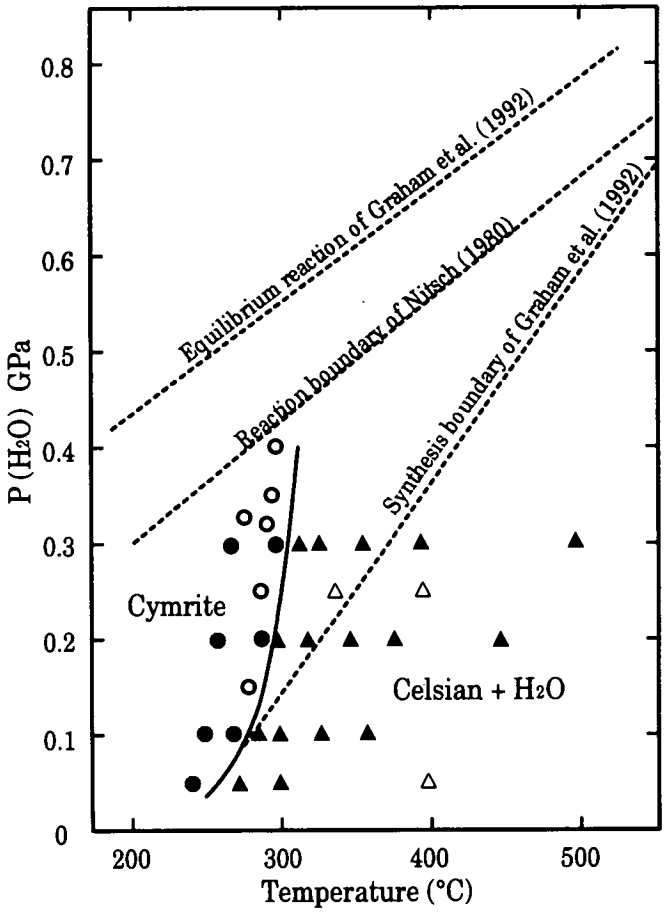

Fig. 2.8. The reversal experiments of Hsu (1994) on the position of the reaction between celsian and water to form cymrite. Circles represent cymrite and triangles celsian. Solid symbols show reversed data points and open symbols represent synthesis experiments. The work of Graham et al. (1992) and Nitsch (1980) are shown for comparison. Redrawn from Hsu (1994).

Hsu's study would explain the common occurrence of cymrite at atmospheric pressures in sedimentary environments without the need for extensive metastable behaviour. However, the reason for the discrepancy between these results and those of Graham et al. were not understood.

The structure of cymrite was determined by Drits et al. (1975) from a sample of cymrite from California. They found the unit cell to be monoclinic with unit cell parameters of a = 0.533 nm, b = 3.66 nm, c = 0.767 nm and $\beta = 90°$. The structure has pseudohexagonal symmetry with slight distortions in the structure reducing the symmetry from hexagonal to monoclinic. This might be caused by slight ordering of the Si and Al atoms and results in small displacements of the Ba atoms along the x-axis and the Si and O atoms along the z-axis. The tetrahedra appear to twist slightly in alternate directions. The resulting diffraction patterns therefore contain satellites on hk0 for Ba atom displacements and weak ones on 0kl for Si and O atom displacements.

Viswanathan et al. (1992), in a paper accompanying that by Graham et al, also studied hydrated barium feldspars. Experiments were carried out on gels of composition $BaAl_2Si_2O_8$ using externally heated cold seal pressure vessels at 0.1-0.3 GPa and piston cylinder apparatus at 0.7-1.0 GPa. Hexacelsian ($BaAl_2Si_2O_8$ with a hexagonal structure), synthesised at atmospheric pressure and 1590°C, and a natural cymrite, were used in dehydration studies. The phases were identified and their lattice constants determined by X-ray diffraction methods.

The natural cymrite was dehydrated over a temperature range of 0-1000°C. Here it was found that cymrite could be partially or completely dehydrated and that the lattice constants varied with water content. Initially the lattice constants were similar to the values for cymrite but when the sample was completely dehydrated they were close to the values for hexacelsian. Dehydration caused an expansion in the c direction and a contraction in the a direction (see Figures. 2.9 and 2.10). Cymrites that had been only partially dehydrated were referred to as intermediate cymrites.

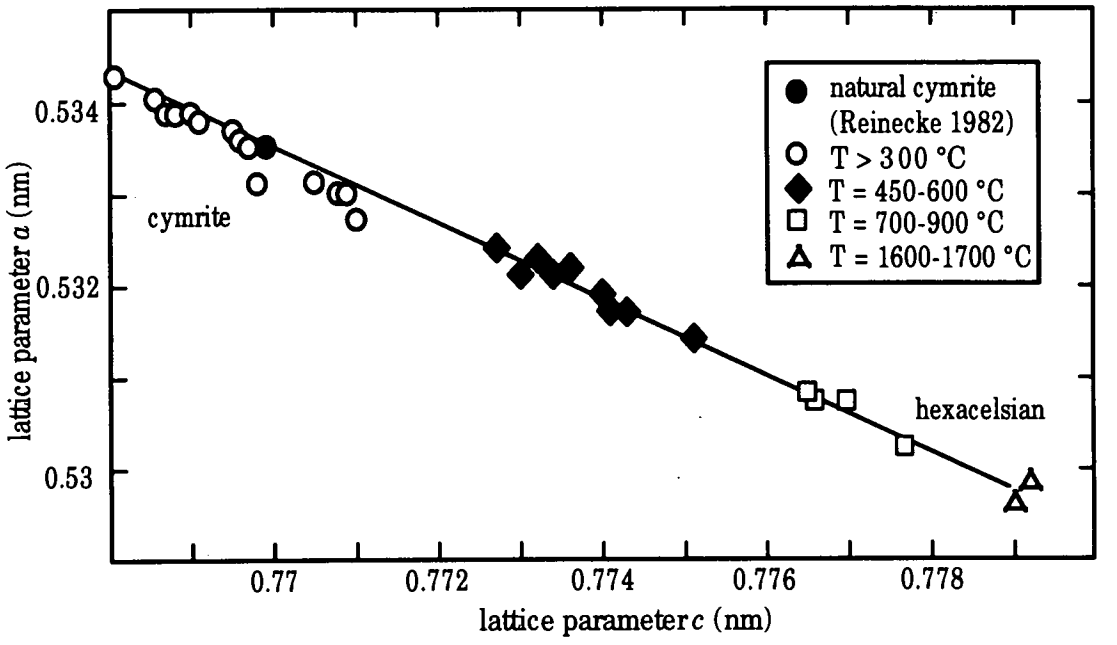

Fig. 2.9. Relation between the lattice parameters *a* and *c* for hexagonal phases produced at stages during the dehydration of cymrite (Viswanathan et al 1992).

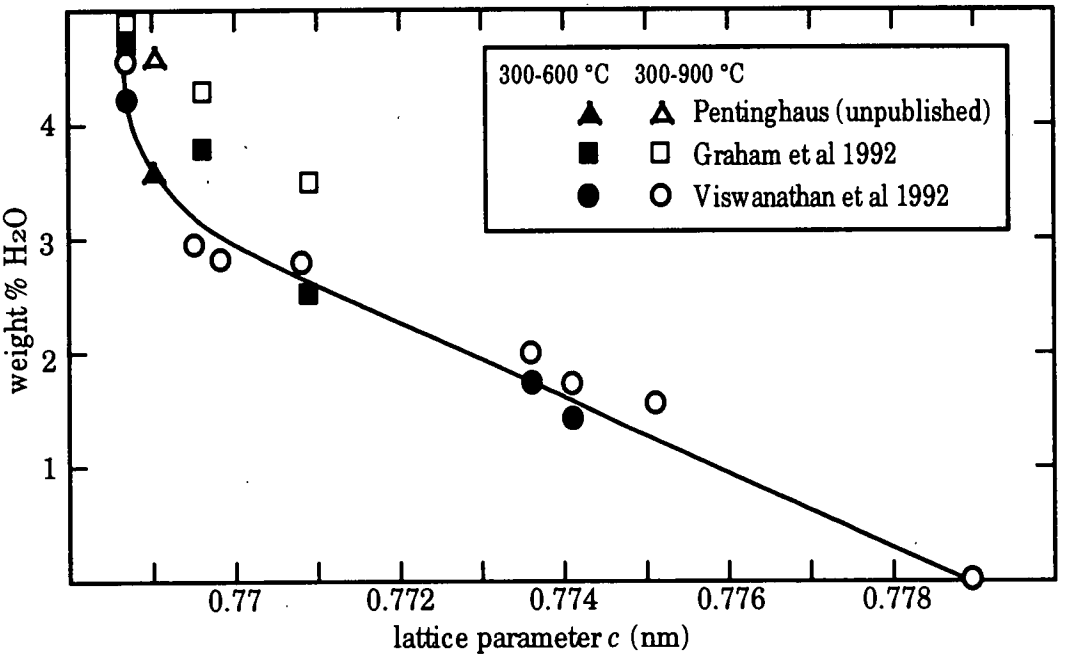

Fig. 2.10. Dependence of the lattice parameter *c* on the water content. (Viswanathan et al., 1992)

Thermogravimetric analysis carried out on synthetic cymrites confirmed the observation of Graham et al (1992), that the main range of dehydration lay between 300 and 600°C. However, with the natural cymrites the temperature range for dehydration was much higher (500-750°C). This could have been due to the difference in the grain size as the synthetic specimens were very fine grained.

Four samples were subjected to dehydration in a Guinier high-temperature camera to determine their change in lattice constants with temperature. Figures. 2.11 and 2.12 show the results. The four samples used were a synthetic hexacelsian, an intermediate cymrite, a synthetic cymrite and a natural cymrite. The hexacelsian, which did not contain water, showed only the effects of thermal expansion. At about 250°C there was a discontinuity which perhaps reflected the change of hexacelsian between its α and β forms as described by Yoshiki and Matsumoto (1951). The natural cymrite seemed to exhibit this α to β transition also and at higher temperatures it showed the contraction in the *a* direction and the expansion in the *c* direction as mentioned previously. The fine grained synthetic cymrites would start to dehydrate at a temperature which would mask the α to β transition if it occurred. The intermediate cymrite showed a smaller water loss effect, as would be consistent with its composition lying between synthetic cymrite and hexacelsian. All samples, when completely dehydrated, converged towards a point where the lattice parameters, at room temperature, were the same as those for hexacelsian. The similarity in the gradients of the curves for the lattice parameter *a* of the three cymrites at temperatures below 250°C suggested that the structure was similar to that of α hexacelsian.

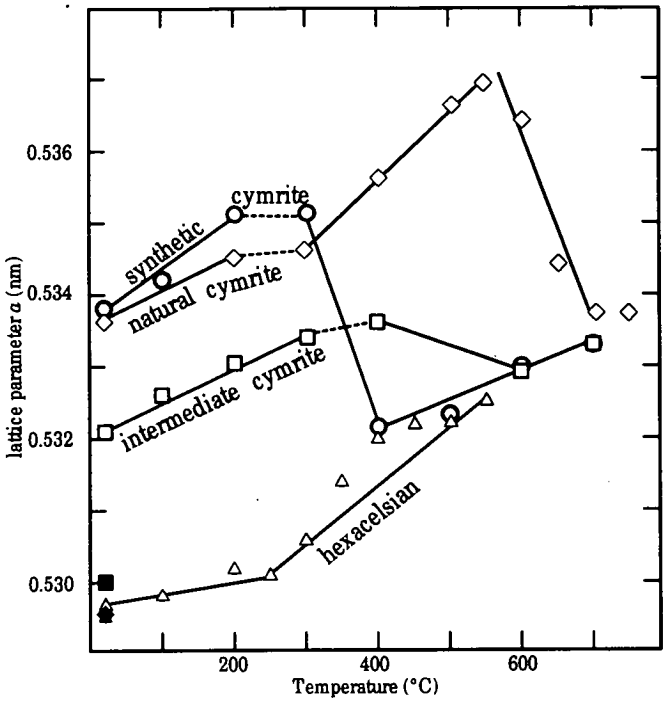

Fig. 2.11. Variation of lattice parameter *a* with temperature. Data for synthetic cymrite from Pentinghaus and Nitsch (1986). Filled symbols show final lattice parameters determined after cooling to room temperature. (Viswanathan et al 1992)

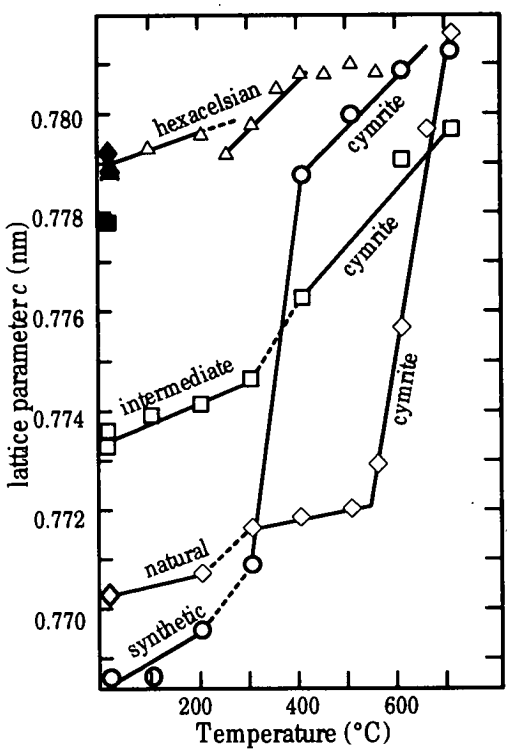

Fig. 2.12. Variation of lattice parameter *c* with temperature. Data for synthetic cymrite from Pentinghaus and Nitsch (1986). Filled symbols: final lattice parameters determined after cooling to room temperature. (Viswanathan et al 1992)

In the stability field of celsian the presence of water could have two contradictory effects. It could either act as a catalyst in suppressing the metastable formation of hexacelsian, favouring celsian instead, or it could extend the metastability of hexacelsian by converting it into hydrated phases (Viswanathan et al 1992). Due to the sluggish rates of the reaction in the formation of celsian from hexacelsian, at low pressure and temperature the latter effect of the presence of water would be dominant and therefore the metastability of hexacelsian would be extended by the formation of hydrous phases. This would explain the existence of the low pressure and temperature field of metastable cymrite growth as found by Graham et al. This readiness to form metastable phases makes the phase diagram more difficult to construct experimentally and therefore the stability field of any cymrite phases with a smaller water content has yet to be determined.

Chapter 3
Experimental and analytical techniques

3.1 Introduction

The primary objectives of this thesis were outlined in Chapter 1. The initial part of the work was to reverse the reaction between sanidine and water to form "sanidine hydrate" in the pressure range of 2.0-3.5 GPa and the temperature range of 400-700°C. Starting materials for these experiments were synthesised at low pressures in the cold seal apparatus and at high pressures in the piston-cylinder apparatus. The reversal experiments were also conducted in the piston-cylinder apparatus. The run products were characterised principally by powder X-ray diffraction.

The phase "sanidine hydrate" was believed to be hydrous for the reasons outlined at the start of Chapter 5. The water content of "sanidine hydrate" was investigated using infrared spectroscopy and thermogravimetric analysis in order to determine the type and quantity of structural "water" respectively. The thermogravimetric analysis produced values that were inconsistent in the high pressure samples. These samples may have been contaminated, perhaps with platinum when the samples were extracted from their capsules. Hence some attempt to quantify the platinum contamination was made using atomic absorption. The techniques of infrared spectroscopy were also used at a later stage in the examination of the water content of samples of synthetic sanidines and some natural feldspars from the Klokken layered syenites from South Greenland.

This chapter describes the methods employed in these experimental and analytical techniques

3.2 Starting materials for high pressure experiments

A supply of $KAlSi_3O_8$ gel, generously donated by Dr D.L. Hamilton of the University of Manchester, was used for the synthesis experiments. The reasons for using a gel rather than a sintered oxide mix were that a gel was more homogenous and its grain size was approximately ten times smaller than a sintered oxide (Odling *pers. comm.*). This meant that a gel was more reactive and hence less likely to cause kinetic problems. The temperatures at which these experiments were performed were low (less than 700°C) and therefore using a gel was less likely to cause problems of metastability or an incomplete reaction. A glass starting material would have been hard to produce as potassium is easily lost in the process. It was important that the gel reacted completely to synthesise sanidine or "sanidine hydrate", since, when the

two were mixed together in order to create a starting material for the reversal experiments, it was assumed that they were wholly crystalline.

Once the sanidine and the "sanidine hydrate" had been synthesised from the gel, they were carefully weighed and mixed together in the proportions 40.1% "sanidine hydrate" to 59.9% sanidine. This mixture was named PTmix. A summary of the synthesis experiments and the proportions in which the sanidine and "sanidine hydrate" were mixed is included in Section 4.2.

In addition to the $KAlSi_3O_8$ gel in synthesis experiments and the sanidine-"sanidine hydrate" mix in reversal experiments, all runs also contained between 6.07 and 9.0 wt% of double deionised and distilled water.

3.3 High pressure experiments using the piston cylinder apparatus

The experiments used to synthesise "sanidine hydrate" and sanidine above 1.0 GPa and to determine the position of the reversal reaction between sanidine and water and "sanidine hydrate" were all conducted in the piston cylinder apparatus.

3.3.1 *Capsule design*

All high pressure experiments used capsules to contain the sample. These capsules were of similar design and varying sizes. Synthesis of "sanidine hydrate", in the piston cylinder apparatus, was carried out using capsules of 4 mm outside diameter and 0.1 mm wall thickness in order to make a large quantity of "sanidine hydrate" for reversal experiments, in fewer experiments. Reversals were carried out in capsules of 3 mm outside diameter as this required less starting material but still produced enough material at the end of the experiment for characterisation by powder X-ray diffraction and subsequent investigation with infrared spectroscopy and thermogravimetric analysis.

Lengths were cut from 3 and 4 mm platinum tubing in order to make the capsules. The 4 mm capsules required lengths of 11-12 mm of platinum tubing. The 3 mm capsules for reversal experiments required only 9-10 mm of tubing as the starting mixture was much denser than the gel used in the 4 mm capsules and so a smaller volume of mixture was sufficient, and the capsule capacity could likewise be reduced.

The platinum tubing was sealed at one end using an electric arc welder. This half sealed capsule was then squashed into the shape of a flat bottomed bucket using a die clamped in a vice. The deionised, distilled water was first placed in the bottom, with the use of a syringe, and then the starting material was loaded on top leaving a gap of more than 3 mm above for ease of sealing the capsule. The quantity of water was always between 6.07 and 9 wt% (6.07 wt% being the amount of water required to make n = 1 in the formula $KAlSi_3O_8.nH_2O$) In the barium analogue, cymrite, the maximum amount of water was one molecule per formula unit. In all synthesis and reversal experiments described in the next chapter there was always free water remaining at the end of the experiment and hence 6.07 wt% was thought to be a sufficient quantity to saturate the system. However, too much water was not desirable as it was possible that, with a large excess of water, a significant amount of the starting material would dissolve incongruently in the vapour phase (see Section 8.6, Stern and Wyllie 1981).

The second end of the platinum tubing was then crimped, welded and pressed flat in a pin press. The capsule was tested for leakages by leaving it in an oven at 110°C overnight. Then, if any weight were lost, the capsule was discarded and the starting material extracted and dried to be reused again. A diagram of the capsule design is shown in Figure 3.1.

3.3.2 *Cell design*

The design of the cell used in the piston cylinder experiments is shown in Figure 3.2.

The platinum capsule containing the sample was held within the centre of a graphite furnace using hot pressed boron nitride (i.e. BN with B_2O_3 as a binder) pieces as spacers. The sleeve around the capsule was thicker for the 3 mm diameter capsules. Any hollows in the walls of the capsule were carefully packed with boron nitride powder. Boron nitride was used as a pressure medium as it is almost frictionless with a fluid-like behaviour at the experimental pressures and temperatures of this study (Odling *pers. comm.* see Section 3.3.4). The capsule was placed with the thinner crimp (the first end) on the top so that the distance between the sample and the thermocouple bead was minimised in order to help reduce any potential problems of thermal gradient (see Section 3.3.5).

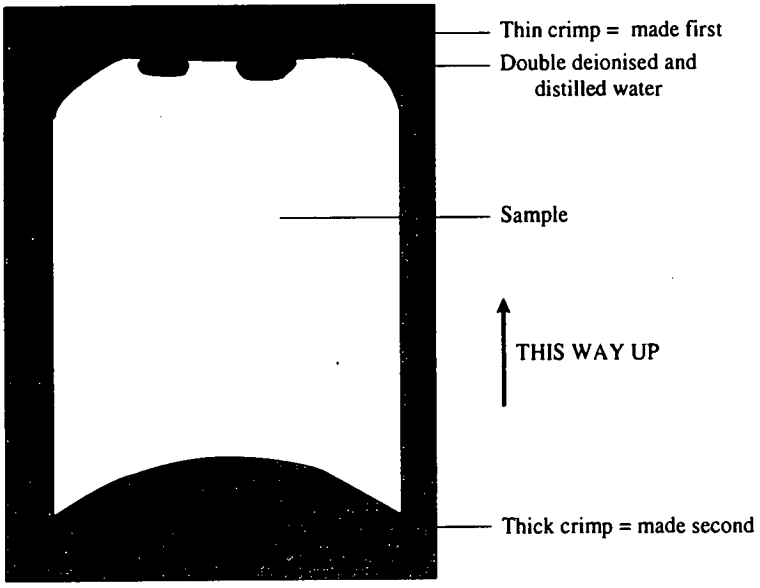

Fig. 3.1. The design of the capsules used in the piston cylinder experiments.
The diameter of capsule was 4 mm for synthesis experiments and 3 mm for reversal experiments

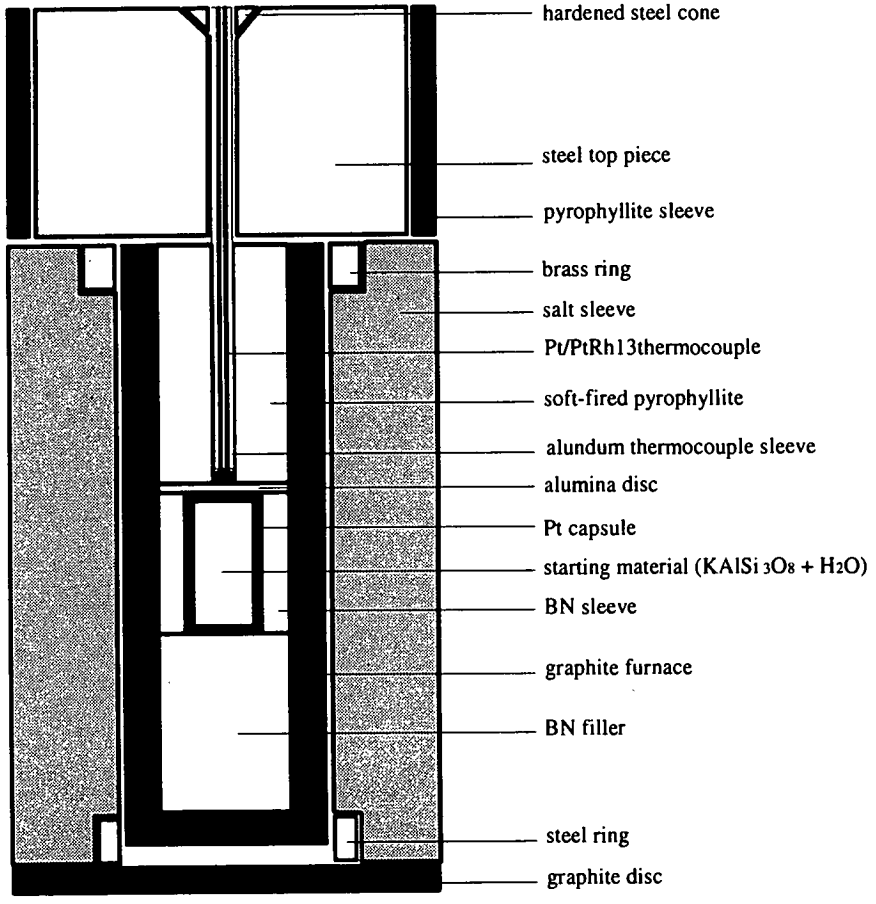

Fig. 3.2. The design of the cell used in the piston cylinder experiments.
The diameter of the cell was 12.7 mm.

A disc of crushable alumina, approximately 0.9 mm thick, was placed on top of the capsule. This was introduced to prevent the thermocouple from punching down through the capsule when the pressure was raised. The thermocouple was made of platinum/rhodium wire within a 2-bore alundum thermocouple sheath.

Soft-fired synthetic pyrophyllite ($Al_4[Si_8O_{22}](OH)_4$) held the thermocouple in position in the top of the furnace. This was used because it clamped the thermocouple when the pressure was raised and helped to prevent it extruding upwards away from the capsule and hence measuring a temperature lower than that of the hot-spot of the furnace. During this series of experiments a new batch of pyrophyllite thermocouple positioners was acquired by the laboratory. It was found that the new batch of soft fired pyrophyllite was strongly contaminated with titanium and iron (see section 3.3.6). However, in these experiments the contaminated pyrophyllite did not seem to have the effect of poisoning the thermocouple and thus altering the temperature reading, presumably because of the low temperature of the experiments. A short length of boron nitride sleeve was added as an extra precaution to all of the reversal experiments where the temperature reading was crucial. It was hoped that this would prevent any of the iron or titanium from touching the thermocouple but would not be too weak to allow the thermocouple to shear. The length of the boron nitride sleeve used was approximately 1 mm.

Surrounding the graphite furnace was a sleeve of NaCl which, like the BN, should act as a frictionless pressure medium. The salt sleeves were made by pressing finely ground Analar salt in a die with a few drops of water. They were then machined to the correct length and indented at each end this allowing a brass ring to be inserted in the top in order to increase the conducting surface of the graphite furnace against the steel top piece above. At the bottom end the salt was made slightly longer than the graphite furnace (1.5 mm) to allow for the extra compressibility of the salt. A steel ring was inserted which was designed to slide up the outside of the graphite furnace and so prevent the salt compressing into the gap at the bottom of the furnace.

Surrounding the salt was a thin sheet of lead lubricated with molybdenum sulphide (MoS_2) grease in order to reduce the friction between the cell and the bomb walls and also prevent the salt from dyking into the tungsten carbide.

On top of the cell, and separating it from the top plate, was a sleeve of soft steel around the thermocouple. This, in turn, was surrounded by a sleeve of soft fired pyrophyllite, which was also well lubricated with MoS_2 grease. Around the top of the

thermocouple was a hardened steel cone which prevented the soft steel dyking up the bore in the tungsten carbide of the top piece

The dimensions of all of the parts of the cell were measured both before and after the experiment so that the causes of any failures could be more readily identified.

3.3.3 *Piston cylinder apparatus*

The cell was loaded into the piston cylinder apparatus as shown in cross section in Figure 3.3.

A confining load of 150 tonnes was applied using the large ram. The pressure of the small ram was then gradually raised, thus applying pressure via the piston to the cell, up to approximately the pressure required during the run. The press was then left for a minimum of two hours in order for it to settle and allow the void space within the cell to compact. During this time the pressure usually dropped by up to 0.15 GPa.

The temperature was raised by passing an electric current through the graphite furnace and measured using a $Pt/Pt_{87}Rh_{13}$ thermocouple. As the temperature increased, the salt expanded and hence the pressure increased. During the heating process the pressure usually increased to 0.05 GPa above the run pressure. The pressure was then bled off, by approximately 0.15 GPa, several times during the first hour or so of the experiment until the system stabilised. After that the pressure only needed adjusting up or down slightly during the longer experiments when the temperature in the room fluctuated or as small leakages lowered the pressure. A record of the e.m.f., pressure, temperature and power values was kept at frequent intervals throughout each experiment.

The experiments were quenched by switching off the power. The temperature decreased to less than 100°C in a few seconds. The apparent pressure dropped by approximately 10% with the temperature and was then lowered to zero by gently bleeding off the oil.

The procedure described above, which brought the sample up to pressure and temperature, probably produced a "piston-out" technique because the salt expanded. However, the exact position of the piston remained uncertain. In some of the longer runs the pressure fell slightly due to leakages or a drop in the ambient temperature which may have resulted in "piston-in" conditions. The position of the piston during the run was therefore unconstrained. In theory this was not too important provided no pressure correction was required during the run (see next section)

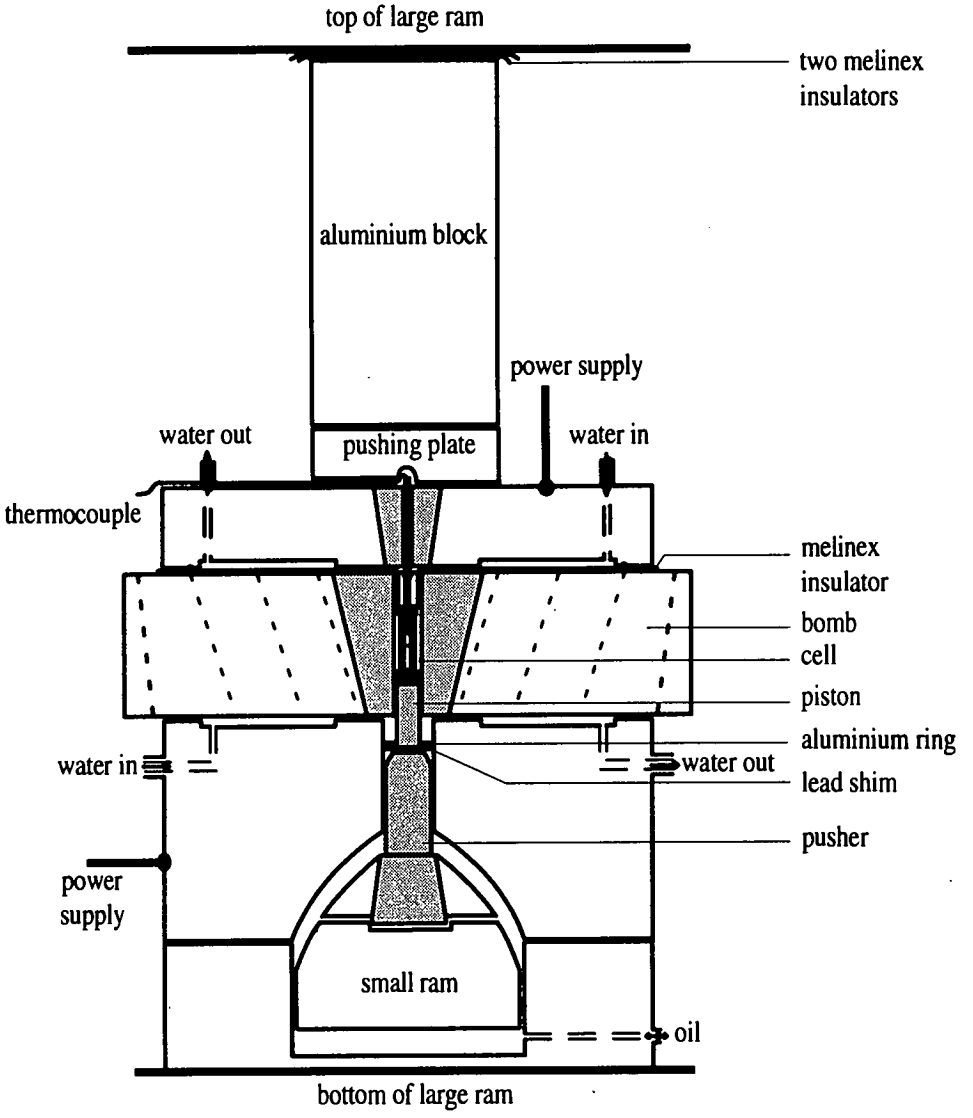

Fig. 3.3. A sketch cross section of the piston cylinder apparatus. Shaded parts were made from tungsten carbide. Diameter of bomb was approximately 250 mm.

3.3.4 *Pressure measurement*

The applied pressure was measured using an oil-filled Heise gauge. However, there were problems with the piston-cylinder apparatus in determining whether this was the true pressure on the sample. This could only properly be solved by calibrating the cell used in the pressure-temperature range of the experiments against a well constrained reaction.

The problems which affected the accurate estimation of pressure were friction, the shear strengths of the pressure media used within the cell and perhaps deformation of the apparatus at high pressures, which may cause an increase in the friction. In these experiments the general effects of friction were minimised as far as possible. The chamber walls were hard and smooth and well lubricated with MoS_2 grease. The salt cell was also lined with lead foil which would also act as a lubricant.

A cell assembly with salt parts on both the inside and outside of the graphite furnace has been calibrated by various authors (Bohlen 1984, Mirwald et al 1975) and one with salt on the inside and CsCl on the outside of the furnace by Bose and Ganguly (1995). These calibrations have been made against the melting of alkali halides and metals. Alkali halides are not ideal for pressure calibration as the melting point varies considerably with temperature. However, the melting of alkali halides can at least be measured using the gas bomb apparatus for comparison. Bohlen (1984) carried out experiments using platinum spheres which fell to the bottom of the capsule as the alkali halide material melted. He discovered that a 25.4 mm diameter salt cell required no pressure correction in the range 0.5 to 2.0 GPa. The data of Mirwald et al (1975) on the melting of LiCl showed that no pressure correction was required for a 12.7 mm cell when compared to the values determined by Clark (1959) for the melting of LiCl. However, Bohlen (1984) found that Clark's values were too low, by 10 - 15°C, and so a pressure correction would also be required for Mirwald et al's data of 0.04 to 0.06 GPa, i.e. the true pressure experienced by the sample was 0.04 to 0.06 GPa lower than the measured pressure. Mirwald et al (1975) also studied the melting of Cu, Ag and Au on compression and decompression strokes and discovered that the friction decreased with time until it appeared to be negligible on the second compression stroke. Bose and Ganguly (1995) calibrated their piston cylinder apparatus for both a 19 mm and a 12.7 mm cell diameter in two ways. Firstly they investigated the hysteresis loop of the relationship between apparent ("nominal") pressure and the piston displacement measured with an "on-line digital pressure transducer". The hysteresis loop shows the decay of friction with time. After approximately 30 hours, also on the second compression stroke, the friction was

reduced to being negligible and hence no pressure correction would be required as the "nominal" pressure would be equal to the true sample pressure. Their second calibration of the piston-cylinder apparatus was from differential thermal analysis of the melting point of LiCl. With this method they found that no pressure correction was required for either of their cells when compared with Clarke's (1959) data with an increase 10°C added to the position of the curve, as was suggested by Bohlen (1984), if the experiments were run for over 30 hours.

In all of the calibration experiments for previous work described above, salt or CsCl was used to surround the furnace with NaCl on the inside of the furnace. In the present experiments boron nitride was used to support the capsule in the centre of the furnace. This may have produced an "anvil" effect (Bell, Mayo and England 1971) where the difference between the shear strengths of the different components of the cell would have resulted in an uneven distribution of the load. The individual components of the cell, however, are all thought to be weak. The graphite furnace was thought to be incapable of supporting a significant load as the furnace would break if it was too long (Carrington 1993). Boron nitride was also thought to be weak under any experimental pressure and temperature (Odling *pers. comm.*). In an experiment of Odling's, boron nitride was found to intrude up the thermocouple bore when pressure was applied and before the temperature was raised. Hence the boron nitride was taken to have no shear strength at any experimental pressure and temperature. Therefore any pressure correction is perhaps most likely to be due to the deformation of the apparatus itself at high pressure.

The pressure correction was measured by calibration against the quartz-coesite reaction, which was thought to be well constrained at the time the calibration experiments were carried out. Bohlen and Boettcher (1982) precisely determined this reaction using a 25.4 mm diameter salt cell which should have required no pressure correction. Their results are plotted in Figure 3.4. The use of quartz-coesite as a calibration reaction for piston cylinder experiments required a reliance on results which were also measured on a piston cylinder apparatus, and thus circular reasoning was involved. However, the original work by Bohlen and Boettcher was performed using a cell which had been calibrated against the melting of CsCl, LiCl and NaCl using the method of sinking platinum spheres. Therefore it was not unreasonable to calibrate the cell assembly, in this instance, against their position for the quartz-coesite reaction. The work of Bose and Ganguly (1995) casts serious doubts on the reliability of Bohlen and Boettcher's data. Bose and Ganguly measured the position of the quartz-coesite reaction using their piston cylinder apparatus which had been

calibrated, as described above, by its friction decay in the hysteresis loop and by differential thermal analysis of the melting of LiCl. They found that the quartz-coesite reaction was parallel to that determined by Bohlen and Boettcher but 0.15 GPa higher. Their results are shown by the dot-dash line in Figure 3.4. The reason for the discrepancy between these two sets of results was not understood by Bose and Ganguly. For this study all the pressures have been calibrated to those of Bohlen and Boettcher.

The results of the pressure calibration experiments are tabulated in Table 3.1. All the calibration experiments were carried out on the same press B in the laboratory at Edinburgh University, as were all the experiments in the rest of this study, which required accurate knowledge of the pressure, rather than on the other press A. The starting material used for the reversal experiments on the quartz - coesite reaction was a mixture (PTQCmix) of 70 % quartz synthesised at 0.1 GPa and 750°C and 30 % coesite synthesised at 3.0 GPa and 550°C. Ten different aliquots of the starting material were scanned using powder X-ray diffraction prior to the reversal experiments. Two large peaks from the powder X-ray diffraction trace were chosen for calibration, one representing quartz and the other coesite, and their average peak height measured. After experiments were completed, the run products were scanned repeatedly and their traces compared for peak heights with those of the starting material. A relative change in peak heights of quartz and coesite indicated to which side of the equilibrium position of the reaction the samples had been at the pressure, temperature conditions of the experiments. The method and criteria used for the estimation of the relative change in peak heights were similar to those used for the reversal experiments of the reaction between sanidine and water to form "sanidine hydrate".

The results of the bracketing experiments are plotted in Figure 3.4. The position of the reaction determined by Bohlen and Boettcher (1982) is shown as a dashed line and that of Bose and Ganguly (1995) as a dot-dash line. At high pressures and temperatures a slight pressure correction is required. However, a straight regression line fitted through the brackets would result in a negative pressure correction at low pressures and temperatures, which would seem an unlikely requirement. Hence a curve was drawn through the brackets at higher pressures which became almost coincident with Bohlen and Boettcher's line at lower pressures. If the pressure were corrected to the data of Bose and Ganguly the observed pressure would need to be increased in order to calculate the true pressure. A negative pressure correction

would be harder to explain than a positive one which could perhaps be caused by the deformation of the apparatus at high pressures increasing the friction.

Table 3.1. Results of reversal experiments on the phase change of quartz to coesite measured in the piston cylinder apparatus B

Run	P	T	H_2O	Length	Type*	Starting	Results***
	GPa	°C	wt %	hours		materials**	
84	2.68	700	5.1	53	pc	PTQCmix	qtz
85	2.72	700	5.2	96	pc	PTQCmix	qtz
86	2.76	700	5.6	47	pc	PTQCmix	no change
87	2.78	700	5.3	72	pc	PTQCmix	95% coes
88	2.64	500	5.6	152	pc	PTQCmix	no change
89	2.68	500	4.9	312	pc	PTQCmix	55% coes
90	2.96	900	11.0	48	pc	PTQCmix	qtz
91	3.05	900	6.3	54	pc	PTQCmix	95% coes
92	2.62	600	7.5	288	pc	PTQCmix	qtz

Notes: * pc = piston cylinder apparatus, R = reversal experiment
PTQCmix = mixture of 30% coesite and 70% quartz
*** coes = coesite, qtz = quartz

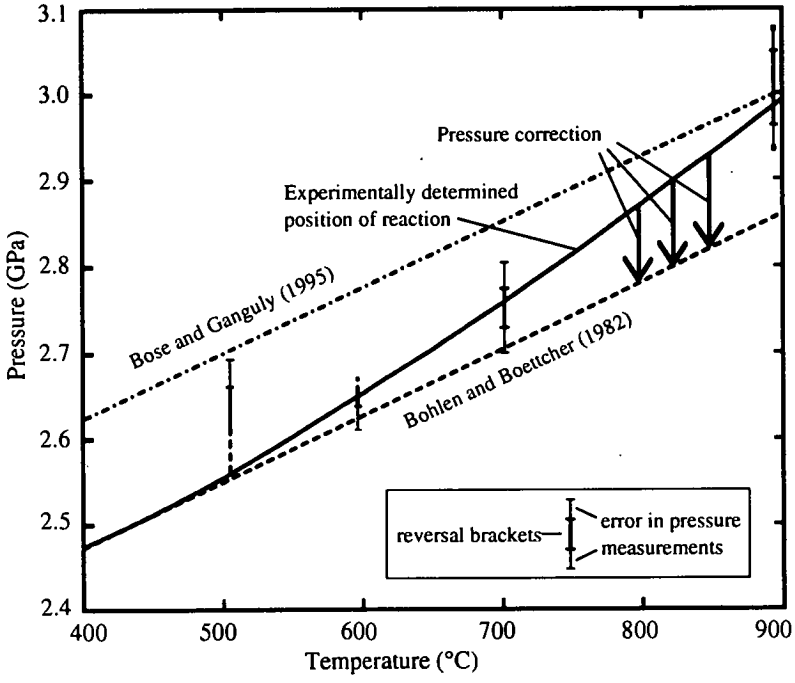

Fig. 3.4. A pressure, temperature graph to show the results of the bracketing reversal experiments for quartz-coesite. The position of the reaction measured by Bohlen and Boettcher (1982) (dashed line) is taken to be the true pressure of the reaction. Therefore the pressure correction is the difference between the best fit curve through the brackets and the true pressure.

If the pressure determined by these experiments (P_{obs}) for the reaction is then plotted against the true pressure (P_{true}) which is taken to be Bohlen and Boettcher's value (Fig. 3.5) then a function can be established to describe this pressure correction. The best fit quadratic functions were found using a curve fitting programme in the software package Cricketgraph.

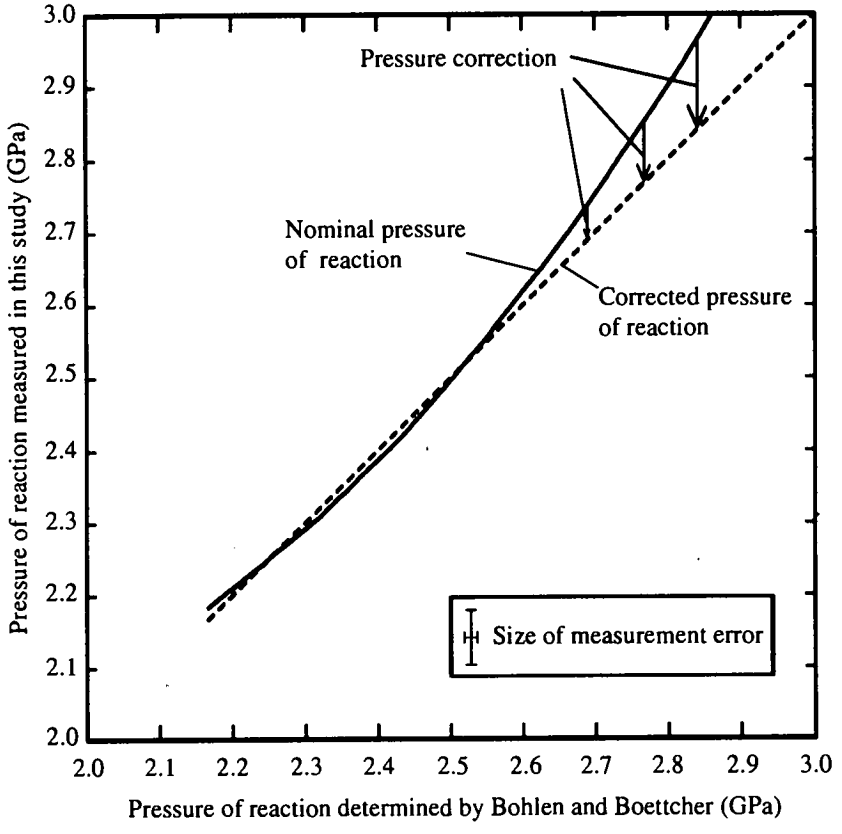

Fig. 3.5. Graph showing the observed pressure plotted against true pressure for the phase change of quartz to coesite. The observed pressure of reaction curve can be described with a quadratic equation and hence a correction function is found.

The true pressure can therefore be calculated using

$$P_{true} = -2.2429 + 2.8906P_{obs} - 0.3971P_{obs}^2$$

where: P_{true} = Corrected pressure (GPa),

P_{obs} = Pressure measured in apparatus (GPa).

Alternatively

$$P_{obs} = 3.7210 - 2.1330P_{true} + 0.6571P_{true}^2.$$

Therefore the pressure correction (P_{corr}) is

$$P_{corr} = P_{obs} - P_{true},$$

$$= 3.7210 - 3.1330P_{true} + 0.6571P_{true}^2.$$

Henceforth all pressures quoted will have been corrected with the use of this function. A few of the synthesis experiments were not performed on Press B and if the pressure correction required is due to deformation of the rig then it is quite probable that Press A would behave differently. However, since an accurate knowledge of the pressure was not so critical to these synthesis experiments the same pressure correction was used for both presses. The error in estimation of the pressure, once the correction has been applied, was within ± 0.05 GPa.

3.3.5 *Temperature measurement*

The temperature within the cell was measured with precision to ± 1°C using a $Pt/Pt_{87}Rh_{13}$ thermocouple junction referenced against a "cold junction" maintained at 0°C in an ice-water bath. The temperature was automatically controlled to within ± 2°C using a Eurotherm controller. The effect of pressure on the temperature reading was unquantifiable and presumed negligible, although this was obviously an additional uncertainty.

The most important factor to affect the temperature reading was the thermal gradient. The temperature was highest within the central part of the graphite furnace and dropped both radially and along the length of the furnace. Odling (*pers. comm*) has measured the temperature gradient within the furnace. His experiment was designed to look at the thermal gradient for a longer capsule at higher temperatures and using a talc/boron nitride cell. However the results are still of some interest. The talc cell should have made little difference and the thermal gradient in lower temperature experiments should be less than in the higher temperature experiments. His results are shown in Figure 3.6. The temperature at either end of the furnace was fixed at approximately 200°C by the flow of cooling water. Thus the inferred lines shown in Figure 3.6 would probably be lower than the true temperature over the region of the capsule as the true temperature would probably be a convex (up temperature) curve passing through these points in order to reach 200°C, without requiring more than one inflection point, by the ends of the furnace. In the lowest temperature case, at

840°C, shown in Figure 3.6 the temperature gradient over a sample 4 mm from the thermocouple bead would be ± 10°C

The effects of the thermal gradient were minimised in the experiments of this project in three ways:

i) the capsule was placed in the central part of the furnace.

ii) the length of the capsule was always less than 5 mm which should restrict the thermal gradient across it to being less than 5°C.

iii) the capsule was always loaded with the thinner crimp (the first one) at the top so that the distance between the thermocouple bead and the sample was always at a minimum.

Therefore, assuming that there was no contamination (see next section), the temperature of the sample would be within ± 10°C of the temperature reading.

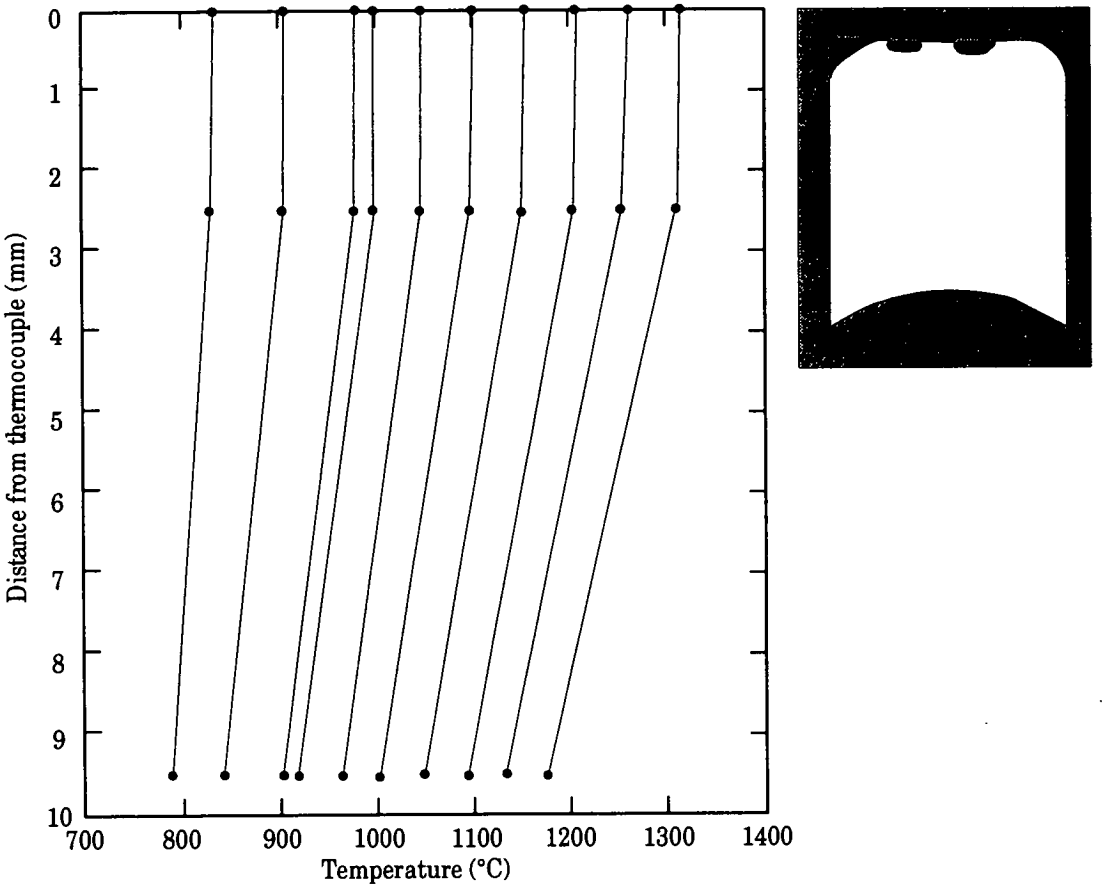

Fig. 3.6. Thermal gradients measured with a triple thermocouple in a graphite furnace within a talc/BN cell. A capsule is shown drawn to scale for comparison. Odling (*pers. comm.*)

3.3.6 *Thermocouple contamination*

During the initial synthesis runs a new batch of soft-fired pyrophyllite ($Al_4[Si_8O_{22}](OH)_4$) thermocouple holders was used. It was found in some runs (Odling, Thomas *pers. comm.*) that the temperature readings became unstable and that during an experiment the power required to maintain the same temperature reading could be increased by up to 10%. This implied that something was happening to the thermocouple that affected its accurate measurement. The most likely explanation was that as the power was increased so the true temperature of the sample rose also. On examination of the thermocouple beads, using the electron microprobe, it was found that they were becoming contaminated with iron. The source of the iron contamination was from the pyrophyllite pieces which were found to contain other phases rich in iron or titanium. This is clearly shown in Figure 3.7.

Figure 3.7 is an electron back scattered image from one of the current experiments showing the edge of the thermocouple bead (top left) and the soft fired pyrophyllite with patches very rich in iron and titanium, which was determined using an Energy Dispersive Spectrometer. In the experiments described in this work the temperature and power readings remained stable implying that contamination did not occur. When the thermocouple bead was analysed, also using Energy Dispersive spectroscopy, even where the bead seemed to be in contact with the iron rich patches (Fig. 3.7), no contamination appeared to exist. The lack of apparent contamination effects in these runs may well have been due to the lower temperature conditions of the experiments compared with those of Odling and Thomas. All of these experiments were at less than 600°C, whereas the ones performed by Odling and Thomas were at temperatures in excess of 1000°C. Above 600°C there may be some process which causes the mobilisation of iron in pyrophyllite.

The problems of thermocouple contamination were encountered during the synthesis experiments where the accuracy of the temperature readings was not so important. Therefore, although there appeared to be no discrepancies, when the reversal experiments were performed, a short sleeve of boron nitride was introduced into the cell to ensure that the temperature reading was accurate. This sleeve was used to isolate the thermocouple bead from the soft-fired pyrophyllite. However its length was restricted as boron nitride is not capable of supporting the thermocouple at experimental pressure and temperature and would allow it to shear (Odling *pers. comm.*). Thus the boron nitride sleeve was always less than 1 mm long in these experiments.

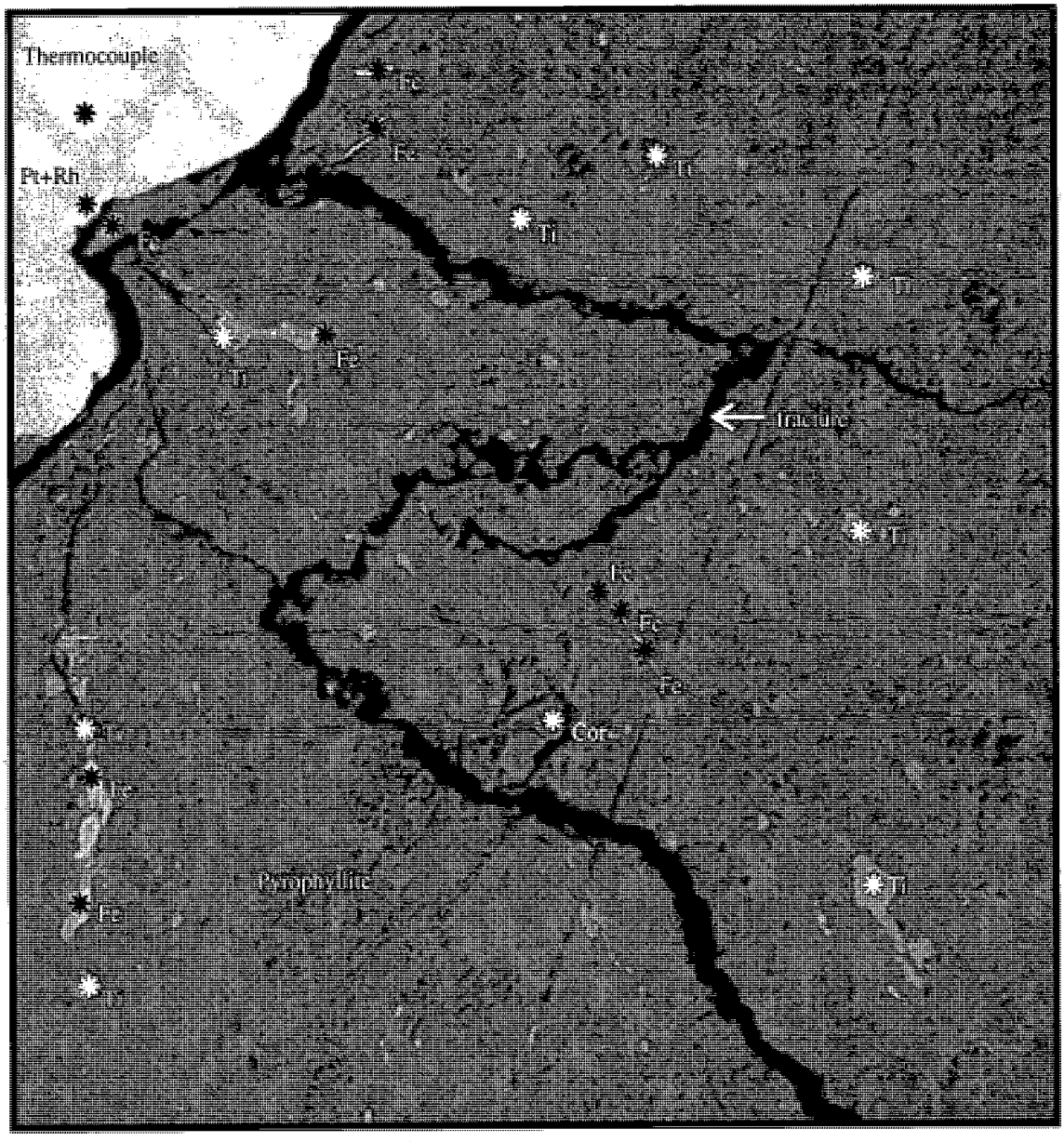

Fig. 3.7 Electron back scattered image showing the edge of the thermocouple bead and the surrounding pyrophyllite in run 48. Stars show the postions of points where the elements were analysed using Energy Dispersive Spectrometry. Parts of the pyrophyllite appear very bright and are very rich in iron or titanium. If these elements can migrate into the thermocouple bead they will contaminate it and therefore affect the temperature reading. However, in this experiment the thermocouple did not seem to have become contaminated. Even a point sampled very close to a position where an iron rich area was almost in contact with the thermocouple bead did not show any iron contamination.
(Fe = iron, Ti = titanium, Pt = platinum, Rh = rhodium and Cor = corundum from polishing)
Diameter of field of view = 1.5 mm

3.4 Low pressure experiments in the cold-seal apparatus

Synthesis of sanidine, for use as part of the mixture used in the reversal experiments, was carried out in the cold-seal apparatus at 0.1 GPa and 750°C

3.4.1 *Capsule design*

The capsules were made from 4 mm diameter and 0.07 mm wall thickness platinum tubing cut into lengths of approximately 30 to 40 mm. The first end was crimped with a three cornered crimp and welded. The capsule was filled with $KAlSi_3O_8$ gel and approximately 2-3 wt% of double deionised and distilled water. The second end was crimped and welded in the same orientation as the first end so that the length of the capsule could be lightly corrugated. This corrugation helped to prevent the capsule from buckling inside the cold-seal bomb which would have made it hard to remove later. The capsule was compressed in a water press before use.

3.4.2 *Cold-seal apparatus*

Figure 3.8 shows the design of the externally heated "Tuttle" cold seal vessels. The capsule was held at the top of the bomb by a filler rod. The pressure medium used was argon gas which was pumped into the bomb at the base through the "olive" seal. The pressure lines for the apparatus are shown in Figure 3.9 The bomb was pressurised prior to heating. The temperature of the external furnace was raised slowly by increasing the set point on a Eurotherm controller. This set the temperature in the controlling thermocouple which was connected to the inside of the furnace. Upon reaching the set temperature within the furnace, the pressure was adjusted to its correct value and both the pressure and temperature were monitored throughout the run.

To quench the experiment the power source for the furnace was switched off, the furnace raised and a jet of compressed air over the bomb was used to bring the temperature down to room temperature in approximately 10 minutes. After the temperature was lowered, the pressure was bled off and the bomb taken apart.

3.4.3 *Pressure measurement*

The pressure was measured using a factory-calibrated Heise gauge which was accurate to $\pm$ 3.0 x 10^{-3} GPa (Welch 1987).

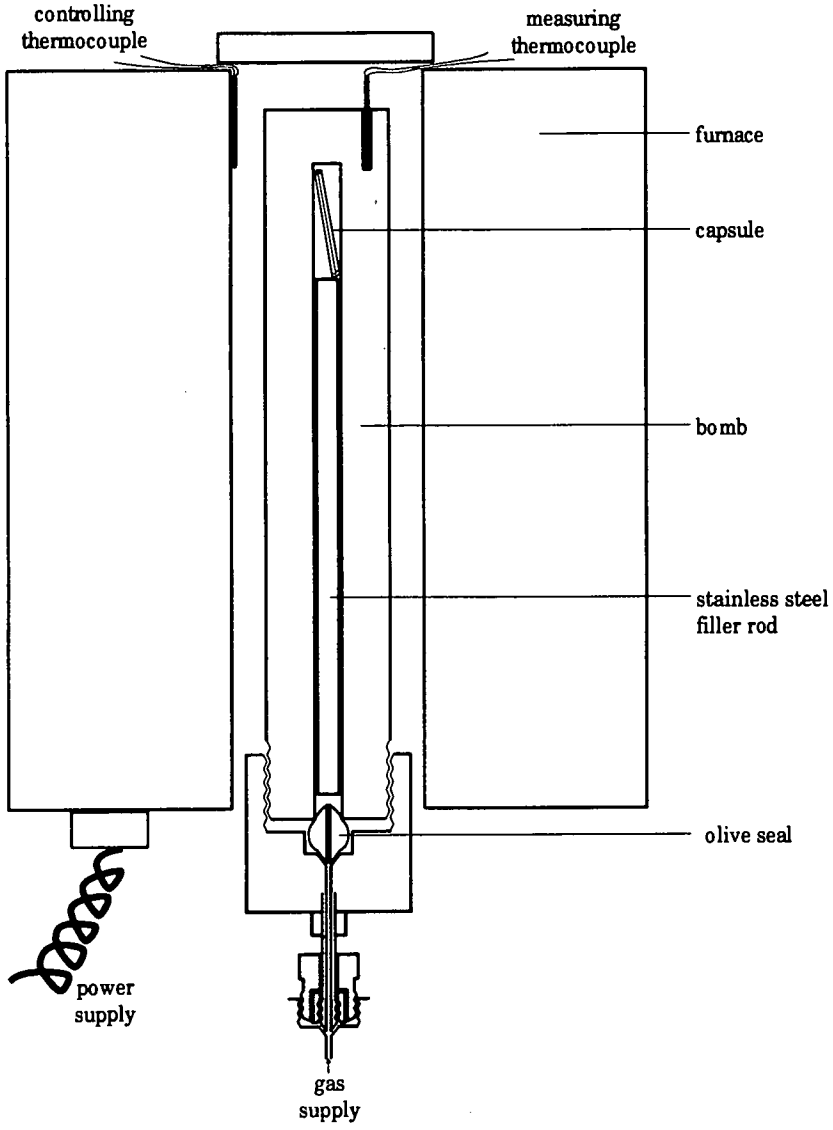

Fig. 3.8. A sketch cross section of the cold seal apparatus used for low pressure experiments. Outside diameter of furnace was approximately 250 mm.

3.4.4 *Temperature measurement*

The thermocouple within the bomb was used to take a precise reading of the temperature by comparing the e.m.f. of the measuring thermocouple with that of a standardised cadmium cell using a Pye potentiometer

The error in the temperature was taken as ± 5°C, this being a combination of the measurement accuracy of ± 3°C (Ford 1972) and the fluctuations in the temperature of the experiment of ± 2°C. The thermal gradient in the cold seal apparatus was measured by Welch (1987) (Fig. 3.10). This showed that the variation in temperature over a 30 to 40 mm capsule would be less than 5°C

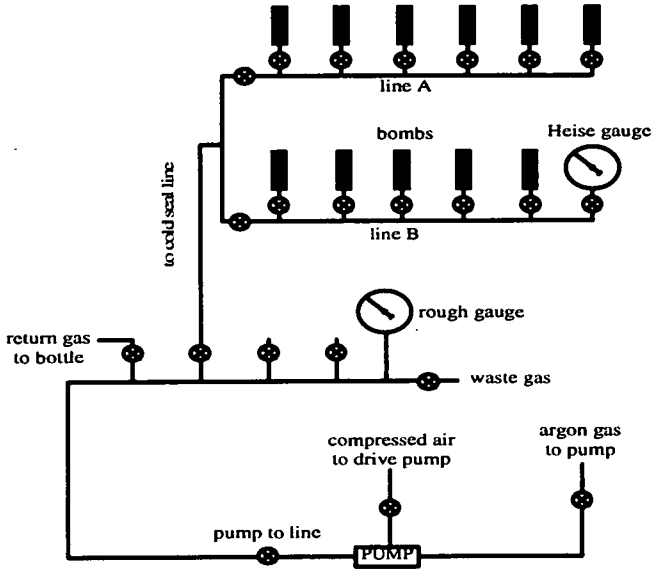

Fig. 3.9. A schematic map of the gas pressure lines used in the cold seal experiments

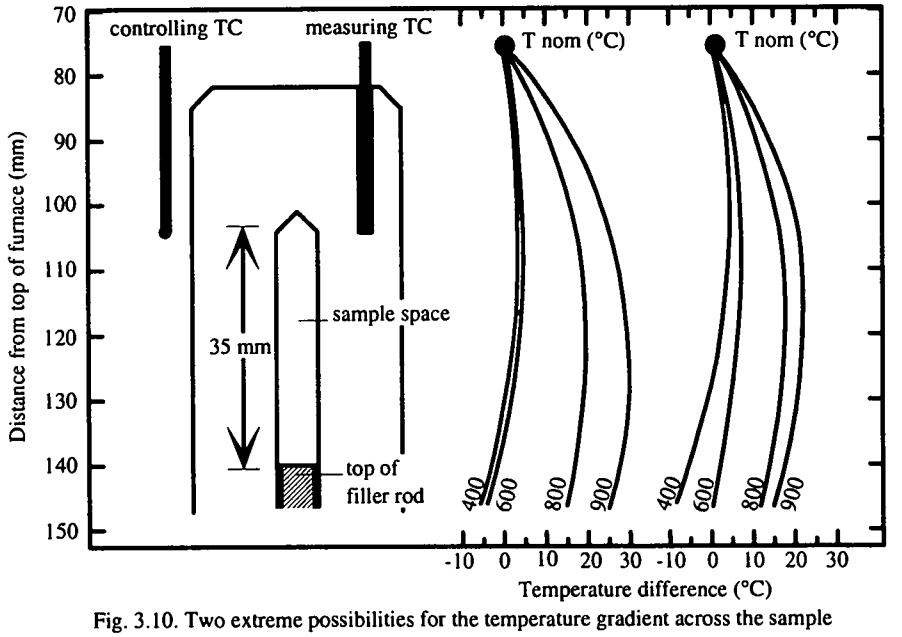

Fig. 3.10. Two extreme possibilities for the temperature gradient across the sample (redrawn from Welch (1987))

3.5 Examination of run products

3.5.1 *Test for capsule failure*

After experiments were completed the capsules were removed carefully and the changes in dimensions of all the pieces were recorded. Any adhering material was removed with a scalpel or needle. The capsule was then examined carefully for leakages and weighed. It was then pierced with a scalpel. If water escaped or if the capsule lost weight after heating to 110°C for a few hours it indicated that the capsule had remained intact throughout the experiment. The total weight loss was then noted, as this gave some indication of the direction of reaction depending on whether the amount of free water increased or decreased.

Retention of water is considered to be a reasonable indication that the capsule remained intact throughout the duration of the reaction. However, Randle (1994) showed that it is possible for a capsule to leak and reseal itself. Many of her experiments showed severe contamination with boron. This quantity of boron was thought to be too large to have just diffused through the capsule walls. However, in most of these runs the water had not escaped. Part of the problem may have been due to the capsule design used. Within that capsule was a solid olivine bucket which may have damaged the capsule during the run. The capsules used in this work were more simple with no solid inner parts

Two of the early synthesis experiments (runs 1 and 2) were tested for boron using Secondary Ion Mass Spectrometry as boron is not detectable with an electron microprobe. Neither of them showed any boron contamination. There was only a trace of boron (36 ppm) throughout both samples. This was probably a slight impurity in the starting material. In the samples of Randle (1994) the quantities of boron ranged from 100 to 100,000 ppm and the samples were therefore more strongly contaminated.

3.5.2 *Extraction and Preparation*

The capsules were opened with a scalpel and the sample scraped out. Samples were usually powdery and the piston cylinder run products were slightly grey in colour. The sample was ground under acetone in an agate mortar for about 10 minutes and a drop of acetone containing some of the sample was pipetted onto a round glass slide for mounting in the powder X-ray diffractometer.

A few crystals were also mounted on a glass slide using a suitable refractive index oil so that they could be examined optically.

3.5.3 *Identification of phases*

The phases present were examined optically but their small grain size made it difficult to identify the two main phases of sanidine and "sanidine hydrate" as they both appeared to be similar. Occasionally, in some of the slightly larger crystals, it was possible to distinguish between the hexagonal "sanidine hydrate" with straight extinction and the monoclinic/triclinic sanidine with inclined extinction. Coesite, although not as abundant, was much easier to identify owing to its high relief.

Powder X-ray diffraction was a more reliable way of identifying phases. The X-ray diffractometer was a Philips PW 1800. The scans used $CuK\alpha_1$ and $CuK\alpha_2$ radiations of wavelengths 0.154060 and 0.154439 nm with the generator set at 40 kV and 50 mA. For identification and determination of the reaction direction the scans used had a step size of 0.02° and a sample time of 3 secs over an angle range of 2 to 60°.

In order to identify the direction of reaction in a reversal experiment the powdered sanidine and "sanidine hydrate" were scanned firstly using X-ray diffraction separately. They were then mixed in an arbitrary proportion of 40.1% "sanidine hydrate" to 59.9% sanidine to form the starting material PTmix and re-scanned. Each of these scans was repeated at least 9 times with a different sample mount each time. Two of the larger peaks on the powder X-ray diffraction pattern that did not interfere with any other peaks were chosen, one representing sanidine at 27.58°2θ, and one representing "sanidine hydrate" at 33.58°2θ. An average peak height from the 9 runs was taken for each peak. After the reversal experiment the run product was also scanned using powder X-ray diffraction at least 9 times and an average of peak heights taken. If the complete reaction to either sanidine or "sanidine hydrate" had not occurred then the heights of the two peaks were compared with the heights of the peaks for the starting mixture. If a reaction had occurred then the peak height of one phase should have increased whilst the peak height of the other should have decreased. However, to be sure the reaction direction was correct, only changes in relative peak heights which indicated a change in the proportions of the phases of greater than 15% were used.

The criteria for identifying reaction direction are shown in Figure 3.11. The ratio of the heights on the powder X-ray diffraction pattern of the "sanidine hydrate" to sanidine peaks in the starting material was 1.5 ± 0.2. From this, the values for the separate components before the mix was made up and assuming that the mix involved no interaction between the two components, a series of rough curves of the

ratio of the intensity of the "sanidine hydrate" to sanidine peaks against the concentration of "sanidine hydrate" could be calculated. Therefore, a good indication of a reaction to form "sanidine hydrate" was taken to be that when the intensity of the "sanidine hydrate" peak divided by the intensity of the sanidine peak was greater than 3.1. A value of less than 0.7 implied that sanidine had been formed in preference to "sanidine hydrate". A result lying between 0.7 and 3.1 was not considered good enough to show the reaction direction. In this way the equilibrium position of the reaction could be determined.

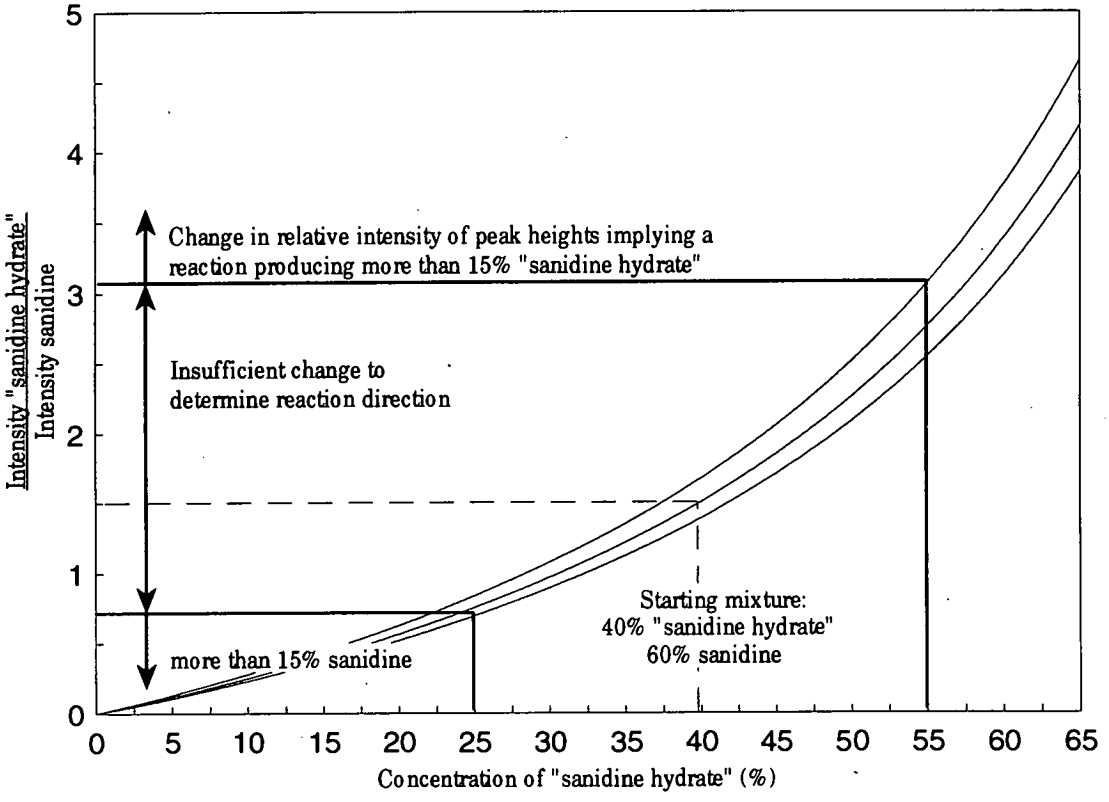

Fig. 3.11. A plot to show the criteria used for identifying reaction direction in reversal experiments. The thin curved lines are the relative peak heights calculated from the initial peak heights of the starting mixture "PTmix". The three lines represent the minimum, maximum and mean values. The starting material contained 40% of "sanidine hydrate" and the reaction direction was only considered good enough for bracketing the reaction if more than 15% of either phase was produced at the expense of the other phase. For example, a value of less than 0.7 for the ratio of peak heights implied that more than 15% of sanidine had formed in the experiment.

3.6 Infrared spectroscopy

Infrared spectroscopy can be used to investigate interatomic covalent and partly covalent bonds in minerals. These bonds have natural modes of vibration in the infrared part of the electromagnetic spectrum at wave numbers between 4000 and 200 cm^{-1}. Therefore, when infrared radiation is passed through the sample, the bonds become excited and the infrared frequencies which correspond to these different vibrations are absorbed. For a vibrational mode to be a good absorber of infrared radiation it has to undergo a change in dipole moment, i.e. a relative movement in the atomic charge centre (Braithwaite, 1990). The fundamental frequencies of particular vibrational modes depend upon the masses of the atoms and the nature of the bonds. At the detector the radiation transmitted is measured for all frequencies. Where a bond has absorbed some of the radiation an absorption peak (or transmission trough) is seen, with a frequency characteristic to that bond.

3.6.1 *The effect of infrared radiation on different "water" types*

Infrared spectroscopy is thus a useful technique for determining the speciation of "water" in minerals (Aines and Rossman 1984). "Water bearing" minerals are those which contain OH groups, some form of H_2O or other H-bearing species. There are four different states in which "water" can occur within feldspars:

(1) H_2O molecules isolated within the crystalline structure,

(2) OH groups isolated within the crystalline structure,

(3) H_2O as free surface water

(4) H_2O held within micropores as fluid inclusions

Other hydrogen defects, such as H^+ or H_3O^+, could perhaps occur but their behaviour with infrared radiation has not been documented. Section 9.1 summarises some of the defects which have been considered by previous authors to explain observations from infrared spectra These alternative hydrogen defects are not mentioned by these authors. Each of these four types produces a characteristic infrared spectrum as described below.

Figure 3.12 shows the three possible internal vibrations of a water molecule that have a frequency in the infrared region of the electromagnetic spectrum. Respectively ν_1 and ν_3 are the symmetric and asymmetric OH stretching vibrations which produce vibrations in the 3000 to 3800 cm^{-1} frequency range, with the symmetric vibration occurring at slightly lower frequencies than the asymmetric vibration. The H_2O

bending vibration, ν_2, has a frequency in the region of 1600 cm^{-1}. These fundamental frequencies produce the highest intensity peaks but the combined vibrational modes can also be used for analysis in the near infrared region above 4000 cm^{-1}. These peaks are used for identification of "water" species where there is interference with the lower frequency peaks of H_2O bending. With a large sample, for instance a single crystal, the ν_2 bending peak is often obscured by interference from vibrations in the tetrahedral framework of aluminium-oxygen and silicon-oxygen bonds.

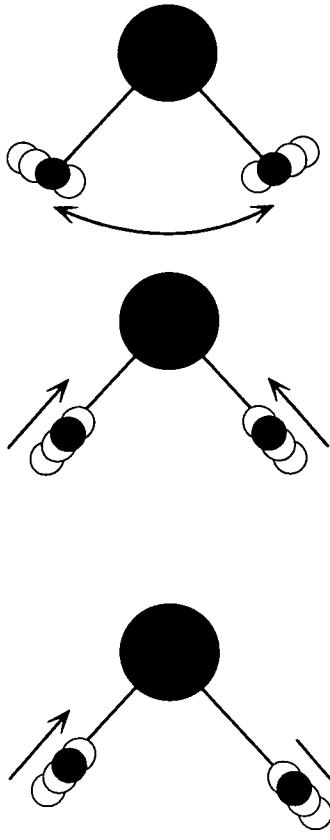

Fig. 3.12. The three possible internal modes of vibration of a water molecule which can be seen in the infrared region of the electromagnetic spectrum. Redrawn from Aines and Rossman (1984)

Hence, the four "water" types listed above have the following characteristic spectra:

(1) Those H_2O molecules that are isolated within the crystalline structure produce three sharp peaks in the infrared absorption spectra. A peak around 1600 cm^{-1} confirms the presence of H_2O molecules. The OH stretching region between 3300

and 3800 cm^{-1} contains two sharp peaks. The lower frequency peak corresponds to symmetrical OH stretching and the higher frequency peak to asymmetric OH stretching. If a single crystal is being studied the orientation of the H_2O molecule can be determined by using polarised infrared radiation. When the incident radiation is polarised in the direction of the two-fold symmetry axis of the H_2O molecule, the vibrations ν_1 and ν_2 will produce peaks. Alternatively when the incident radiation is polarised perpendicular to this two fold symmetry axis, but is still in the plane of the molecule, the vibration ν_3 will produce a peak. Figure 3.13 shows the spectrum of gypsum which contains structural H_2O

(2) Obviously OH groups cannot produce a bending vibration and this lack of a bending vibration is the primary means of distinguishing OH groups from H_2O molecules. In addition, in the OH stretching region only a single peak should occur on the infrared trace. Figure 3.13 also shows the theoretical spectrum of a phlogopite containing only structural OH.

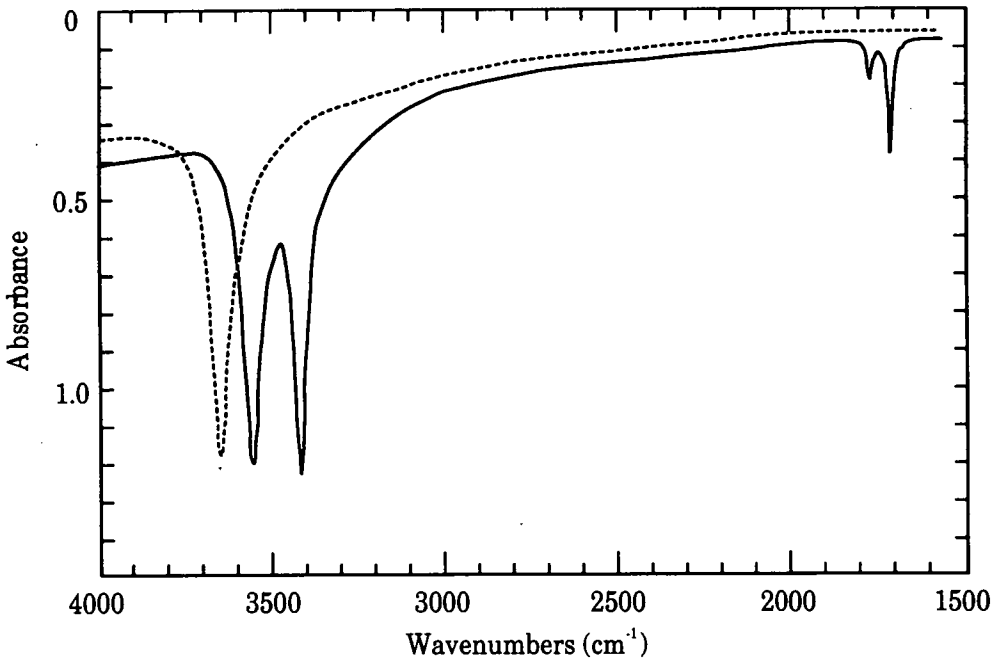

Fig. 3.13. The solid line shows the spectrum of gypsum $Ca_2SO_4.2H_2O$ (redrawn from Aines and Rossman, 1984). Gypsum contains structural H_2O and so shows three peaks in the infrared trace, two between 3400 and 3600 cm^{-1} corresponding to the two OH stretching vibrations and one at 1620 cm^{-1} as a result of the H_2O bending vibration. For comparison, a theoretical spectrum of the end member trioctahedral mica, phlogopite, is shown (dashed). Micas contain structural OH and hence only have one OH stretching peak in this part of the electromagnetic spectrum. Most natural micas have more than one peak in this region because the frequency of the OH stretching peak will vary depending upon the attraction of its nearest neighbour atom. In phlogopite the nearest neighbour is always magnesium and so only one peak will be produced.

(3) & (4) The H_2O molecules occurring either as free surface water or as groups of molecules held within a fluid inclusion should produce a bending peak in the 1600 cm^{-1} region as shown in Figure 3.14. However, unlike isolated H_2O molecules in the crystalline structure, in the OH stretching region a single broad hump is seen in the infrared spectrum. Hydrogen bonding between water molecules has the effect of broadening the two OH stretching peaks into this one hump. The lack of a modulating silicate lattice to hold the H_2O molecules allows the frequencies of the OH stretching vibrations to be displaced to lower values than is seen with structural H_2O.

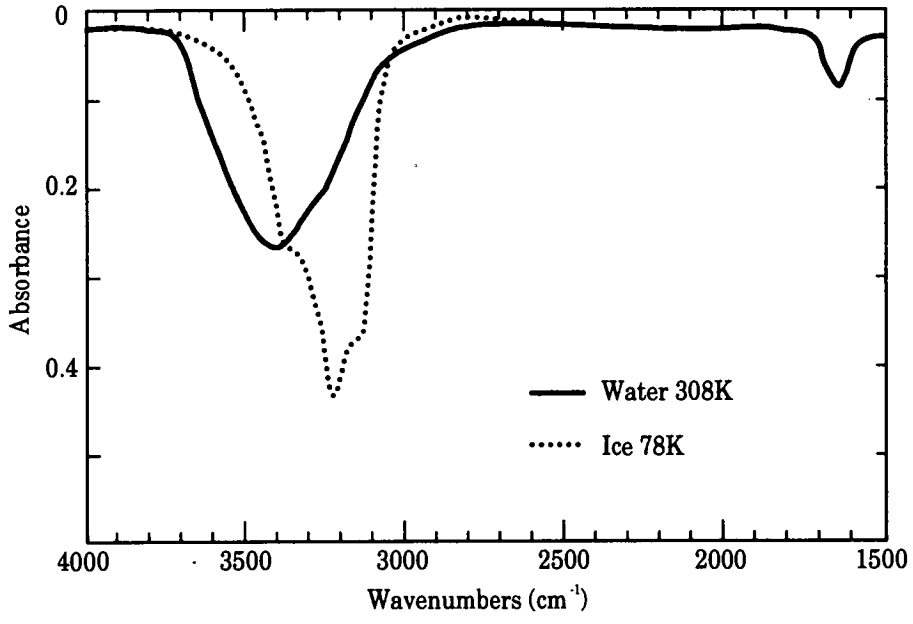

Fig. 3.14. The solid line is the infrared absorption spectrum of a thin film (1μm thick) of water held between two glass slides showing the overlapping OH stretching modes near 3400 cm^{-1} and the bending mode near 1630 cm^{-1}. For comparison the spectrum of the same thickness of ice at 78K is shown which contains an extra peak near 3200 cm^{-1}. Redrawn from Aines and Rossman (1985)

Liquid water can be further distinguished from crystallographic water by cooling the sample to 78K with liquid nitrogen. Fig. 3.14 shows the difference in the spectra between water and ice. Ice produces an extra peak at 3200 cm^{-1} and so the presence of this additional peak, when the sample is frozen, shows that the sample contains free water unconnected to any of the surrounding structure. At 78K water in fluid inclusions should show an extra peak at 3200 cm^{-1} whereas structural "water" should not. However, it is possible to get large variations in the size of fluid inclusions with the smallest of these containing only a few molecules. If an inclusion contains fewer than of the order of 1000 molecules, molecular interactions may prevent the formation of ice even at the temperature of liquid nitrogen (78K).

3.6.2 *Methods of infrared spectroscopy*

The instrument bench used was a Nicolet 510P Fourier Transform Infrared (FTIR) spectrophotometer with a Nicolet Nicplan microscope attachment. A helium/neon laser was used which measured between 5800 cm^{-1} and 200 cm^{-1} with a KBr beam splitter and a CsI detector. Each spectrum was measured using 128 scans at a resolution of 2 cm^{-1}. Three methods of infrared spectroscopy were used at different stages in the research. The three methods used were of transmission through a potassium bromide disc, diffuse reflectance off the surface of a crystal or powder and transmission through a single crystal with the aid of the Nicplan microscope.

a) Potassium bromide disc method

Powdered samples were mixed with potassium bromide (KBr) and pressed into a disc. Potassium bromide was used as it is transparent to infrared radiation down to 400 cm^{-1}. One problem with potassium bromide which is particularly inconvenient for studies of water speciation is that it is hygroscopic. Therefore during sample preparation every precaution was taken to minimise the amount of water absorbed by the potassium bromide. The sample, potassium bromide and pressing die were kept in a warmed desiccator and only taken out for as brief a period as possible in order to mix the sample with the potassium bromide and then to press the disc. The samples and the reference blank sample were made using a standard method which involved equivalent durations of exposure to atmospheric water.

The bench was purged with clean dry carbon dioxide for approximately five minutes to remove the effects of atmospheric water. A reference blank sample containing only potassium bromide was prepared and the spectrum of every sample had this standard spectrum automatically subtracted from it. This procedure removed any effects of the potassium bromide background and also minimised the adsorbed surface water component of the hygroscopic potassium bromide disc. Frequently the automatic subtraction of the background did not remove all of the carbon dioxide peaks in the 2500 to 2300 cm^{-1} range. With the synthetic samples there should be very little carbon dioxide present and, if the background was removed manually until these peaks disappeared, it generally appeared to reduce the noise level of the spectrum.

b) Diffuse reflectance method

This method measures the radiation reflected off the surface of the samples. Samples can be a single crystal, a number of small crystals or a powder. The samples are placed in a cup held within a system of mirrors which is fitted into the sample chamber within the instrument bench. The background is measured with no sample in the chamber and again this background reading is removed automatically from the sample spectra. The instrument bench was purged for five minutes before each measurement in order to reduce the effect of atmospheric water and carbon dioxide.

This method is less commonly used than either of the other two methods, but for powdered samples it should avoid the slight problem, found with the potassium bromide disc method, of the hygroscopic nature of the potassium bromide, however, the powdered sample may also adsorb some water. For synthetic samples, which were powdered crystals, the microscopic method could not be used and therefore this method was the only alternative to the potassium bromide disc method. The other advantage to this method, when studying powders, is that it should take an average spectrum over a large number of randomly oriented crystals. Spectra measured with the microscope vary depending on the orientation of the crystal through which the radiation is transmitted. The diffuse reflectance method was therefore used when trying to calculate the relative quantities of water in natural samples as well as in synthetic ones. This calculation was attempted by normalising the area of the OH stretching peaks, when plotted as absorbance, to a peak produced by vibrations of the silicate framework. The method produced different results when the areas were calculated using the reflectance plots, as illustrated in the figures of this work. Previous authors use the area measured using an absorbance method on a microscope and so the absorbance values are quoted here. The method did not appear to be very successful perhaps because the reference peaks were often partly below the linear range of the spectrum (Brian Jackson, *pers comm.*). The only drawback to this diffuse reflectance method is that it tends to produce peaks at 3840 and 3750 cm^{-1} and in the region of 1600 to 1650 cm^{-1}, which are not seen with any of the methods and are therefore presumably due to interference of some sort.

c) Infrared microscopy

Natural samples of feldspar can be analysed using the Nicplan infrared microscope. Crystals have to be approximately 50 μm in size or more, but thin enough that they are transparent to infrared radiation. Crystals can be up to 2 mm or more in diameter

if they are relatively clear. Samples need to be cut into thin enough slabs so that crystals can be found that fill the entire thickness of the slab. Cutting such a thin slab is not easy and therefore larger crystals are easier to study. The polish on both surfaces does not need to be too perfect as this reduces the interference of reflected radiation.

In this study the infrared radiation was passed through an aperture of 1 mm in diameter. The beam is focused onto the sample using a condenser which results in a sampling area of approximately 0.18 mm in diameter. The effects of variations in the water contents of the atmosphere were minimised by covering the sample with a hood purged with dry nitrogen. In addition a background spectrum was measured with no sample on the stage and then automatically subtracted from each of the sample spectra.

3.7 Thermogravimetric analysis

Thermogravimetric analysis is one method that can be used to accurately determine the percentage of a volatile component within a sample. By this method the sample is heated up at a constant rate and the change in weight is measured in comparison to a standard. The standard should be of a substance which does not change in weight over the entire range of temperature measurement. The graph of results produced may show several phases of weight loss which may, in turn, be interpreted as different types of volatile loss. The thermogravimetric method of analysis is particularly useful for very small aliquots of sample, and so it was used in this instance as the run product of the piston cylinder reversal experiments usually only produced in the order of approximately 25 mg of sample.

3.7.1 *Thermogravimetric techniques*

The thermogravimetric analysis machine used was a Thermal Analyst 2000, STD 2690 Simultaneous DTA-DTG (based at the University of St Andrews Chemistry Department). The balance was tared with an empty alundum crucible prior to each run. An alumina (Al_2O_3) reference sample of a similar weight to the sample to be measured, i.e. around 10 mg, was placed on an adjacent balance within the machine. This was used to compare with the sample throughout the run as pure alumina should not change in weight on heating. A finely ground sample of "sanidine hydrate" of

approximately 10 mg was placed into the alundum crucible. The equipment was then programmed to run up to the desired temperature whilst the weight change was recorded throughout. The sample chamber was purged with dry oxygen during the run to remove any atmospheric water. The programme used involved holding the sample at room temperature for 10 minutes to allow the balance to stabilise before steadily heating the sample at a fixed rate of 10°C per minute up to the desired temperature. Once this temperature was achieved it was held steadily for a further 10 minutes before cooling to room temperature again with the use of a fan. The initial samples were run up to a temperature of 1200°C. However, once it had been shown that there were no significant weight variations above 800°C the samples were only run up to this temperature. The remains of samples left after thermogravimetric analysis were kept for further investigation (see Sections 5.2 and 6.3).

After a run was completed, graphs were then plotted to show percentage weight loss and the first derivative of weight loss with respect to temperature (i.e. %loss/°C) against temperature.

3.7.2 *Errors in thermogravimetric results*

The thermogravimetric results seemed to have variations which were far larger (see Section 5.3) than the measurement errors on the equipment should have been and yet did not show any systematic trends with pressure, temperature or the duration of the experiment. These significant variations were probably due to the nature of the samples themselves and not the measuring equipment and yet were unlikely to reflect true variations in the percentage water content of the "sanidine hydrate" itself. The weight loss in the sample is measured as a percentage weight loss and therefore a discrepancy could arise if there was any contamination of the "sanidine hydrate" or sanidine with any other phases.

In these samples there were three possible sources of contamination which could account for these difficulties.

(1) Firstly coesite was a by-product in all of the high pressure experiments. The cause and extent of this effect was discussed in Section 4.4. Two of the experiments were calibrated approximately for coesite by investigating the difference in peak heights, using powder X-ray diffraction, both before and after the addition of a known amount of coesite. This showed that the quantity of coesite was approximately 3 wt% or less. Samples which were not synthesised in the coesite stability field probably would have instead contained similar amounts

of quartz. However, these samples were invariably those ones which contained sanidine because the quartz-coesite and the sanidine+water-"sanidine hydrate" reactions were nearly coincident. Because of interference of the quartz and sanidine peaks in the powder X-ray diffraction pattern it was impossible to identify the presence of a minor quantity of quartz. So, if there was some quartz contamination, its quantity was presumed to be of a similar order of magnitude to the coesite and therefore small enough to be ignored.

(2) A second difficulty arose when the "sanidine hydrate" or sanidine was not entirely crystalline. This situation was hard to identify and quantify. The only way to observe amorphous material was by inspection under an optical microscope where the amorphous material should appear isotropic. But in this case the crystal size of the samples was less than a micron in diameter and so the birefringence colours of the crystalline material were very low even in orientations parallel to the optic axis. In consequence the difference between isotropic material and anisotropic material was not always apparent. Since a large proportion of each sample was definitely crystalline, it was presumed that any remaining material was crystalline but with birefringence colours too low to identify. There was no positive evidence for the existence of any amorphous material and so it was taken that none was present.

(3) The third source of contamination was potentially more serious. Experiments in the piston cylinder apparatus required samples to be sealed in platinum capsules. The pressures for these runs were so high that by the end of the experiments the capsules had shortened considerably resulting in thickening of the platinum walls of the capsules by folding. This, coupled with the extremely small size of the capsules (3mm by 3mm), made the extraction of the run products difficult. Some degree of force was required to open the capsule and remove the contents. This invariably caused small flakes of platinum and occasionally pieces of scalpel blade to contaminate the sample. Where possible these pieces were carefully removed under the microscope with a dampened needle, although, inevitably there were always some fragments remaining. The high density of platinum compared to that of "sanidine hydrate" means that even a small amount of platinum can produce a high percentage weight of the metal within the sample.

The occurrence of platinum contamination was not encountered by Graham et al. (1992) as their experiments were performed in gas bombs. The capsules produced for their experiments were larger, containing much more material, and were not so

severely compressed during the experiment as the capsules removed from the piston cylinder apparatus. Thus the samples would be more easily extracted from their capsules.

Atomic absorption (see next section) was used to attempt to quantify the amount of platinum in some of these samples produced in the piston cylinder. If successful this would make it possible to recalculate the thermogravimetric data to see if the platinum contamination was the cause of the discrepancies in the data.

The three possible impurities discussed should have the same resultant effect on the thermogravimetric results. All three contaminants (coesite, non-crystalline material and platinum) are anhydrous, so when they are added to "sanidine hydrate" they would make the percentage weight loss measured appear lower than if the sample was entirely of "sanidine hydrate". Although some attempt was made to determine the effect of the concentration of platinum on the sample, the overall effect of these impurities could not be entirely quantified. The degree of contamination varied between samples and hence no correction could be made. Therefore the percentage weight loss measured is a minimum figure and the true value could be higher.

3.8 Atomic absorption

The samples remaining after thermogravimetric analysis were analysed, using atomic absorption, to determine the quantity of platinum within them. The thermogravimetric results could then be recalculated to remove the effect of platinum contamination. Atomic absorption is a technique employing the excitation of atoms. Changing the energy levels of atoms requires a frequency in the ultraviolet or visible parts of the electromagnetic spectrum. Hence when a sample is placed in the path of ultraviolet or visible radiation, frequencies are absorbed which depend on the type of atoms present and the difference in the energy levels of the excited and normal states. The samples must be decomposed and converted into the gaseous elementary particles of atoms or ions prior to analysis so that the atomic energy levels are not affected by any bonding effects.

The wavelength at which platinum is best excited is at 265.9nm and therefore the source of radiation was set to this wavelength. A solution of the sample dissolved in dilute acid was sprayed into a chamber containing an air-acetylene flame which should convert the dissolved sample into a gas. The quantity of platinum in the

sample was approximately determined by comparing its absorption with that of five standard solutions of differing concentrations. However, it was found that the platinum absorption peak was depressed by interference. There are two types of interference which could cause this. The possibility of the depression of the absorbance peak by interference with a species produced by combustion of the flame was removed by switching the fuel from air-acetylene to hydrogen. This had no effect on the platinum absorption peak height. Therefore the depression of the platinum frequency peak must have been caused by chemical interference with other atoms in the sample. To overcome this problem a "standard additions" method was used. Four aliquot parts of the sample were taken and varying amounts of the platinum standard were added to each. This required an estimation of the quantity of platinum (as determined before) so as to keep the total concentration of platinum in each addition well within the linear portion of the calibration curve at approximately 0 - 40 ppm. In addition a quantity of lanthanum solution was added as this had the effect of reducing the depression of the platinum absorbance peak. This effect may be due to the lanthanum reacting preferentially with the species that was interfering with the platinum and hence preventing it from causing the platinum peak to be depressed. The platinum peak was then larger and so easier to detect at very small concentrations.

If the relationship between absorbance and concentration is linear

$$C_x = C_s \frac{A_x}{(A_s - A_x)}$$

where C_S = concentration of platinum
A_S = absorbance of platinum
C_X = concentration of platinum in sample
A_X = absorbance of platinum in sample

Therefore, if A_s is plotted against C_s, the resulting straight line can be extrapolated to $A_s = 0$ where $C_x = -C_s$, and hence the concentration of the platinum in the sample can be determined.

3.8.1 *Sample preparation and techniques used in atomic absorption*

The entire sample remaining from thermogravimetric analysis (approximately 0.009 g) was dissolved in 3 ml of aqua regia. The platinum dissolved slowly and so it was necessary to maintain the temperature near boiling for some two hours in a covered beaker to ensure that dissolution was complete. The excess acid was removed by

evaporating to dryness on the steam bath. The resulting residue was dissolved in 0.25 ml of HCl and then diluted to 25 ml.

A standard concentrate was prepared by dissolving 0.22006 g of platinum in 8 ml of hot aqua regia. Some of the platinum remained undissolved and this was filtered off and weighed. This left 0.21698 g of platinum in solution. The solution was diluted to 200 ml to give a standard 1084.9 ppm platinum solution. This, in turn, was diluted to produce five working standards of between 0 and 100 ppm platinum with HCl added to make the concentration of HCl in each standard similar to that of the sample. Any aqua regia in the aliquots of the concentrated standard was ignored as it was relatively low at a maximum of 1/8 ml.

These five standards and a blank were then run in a SpectAA atomic absorption spectrometer in order to draw a graph of absorbance against concentration for the platinum frequency being measured. The plot was near linear in the 0 to 40 ppm range of platinum concentration. The absorbance for a sample was then compared to this graph in order to estimate the amount of platinum in the sample. Unfortunately the interference effects, as outlined above, reduced the platinum absorbance and so made the quantity of platinum appear less than its true value. Thus it was necessary to recalculate the quantity of platinum using a method of standard additions.

In order to prepare the standard additions solutions, four 4 ml portions of the sample solution were pipetted out into separate containers. To one aliquot part of sample 0.05 ml of 1085 ppm standard solution was added. To the next aliquot part 0.075 ml of 1085 ppm standard solution was added and to the third 0.1 ml of 1085 ppm standard solution. No standard was added to the fourth aliquot part. The different volumes of these solutions were all diluted to 11.1 ml. Thereafter 3 ml of 5% lanthanum 25% HCl solution were added to the four solutions. A blank was also made up with 11.1 ml of de-ionised water and 3 ml of the 5% lanthanum 25% HCl solution. The concentration of platinum in all of these samples was well within the linear portion of the calibration curve. Dilution of the aliquot parts was kept as low as possible as the concentration of platinum was low. No attempt was made to balance the concentration of HCl in all the solutions but this did not seem to make a difference, as a linear calibration on a graph of absorbance against concentration was nevertheless obtained.

Chapter 4

Phase equilibrium studies

4.1 Introduction

In order to determine the equilibrium position of the reaction

$$KAlSi_3O_8 + nH_2O = KAlSi_3O_8.nH_2O$$
$$\text{sanidine} + \text{water} = \text{"sanidine hydrate"}$$

reversal experiments were performed on a mixture of sanidine and the hydrate phase "sanidine hydrate" ($KAlSi_3O_8.nH_2O$). This chapter describes the synthesis of the starting materials, the reversal experiments and synthesis of "sanidine hydrate" and sanidine for use in further investigations described in subsequent chapters. During the course of these experiments it was found that coesite was a minor component of all run products at pressures in the coesite stability field. The quantity of coesite was roughly calibrated in some runs in order to establish the severity of the problem. The metastable behaviour of "sanidine hydrate" may explain any discrepancy between the reversal data found here and Seki and Kennedy's (1964a) synthesis results.

4.2 Starting materials

Sanidine was synthesised, as described in Section 3.4, in the cold seal apparatus at 0.1 GPa and 750°C from a gel of potassium feldspar ($KAlSi_3O_8$) composition. This gel was kindly supplied by Dr D.L. Hamilton of the University of Manchester. A summary of these synthesis experiments is given in Table 4.1.

Table 4.1. Synthesis of sanidine for use in reversal experiments

Run	P	T	H_2O	Length	Type	Starting	Results***
	GPa	°C	wt %	hours	*	materials**	
29	0.100	750	3.01	144	cs	DLH gel	san - only one tiny extra peak
30	0.100	750	2.94	144	cs	DLH gel	san only
37	0.100	750	3.8	240	cs	DLH gel	san only
38	0.100	750	3.9	240	cs	DLH gel	san only
39	0.100	750	3.7	240	cs	DLH gel	san only

Notes: * cs = cold seal apparatus
** DLH gel = gel donated by DL Hamilton of the University of Manchester
*** san = sanidine

"Sanidine hydrate" was synthesised from this same gel, donated by Dr D.L. Hamilton, at 3.0 GPa and 550°C in the piston cylinder apparatus as described in Section 3.3. The experimental conditions for the synthesis of "sanidine hydrate" and the results of these experiments are summarised in Table 4.2. The occurrence of coesite is discussed in Section 4.4.

Run products of both sanidine and "sanidine hydrate" were characterised using X-ray diffraction. Both minerals showed no extraneous peaks when their patterns were compared with those taken from the Joint Committee of Powder Diffraction Standards measured by Scheel (1971) for sanidine and Seki and Kennedy for "sanidine hydrate". The composition of the minerals could not be ascertained as the grain size was too small for microprobe analysis. Identification of the crystals optically was not possible also because of the small grain size.

Table 4.2. Synthesis of "sanidine hydrate" for use in reversal experiments

Run	P	T	H_2O	Length	Type	Starting	Results***
	GPa	°C	wt %	hours	*	materials**	
31	2.867	550	8.88	26	pc	DLH gel	SH + coes only - (< 3% coes)
33	2.949	650	6.98	25	pc	DLH gel	SH + coes only
34	2.867	550	7.63	51	pc	DLH gel	SH + coes only
35	2.879	550	7.7	44	pc	DLH gel	SH + coes
40	2.855	550	7.5	39.5	pc	DLH gel	SH + coes + trace of musc
41	2.849	550	6.68	26	pc	DLH gel	SH + coes + trace of musc
48	2.891	550	6.33	26	pc	DLH gel	SH + traces of coes and ?musc

Notes: * pc = piston cylinder apparatus
** DLH gel = gel donated by DL Hamilton of the University of Manchester
*** SH = "sanidine hydrate", coes = coesite, musc = muscovite

A typical X-ray diffraction trace of "sanidine hydrate" is shown in Figure 6.2. These phases were difficult to identify optically in experimental run products as their grain size was too small. It was even difficult to distinguish crystalline material from amorphous material as the birefringence was so low. It was sometimes possible to identify traces of coesite in the run products as a result of its high relief. Attempts at checking the composition of "sanidine hydrate" using the electron microprobe were unsuccessful, again as a result of the extremely small grain size. The electron microprobe did show the aluminium to silicon ratio to be correct, but the quantities of potassium were lower than expected, perhaps as a result of the mobilisation of the

potassium ions by the electron beam. The absolute values obtained by the electron microprobe were not useful as the high concentrations of water caused low total counts and hence the correction functions did not work properly.

Once the sanidine and the "sanidine hydrate" had been synthesised from Dr D.L. Hamilton's gel, they were carefully weighed and mixed together in the proportions 40.1% "sanidine hydrate" to 59.9% sanidine. This mixture was referred to as "PTmix". The proportions of sanidine and "sanidine hydrate" used in making the mixture "PTmix" from all of the different synthesis experiments is summarised in Table 4.3.

Table 4.3. Weights of sanidine and "sanidine hydrate" used in the manufacture of "PTmix", the starting material used for all reversal experiments

"sanidine hydrate"		sanidine	
Run no.	weight (g)	Run no.	weight (g)
31	0.02209	29	0.04408
33	0.031485	30	0.04369
34	0.03168	37	0.070615
35	0.028275	38	0.063495
40	0.02783	39	0.088935
41	0.03217		
48	0.03418		
Total	0.20771	Total	0.310815
Total after XRD	0.20638	Total after XRD	0.307956
Proportion	40.1%	Proportion	59.9%
Total weight of mix (g)		0.514336	
Weight remaining after XRD (g)		0.51080	

4.3 Reversal experiments

In order to find the equilibrium position of the reaction between sanidine and "sanidine hydrate", reversal experiments were performed at a variety of pressures and temperatures on the mixture "PTmix". Reaction directions were determined, as described in Section 3.5, by comparing the peak heights of sanidine and " sanidine hydrate", in a powder X-ray diffraction pattern, both before and after the experiment. This gave an approximate percentage of "sanidine hydrate" in the run product. Only reactions which produced more than 15% of either sanidine or "sanidine hydrate" were considered good enough indicators of reaction direction to show where the position of the equilibrium reaction was. The results of the reversal experiments are summarised in Table 4.4.

Table 4.4. Reversal experiments on the reaction between sanidine and water to form "sanidine hydrate"

Run	P	T	H_2O	Length	Type	Starting	Results***
	GPa	°C	wt %	hours	*	materials**	
49	2.500	550	5.4	24	pcR	PTmix	san but <10% -coes peaks gone
50	2.855	550	5.88	24.5	pcR	PTmix	only SH with coes
51	2.000	550	6.36	24	pcR	PTmix	san only no SH or coes
52	2.667	550	6.09	25	pcR	PTmix	≈75% SH but still some san + coes
53	2.300	550	6.43	24	pcR	PTmix	san only no SH or coes
54	2.400	550	6.26	24.5	pcR	PTmix	≈20 % SH = mostly san - no coes
55	2.590	550	7.05	24.5	pcR	PTmix	≈60 % SH but still some san + coes
56	2.855	650	6.28	24	pcR	PTmix	SH + coes only
57	2.500	650	6.35	24.5	pcR	PTmix	san only - no coesite
58	2.667	650	6.15	42	pcR	PTmix	san only - poss. slight trace of coes
59	2.737	650	6.22	24	pcR	PTmix	≈90% SH but still some san + coes
60	2.350	450	6.36	168	pcR	PTmix	≈10% SH - mostly san - no coes
61	2.721	680	6.67	20	pcR	PTmix	all SH - coesite present
62	2.696	680	6.38	24	pcR	PTmix	mostly san but traces of SH + coes
63	2.450	450	6.67	144	pcR	PTmix	v. slight shift to SH -trace of coes
65	2.500	550	6.9	63	pcR	PTmix	≈ 20% SH - mostly san - no coes
68	2.500	450	9.1	168	pcR	PTmix+qtz/coes	≈ 55% SH but still some san + coes

Notes: * pc = piston cylinder apparatus, R = reversal experiment
** PTmix = mixture of 40.1% "sanidine hydrate" and 59.9% sanidine
*** SH = "sanidine hydrate", san = sanidine, coes = coesite

These experimental results showed the equilibrium position of the reaction for a specific temperature to be restricted to lying between four reasonably tight pressure brackets. The equilibrium reaction lay between 2.350 GPa and 2.500 GPa at 450°C, 2.400 GPa and 2.590 GPa at 550°C, 2.667 GPa and 2.737 GPa at 650°C and between 2.696 GPa and 2.721 GPa at 680°C. The brackets at lower temperatures were much broader due to the poorer kinetics of the reaction under these conditions. The duration of the experiments at 450°C had to be increased substantially to obtain a reaction. The results of these experiments are plotted in Figure 4.1

If the reaction appears linear when plotted on a pressure versus temperature graph it must lie in a position similar to the thick dashed line shown in Figure 4.1. The two thick solid lines show the limiting positions between which the reaction must occur. However, it is possible that the change in reaction position with pressure and temperature is not linear. If the water content of the "sanidine hydrate" varied with pressure and temperature then the reaction stoichiometry and the composition of the "sanidine hydrate" could change along the equilibrium reaction and the reaction surface in the system sanidine - "sanidine hydrate" - water would not be planar, resulting in a curved line on a pressure, temperature graph. This was found to occur in cymrite by Graham et al. (1992) (see section 2.3). Therefore, in order to calculate the curvature of the sanidine to "sanidine hydrate" reaction on the pressure-temperature graph, the variation of the water content with pressure and temperature of synthesis needed to be determined. This was attempted using thermogravimetric analysis as described in Section 5.3, where samples of "sanidine hydrate" were slowly heated to measure the variation of percentage weight loss with temperature. This gave an indication of the quantity of H_2O in the crystal structure although the results were not good enough to show how this quantity varied with pressure and temperature (see Section 5.3.1). Therefore the curvature of the reaction, if any, on a pressure-temperature graph could not be calculated.

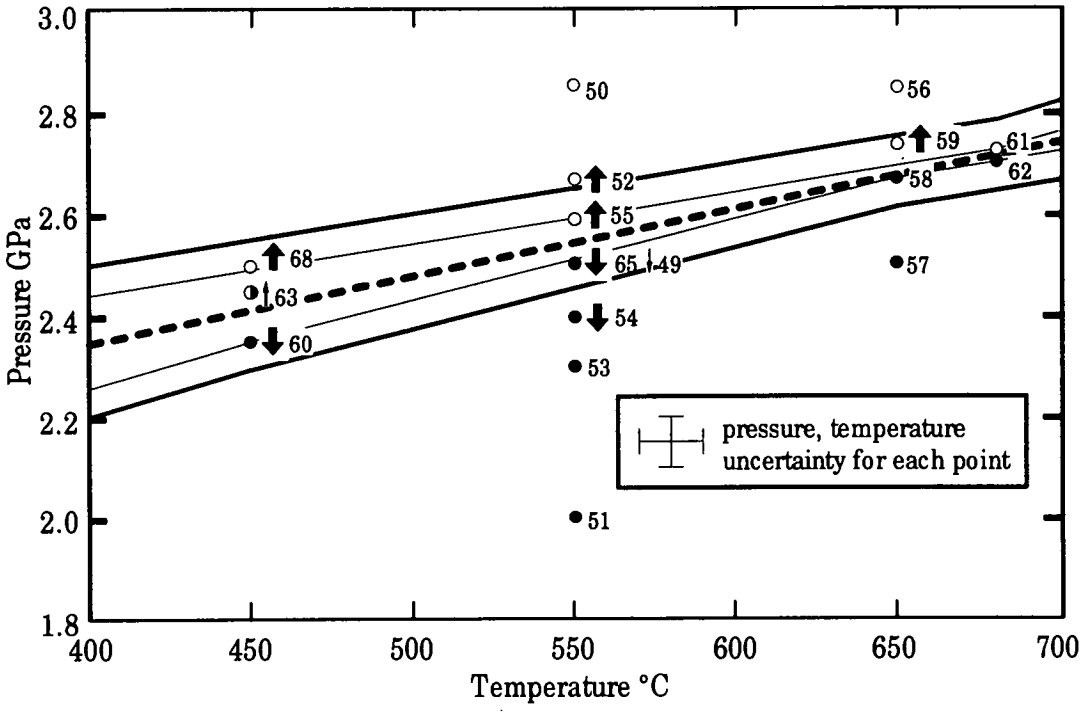

Fig. 4.1. Results of the reversal experiments on the reaction between sanidine and water to form "sanidine hydrate". The numbers refer to the run numbers as given in Table 4.3. The large arrows show the reaction direction when the reaction was not complete. The small arrows show when the reaction produced less than 15% of sanidine or "sanidine hydrate" and was considered insufficient to determine the reaction direction. The reaction must lie in a position between the two solid lines. A possible example of the position is shown by the heavy dashed line.

4.4 The coesite problem

As can be seen in Tables 4.2 and 4.4, all of the high-pressure experiments that were at a high enough pressure formed coesite in small quantities in addition to the other phases present. This could have serious implications affecting the reversal results. It is also possible that quartz was a by-product in some of the lower pressure experiments. However, quartz would not be apparent in such small quantities in a powder X-ray diffraction pattern, when it is in the presence of sanidine, because all of the quartz peaks would be hidden by larger sanidine peaks. The quartz-coesite boundary is almost coincident with the sanidine-"sanidine hydrate" reaction and therefore coesite was only ever found in the presence of "sanidine hydrate". This would imply that quartz was actually present in those runs which produced sanidine but the quartz could not be observed.

In order to establish the severity of this problem of the appearance of coesite in the higher pressure experiments, the quantity of the coesite in two of the run products

(runs 14 and 31) was measured approximately. This was accomplished by adding a small amount (< 5%) of a known weight of coesite to the run product. This should increase the size of the coesite peak in the powder X-ray diffraction pattern. If it is assumed that the size of the coesite peak is roughly proportional to the quantity of coesite in the sample, by examining the X-ray diffraction pattern, both before and after the addition of coesite, the increase in the size of the coesite peak should give an indication of the quantity of coesite in the original run product. In both of the experiments that were calibrated for coesite, the quantity of coesite was found to be small (see Table 4.5). The X-ray diffraction traces of these two experiments showed similarly sized coesite peaks to all of the other experiments and so it was presumed that the quantity of coesite was also small in all of the experiments.

Table 4.5. Experiments to investigate the coesite found in the higher pressure experiments

Run	P	T	H_2O	Length	Type	Starting	Results***
	GPa	°C	wt %	hours	*	materials**	
13	2.913	550	3.7	68	pc	P3K100 us	san +SH + trace of coes
14	2.919	550	8.03	69.5	pc	P3K100	SH + trace of coes (1.5%)
20	0.100	800	2.01	48	cs	P3K100	san + odd peaks possibly lc + ks
31	28.67	550	8.88	26	pc	DLH gel	SH + coes only - (< 3% coes)

Notes: * pc = piston cylinder apparatus, cs = cold seal apparatus
** P3K100 = gel synthesised by the author (Appendix A), us = undersaturated with water
DLH gel = gel donated by DL Hamilton of the University of Manchester
***SH = "sanidine hydrate", san = sanidine, coes = coesite, lc = leucite, ks = kalsilite

The formation of coesite in these experiments is not easily explained. There are, however, three possible explanations.

One possibility was that the gel donated by Dr D.L. Hamilton was not of the correct composition ($KAlSi_3O_8$). When producing a gel it is more common to have a problem of silica deficiency rather than any excess of silica. This is because the source of silica that is most commonly used is tetraethyl orthosilicate ($Si(OC_2H_5)_4$), which is volatile and prone to loss by evaporation until it has been fully hydrolysed by the ammonia solution during gel preparation. Coesite was also a by-product of experiments using other gels (for example runs 13 and 14 in Table 4.5). Gel P3K100 was a gel produced by the author (see Appendix A) which was not used in reversal experiments because it formed peaks at low pressure, which may have been those of leucite and kalsilite (run 20, Table 4.5). However, at high pressure (run 14, Table

4.4) this gel also produced coesite. This would imply that if the composition of the gel was not correct, it was silica rich at high pressure but it was silica poor at low pressure, which would be impossible.

A more probable explanation would be that the water in the capsule dissolved a small amount of the gel used. If the potassium and aluminium components were more soluble than the silica component it should have encouraged the excess silica to precipitate out as coesite or quartz. Therefore, at the end of the experiment, the products should have been mostly "sanidine hydrate" or sanidine with a small amount of coesite or quartz, and the remaining water should be rich in potassium and aluminium. If this were the case then varying that quantity of water used in the experiments should change the size of the coesite peak. Run 13 (Table 4.5) contained only 3.7 wt% of water in the capsule before the start of the experiment. This was not enough water to form entirely "sanidine hydrate" and therefore it was undersaturated. However, despite the fact that the run produced both "sanidine hydrate" and sanidine the relative height of the coesite peak was still of a similar size to all of the water-saturated experiments. One would expect that when the proportion of water was reduced a smaller quantity of the potassium and aluminium components would dissolve and therefore leave less silica to precipitate as coesite, resulting a decrease in the size of the coesite peak. Since the size of the coesite peak was not reduced by decreasing the quantity of water it seems unlikely that the formation of the coesite was caused by preferential dissolution of components of the gel. The preferential dissolution of potassium and aluminium would not agree with the work of Anderson and Burnham (1983) on the dissolution of feldspars which, in the presence of water, tend to precipitate micas or feldspathoids at different temperature conditions. Their work showed no pressure effect on the dissolution properties but their studies only included data obtained below 0.6 GPa. In the current experiments it is perhaps the gel dissolving which may behave in a different fashion to the dissolution of sanidine.

Another explanation is that the "sanidine hydrate" which formed in the present experiments did not have the same quantity of silica as is given by the formula $KAlSi_3O_8.nH_2O$. Therefore the silica remaining from the $KAlSi_3O_8$ gel precipitated to form coesite or quartz. This explanation was hard to prove as it was not possible to determine the composition of the crystals using the electron microprobe because the diameter of the crystals was generally less than a micron and thus inaccessible to microprobe analysis. Even the use of a large rastered beam over a number of crystals did not give any intelligible results.

However, since the quantity of coesite was small, the problem was perhaps not so significant to the overall results.

4.5 Metastable behaviour of "sanidine hydrate" and sanidine

Figure 4.2 shows how these reversal results compare with the previous results of Seki and Kennedy (1964a). Their "synthesis" reaction boundary was at slightly lower pressure and a slightly larger gradient than the one determined here. Initially it was thought that this might be due to the fact that their experiments were not reversal experiments. All of their experiments were synthesis experiments from a gel or glass starting material and the duration of all of their experiments was less than 2 or 3 hours. It is possible that such short experiments only produced metastable products. If this were the case then it would explain the discrepancy between two positions for the reaction. To test this hypothesis two experiments were performed to see if it was possible to reproduce Seki and Kennedy's results. Run 67 (see Table 4.6 and Fig. 4.2) was a synthesis experiment of only three hours duration at 2.350 GPa and 550°C. This chosen pressure and temperature lay between the two positions for the reaction given by Seki and Kennedy and found in this current work. However, the experiment only produced sanidine and no metastable "sanidine hydrate". In order to make more certain that Seki and Kennedy's results were not reproducible, the same experiment was then repeated (run 71) but this time using a starting material of a gel which was seeded with crystals of "sanidine hydrate". This should have encouraged the "sanidine hydrate" to grow metastably. This experiment was run for 2 hours but it still only crystallised sanidine and even the seeds of "sanidine hydrate" were not apparent. Therefore it was not possible, in this case, to reproduce Seki and Kennedy's results.

The discrepancy between the results of this investigation and those of Seki and Kennedy may be a result of slight variations in the apparatus, or an effect of the use of different starting materials. Seki and Kennedy's experiments used either pure sanidine crystallised from a $KAlSi_3O_8$ glass or a natural orthoclase containing 4.40% Na_2O and 11.7% K_2O, whereas these synthesis experiments used a gel of composition $KAlSi_3O_8$.

During further experiments it was found that it was possible to crystallise sanidine metastably in the "sanidine hydrate" field. Run 73, at 2.667 GPa and 550°C, and run 74, at 2.737 GPa and 650°C, (Table 4.6) were both designed to synthesise "sanidine hydrate" at different pressures and temperatures, and thus obtain samples for subsequent study by infrared spectroscopy and thermogravimetric analysis (see Sections 5.2 and 5.3). However, both of these experiments produced metastable sanidine. These two experiments were the closest to the equilibrium boundary (see Table 4.6). This metastable behaviour opposes to that shown by cymrite (Graham et

al 1992). Cymrite, the high-pressure phase, forms metastably in short duration runs on the low pressure side of the reaction. Here it seems that the low-pressure phase grows metastably on the high pressure side of the reaction.

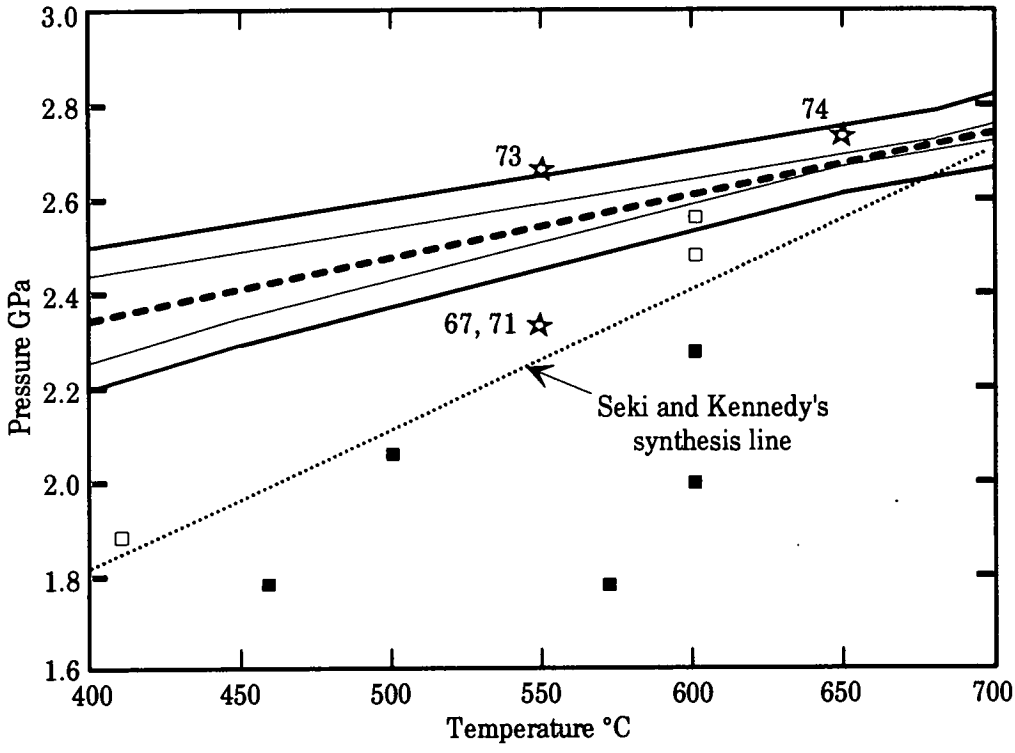

Fig. 4.2. A graph to show the difference between the results of the present work and the results of Seki and Kennedy (1964a). (□ = "sanidine hydrate", ■ = sanidine). Numbered points marked ☆ show where experiments were performed by the author to investigate the metastable crystallisation behaviour of sanidine and "sanidine hydrate" (see Table 4.5)

Table 4.6 . Experiments to investigate the metastability of "sanidine hydrate" and sanidine

Run	P	T	H_2O	Length	Type	Starting	Results***
	GPa	°C	wt %	hours	*	materials**	
67	2.350	550	13.66	3	pc	DLH gel	san only no metastable SH
71	2.350	550	9.88	2	pc	DLH+ SH seeds	san + trace of musc, no SH
73	2.667	550	8.18	48	pc	DLH gel	SH + san + poss. trace of coes
74	2.737	650	7.4	22	pc	DLH gel	SH + san - no coes - trace of musc

Notes: * pc = piston cylinder apparatus
** DLH gel = gel donated by DL Hamilton of the University of Manchester
*** SH = "sanidine hydrate", san = sanidine, coes = coesite, musc = muscovite

4.6 Synthesis experiments for subsequent analysis

Following the reversal experiments the nature of the "sanidine hydrate" phase needed to be investigated in more detail in order to identify the "water" species in the structure, the quantity of water and the cell parameters. This was performed using infrared spectroscopy, thermogravimetric analysis and powder X-ray diffraction techniques. The results of these investigations are summarised in the succeeding chapters. However, in order to do this more "sanidine hydrate", synthesised over a range of pressures and temperatures, was required. The water content of some synthetic sanidines was also examined using infrared spectroscopy.

Table 4.7 lists a summary of all the experiments which produced almost entirely "sanidine hydrate". The run products of these experiments were used for the subsequent analysis by the above mentioned techniques. Figure 4.3 shows the pressures and temperatures at which these experimental runs were performed to produce the "sanidine hydrate". Table 4.8 summarises the experiments used for the investigation of the water content of the synthetic sanidines.

Table 4.7. Synthesis and reversal experiments used to produce "sanidine hydrate" for analysis by infrared spectroscopy and thermogravimetric analysis

Run	P	T	H_2O	Length	Type*	Starting	Results***
	GPa	°C	wt %	hours		materials**	
16	2.930	550	6.9	39	pc	P3K100	SH + trace of coes
17	2.923	550	6.34	51	pc	P3K100	SH + trace of coes
22	2.868	550	6.22	67.5	pc	IP gel	SH + trace of coes
50	2.855	550	5.88	24.5	pcR	PTmix	SH + trace of coes
56	2.855	650	6.28	24	pcR	PTmix	SH + trace of coes
61	2.721	680	6.67	20	pcR	PTmix	SH + trace of coes
72	2.855	450	8.43	72	pc	DLH+ SH seeds	SH with trace of coes + ?lc or qtz?
75	2.737	500	9.0	60.5	pc	DLH gel	SH - trace of coes but qtz instead??
76	2.737	600	9.67	21	pc	DLH gel	SH + coes + minor trace of qtz??
77	2.855	680	11.1	9+?	pc	DLH gel	SH + coes + minor trace of qtz??

Notes: * pc = piston cylinder apparatus, R = reversal experiment
** IP gel = a gel supplied by I Parsons and made by JC Rushton
P3K100 = gel synthesised by the author (see Appendix A)
DLH gel = gel donated by DL Hamilton of the University of Manchester
PTmix = mixture of 40.1% "sanidine hydrate" and 59.9% sanidine
*** SH = "sanidine hydrate", coes = coesite, qtz = quartz, musc = muscovite, lc = leucite

Table 4.8. Synthesis and reversal experiments used to produce sanidine for analysis by infrared spectroscopy

Run	P GPa	T °C	H_2O wt %	Length hours	Type*	Starting materials**	Results***
62	2.74	680	6.38	24	pcR	PTmix	san (+ SH trace)
57	2.50	650	6.35	24	pcR	PTmix	san only
51	2.00	550	6.36	24	pcR	PTmix	san only
93	1.50	700	10.9	48	pc	DLH gel	san only
97	0.50	700	9.0	82	gb	DLH gel	san only
98	0.10	700	11.8	96	cs	DLH gel	san only
99	0.10	700	11.8	96	cs	DLH gel	san only
96	0.50	700	10.4	82	cs	P3K100	san only
18	0.10	750	1.87	66	cs	P3K100	san (+ lc + kal trace)
20	0.10	750	2.01	67	cs	P3K100	san (+ lc + kal trace)
11	0.10	750	2.63	108	cs	P3K100	san only
19	0.10	750	2.03	67	cs	P3K100	san (+ lc + kal trace)
15	0.10	750	5.90	24	cs	P3K100	san (+ lc trace)
9	0.10	750	2.73	108	cs	P3K100	san (+ kal trace)
45♣	0.10	750	----	144	cs	P3K100	san only

Notes: * pc = piston cylinder, cs = cold seal, gb = gas bomb, R = reversal experiment
** P3K100 = gel synthesised by the author (see Appendix A)
DLH gel = gel donated by DL Hamilton of the University of Manchester
PTmix = mixture of 40.1% "sanidine hydrate" and 59.9% sanidine
*** san = sanidine, SH = "sanidine hydrate", lc = leucite, kal = kalsilte
♣ fired to 1100°C for 20 hours

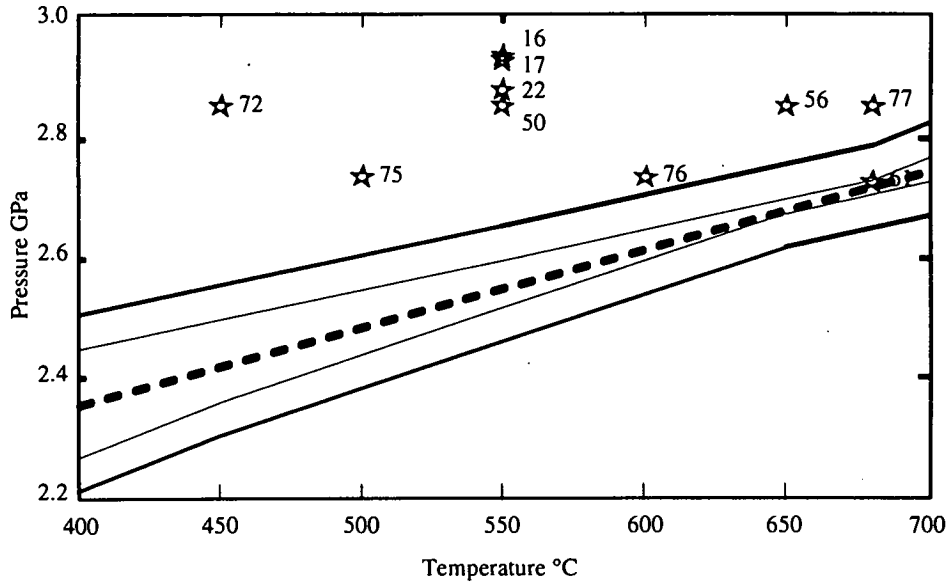

Fig. 4.3. Experiments used to produce "sanidine hydrate" for subsequent analysis using thermogravimetric analysis, infrared spectroscopy and powder X-ray diffraction. The numbers refer to the experiments summarised in Table 4.6. Lines show brackets as determined in Fig. 4.1.

4.7 Conclusions

The position of the reaction

$$KAlSi_3O_8 + nH_2O = KAlSi_3O_8.nH_2O$$
$$\text{sanidine} + \text{water} = \text{"sanidine hydrate"}$$

has been shown to lie between the four reversal brackets 2.350 GPa and 2.500 GPa at 450°C, 2.400 GPa and 2.590 GPa at 550°C, 2.667 GPa and 2.737 GPa at 650°C and between 2.696 GPa and 2.721 GPa at 680°C.

The quantity of coesite in all the high pressure experiments was roughly calibrated and found to be small, perhaps less than 5% in most runs. The cause of this coesite was not determined but the three potential problems were that the gel was off composition, water preferentially dissolves the potassium and aluminium components of the gel or that the "sanidine hydrate" was not of the same stoichiometry as the formula given above.

Attempts to reproduce Seki and Kennedy's (1964a) synthesis results were unsuccessful. The discrepancy between their results and the ones found here was therefore not a result of the metastable behaviour of "sanidine hydrate". This behaviour is not analogous with that of the metastable behaviour of cymrite as found by Graham et al. (1992). In fact it was possible to crystallise sanidine metastably just inside the "sanidine hydrate" stability field when a gel was used as a starting material. Reversal experiments, which used the crystalline starting material PTmix, were run at similar pressures and temperatures to the ones that crystallised sanidine metastably and formed "sanidine hydrate" alone.

Chapter 5
"Water" content of "sanidine hydrate"

5.1 Introduction

In the reversal experiments of Chapter 4 the phase produced on the high pressure side of the reaction, "sanidine hydrate", was thought to be a hydrous phase. In the absence of water, sanidine has been shown to be stable up to pressures of 4 to 10 GPa in the temperature range 800 to 2000°C (Kinomura et al 1975) but in the presence of water a reaction occurs. The sanidine reacts with this water and thus the resulting high pressure phase is hydrated. Also in the reversal experiments which produced "sanidine hydrate" there was less water in the capsule at the end of the experiment than at the beginning which could imply that some of the water was consumed by the reaction. In the work on cymrite, a potential analogue to "sanidine hydrate", Graham et al (1992) found that the composition of cymrite was $BaAl_2Si_2O_8.nH_2O$, where $0 \leq n \leq 1$. In their work the water content of cymrite was investigated by infrared spectroscopy and found to be molecular H_2O held within the crystalline structure. Therefore the type of water species in "sanidine hydrate" was here also examined by infrared spectroscopy to see if it too contained molecular H_2O.

The reversal of the reaction between sanidine ($KAlSi_3O_8$) and water to form "sanidine hydrate" ($KAlSi_3O_8.nH_2O$) was discussed in Chapter 4. The reversal experiments restricted the reaction to lie between four tight pressure brackets at different temperatures. It was possible to fit a number of straight lines to lie within these brackets which could represent the true equilibrium position of the reaction. If the compositions of any of the phases vary with pressure and temperature, however, it is possible that the reaction would not appear as linear on a pressure-temperature graph. In Chapter 2 the work of Graham et al. (1992) on cymrite ($BaAl_2Si_2O_8.nH_2O$) was considered as a potential analogue to "sanidine hydrate". They discovered that cymrite had a variable water content by investigating samples synthesised at different pressures and temperatures with thermogravimetric analysis. The water content varied from one molecule of H_2O per formula unit at high pressures and low temperatures to probably being free of water at low pressures and high temperatures (see Fig. 2.7). As a result the reaction could not be linear on a pressure-temperature graph. The water contents determined by thermogravimetric analysis were contoured on a graph of the partial pressure of water against temperature. These variation in water content could then be used to calculate the curvature of the reaction between sanidine and water to form "sanidine hydrate" by thermodynamic analysis. Graham et al. calculated that the reaction was slightly convex up with pressure i.e. $d^2P/dT^2 > 0$. In the light of these results, thermogravimetric analysis was also performed in this study on samples of "sanidine hydrate", previously synthesised at various pressures

and temperatures, in order to see if the value of "n" in the formula $KAlSi_3O_8.nH_2O$ could be determined and also to see if it varied with the pressure and temperature of synthesis.

The experimental methods employed for all of the techniques mentioned in this Chapter were as described in Chapter 3.

5.2 Infrared spectroscopy of "sanidine hydrate"

Two typical infrared spectra of "sanidine hydrate" are shown in Figure 5.1 (runs 17 and 56). The difference in intensity of transmission between the two traces only reflects the different quantities of sample used. At 1610 cm^{-1} there is an absorption peak (or transmission trough) which would indicate the presence of molecular H_2O. In the OH stretching region there are two sharp absorption peaks at 3530 and 3620 cm^{-1} which are the result of isolated structurally bound H_2O molecules. In the samples synthesised at different pressures and temperatures the position of the absorption peaks does not vary by more than $\pm$ 10 cm^{-1}. In the OH stretching region of the spectra there is also a smaller broad background hump at a slightly lower frequency. This absorption hump indicates the existence of surface water or water held within micropores. Some surface water is hard to avoid when using a hygroscopic KBr disc. In addition micropores containing water as fluid inclusions are also probable in samples synthesised hydrothermally as these samples were dried to 100°C which should remove most of the surface water, but not necessarily the fluid inclusion water. Samples were also investigated in the near infrared at wavenumbers between 4000 and 5800 cm^{-1} in order to look for overtones of these fundamental vibrations seen at lower wavenumbers. However, no combination modes were seen and therefore no additional information on the nature of the structural "water" could be obtained.

Goldman et al (1977) studied single crystals of cordierite using polarised infrared spectroscopy. In the OH stretching region four absorption peaks were identified on an infrared spectrum (Fig. 5.2). These four peaks were thought to represent two different sites for H_2O molecules within the hexagonal channels of the crystals. The orientation of these water molecules could be shown to have the H-H vector of the water molecule either parallel or perpendicular to the channel axis by using polarised infrared radiation (Schreyer, 1985) (Fig. 5.3). However, in the H_2O bending region there are more than two absorption peaks, which does not entirely fit this

explanation. Although this work of Goldman et al. utilised polarised infrared radiation and a single crystal technique, the corresponding powder pattern would presumably resemble the combination of the three traces of Figure 5.2. Therefore a comparison of the pattern of the infrared spectrum of cordierite with that of "sanidine hydrate" showed that there must be only one site for the H_2O within the "sanidine hydrate" structure. Work by Schmetzer and Kiefert (1990) has shown that the presence of two H_2O sites in the crystal structure, in an orientation parallel and perpendicular to the channel axis within the crystal, is also a property of beryl.

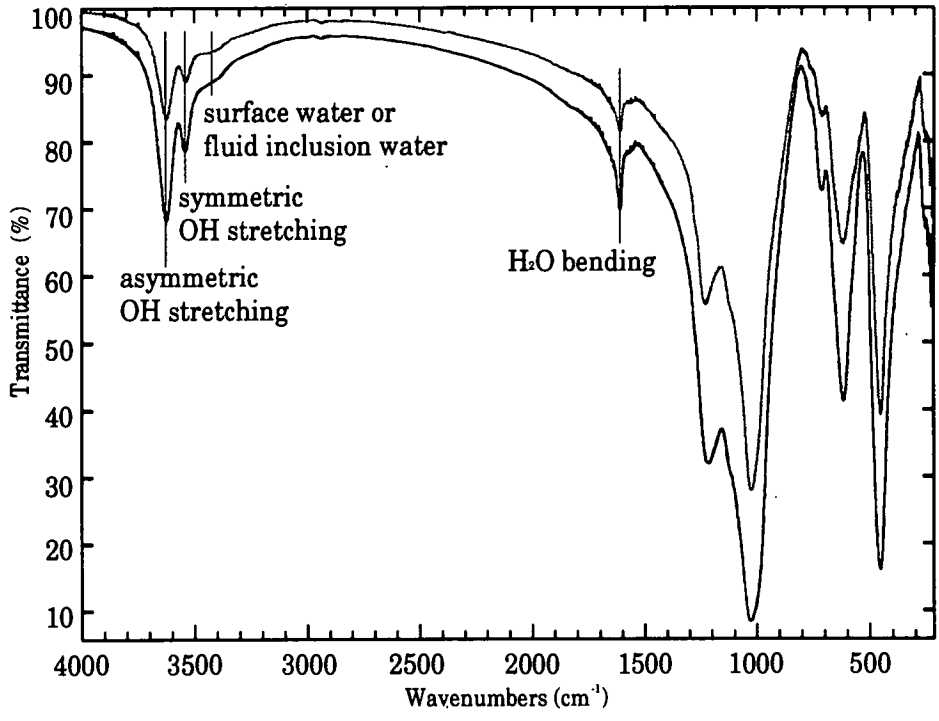

Fig. 5.1. Infrared spectra of two samples of "sanidine hydrate". The feinter top trace is of run 56 and the lower darker one is that of run 17. Both traces appear very similar showing evidence for the presence of structural H_2O molecules and free water as either surface water or water in fluid inclusions.

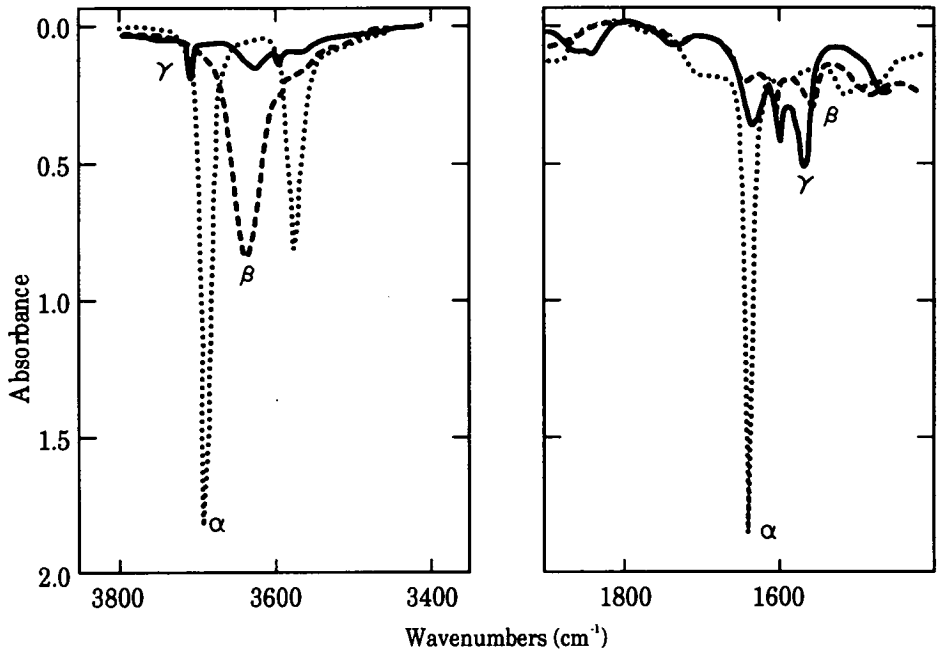

Fig. 5.2. Infrared spectra of water in cordierite from three different orientations through the crystal. The spectrum, taken in polarised radiation, shows more than two features in the 3600 wavenumber region. At 78K the β orientation resolves into two peaks. These four peaks have been interpreted as showing there are two water sites within the hexagonal channels in the structure of cordierite (see Fig. 5.3). (redrawn after Goldman et al., 1977)

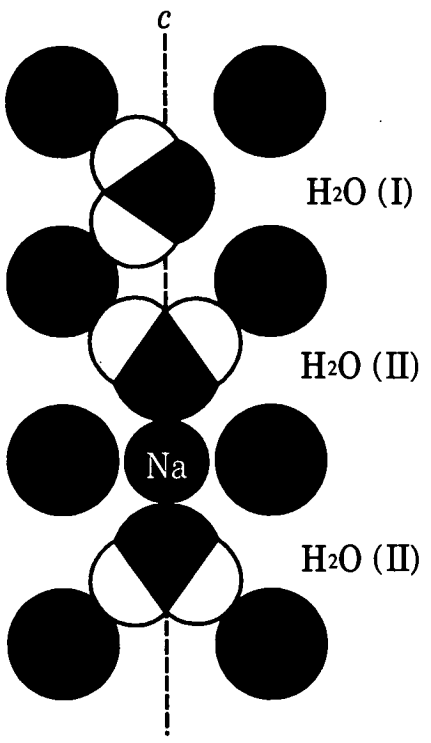

Fig. 5.3. A sketch section through the hexagonal channel of cordierite parallel to the *c* axial direction showing the two orientations in which H_2O can occur within the channel. The presence of a cation, such as sodium, seems to encourage the H_2O molecule to take a position with the H-H vector perpendicular to the *c* axis type (II). (redrawn after Goldman et al., 1977)

These infrared spectra for "sanidine hydrate" are similar to the spectra for cymrite prepared at 0.965 GPa and 740°C (Fig. 5.4). The positions of the OH stretching absorption peaks in "sanidine hydrate" are shifted to higher frequencies than in cymrite but not to such high frequencies as are found in cordierite or beryl. This frequency shift implies that the strengths of the bonds holding the H_2O molecules in the "sanidine hydrate" structure are slightly stronger than those in cymrite but not as strong as those in cordierite or beryl.

There is no evidence, from infrared spectroscopy, for any OH groups within the "sanidine hydrate" structure as there is no single OH stretching absorption peak. However, it would probably be difficult to observe a small OH stretching peak if its frequency lay in the range of OH stretching of an H_2O molecule.

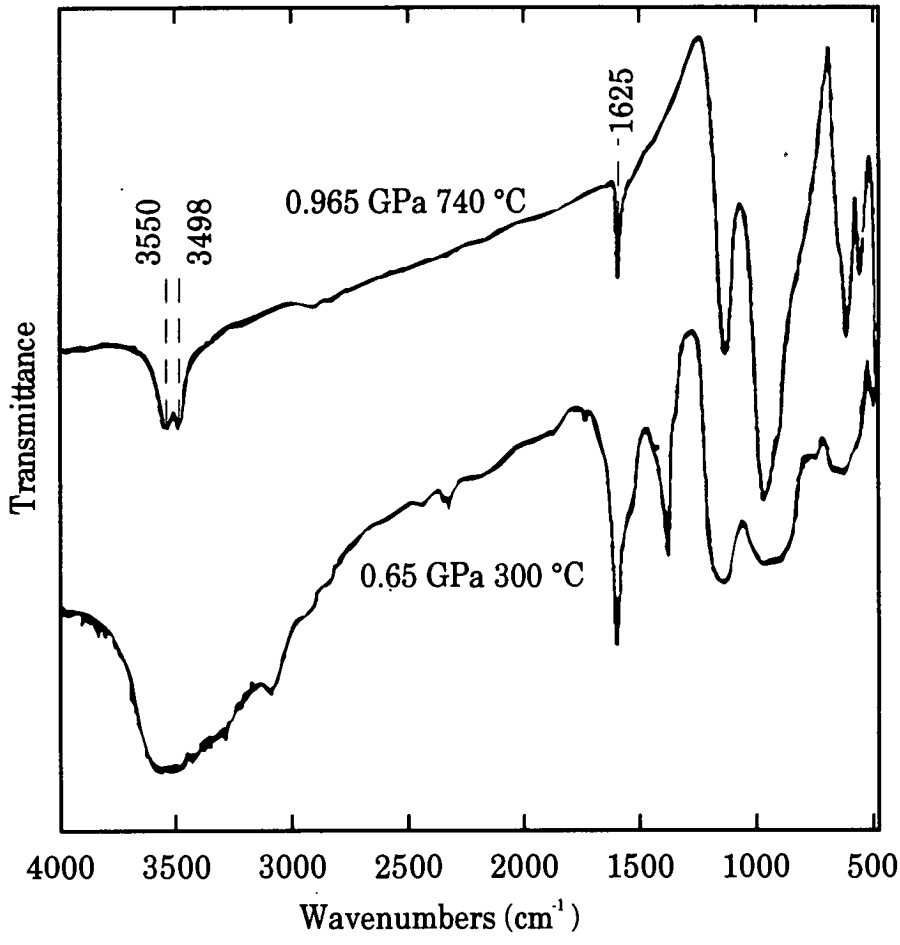

Fig. 5.4. Two infrared spectra of cymrite synthesised under different pressure and temperature conditions (redrawn from Graham et al 1992, fig. 7).

Thermogravimetric analysis of the samples of "sanidine hydrate" was then performed (see next section). The samples were heated up until no further weight loss occurred. This constant weight at increasing temperatures was thought to imply that all of the structural "water" had been removed. As a further check that this was indeed the case, samples which had been subjected to thermogravimetric analysis, which are subsequently referred to as "hexasanidine", were re-investigated using infrared spectroscopy. Two typical results of samples of runs 76 and 61, mounted in a KBr disc, are shown in Figure 5.5. Both samples show only a broad peak in the OH stretching region which is probably caused by surface water adsorbed by the KBr disc. There is no evidence for either structural H_2O or structural OH. This dehydrated material could be similar to the barium analogue, hexacelsian of Viswanathan et al. (1992) and Graham et al. (1992). In order to see if this was the case the cell parameters of "sanidine hydrate" and "hexasanidine" were measured for comparison with cymrite and hexacelsian (see Chapter 6)

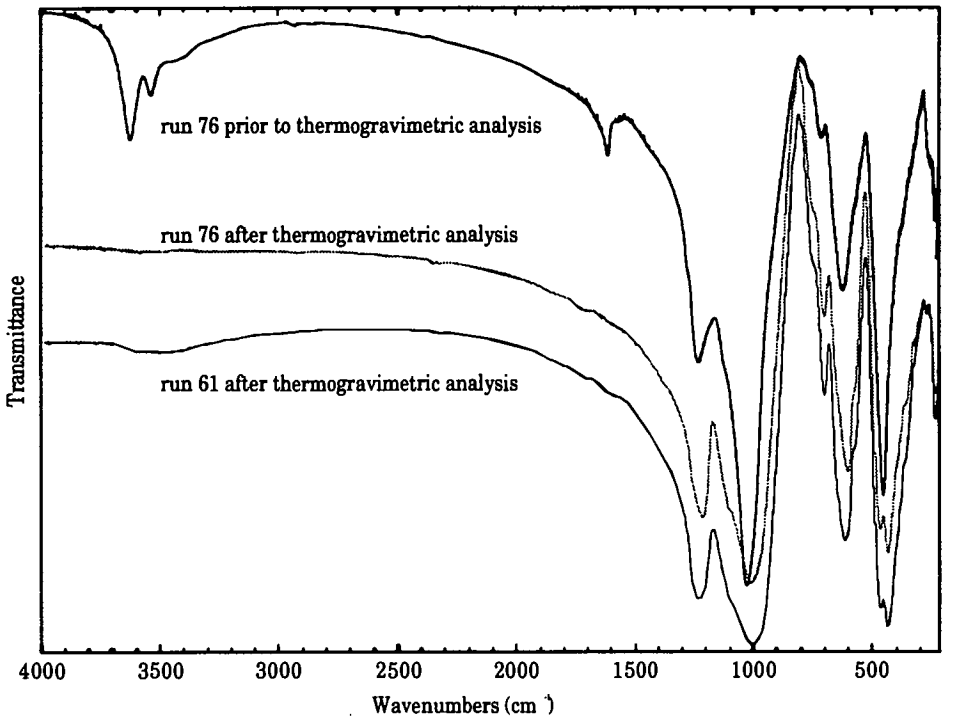

Fig. 5.5. Infrared spectra of two samples of "hexasanidine" synthesised by dehydrating "sanidine hydrate" during thermogravimetric analysis. The feinter trace is of run 76 and the lower darker one is that of run 61 compared with the material prior to dehydration of run 76 shown in the top trace. Both traces show no evidence for the presence of structural "water". The features in the OH stretching region and the H_2O bending region are probably a result of adsorbed surface water on the KBr disc.

5.3 Thermogravimetric analysis of "sanidine hydrate"

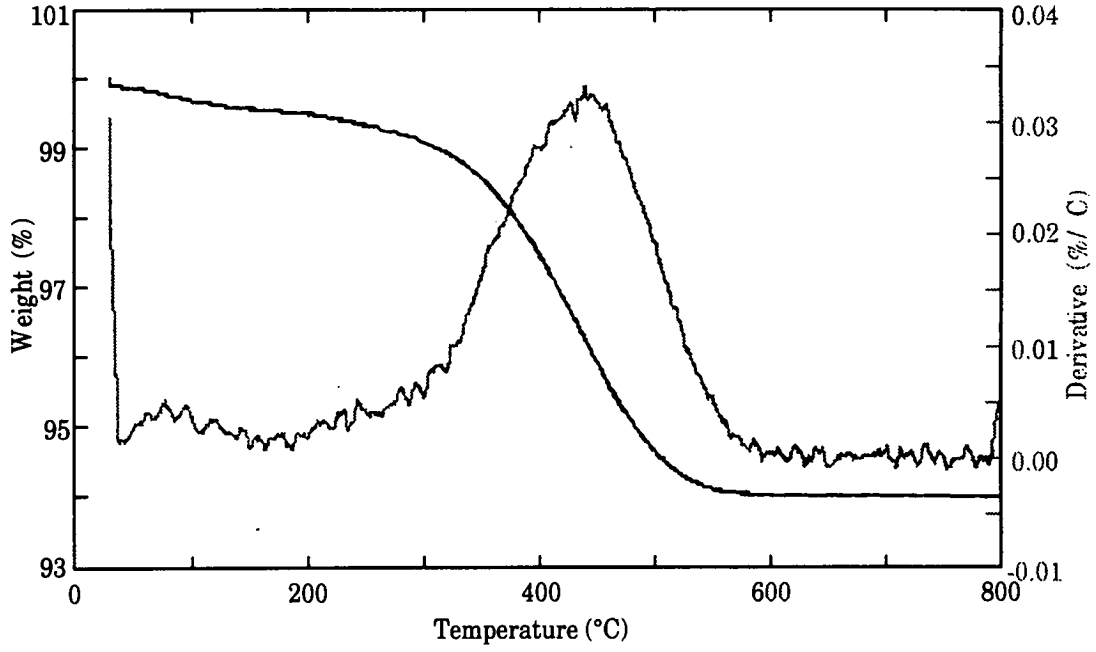

Fig. 5.6. A typical thermogravimetric result of a "sanidine hydrate" sample (run 17) showing the weight loss (heavier black line) and the derivative of the weight loss with respect to temperature (feinter grey line) plotted against temperature. The major weight loss event between 200 and 600°C is probably caused by the loss of structurally bound H_2O molecules. The small and variable weight losses below 300°C and above 600°C were perhaps due to surface water and structurally bound OH groups respectively.

A typical graph of the results of thermogravimetric analysis of a "sanidine hydrate" sample (run 17) is shown in Figure 5.6. All the graphs of the thermogravimetric analysis of the samples exhibited a similar shaped curve. Up to around 300°C there was a very slight and variable weight loss. Above 300°C but below 550°C there was a substantial loss of weight. Above 550°C and up to around 800°C the weight sometimes appeared to drop slightly, by less than 0.2 wt%, but up to 1200°C the weight rose again slightly. The small increase in weight above 800°C was probably caused by a slight drift in the measurement of the machine as was seen in an anhydrous sample of run 45 which was fired before analysis (see Fig. 9.9). Hence there was probably no further weight loss above 800°C. The derivative of the weight loss with respect to temperature was also drawn up as this could show more clearly when there was a change in slope. All of these samples showed only one strong peak in the derivative in the 300-550°C region and a minimal one below 300°C. To calculate the percentage weight loss over a weight loss event, two positions were chosen on the curve outside the temperature range of the weight loss event. Tangents

were drawn at these two positions and another at the point of inflection where d(wt%)/dT was at a maximum. The two points of intersection of these three tangents were then used to measure the weight loss without the effect of the background of measurement drift and weight loss from other events. Figure 5.7 shows how these tangents were drawn on the graph of weight loss against temperature.

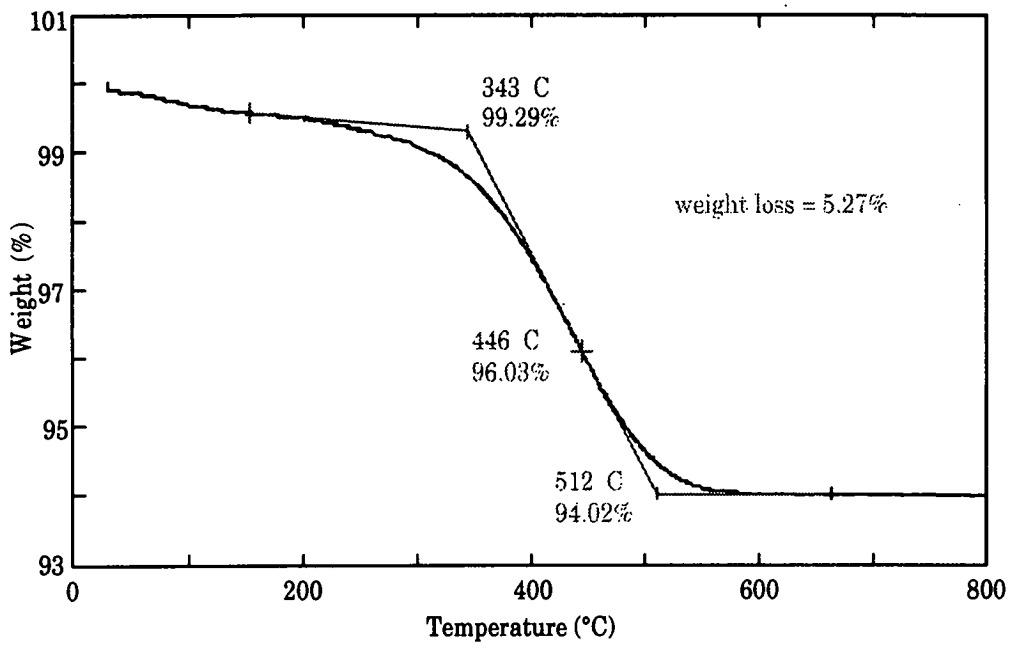

Fig. 5.7. Diagram to show the method of tangent construction used to measure the percentage weight loss over a weight loss event. The measurement shown here is for the main weight loss event between 300 and 550°C which may correspond to the loss of structurally bound H_2O molecules in "sanidine hydrate".

5.3.1 *Interpretation of the weight losses*

The weight loss exhibited by "sanidine hydrate" on heating from 0 to 800°C can be viewed as three weight loss events over the separate temperature ranges of around 0-300°C, 300-550°C and 550-800°C.

The weight loss up to approximately 300°C was thought to be mostly that of surface water lost from the sample.

The major weight loss event between 200 and 600°C was taken to be the loss of the H_2O molecules from within the crystalline structure as identified using infrared spectroscopy (see Section 5.2).

Above 550°C but below 800°C there was a small weight loss in some of the samples. This weight loss may have been that of a small amount of structural OH, as was suggested by Graham et al (1992) for a similar small weight loss observed in cymrite. Any further evidence for structural OH could not be found using infrared spectroscopy, as it is hard to see evidence of structural OH in the presence of large amounts of structural H_2O.

The percentage weight loss of 10 run products from piston cylinder experiments which produced "sanidine hydrate" were measured over these three temperature ranges to evaluate the percentage weight loss and to see if the weight loss varied with the pressure and temperature of synthesis. Three of these samples were re-run to check for consistency. At this stage material remaining from the original samples was exhausted thus prohibiting any further checks. The percentage weight loss for these thermogravimetric experiments is listed in Table 5.1. Figure 5.8 shows the plot of these results for the pressure and temperature conditions of all of the piston cylinder experiments with the percentage weight loss of the main water loss event between 300 and 550°C shown in bold type. Unlike the work of Graham et al. (1992) these samples showed no obvious systematic variation in percentage weight loss with pressure and temperature. The values ranged from 4.42 to 5.85 wt% but in an irregular order. Repeat thermogravimetric runs on the same samples (runs 50, 56 and 77 in Table 5.1) showed differences in the percentage weight loss within the same sample were almost within the measurement error of the machine itself which was ± 0.1 wt%. However, samples which were synthesised at similar pressures and temperatures (e.g. runs 16 and 17 and runs 22 and 50) showed differences which were larger than 0.1 wt%. These could imply that the overall error in measurement was greater than ± 0.1 wt%, perhaps of the order of ± 0.3 wt% or possibly more. This was most likely to be a property of the samples themselves rather than the thermogravimetric machine (see Section 3.7.2). The degree of systematic variation was checked by examining the thermodynamics of the dehydration of "sanidine hydrate" in Section 7.6 and found to be poor. Therefore the percentage weight loss could not be contoured with isopleths of constant water content as was calculated by Graham et al. (1992) for the barium analogue (see Section 2.3). However, it is interesting to note that the weight loss between 300-550°C in all of the samples was within ± 0.8 wt% from the mean value of 5.07 wt%. In addition the maximum value of weight loss in this event was 5.85 wt% which is less than 6.07 wt% which would be the weight percentage of H_2O if there was one H_2O molecule per formula unit.

Table 5.1. Table of percentage weight losses of samples of "sanidine hydrate" measured by thermogravimetric analysis. The three temperature ranges in which different weight loss events occurred are shown as well as the pressures and temperatures of synthesis of the ten piston cylinder run products.

Run number	Pressure of synthesis (GPa)	Temperature of synthesis (°C)	Weight loss (0 - 300°C) (%)	Weight loss (300-550°C) (%)	Weight loss (550 - 800°C) (%)
72.1	2.855	450	0.51	5.38	0.31
50.1	2.855	550	0.03	4.77	0.28
50.2	2.855	550	0.25	4.81	0.31
22.1	2.868	550	0.56	5.07	0.5
17.1	2.923	550	0.61	5.27	0.03
16.1	2.930	550	0.51	5.85	0.00
56.1	2.855	650	0.75	4.50	0.37
56.2	2.855	650	0.90	4.42	0.29
77.1	2.855	680	0.60	4.66	0.27
77.2	2.855	680	0.35	4.42	0.27
75.1	2.737	500	0.34	5.42	0.13
76.1	2.737	600	0.27	5.15	0.27
61.1	2.721	680	0.89	4.59	0.37

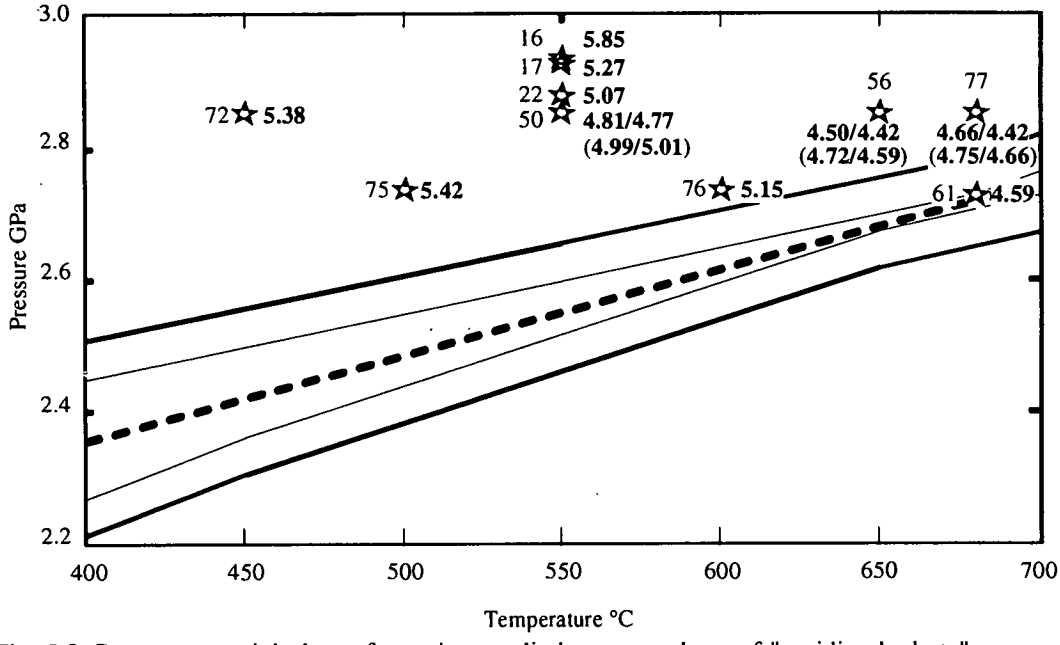

Fig. 5.8. Percentage weight loss of ten piston cylinder run products of "sanidine hydrate", measured by thermogravimetric analysis, in the 300 - 550°C temperature range plotted in the position of their pressures and temperatures of synthesis. Measurement errors in the thermogravimetric data should be ± 0.1 wt%. The figures shown in parentheses are the corrected weight losses after the platinum content was measured using atomic absorption. The solid and dashed lines show possible positions of the reversed reaction as described in Chapter 4, Fig. 1.1.

5.3.2 *Correction of the weight losses using the admixed platinum contents*

One of the potential difficulties with the thermogravimetric measurements was the contamination of the solid media samples with platinum (see Section 3.7). This contamination may hide any pattern in the variation of the water content with the pressure and temperature of synthesis, as shown in Figure 5.8, and therefore the technique of atomic absorption was used to try to measure the quantity of platinum in each sample. The techniques used for atomic absorption were also described in Section 3.8.

The standard additions method showed that there was severe depression of the platinum absorption peak, presumably because some other part of the sample was being simultaneously dissolved and interfering with the platinum atoms. This method yielded the results shown in Table 5.2. The error values for these figures were probably $\pm$ 0.02 mg.

The thermogravimetric data were then recalculated to account for the known platinum contamination using the equation:

$$\alpha = \frac{\beta X}{(X - Y)}$$

where α = corrected percentage weight loss in "sanidine hydrate" alone
β = percentage weight loss in "sanidine hydrate" + platinum
X = weight of "sanidine hydrate" + platinum + H_2O before thermogravimetric analysis
Y = weight of platinum in sample

The samples chosen for measurement using atomic absorption were the ones on which repeat thermogravimetric runs had been performed, run numbers 50, 56 and 77. They were also the ones with low weight loss values which may therefore have been more contaminated. The final column of data in Table 5.2 and the numbers in parentheses in Figure 5.8 show the result that these recalculated figures would have on the thermogravimetric data.

Inevitably, as these figures rely on calculating the total platinum in the sample, the value would be smaller than the true value if some of the platinum was lost before atomic absorption was performed. So if the measured quantity of platinum was incorrect, it is probable that the true quantity would be larger and in this case would recalculate to result in yet higher values for the weight percentage of water lost from "sanidine hydrate" during thermogravimetric analysis

Table 5.2. Corrected values for the percentage weight loss of the main weight loss event in "sanidine hydrate" between 300 and 550°C during thermogravimetric analysis after measuring the platinum content (column 4) using results from atomic absorption techniques.

Run number	Weight of sample before TGA (mg)	Weight loss before correction (%)	Weight of platinum (mg)	Corrected weight loss (%)
50.1	10.8	4.77	0.478	4.99
50.2	9.2	4.81	0.362	5.01
56.1	10.3	4.50	0.472	4.72
56.2	9.9	4.42	0.377	4.59
77.1	10.4	4.66	0.196	4.75
77.2	7.3	4.42	0.385	4.66

It seems that the quantity of platinum as determined by atomic absorption does not explain the variation seen in the thermogravimetric data. The platinum in all the samples run had the reasonably consistent effect of increasing the weight percentages of the main water loss event by 0.2 to 0.3 wt%. Any agreement between the three repeated runs was not improved by a corrected weight figure and therefore it is probable that some of the platinum was lost prior to atomic absorption analysis. Hence the platinum correction did not aid an explanation for the variation from samples synthesised under different conditions, either by systematic differences or as a consistent quantity of water lost over the entire range of pressures and temperatures at which they were studied.

The platinum correction was not sufficiently good to merit more of the samples being used up in atomic absorption analysis. The remaining samples were needed for repeat powder X-ray diffraction scans to calculate the consistency of the unit cell parameter measurements. Each of these scans would result in more of the original platinum content being lost and so would cause the accuracy of the platinum correction to decrease. Therefore only 6 of the thermogravimetric samples were corrected for platinum content.

5.4 Conclusions

The phase "sanidine hydrate" was shown from infrared spectroscopy to contain structural H_2O molecules which were limited to one site within the crystalline structure. Thermogravimetric analysis did not show that the water content varied in a clear systematic fashion with pressure and temperature over the pressure-temperature range studied. The mean weight loss between 300 and 550°C, which was thought to represent the structural H_2O component, was 5.07 wt%. This weight loss corresponds to 0.83 molecules per formula unit, i.e. the formula of "sanidine hydrate" was

$$KAlSi_3O_8.0.83H_2O$$

This value may not be significant but was used to try and calculate some thermodynamic parameters over the pressure-temperature range studied in Chapter 7. The accuracy of these weight losses may be poor. There was some variation about the mean value with the maximum value being almost 1 H_2O molecule per formula unit. The cause of this variation could be contamination rather than true differences in the water content of "sanidine hydrate". The overall effect of the contamination was difficult to demonstrate, although some samples were shown to contain significant quantities of platinum. The products of thermogravimetric analysis of "sanidine hydrate" up to 800°C showed no remaining structural "water" peaks in the infrared spectra and was hence termed "hexasanidine". Since "hexasanidine" could be synthesised it would imply that "sanidine hydrate" could have a water content which varied between 1 and 0 molecules per formula unit as was found in the barium system (see Section 2.3).

Chapter 6
Unit cell parameters

6.1 Introduction

In Chapter 5 the water content of "sanidine hydrate" was investigated. It was thought that perhaps the value of n in the formula $KAlSi_3O_8.nH_2O$ might vary systematically with the pressure and temperature of synthesis in a similar fashion to the barium feldspar hydrate, cymrite (Graham et al 1992). In Section 5.3 the results of thermogravimetric analysis of samples of "sanidine hydrate" were documented. Figure 5.8 showed that these results varied slightly with pressure and temperature of synthesis, but not in a systematic manner as shown by the thermodynamic analysis described in Section 7.6. It was postulated in Section 5.3.1 that contamination of the sample might be affecting the results. If the quantity of water in the "sanidine hydrate" structure does vary significantly with pressure and temperature of synthesis then the size of the unit cell may reflect this. Viswanathan et al. (1992) calculated the cell parameters of the barium feldspar hydrate, cymrite and its dehydrated form hexacelsian. They showed that the cell parameters of cymrite changed progressively with dehydration and hence cymrite and hexacelsian formed end members of a solid solution series. If "sanidine hydrate" and "hexasanidine" behave similarly then they too may be part of a solid solution series with variable amounts of water in the structure, and therefore the structural "water" content should vary with pressure and temperature of synthesis and hence the results of thermogravimetric analysis shown in Figure 5.8 were probably affected by contamination.

Cell parameters were calculated, using powder X-ray diffraction, for "sanidine hydrate" synthesised under a variety of pressure temperature conditions in order to investigate any variation in cell structure. Cell parameters were also calculated for some of the same samples that were dehydrated during thermogravimetric analysis ("hexasanidine"). This showed the maximum possible variation in water content from a fully hydrated sample to a dehydrated sample.

6.2 Techniques used in calculating cell parameters

The sample was mixed thoroughly with a small amount of internal standard. A good internal standard is one which has a very well known structure and hence the position of its peaks on a powder X-ray diffraction pattern is well defined. In addition the internal standard must have X-ray diffraction peaks over a similar angle range as the sample and minimal overlap with those peaks generated by the sample. The internal standard used for samples of "sanidine hydrate" and "hexasanidine" was quartz.

The sample containing the internal standard was mounted on a glass slide with acetone and scanned with X-rays using a Philips PW 1800 X-ray diffractometer. The scans used CuKα_1 and CuKα_2 radiation of wavelengths 0.154060 and 0.154439 nm with the generator set to 40 kV and 50 mA. For accurate crystallographic work the scan was set to run from 2°2θ to 140°2θ using a step size of 0.015°2θ and a measurement time of 3 seconds per step on a spinning sample. A slow scan, of eight hours duration, was required to achieve a better definition of the peaks. The scan was run up to a large angle as the position of the peaks at higher values of 2θ is better known and therefore increases the precision of the cell parameters calculation.

The Philips APD 1700 software automatically generated a data file of peak positions and intensities. This file was carefully edited by automatically removing the Kα_2 peaks and then edited manually on the screen to ascertain that all the peaks were correctly positioned and were genuine sharp peaks. Any peaks that were known to be indicative of other phases, in particular those peaks for coesite, were deleted at this stage. The remaining peaks data file was then corrected using the systematic error correction programme of the Philips software. This software creates a "best fit function" which corrects the peaks of the quartz internal standard back to their theoretical value. The best fit function could then be plotted to check that there were no outlying peaks that altered the position of the best fit curve so that it did not run through the majority of the points. If the curve did not lie in a reasonable position then these outlying peaks could be ignored and another best fit function calculated. Figure 6.1 shows these outlying peaks as an "O". The "best fit function" as fitted through all of the points is the dotted curve. An improved "best fit function", which ran through the main array of points and is shown in Figure 6.1 as a solid black line, was obtained by ignoring the outlying peaks. The outlying peaks were often low intensity peaks at higher angles which may not have been caused by the quartz internal standard

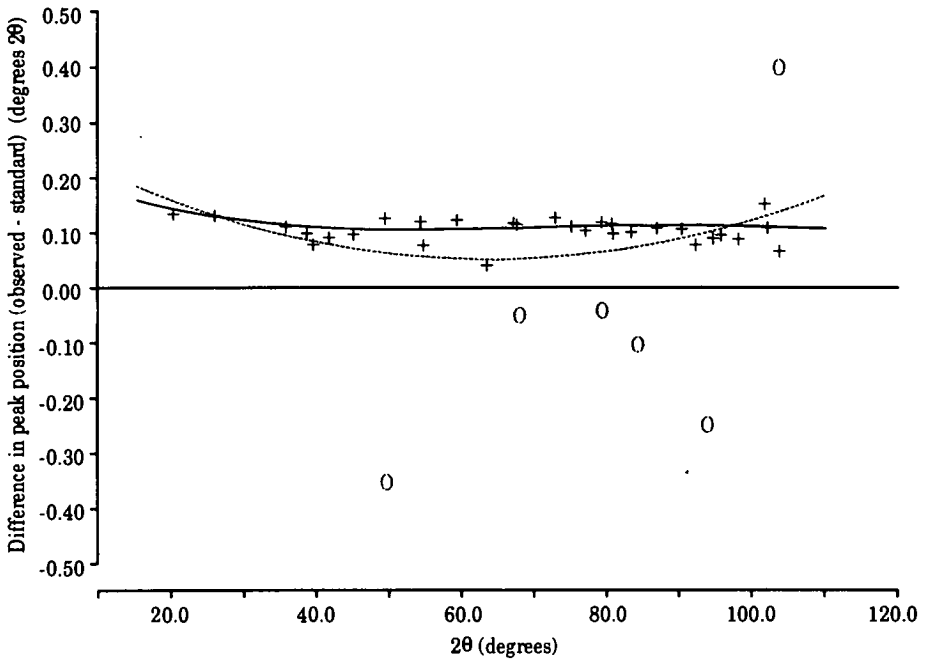

Fig. 6.1. Diagram to show how the systematic error correction was applied. Crosses and circles represent peaks identified by the software as quartz peaks. The y-axis shows the difference between these peaks and their true value in quartz. Initially a best fit function was applied to all of these peaks (dotted line). Some of the peaks (circles) were not close to the main array of peaks. These outlying peaks affected the shape of the best fit curve substantially and were therefore ignored and a second best fit curve produced (black solid line). The entire peaks data file was then adjusted using a function which corrected for this systematic error.

When a good systematic error correction function had been evaluated it was applied to the data file for the entire angle range. This procedure corrects for variations of the positions of the peaks that are due to differing sample thickness and heights of the mount.

In order to use the crystallography component of the Philips APD 1700 software package it was necessary to have a peaks data file which contained only the peaks of the phase of interest. Hence a new data file was created. It was also useful, as a cross check, to write a file which contained the quartz peaks from the error corrected file. The internal standard should show the cell parameters of quartz. The cell parameters of "sanidine hydrate" and "hexasanidine" were refined from an initial starting point of Seki and Kennedy's (1964a) values for the cell parameters of a = 0.533 nm and c = 0.77 nm using a hexagonal primitive cell. The potentially analogous barium feldspar hydrate, cymrite, has a monoclinic symmetry with unit cell parameters of a = 0.533 nm, b = 3.66 nm and c = 0.767 nm but the structure can be refined as pseudohexagonal with a space group $P2_1$ (Drits et al 1975, Drits and Kashaev 1969). The cell parameters of Viswanathan et al (1992) are all calculated using this

pseudohexagonal symmetry. "Sanidine hydrate" has a very similar powder X-ray diffraction pattern to cymrite and hence it is possible that it also has pseudohexagonal symmetry and is really monoclinic. This may explain the difficulty in indexing all of the unknown peaks which might have been "sanidine hydrate".

Using the Philips APD 1700 software programme it was possible to vary the number of refinements and the size of the final 2θ error window. These were modified until the number of reflections with a unique explanation increased, preferably to explain all of the peaks, and the number of reflections with two or more explanations decreased, preferably to zero. A good refinement normally had a final error window in the peak positions of 0.05°2θ or less. This degree of refinement was not attainable in this instance for all of the available peaks and it was found that the peaks present varied from sample to sample. In order to make a comparison of the different samples and to improve the refinement, 10 peaks were chosen. The peaks selected were ones that occurred in the trace of every sample and included some of the higher angle peaks to increase the precision of the refinement and also most of the more intense lower angle peaks. The choice of these peaks did have an effect on the cell parameters calculated and several combinations of peaks were investigated. None of these choices could explain the existence of all of the unknown peaks in the trace especially if the highest angle peaks were selected. The final choice of peaks was that which refined with a better final error window and yet contained most of the larger peaks. Table 6.1 shows the average positions of the peaks used for cell refinement of "sanidine hydrate" and "hexasanidine".

For comparison the indexed pattern generated by this method was then used to recalculate the cell parameters with the aid of a programme written by Dr P Champness of Manchester University. This programme gave slightly different values for the cell parameters but a better idea of the errors involved in each calculation. The figures for the cell parameters in Tables 6.2 and 6.3 are those generated by this programme.

Table 6.1. Approximate positions of reflections used to refine the cell parameters for the structures of "sanidine hydrate" and "hexasanidine". 2θ is the peak position on the X-ray diffraction pattern and h, k and l are the Miller indices assigned to that peak by the Philips software

"sanidine hydrate"				"hexasanidine"			
2θ position	h	k	l	2θ position	h	k	l
19.178	1	0	0	19.366	1	0	0
22.406	1	0	1	22.482	1	0	1
23.040	0	0	2	22.729	0	0	2
30.153	1	0	2	30.031	1	0	2
33.555	1	1	0	33.875	1	1	0
38.940	2	0	0	41.040	2	0	1
40.274	2	0	1	49.041	1	1	3
47.084	0	0	4	58.247	2	1	2
57.900	2	1	2	71.276	2	2	0
70.524	2	2	0	137.933	1	1	9

6.3 Results of cell refinement calculations

Figures 6.2 and 6.3 show a typical X-ray diffraction trace for "sanidine hydrate" and "hexasanidine" respectively in the 0 to 140°2θ angle range. These two traces are similar but they do show a slight shift in peak positions as shown in more detail in Figure 6.4, which is a comparison of the traces of these samples in the 0 to 60°2θ angle range. It is these shifts that give rise to the small differences in the size of the unit cell parameters for "sanidine hydrate" and "hexasanidine". Tables 6.2 and 6.3 list the results of unit cell refinement calculations for "sanidine hydrate" and "hexasanidine" respectively. Although the unit cell parameters were calculated for samples synthesised at a variety of pressures and temperatures, there was little variation in unit cell parameters between samples and that slight variation was not systematic with the conditions of synthesis. Repeat calculations for four of the samples (runs 16, 50, 56 and 61) using different aliquots of the same sample showed that the variation between different samples and repeat runs of the same sample were of a similar order of magnitude. All of the calculated unit cell parameters for the samples lay within a reasonable error of ±0.001 nm or less of the mean values shown at the bottom of the tables. These calculated cell parameters clearly do not offer an explanation for all of the peaks shown in Figures 6.2 and 6.3. The reason for this uncertainty may be that the unit cell for both "sanidine hydrate" and "hexasanidine" is actually monoclinic, with a pseudohexagonal symmetry similar to that believed to occur in cymrite (see previous section), rather than a hexagonal primitive unit cell as was assumed for these samples. Tables 6.4 and 6.5 show a list of all the possible positions of peaks that these unit cell parameters could give rise to using a hexagonal cell.

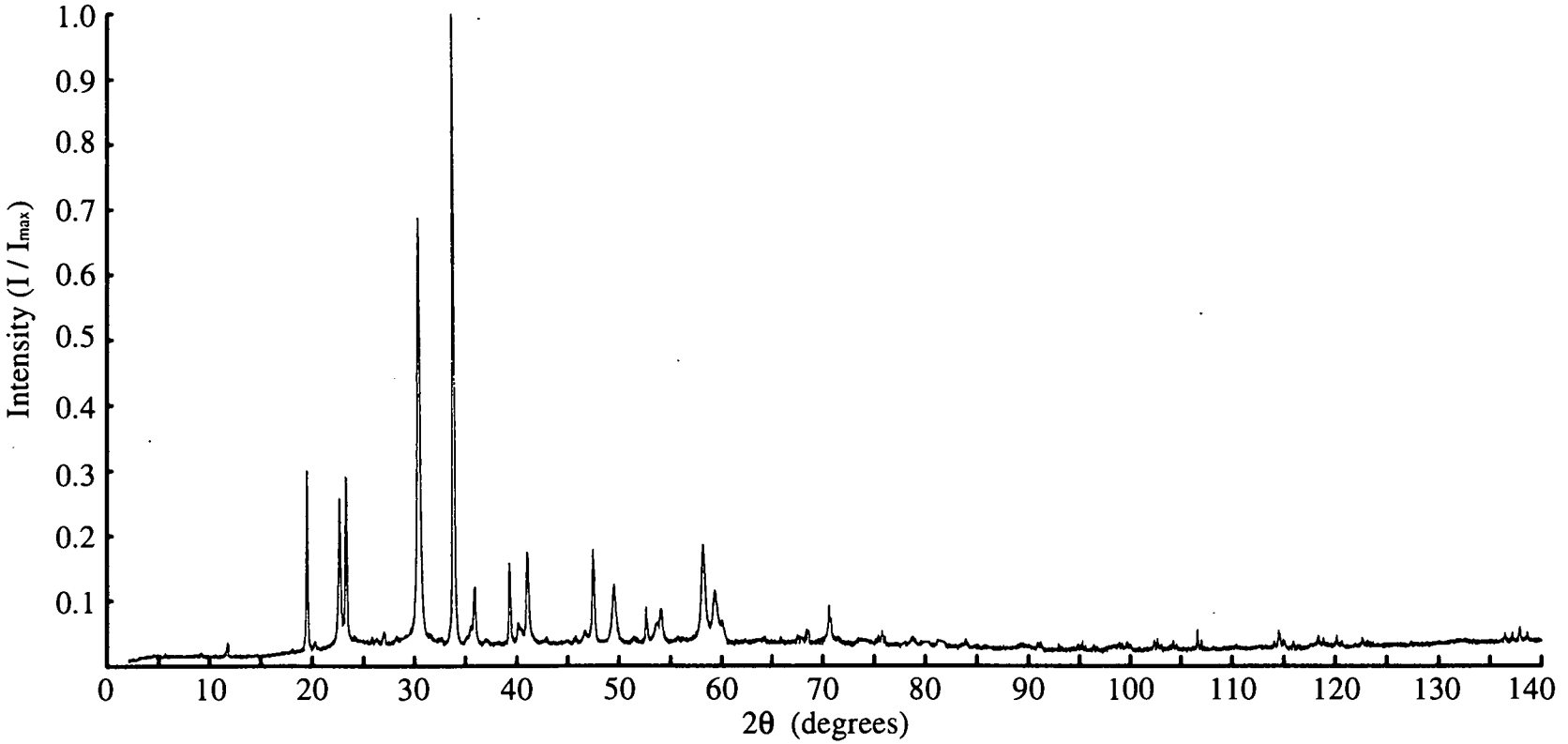

Fig. 6.2 Typical powder X-ray diffraction pattern of "sanidine hydrate" (run 56)

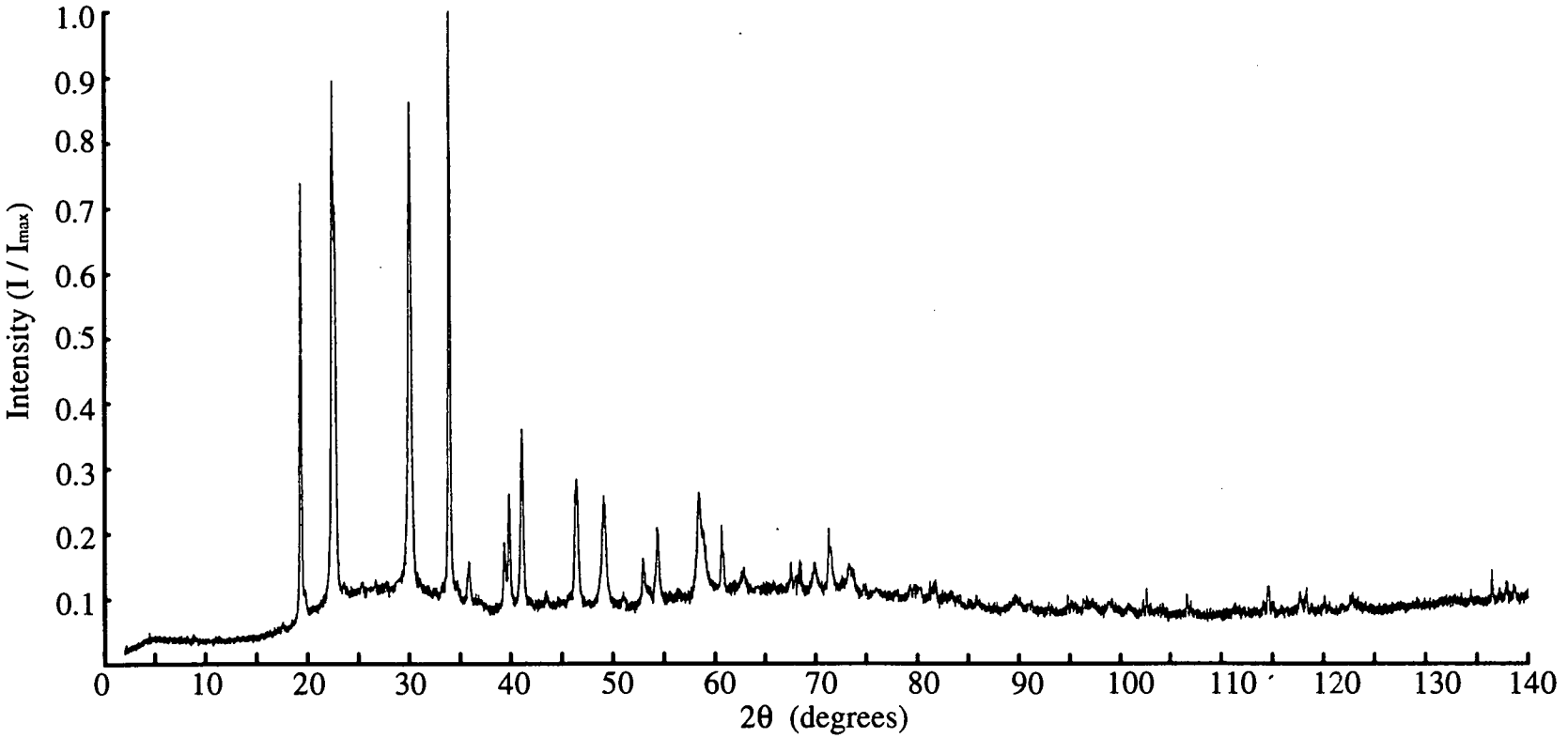

Fig. 6.3 Typical powder X-ray diffraction pattern of "hexasanidine" ("sanidine hydrate" from run 61 after dehydration by thermogravimetric analysis)

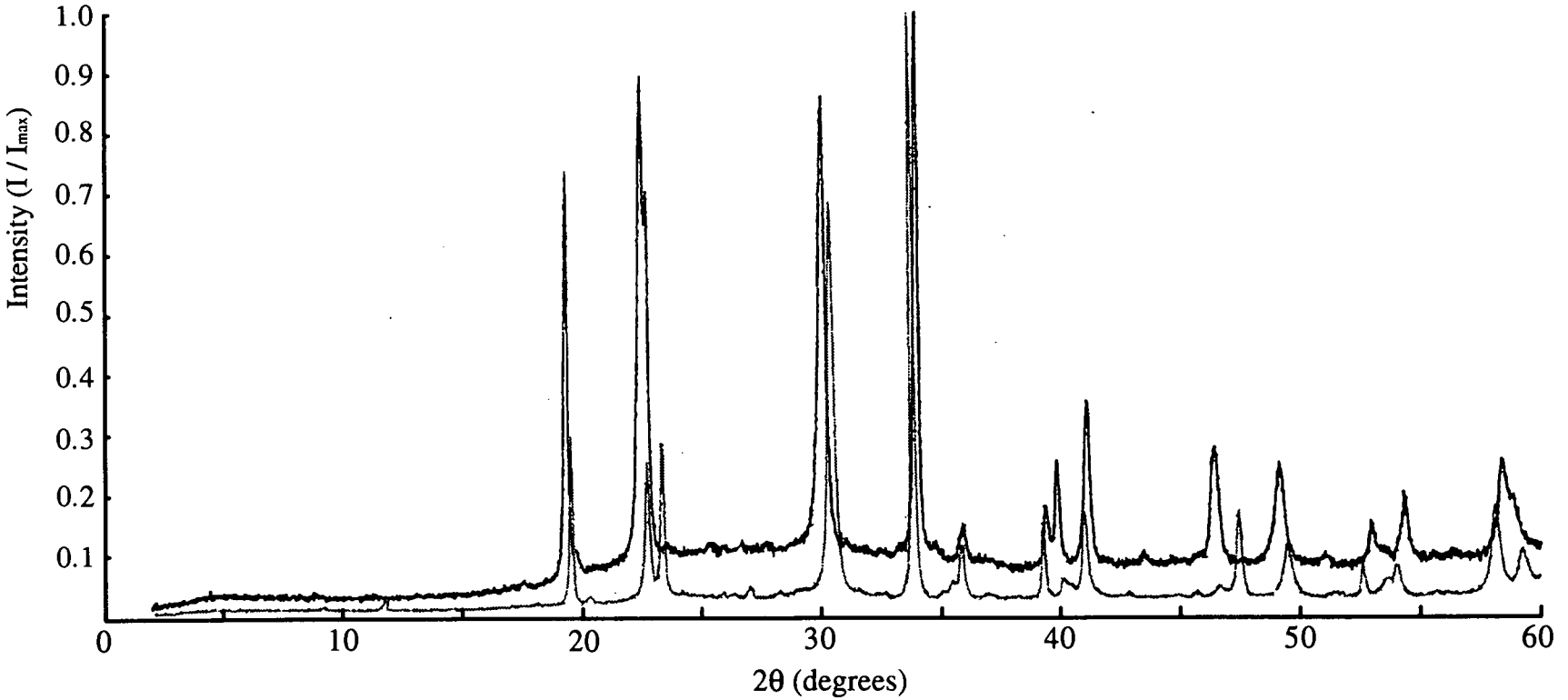

Fig. 6.4. An enlarged comparison of the powder X-ray diffraction patterns shown in Figures 6.2 and 6.3 in the 0 to 60 2θ range. "Sanidine hydrate" (run 56) is shown in grey and "hexasanidine" (run 61) is shown in black. The difference in the background intensity is probably the result of the different quantities of sample used although it could also be caused by amorphous material within the sample. A smaller quantity of sample was used for the "hexasanidine" and so the background shows more of the intensity resulting from the glass mounting slide.

Table 6.2. Unit cell parameters calculated, using a hexagonal primitive cell, for samples of "sanidine hydrate" synthesised at various pressures and temperatures.

Run number	Pressure (GPa)	Temperature (°C)	a (nm)	c (nm)	volume (nm^3)	c/a
16a	2.930	550	0.5337	0.7705	0.1901	1.444
16b	2.930	550	0.5337	0.7712	0.1902	1.445
17	2.923	550	0.5337	0.7714	0.1903	1.445
22	2.879	550	0.5337	0.7711	0.1902	1.445
50a	2.855	550	0.5338	0.7718	0.1905	1.446
50b	2.855	550	0.5339	0.7716	0.1905	1.445
72	2.855	450	0.5338	0.7709	0.1902	1.444
56a	2.855	650	0.5336	0.7718	0.1903	1.446
56b	2.855	650	0.5338	0.7710	0.1903	1.444
77	2.855	680	0.5335	0.7716	0.1902	1.446
75	2.737	500	0.5338	0.7712	0.1903	1.445
76	2.737	600	0.5334	0.7712	0.1901	1.446
61a	2.721	680	0.5336	0.7718	0.1903	1.446
61b	2.721	680	0.5336	0.7718	0.1903	1.447
Mean			0.5337	0.7714	0.1903	1.445
Range			± 0.0003	± 0.0009	± 0.0002	± 0.002

Table 6.3. Unit cell parameters calculated, using a hexagonal primitive cell, for samples of "hexasanidine" synthesised by dehydrating samples of "sanidine hydrate" using thermogravimetric analysis (see Section 5.3).

Run number	Pressure (GPa)	Temperature (°C)	a (nm)	c (nm)	volume (nm^3)	c/a
61	2.721	680	0.5290	0.7815	0.1894	1.477
72	2.855	450	0.5289	0.7819	0.1895	1.448
75	2.737	500	0.5278	0.7819	0.1895	1.479
76	2.737	600	0.5288	0.7823	0.1894	1.479
16a	2.830	550	0.5291	0.7818	0.1895	1.478
16b	2.930	550	0.5289	0.7818	0.1894	1.478
17a	2.923	550	0.5289	0.7818	0.1894	1.478
17b	2.923	550	0.5291	0.7817	0.1895	1.477
Mean			0.5288	0.7818	0.1895	1.478
Range			±0.0010	±0.0005	±0.0001	±0.0001

Table 6.4. The positions of potential X-ray diffraction peaks for "sanidine hydrate" if the cell parameters are taken as a = 0.5337 nm and c = 0.7714 nm and the unit cell is hexagonal primitive.

2θ	h	k	l	2θ	h	k	l	2θ	h	k	l
11.462	0	0	1	73.867	3	1	0	109.380	1	0	8
19.187	1	0	0	75.053	3	1	1	110.243	4	1	3
22.406	1	0	1	75.306	2	2	2	111.469	2	1	7
23.040	0	0	2	76.907	1	0	6	111.993	3	2	4
30.153	1	0	2	78.574	3	1	2	112.612	2	2	6
33.555	1	1	0	79.573	3	0	4	112.788	4	0	5
34.863	0	0	3	81.145	2	2	3	112.875	5	0	0
35.569	1	1	1	83.371	1	1	6	114.120	5	0	1
38.940	2	0	0	83.534	2	1	5	116.107	3	1	6
40.095	1	0	3	83.614	4	0	0	116.291	1	1	8
40.724	2	0	1	84.354	3	1	3	117.936	5	0	2
41.098	1	1	2	84.763	4	0	1	118.496	3	0	7
45.730	2	0	2	86.566	2	0	6	119.051	4	1	4
47.084	0	0	4	88.197	4	0	2	119.900	2	0	8
49.166	1	1	3	88.691	0	0	7	119.988	3	3	0
51.290	1	0	4	89.178	2	2	4	121.316	3	3	1
52.327	2	1	0	89.913	3	0	5	123.640	3	2	5
53.250	2	0	3	91.874	1	0	7	123.736	4	2	0
53.757	2	1	1	92.361	3	1	4	124.624	5	0	3
57.900	2	1	2	93.177	3	2	0	125.121	4	2	1
59.051	1	1	4	93.914	4	0	3	125.421	3	3	2
59.904	0	0	5	94.322	3	2	1	127.351	4	0	6
59.996	3	0	0	96.128	2	1	6	127.974	0	0	9
61.307	3	0	1	97.770	3	2	2	129.429	4	2	2
62.695	2	0	4	98.268	1	1	7	130.071	2	2	7
63.519	1	0	5	99.505	2	2	5	131.688	4	1	5
64.426	2	1	3	99.586	4	1	0	131.692	2	1	8
65.147	3	0	2	100.746	4	1	1	132.133	1	0	9
70.439	1	1	5	101.499	2	0	7	132.788	3	3	3
70.524	2	2	0	101.996	4	0	4	134.370	3	1	7
71.302	3	0	3	102.583	3	0	6	135.055	5	0	4
71.731	2	2	1	102.749	3	1	5	136.220	5	1	0
73.017	2	1	4	103.586	3	2	3	137.294	4	2	3
73.615	0	0	6	104.258	4	1	2	137.898	5	1	1
73.784	2	0	5	106.039	0	0	8				

Table 6.5. The positions of potential X-ray diffraction peaks for "hexasanidine" if the cell parameters are taken as a = 0.5228 nm and c = 0.7818 nm and the unit cell is hexagonal primitive.

2θ	h	k	l	2θ	h	k	l	2θ	h	k	l
11.309	0	0	1	74.667	3	1	0	107.406	1	0	8
19.366	1	0	0	75.818	3	1	1	110.329	2	1	7
22.482	1	0	1	75.849	1	0	6	111.283	4	1	3
22.729	0	0	2	75.916	2	2	2	112.206	2	2	6
30.031	1	0	2	79.236	3	1	2	112.688	3	2	4
33.875	1	1	0	79.624	3	0	4	112.998	4	0	5
34.385	0	0	3	81.589	2	2	3	114.350	1	1	8
35.822	1	1	1	82.455	1	1	6	114.492	5	0	0
39.316	2	0	0	83.192	2	1	5	115.721	5	0	1
39.764	1	0	3	84.567	4	0	0	115.754	3	1	6
41.040	2	0	1	84.854	3	1	3	117.425	3	0	7
41.185	1	1	2	85.684	4	0	1	117.962	2	0	8
45.892	2	0	2	85.714	2	0	6	119.487	5	0	2
46.421	0	0	4	87.211	0	0	7	119.926	4	1	4
49.041	1	1	3	89.025	4	0	2	121.853	3	3	0
50.745	1	0	4	89.406	2	2	4	123.172	3	3	1
52.849	2	1	0	89.692	3	0	5	124.087	3	2	5
53.206	2	0	3	90.454	1	0	7	124.933	0	0	9
54.232	2	1	1	92.649	3	1	4	125.755	4	2	0
58.247	2	1	2	94.305	3	2	0	126.108	5	0	3
58.694	1	1	4	94.592	4	0	3	127.138	4	2	1
59.028	0	0	5	95.422	3	2	1	127.176	4	0	6
60.610	3	0	0	95.452	2	1	6	127.257	3	3	2
61.879	3	0	1	96.955	1	1	7	128.991	1	0	9
62.417	2	0	4	98.785	3	2	2	129.074	2	2	7
62.739	1	0	5	99.461	2	2	5	129.690	2	1	8
64.584	2	1	3	100.234	2	0	7	131.451	4	2	2
65.601	3	0	2	100.850	4	1	0	132.347	4	1	5
69.826	1	1	5	101.985	4	1	1	133.386	3	1	7
71.276	2	2	0	102.016	3	0	6	134.626	3	3	3
71.578	3	0	3	102.472	4	0	4	136.486	5	0	4
72.447	2	2	1	102.765	3	1	5	137.933	1	1	9
72.479	0	0	6	104.038	0	0	8	138.747	3	0	8
72.946	2	1	4	104.466	3	2	3	138.944	5	1	0
73.244	2	0	5	105.420	4	1	2	139.381	4	2	3

6.4 Conclusions

The unit cell parameters for "sanidine hydrate" do not vary systematically with pressure and temperature of synthesis. The range in values is small with the mean values for the cell parameters being a = 0.5337 (±0.0003) nm, c = 0.7714 (±0.0009) nm, V = 0.1903 (±0.0002) nm^3 and c/a = 1.445 (±0.002). This seems to imply that there is no variation in the water content over the pressure and temperature range studied, however, the maximum variation cannot be large as the cell parameters of "hexasanidine", which contains no structural "water", are not very different to those for "sanidine hydrate". The cell parameters of "hexasanidine" are a = 0.5288 (±0.001) nm, c = 0.7818 (±0.0005) nm, V = 0.1895 (±0.0001) nm^3 and c/a = 1.478 (±0.0001). The difference in cell parameters between samples with an average water content of 0.83 moles per formula unit ("sanidine hydrate") and samples with no water in their structure ("hexasanidine") are a = -0.0049 and c = 0.0104. Hence any slight variation in the cell parameters as a result of variation in the water content may well be hard to detect. The fact that "hexasanidine" can be synthesised means that the water content of "sanidine hydrate" can vary but does not appear to do so significantly for the pressure and temperature range studied.

If these cell parameters are compared with those calculated by Viswanathan et al (1992) (Fig. 2.9, Chapter 2), for cymrite and hexacelsian, the "sanidine hydrate" and "hexasanidine" analogues respectively, it can be seen that the values are similar and that the dehydration of "sanidine hydrate" also results in a contraction in the a direction but an expansion in the c direction of the unit cell (Table 6.6).

Table 6.6. A comparison of the cell parameters for "sanidine hydrate", "hexasanidine", cymrite and hexacelsian. Data for cymrite and hexacelsian is taken from Viswanathan et al. (1992)

	a	change	c	change
"sanidine hydrate"	0.5337	} -0.0049	0.7714	} 0.0104
"hexasanidine"	0.5288		0.7818	
cymrite	0.534	} -0.004	0.769	} 0.008
hexacelsian	0.530		0.778	

Chapter 7
Thermodynamic Analysis

7.1 Introduction

In the previous chapters new data on the properties of the phase "sanidine hydrate" and constraints on its reaction to form sanidine and water have been described (reaction 1).

$$KAlSi_3O_8.nH_2O = KAlSi_3O_8 + nH_2O. \quad (1)$$
$$\text{"sanidine hydrate"} = \text{sanidine} + \text{water.}$$

In theory these data can be used to evaluate some of the thermodynamic parameters associated with this reaction (1), and thus to calculate the pressure-temperature locus of the reaction outside the range of the experimental brackets and to predict the position of further reactions.

This chapter describes attempts to estimate the thermodynamic parameters of enthalpy and entropy of the reaction of "sanidine hydrate" to form sanidine and water (1) using new data reviewed below (see next section). The thermogravimetric data did not give sufficiently well-constrained results to describe the regular variation of structural H_2O in "sanidine hydrate". The thermodynamics of the dehydration of "sanidine hydrate" to form "hexasanidine" are considered. This shows more clearly that the thermogravimetric data were insufficient and not of good enough quality to calculate isopleths of constant structural "water" content on a pressure-temperature graph.

Two methods of thermodynamic analysis of reaction (1), which assumed no variation in the water content, were therefore attempted and are described below. The first is that as described by Chatterjee (1991) and calculates the average enthalpy and entropy over the region of the experimental brackets. The method takes no account of the variation of the heat capacity with temperature. Thus these figures cannot be used to extrapolate far beyond the experimental range. The second method takes into account the variation of the heat capacity of the reaction with temperature which should allow the extrapolation of the reaction on a pressure-temperature graph to be extended further than with the first method. However, in this case the data were not of a sufficient quality to make this method a significant improvement on Chatterjee's method. Both these methods were limited by the quality of the data. Ideally the reversal brackets should cover a larger temperature range, limit the reaction to a smaller pressure bracket and be at more frequent temperature intervals. In this instance it was not possible to improve on the data, as at higher temperatures the sample would be at least partially molten (Goldsmith and Peterson 1990) and at lower temperatures the duration of the experiment would be impracticably long. The size of the pressure bracket was as narrow as could be measured accurately with the solid media apparatus (see Section 3.3.4).

7.2 Review of the new data acquired in this study

Chapter 4 presented the results of reversal experiments on the reaction

$$KAlSi_3O_8.nH_2O = KAlSi_3O_8 + nH_2O. \quad (1)$$

"sanidine hydrate" = sanidine + water.

These experiments limited the equilibrium position of the reaction to lie within four pressure-temperature brackets. If the error in measuring the pressure is taken into account then the reaction must lie between 2.30 GPa and 2.55 GPa at 450°C, 2.33 GPa and 2.63 GPa at 550°C, 2.60 GPa and 2.80 GPa at 650°C and 2.63 GPa and 2.76 GPa at 680°C.

In addition the water content of "sanidine hydrate" was measured by thermogravimetric analysis. The results of that investigation are listed and discussed in Section 5.3. The water content of "sanidine hydrate" did not appear to vary systematically with the pressure and temperature of synthesis (see Section 5.3 and Table 5.1). The lack of systematic variation in the measured structural "water" contents meant that calculations of the thermodynamic properties of the dehydration of "sanidine hydrate" was not possible (see Section 7.5). Taken together the samples gave an average water content of 0.83 molecules per formula unit, with a large margin of error. The error may have been the result of a variety of potential contaminants. Contaminants with no volatile component would cause the thermogravimetric samples to appear to have less water per formula unit of "sanidine hydrate". Therefore it was considered possible that the water content could be as much as one molecule per formula unit, comparable to that of cymrite.

Here the two cases are considered where n, the number of molecules of H_2O per formula unit of "sanidine hydrate", first has the average value of 0.83, taken from the thermogravimetric weight losses, and second if the thermogravimetric samples were strongly contaminated, when n = 1.

In the first case when n = 0.83 equation (1) becomes

$$KAlSi_3O_8.0.83H_2O = KAlSi_3O_8 + 0.83H_2O, \quad (2)$$

or alternatively if n = 1,

$$KAlSi_3O_8.H_2O = KAlSi_3O_8 + H_2O. \quad (3)$$

Finally in Chapter 6 the unit cell volume of "sanidine hydrate", calculated from powder X-ray diffraction, was found to be 0.1903 nm^3.

7.3 List of symbols used in Chapter 7

The symbols used in the thermodynamic calculations in this chapter are listed below.

ΔC_p = Heat capacity change of the reaction at fixed pressure,

$f(H_2O)$ = Fugacity of water at T and P,

$\Delta G^{\circ}_{(r)\,T,P}$ = Molar Gibbs energy change of the reaction at T and P,

$\Delta H^{\circ}_{(r)\,T,P}$ = Molar enthalpy change of the reaction at T and P,

$\Delta H^{\circ}_{(r)<T>}$ = Average molar enthalpy change of the reaction over the bracketed temperature range,

$\Delta S^{\circ}_{(r)\,T,P}$ = Molar entropy change of the reaction at T and P,

$\Delta S^{\circ}_{(r)<T>}$ = Average molar entropy change of the reaction over the bracketed temperature range,

$\Delta V^{\circ}_{s\,T}$ = Molar volume change of solids at T,

α = Coefficient of isobaric thermal expansion,

β = Coefficient of isothermal compressibility,

K = Equilibrium constant of the reaction,

n = Number of moles of H_2O used in reaction (1),

P = Pressure (calculations use bars apart from the fugacity polynomial),

R = Gas constant, 8.3143 J $K^{-1}mol^{-1}$,

T = Temperature (calculations in Kelvin).

a(P), b(P), c(P) = Temperature coefficients, expressed as a function of pressure, in the fugacity polynomial (equation 5) for $RT\ln f(H_2O)$

$\Delta G^{*}_{(r)}$ = expression for the Gibbs energy involving only the terms with errors that need to be propagated in the pressure-temperature extrapolation of the reaction

$\sigma_{\Delta G^*}$ = propagated error in $\Delta G^{*}_{(r)}$,

σ_T = propagated error in the temperature position of the reaction

Conventionally σ represents a standard deviation but in this work there were not enough data points to justify calculating a standard deviation and therefore the values of σ represent the maximum and minimum variation. The values quoted should be greater than the standard deviation and roughly equivalent to 2σ or 3σ.

7.4 General theory and assumptions

For an ideal solution involving solids and fluids a general equation for the change in free energy of a reaction (e.g. Spear, 1993, Chatterjee, 1991) would be

$$\Delta G^{\circ}_{(r)} = \Delta H^{\circ}_{(r)1,298} + \int_{298}^{T} \Delta C_P dT - T\Delta S^{\circ}_{(r)1,298} - T\int_{298}^{T} \frac{\Delta C_P}{T} dT$$

$$+ (P-1)(\Delta V^{\circ}_{s\,298} + \Delta(\alpha V^{\circ}_{s\,298})(T-298) - \Delta(\beta V^{\circ}_{s\,298})P/2) \qquad (4)$$

$$+ nRT \ln f(H_2O) + RT \ln K$$

The symbols used in this equation are listed in Section 7.3.

In this case it will be assumed that the volume change of the solids with pressure and temperature is negligible as there are no data on the compressibility (β) and thermal expansion (α) of "sanidine hydrate". This may be a rash assumption since these values in other devolatilisation reactions can become quite significant at high pressures (Powell and Holland, 1985). $\Delta V_{s\,298}$ can be calculated from the unit cell volumes measured by powder X-ray diffraction (Chapter 6).

Molar volume of "sanidine hydrate" = unit cell volume x Avagadro's number
= 0.1903 x 6.022 x 10^{23} nm^3
= 1.146 x 10^{23} nm^3
= 11.46 $Jbar^{-1}$.

The unit cell for sanidine has a volume of 0.7229 nm^3 (Smith and Brown, 1988). This unit cell has a C2/m structure containing four formula units per unit cell. The primitive cell would therefore have a volume of 0.1807 nm^3.

Molar volume of sanidine = 1.088 x 10^{23} nm^3
= 10.88 $Jbar^{-1}$.

Therefore for the order the equation is written in (1), where "sanidine hydrate" is the reactant $\Delta V_{s\,298}$ = - 0.58 $Jbar^{-1}$.

In Section 7.5 the dehydration reaction of "sanidine hydrate" to form "hexasanidine" (equation 7) is considered. It is probable that "sanidine hydrate" has a variable water content but the thermodynamic data were inadequate and hence the variation with pressure and temperature is not known. Therefore the best approximation available for calculation of the thermodynamic properties of the reaction between sanidine and water to form "sanidine hydrate" (equation 1) is to consider the case where "sanidine hydrate" shows no variation of this water content with pressure and temperature.

Thus two cases are considered here. In the first case (equation 2) the average value for the water content of "sanidine hydrate", of 0.83 molecules of H_2O per formula unit, was used. In order to see how a different water content affects the values obtained a second case was evaluated in which "sanidine hydrate" contains 1 molecule of H_2O per formula unit (equation 3). This value might be the maximum possible water content of "sanidine hydrate". Since in both the cases considered in equations (2) and (3) the composition of "sanidine hydrate" does not change the phase can therefore be considered as pure, showing no solid solution. In this case the equilibrium constant K for the reaction will be of value 1. Hence RTlnK = 0. This assumption may not be valid outside the pressure-temperature range studied.

$RT\ln f(H_2O)$ can be calculated at various pressures and temperatures from the fugacity polynomial for H_2O of Holland and Powell (1985), as shown in equation (5), which is valid up to 3.0 GPa. Temperatures used must be in Kelvin and pressures in kilobars.

$$RT\ln f(H_2O) = a(P) + b(P)T + c(P)T^2 \quad \text{in kJmol}^{-1} \qquad (5)$$

where: $a(P) = a_1 + a_2P + a_3P^2 + a_4P^{-1} + a_5P^{-2}$

$b(P) = b_1 + b_4P^{-2}$

$c(P) = c_1 + c_2P + c_3P^{-2} + c_4P^{-0.5} + c_5P^{-1} + c_6P^{-3}$

and:

$a_1 = -40.388$	$b_1 = 0.117372$	$c_1 = -7.3681 \times 10^{-6}$
$a_2 = 1.6474$		$c_2 = 1.10295 \times 10^{-7}$
$a_3 = -0.0062115$		$c_3 = -9.8774 \times 10^{-7}$
$a_4 = 2.0068$	$b_4 = -0.0004671$	$c_4 = -2.4819 \times 10^{-5}$
$a_5 = 0.0562929$		$c_5 = 8.2948 \times 10^{-6}$
		$c_6 = 8.33667 \times 10^{-8}$

Equation (4) thus reduces to

$$\Delta G^\circ_{(r)} = \Delta H^\circ_{(r)1,298} + \int_{298}^{T} \Delta C_P dT - T\Delta S^\circ_{(r)1,298} - T\int_{298}^{T} \frac{\Delta C_P}{T} dT + \Delta V^\circ_{s\,298}\,(P-1) + nRT\ln f(H_2O) \qquad (6)$$

where the unknowns are $\Delta H^\circ_{(r)1,298}$, $\Delta S^\circ_{(r)1,298}$ and ΔC_P.

7.5 Thermodynamics of the "water" in "sanidine hydrate"

It was shown in Section 5.3 that the water content of "sanidine hydrate" could vary, as it was possible to dehydrate it to form an anhydrous phase with a similar structure and cell parameters. Attempts to find a systematic variation in the water content with pressure and temperature of synthesis did not appear to give useful results. However, it would be interesting to see if this water content data did show any systematic variation by calculating the thermodynamic parameters of the dehydration of "sanidine hydrate" (reaction 7). If the thermogravimetric data were systematic the thermodynamic parameters might be reasonably similar to those for the dehydration of cymrite to form hexacelsian.

$$KAlSi_3O_8 + nH_2O = KAlSi_3O_8.nH_2O. \quad (7)$$
"hexasanidine" + water = "sanidine hydrate".

where n lies between 1 and 0 as shown in Chapter 5 and is assumed to be a continuous ideal solid solution between these values.

Taking the standard states at the pressure and temperature of interest and the maximum solubility of water as n = 1, then equation (4), at equilibrium, can be rewritten as

$$\Delta G^{\circ}_{(r)} = \Delta H^{\circ}_{(r)1,T} - T\Delta S^{\circ}_{(r)1,T} + \Delta V^{\circ}_{s\,298}(P-1) - RT\ln f(H_2O) + RT\ln K = 0. \quad (8)$$

where K = X/(1-X) and X is the mole fraction of the hydrous $KAlSi_3O_8.H_2O$ end member and may be calculated for each thermogravimetric datum from Table 5.1. $\Delta V^{\circ}_{S,298}$ for reaction (7) calculated from the change in cell parameters is -0.0008 nm^3 and may be ignored.

Rearranging equation (8) gives

$$\frac{\Delta H^{\circ}_{(r)1,T}}{T} - \Delta S^{\circ}_{(r)1,T} = -R\ln\left(\frac{X}{1-X}\right) + \frac{RT\ln f(H_2O)}{T} \quad (9)$$

The function for $RT\ln f(H_2O)$ is known from the fugacity polynomial for water given in equation (5). If $(RT\ln f(H_2O))/T$ is calculated for each of the points at which X is known, a plot of the right hand side of equation (9) against 1/T should show a linear correlation with a slope of $\Delta H^{\circ}_{(r)1,T}$ and an intercept at 1/T = 0 of $-\Delta S^{\circ}_{(r)1,T}$. These values should be the enthalpy and entropy, respectively, of reaction (7). The results are shown in Figure 7.1.

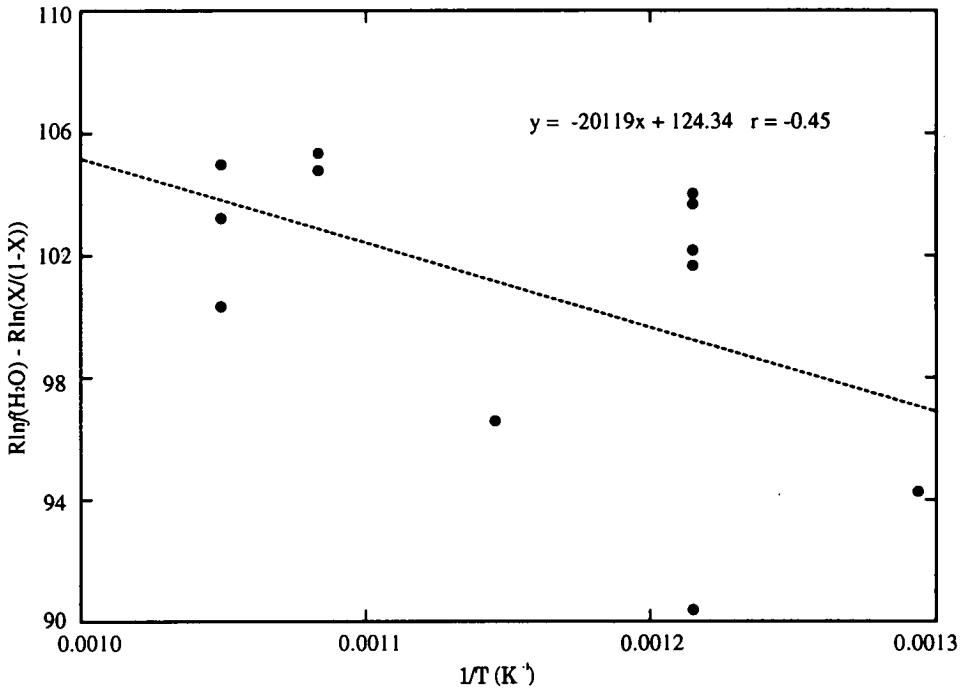

Fig. 7.1. Method of determining $\Delta H^{\circ}_{(r)1,T}$ and $\Delta S^{\circ}_{(r)1,T}$ for the dehydration of "sanidine hydrate" (reaction 26). The slope of the best fit straight line is $\Delta H^{\circ}_{(r)1,T}$ and the intercept at $1/T = 0$ is $-\Delta S^{\circ}_{(r)1,T}$

The correlation shown in Figure 7.1 is not good and therefore the values determined from the best fit line should be treated with caution. The best fit line, determined by linear "least-squares" regression, gives values of -20119 (±40900) $Jmol^{-1}$ for $\Delta H^{\circ}_{(r)1,T}$ and -124.34 (±48.04) $JK^{-1}mol^{-1}$ for $\Delta S^{\circ}_{(r)1,T}$. The errors in these measurements are the standard deviation in the points from the line. The values for the barium analogue reaction between cymrite and hexacelsian were $\Delta H^{\circ}_{(r)1,T}$ = -59000 (±3000) $Jmol^{-1}$ and $\Delta S^{\circ}_{(r)1,T}$ = -133.47 (±3.2) $JK^{-1}mol^{-1}$. These respective values for the "sanidine hydrate"- hexasanidine and cymrite-hexacelsian reactions are reasonably similar to each other, although the errors are considerably larger for the values calculated here.

It is possible to calculate isopleths of constant water content if these values for $\Delta H^{\circ}_{(r)1,T}$ and $\Delta S^{\circ}_{(r)1,T}$ are put back into equation (9). If the fugacity polynomial from equation (5) is also put into equation (9) it can be rewritten as

$$0 = c(P)T + \left(\Delta S^{o}_{(r)1,T} - R\ln\left(\frac{X}{1-X}\right) + b(P)\right) + \frac{a(P) - \Delta H^{o}_{(r)1,T}}{T} \qquad (10)$$

where $a(P)$, $b(P)$ and $c(P)$ are the coefficients of temperature from the fugacity polunomial.

If equation (10) is multiplied throughout by T it gives a quadratic equation in T as shown in equation (11)

$$0 = c(P)T^2 + \left(\Delta S^{o}_{(r)l,T} - R\ln\left(\frac{X}{1-X}\right) + b(P) \right)T + \left(a(P) - \Delta H^{o}_{(r)l,T}\right) \qquad (11)$$

At each value of X chosen, this equation will result in two solutions for temperature for each value of pressure. One set of the solutions should be a reasonable explanation of the thermodynamic data. If different values of X are chosen a plot of isopleths of constant water composition can be drawn for each value of X. If the mean values for the enthalpy and entropy are used the resultant plot would look similar to that for the dehydration of cymrite, calculated by Graham et al. (1992), and shown in Figure 2.7 in Chapter 2. However, the errors in the enthalpy and entropy are too large to make a plot like this useful. If the errors in the enthalpy and entropy are propagated, using the same techniques as described in section 7.6.1, to calculate the standard deviation in the temperature position of the reaction (σ_T) for each of the isopleths the errors are large. For example σ_T is 300°C at 100°C and 400°C at 1000°C.

The values for the enthalpy and entropy of the "sanidine hydrate" to hexacelsian transformation, calculated above, were therefore not considered to be adequate for use in the calculation of the thermodynamic properties of the reaction between sanidine and water to form "sanidine hydrate". Hence the water content of "sanidine hydrate" was assumed to be constant in the calculations described in the subsequent sections. The effect of the structural "water" variation in cymrite did not alter the pressure-temperature position of the reaction substantially and therefore the assumption of constant water content in "sanidine hydrate" should result in a reaction position not far removed from the true one in the range of the experimental brackets.

7.6 Chatterjee's method

The method of Chatterjee (1991) calculates the average enthalpy $\Delta H^{\circ}_{(r)<T>}$ and average entropy $\Delta S^{\circ}_{(r)<T>}$ over the pressure and temperature range of the experiments, and thus equation (6) can be rewritten as

$$\Delta G^{\circ}_{(r)} = \Delta H^{\circ}_{(r)<T>} - T\Delta S^{\circ}_{(r)<T>} + \Delta V^{\circ}_{s\,298}\,(P-1) + nRT\ln f(H_2O)\,. \qquad (12)$$

At equilibrium $\Delta G^{\circ}_{(r)} = 0$ so equation (12) becomes

$$T\Delta S^{\circ}_{(r)<T>} - \Delta H^{\circ}_{(r)<T>} = \Delta V^{\circ}_{s\,298}\,(P-1) + nRT\ln f(H_2O)\,. \qquad (13)$$

This method avoids knowing the heat capacity function of the reaction but means that the variation of $\Delta H^{\circ}_{(r)}$ and $\Delta S^{\circ}_{(r)}$ with temperature is not known and therefore will result in some uncertainty in the extrapolation of the pressure-temperature curve.

In order to calculate $\Delta H^{\circ}_{(r)<T>}$ and $\Delta S^{\circ}_{(r)<T>}$ the right hand side of equation (13) is plotted against temperature for each of the reversal brackets. The values of pressure taken for the reversal brackets include the uncertainty in the pressure measurement i.e. the brackets are the widest possible pressure variation. The plotted points derived from equation (13) should lie on either side of an equilibrium line. The "best fit" line determined by linear least squares regression should have a slope of $\Delta S^{\circ}_{(r)<T>}$ and an intercept of $-\Delta H^{\circ}_{(r)<T>}$. The two cases when n = 0.83 (black) and when n = 1 (grey) are shown in Figure 7.2. The best fit straight lines through the centre of each bracket have a correlation coefficient of 1. For n = 0.83 $\Delta S^{\circ}_{(r)<T>}$ = 92.75 $JK^{-1}mol^{-1}$ and $\Delta H^{\circ}_{(r)<T>}$ = 18107 $Jmol^{-1}$. When n = 1, however, $\Delta S^{\circ}_{(r)<T>}$ = 113.25 $JK^{-1}mol^{-1}$ and $\Delta H^{\circ}_{(r)<T>}$ = 20023 $Jmol^{-1}$.

The error in these values can be determined by calculating the shallowest and steepest lines which lie between the limits of the brackets as shown in Figure 7.2. The slopes and intercepts of these lines represent the maximum possible variation in the enthalpy and entropy respectively as they include the pressure uncertainty. The uncertainty in the temperature measurement was not taken into account because the uncertainty in the temperature is relatively small in comparison to the pressure uncertainty and hence its effect would only reduce the error in the calculated

enthalpy and entropy if the errors were propagated. The maximum error in $\Delta S^{\circ}_{(r)<T>}$ is ± 8 $JK^{-1}mol^{-1}$ and the maximum error in $\Delta H^{\circ}_{(r)<T>}$ is ± 7000 $Jmol^{-1}$ when n = 1.

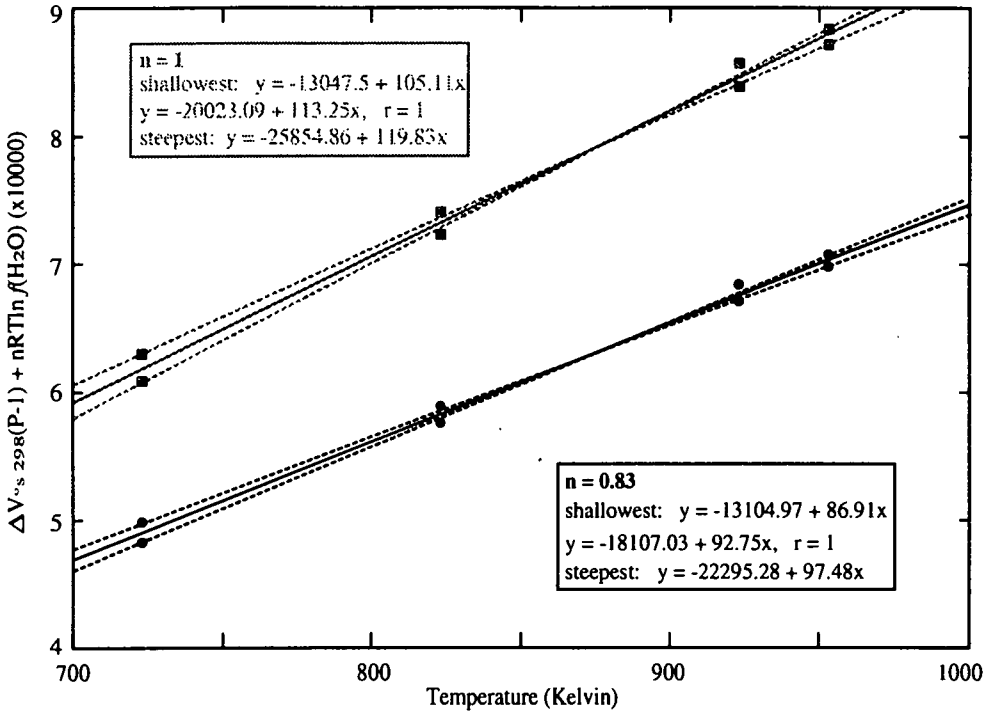

Fig. 7.2. Chatterjee's method for determining $\Delta S^{\circ}_{(r)<T>}$ and $\Delta H^{\circ}_{(r)<T>}$ of reaction 1. $\Delta S^{\circ}_{(r)<T>}$ is given by the slope of the straight line and $-\Delta H^{\circ}_{(r)<T>}$ is the intercept. The error in these figures is calculated from the lines of maximum and minimum gradient that fit between the brackets. r is the correlation coefficient of the best fit straight line through the centre of each bracket.

It is of interest to see how these values would affect the pressure and temperature extrapolation of the reaction outside the experimental range. If these values for $\Delta S^{\circ}_{(r)<T>}$ and $\Delta H^{\circ}_{(r)<T>}$ are put back into equation (13) the position of the reaction can be evaluated at other pressures and temperatures. Given the lack of information about ΔC_p this extrapolation will not be reliable outside the bracketed region.

Equation (13) can be written as

$$0 = nc(P)T^2 + (nb(P) - \Delta S^{\circ}_{(r)<T>})T + \Delta H^{\circ}_{(r)<T>} + \Delta V_s(P-1) + na(P) \qquad (14)$$

where a(P), b(P) and c(P) are the pressure function parts of the $RTlnf(H_2O)$ polynomial.

This is a quadratic equation which will always result in two values for each pressure chosen. However, only one of these two sets of numbers will pass within the reversal brackets and it is this set which is the relevant solution.

Figure 7.3 shows the pressure versus temperature curve for the reaction determined in this way. The two cases when n = 1 and n = 0.83 are almost coincident on the pressure-temperature graph.

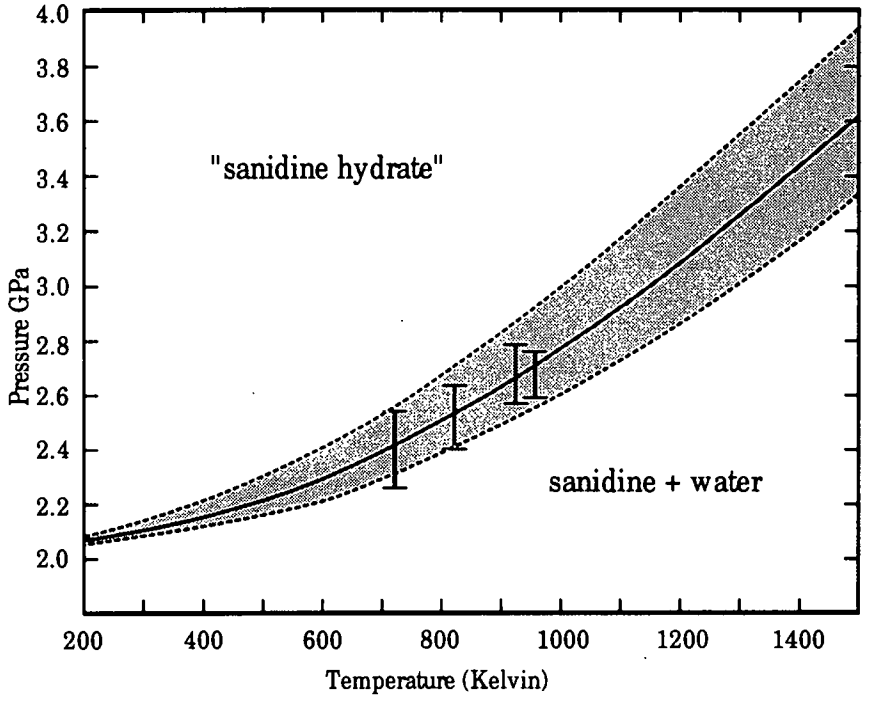

Fig. 7.3. Extrapolation of the reaction between sanidine and water to form "sanidine hydrate" (reaction 1, solid line) to pressures and temperatures outside the reversal brackets shown. The two cases where n = 1 and n = 0.83 are coincident on this plot. This method assumes the unlikely condition that the enthalpy and entropy do not change with pressure and temperature.
The maximum error in the value of the temperature (σ_T) at any equilibrium pressure is shown by the dotted lines (see Section 7.5.1). The extrapolated reaction could lie anywhere within the shaded area if only the calculated values for the enthalpy and entropy are taken into account.

7.6.1 *Error propagation*

In the previous section the values of the average enthalpy and entropy over the bracketed region were calculated. In addition the errors for these two figures were estimated. The extrapolation of the pressure-temperature position of the reaction was then shown in Figure 7.3, ignoring the variation of the change in heat capacity function of the reaction with temperature. The uncertainties in the enthalpy and

entropy measurements will result in a similarly large error (σ_T) in the temperature position of the reaction shown in Figure 7.3. This error can be evaluated by propagating the previously determined uncertainties in the enthalpy and entropy, using the methods of Chatterjee (1991).

If it is assumed that the quantities $\Delta V^{\circ}_{s\,298}$ and RTln$f$(H_2O) are known exactly then equation (12) can be rewritten as

$$\Delta G^{*}_{(r)} = \Delta H^{\circ}_{(r)<T>} - T\Delta S^{\circ}_{(r)<T>} + \Delta V^{\circ}_{s\,298}(P-1) + C \qquad (15)$$

where C includes all the terms with no errors.

A general equation for the propagation of errors of a function f(u,v) is

$$\sigma_x^2 = \left(\frac{\delta x}{\delta u}\right)_v^2 \sigma_u^2 + \left(\frac{\delta x}{\delta v}\right)_u^2 \sigma_v^2 + 2\rho_{uv}\sigma_u\sigma_v\left(\frac{\delta x}{\delta u}\right)_v\left(\frac{\delta x}{\delta v}\right)_u \qquad (16)$$

where σ is the standard deviation of a variable and ρ_{uv} is the correlation coefficient of variables u and v (Chatterjee, 1991).

If ΔG^* is considered as $\Delta G^* = f(T,P)$ then using equation (16)

$$\sigma^2_{\Delta G^*} = \left(\frac{\delta \Delta G^*}{\delta T}\right)_P^2 \sigma_T^2 + \left(\frac{\delta \Delta G^*}{\delta P}\right)_T^P \sigma_P^2. \qquad (17)$$

as P and T are non-covariant.

In order to solve for σ_T at any given equilibrium P (for which $\sigma_P = 0$) and by taking the derivative of equation (15) with respect to T, equation (17) can be rearranged to give

$$\sigma_T = \frac{\sigma_{\Delta G^*}}{\left|-\Delta S^{\circ}_{<T>}\right|}. \qquad (18)$$

$\sigma_{\Delta G^*}$ can be determined by considering equation (15) as $\Delta G^* = f(\Delta H^{\circ}_{(r)<T>}, \Delta S^{\circ}_{(r)<T>})$ and applying equation (16) to it i.e.

$$\sigma^2_{\Delta G^*} = \left(\frac{\delta \Delta G^*}{\delta \Delta H_{<T>}}\right)_P^2 \sigma^2_{\Delta H_{<T>}} + \left(\frac{\delta \Delta G^*}{\delta \Delta S_{<T>}}\right)_P^2 \sigma^2_{\Delta S_{<T>}} + 2\rho_{\Delta H_{<T>},\Delta S_{<T>}} \sigma^2_{\Delta H_{<T>}} \sigma^2_{\Delta S_{<T>}} \left(\frac{\delta \Delta G^*}{\delta \Delta H_{<T>}}\right)_P \left(\frac{\delta \Delta G^*}{\delta \Delta H_{<T>}}\right)_P \qquad (19)$$

If equation (19) is evaluated using the partial differentials of equation (15) and then substituted into equation (18) the error in the temperature position of the reaction calculated from the values of $\Delta H^{\circ}_{(r)<T>}$ and $\Delta S^{\circ}_{(r)<T>}$ alone is

$$\sigma_T = \frac{\left[\sigma^2_{\Delta H_{<T>}} + T^2\sigma^2_{\Delta S_{<T>}} - 2T\rho_{\Delta H_{<T>}\Delta S_{<T>}}\sigma_{\Delta H_{<T>}}\sigma_{\Delta S_{<T>}}\right]^{0.5}}{\left|-\Delta S_{<T>}\right|}. \qquad (20)$$

As the greatest possible deviation of $\Delta H^{\circ}_{(r)<T>}$ and $\Delta S^{\circ}_{(r)<T>}$ is known, the standard deviation must be less but with so few data points available it is meaningless to attempt a calculation of this deviation.

> "We might also comment that if the difference between N and (N-1) ever matters to you, then you are probably up to no good - e.g. trying to substantiate a questionable hypothesis with marginal data."
>
> Press et al (1992) page 605

In this case N = number of data points = 4 and hence the maximum deviation was used in these calculations rather than the standard deviation

If σ_T is calculated using the largest deviation in the enthalpy and entropy instead of the standard deviation the extrapolated pressure temperature position of the reaction must lie between the two dotted lines within the shaded area shown in Figure 7.3. The shaded area represents all of the potential positions of the reaction that could be calculated from the enthalpy and entropy values calculated in the previous section if the positions of the bracketing experiments are not taken into account. In the region of the brackets the position of the reaction is, of course, further restricted to lie between them.

7.7 An alternative method

It is possible to take account of the heat capacity change of the reaction ΔC_p without direct measurement of the heat capacity function of "sanidine hydrate" (C_{PSH}). In theory this should improve the extrapolation of the reaction to pressures and temperatures outside the reversal brackets as it does not assume that the heat capacity of the reaction (ΔC_p) does not vary with pressure and temperature. In practice, however, the data are not of a sufficient quality to make this method any more reliable. The method is explained below.

At equilibrium, reaction (6) becomes

$$0 = \Delta H^{\circ}_{(r)1,298} + \int_{298}^{T} \Delta C_P dT - T\Delta S^{\circ}_{(r)1,298} - T\int_{298}^{T} \frac{\Delta C_P}{T} dT + \Delta V^{\circ}_{s\,298}(P-1) + nRT \ln f(H_2O). \quad (21)$$

If we set

$$\Delta G^{\circ}_{(r)1,T} = \Delta H^{\circ}_{(r)1,298} + \int_{298}^{T} \Delta C_P dT - T\Delta S^{\circ}_{(r)1,298} - T\int_{298}^{T} \frac{\Delta C_P}{T} dT, \quad (22)$$

then at equilibrium if equation (22) is substituted into equation (6)

$$\Delta G^{\circ}_{(r)1,T} = -\Delta V^{\circ}_{s\,298}(P-1) - nRT \ln f(H_2O). \quad (23)$$

If equation (22) is differentiated twice with respect to temperature at constant pressure we get

$$\frac{\delta^2}{\delta T^2}(\Delta G^{\circ}_{(r)1,T})_P = -\frac{\Delta C_P}{T}$$

$$\Delta C_P = -T\frac{\delta^2}{\delta T^2}(\Delta G^{\circ}_{(r)1,T})_P \quad (24)$$

Therefore the heat capacity of the reaction can be determined by differentiating equation (22) twice with respect to temperature at constant pressure.

Rewriting equation (23) using the polynomial for the fugacity of water we get

$$\Delta G^{\circ}_{(r)1,T} = -\Delta V^{\circ}_{s\,298}(P-1) - n(a(P) + b(P)T + c(P)T^2)$$

which can be differentiated twice with respect to temperature at constant pressure to give

$$\frac{\delta^2}{\delta T^2}(\Delta G^{\circ}_{(r)1,T})_P = (-2nc(P))_P. \quad (25)$$

Therefore the heat capacity function of the reaction can be obtained by substituting (25) into (24) i.e.

$$\Delta C_P = (-2nc(P)T)_P. \quad (26)$$

In order to solve equation (21) we need to know

$$\int_{298}^{T} \Delta C_P dT = \int_{298}^{T} (-2nc(P)T)dT = \left[-nc(P)T^2\right]_{298}^{T} \quad (27)$$

and

$$\int_{298}^{T} \frac{\Delta C_P}{T} dT = \int_{298}^{T} (-2nc(P))dT = \left[-nc(P)T\right]_{298}^{T}. \quad (28)$$

If these are then put back into equation (21) we get

$$T\Delta S^{\circ}_{(r)1,298,} - \Delta H^{\circ}_{(r)1,298} = 2nc(P)T^2 + (nb(P) - 2x298nc(P))T + na(P) + \Delta V^{\circ}_{s\,298}(P-1). \quad (29)$$

If the right hand side of equation (29) is plotted for each of the pressure, temperature conditions of the reversal brackets then the "best fit" straight line which passes between these points should have $-\Delta H^{\circ}_{(r)1,298}$, as the intercept and $\Delta S^{\circ}_{(r)1,298}$ as the slope.

The result is shown in Figure 7.4 for the two cases where n = 1 (grey lines) and n = 0.83 (black lines). The best fit straight lines through the centre of each bracket have a correlation coefficient of 1. For n = 0.83 $\Delta S^{\circ}_{(r)<T>}$ = 85.01 $JK^{-1}mol^{-1}$ and $\Delta H^{\circ}_{(r)<T>}$ = 13199 $Jmol^{-1}$. When n = 1, however, $\Delta S^{\circ}_{(r)<T>}$ = 103.92 $JK^{-1}mol^{-1}$ and $\Delta H^{\circ}_{(r)<T>}$ = 14110 $Jmol^{-1}$. The errors in estimating $\Delta H^{\circ}_{(r)1,298}$, and $\Delta S^{\circ}_{(r)1,298}$ can again be evaluated by calculating the lines of maximum and minimum gradient that pass through the data points. The maximum deviation of $\Delta H^{\circ}_{(r)1,298}$ is 7000 $Jmol^{-1}$ and of $\Delta S^{\circ}_{(r)1,298}$ is 8.5 $JK^{-1}mol^{-1}$ when n = 1

Comparing the values of Figures 7.2 and 7.4 in Table 7.1 it is evident that the two methods show similar values for $\Delta H^{\circ}_{(r)1,298}$, and $\Delta H^{\circ}_{(r)<T>}$, and $\Delta S^{\circ}_{(r)1,298}$ and $\Delta S^{\circ}_{(r)<T>}$ for both methods of calculation.

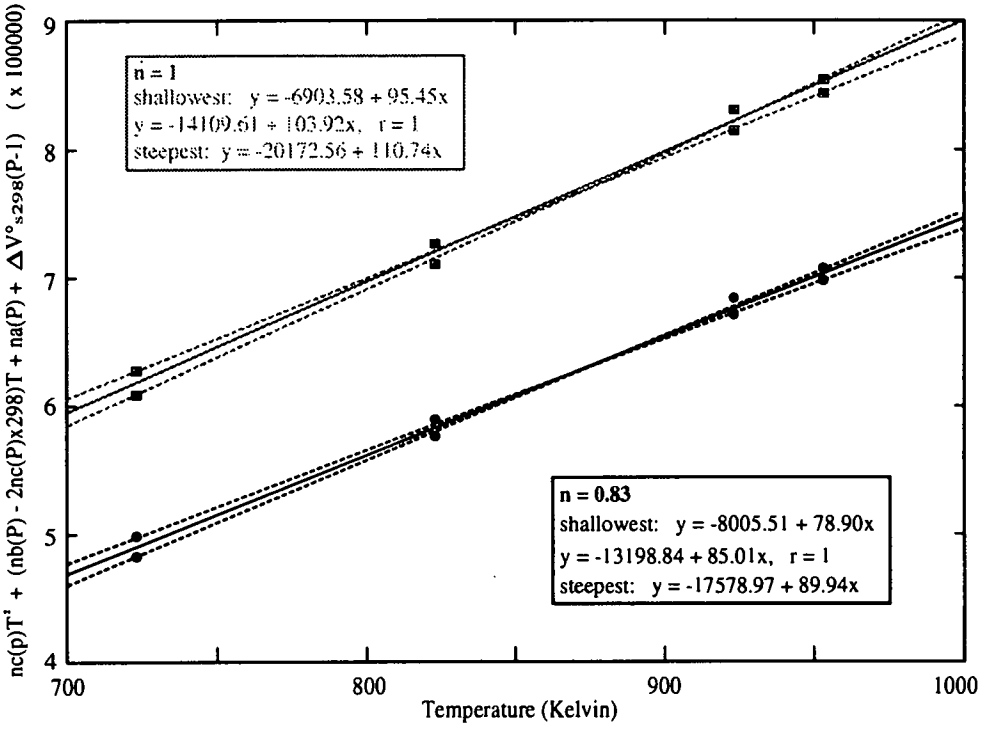

Fig. 7.4. Method for determining $\Delta H^{\circ}_{(r)1,298}$, and $\Delta S^{\circ}_{(r)1,298}$ of reaction 1. $\Delta S^{\circ}_{(r)1,298}$ is given by the slope of the straight line and $-\Delta H^{\circ}_{(r)1,298}$ is the intercept. The error for these figures is calculated from the lines of maximum and minimum gradient that fit between the brackets. r is the correlation coefficient of the best fit straight line through the centre of each bracket.

Table 7.1. A comparison of the values of enthalpy and entropy calculated from Chatterjee's method and the alternative method which takes account of the heat capacity of the reaction for the reaction between sanidine and water to form "sanidine hydrate".

	Chatterjee's method		Alternative method	
n = 0.83	$\Delta H^{\circ}_{(r)<T>}$	= 18107.03 $Jmol^{-1}$ + 4188.25 - 5002.06	$\Delta H^{\circ}_{(r)1,298}$	= 13198.84 $Jmol^{-1}$ + 4380.13 - 5913.33
	$\Delta S^{\circ}_{(r)<T>}$	= 92.75 $JK^{-1}mol^{-1}$ + 4.73 - 5.84	$\Delta S^{\circ}_{(r)1,298}$	= 85.01 $JK^{-1}mol^{-1}$ + 4.93 - 6.11
n = 1	$\Delta H^{\circ}_{(r)<T>}$	= 20023.09 $Jmol^{-1}$ + 5831.77 - 6976.59	$\Delta H^{\circ}_{(r)1,298}$	= 14109.61 $Jmol^{-1}$ + 6062.95 - 7206.03
	$\Delta S^{\circ}_{(r)<T>}$	=113.25 $JK^{-1}mol^{-1}$ + 6.58 - 8.14	$\Delta S^{\circ}_{(r)1,298}$	=103.92 $JK^{-1}mol^{-1}$ + 6.82 - 8.47

If these values for $\Delta H^{\circ}_{(r)1,298}$, and $\Delta S^{\circ}_{(r)1,298}$ are put back into equation (29) then a quadratic equation in T is generated i.e.

$$0 = 2nc(P)T^2 + (nb(P) - 2x298nc(P) - \Delta S^{\circ}_{(r)1,298})T + na(P) + \Delta V^{\circ}_{s\,298}(P-1) + \Delta H^{\circ}_{(r)1,298}. \quad (30)$$

If equation (30) is solved for chosen temperatures two sets of solutions will be found. The set chosen as the solution would be the one which passes through the reversal brackets. In theory if the reversal brackets were good equation (30) would produce an improved extrapolation of the reaction at pressures and temperatures outside the range of the reversal experiments. The solid line in Figure 7.5 shows the extrapolated position of the reaction using this method. The error in the temperature position of the reaction (σ_T) would be of a similar order of magnitude to that determined for Chatterjee's method but slightly larger because the errors in $\Delta H^{\circ}_{(r)1,298}$, and $\Delta S^{\circ}_{(r)1,298}$ are a little larger. The position of the reaction determined using Chatterjee's method, shown by a dotted line in Figure 7.5, lies in a similar position to that determined here if the errors are taken into account. The only large difference occurs at low temperatures.

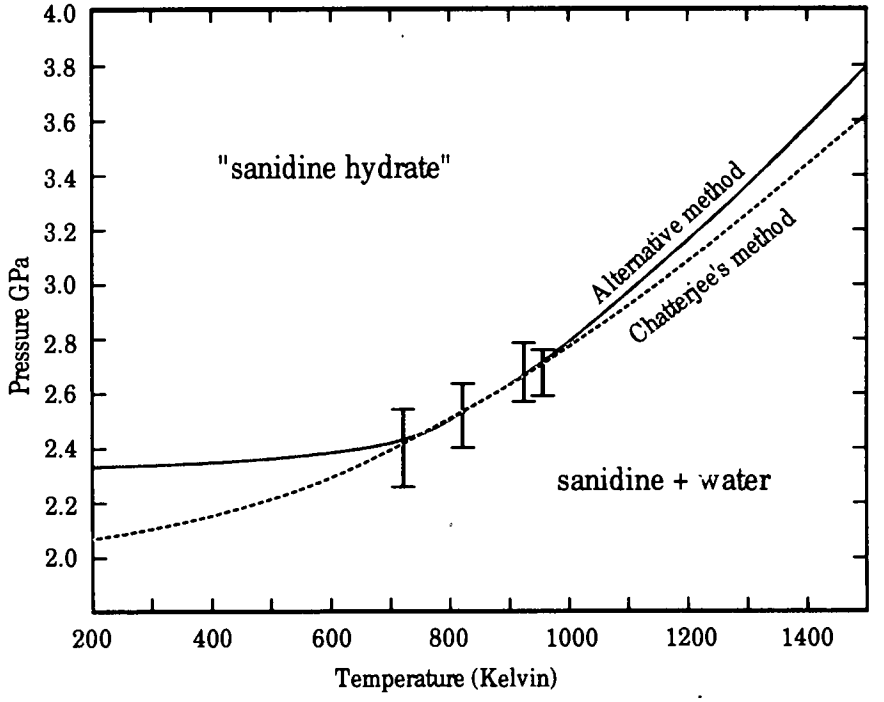

Fig. 7.5. The position of the reaction calculated from a method which does not assume that the enthalpy and entropy are constant with pressure and temperature. The reaction position determined using the methods of Chatterjee (Fig. 7.3) is shown for comparison.

7.8 Conclusions

Thermodynamic analysis of the dehydration of "sanidine hydrate" was not feasible as the quality of the thermodynamic data was inadequate. If the water content of "sanidine hydrate" was presumed constant over the pressure-temperature range of the experiments, then the enthalpy and entropy of the reaction between sanidine and water to form "sanidine hydrate" could be calculated by two different methods. The results of these calculations are summarised in Table 7.1. The change in enthalpy of the reaction in the pressure-temperature range studied, where n has an average value of 0.83 molecules per formula unit, was found to be 18000 (±5000) $Jmol^{-1}$ if the calculation methods of Chatterjee (1991) were used. The equivalent entropy was 92.75 (±5.8) $JK^{-1}mol^{-1}$. The equivalent values for the reaction between celsian and water to form cymrite, using a similar method of calculation but when a variable quantity of water is considered, are $\Delta H^{\circ}_{(r)<T>}$ = 37425 $Jmol^{-1}$ and $\Delta S^{\circ}_{(r)<T>}$ = 116.37 $JK^{-1}mol^{-1}$. The values calculated in this study are similar to those calculated for the barium analogue as would be expected given the strong structural similarities. The value of the entropy is smaller then the entropy of the cymrite-celsian reaction. Since the change in volume of the solids calculated from the cell parameters in Chapter 6 is similar to the cell volume change in the barium system, the smaller entropy will result in a shallower gradient for the reaction from the Clausius-Clapeyron relationship

$$\frac{dP}{dT} = \frac{\Delta S^{\circ}_{(r)}}{\Delta V^{\circ}_{(r)}} \qquad (31)$$

Chapter 8
Geological significance of "sanidine hydrate"

8.1 Introduction

In the preceding chapters a detailed study of the phase "sanidine hydrate" has been described. This chapter considers the possible geological conditions in which "sanidine hydrate" may occur.

The reversal data on the reaction of sanidine and water to form "sanidine hydrate" were presented in Chapter 4. These data limit the stability field of "sanidine hydrate" to high pressures. At higher temperatures "sanidine hydrate" must melt. The position of this melting curve is constrained by the position of the wet melting of sanidine. Hence the pressure temperature stability field of "sanidine hydrate" is limited to low temperatures at high pressures. The geological occurrences of such low temperature, high pressure conditions may be rare. Evidence for these conditions from geotherms and rocks at the surface of the earth does exist but is not common. The occurrence of these conditions may be more common in subduction zones which are dynamic systems and therefore the variation in the conditions with depth is difficult to predict. Numerical simulations of subduction zones show some idea of the primary controls on the temperature-depth profile.

The stability field of "sanidine hydrate" may also be changed by the presence of more components. This study only considered a simplified situation. Natural systems are much more complicated. The effect of the addition of extra components to the system is not known and therefore "sanidine hydrate" may form by other reactions than the one studied here. However, since the pressures and temperatures at which sanidine and water will react to form "sanidine hydrate" have been determined, the formation of "sanidine hydrate" by this reaction, on metamorphism, is restricted by the stability field of sanidine in the presence of water. Hence the reactions with other phases which would remove sanidine when in the presence of water at lower pressures need to be considered.

Finally the likelihood of sanidine and water coexisting up to the pressures and temperatures required to form "sanidine hydrate" in most common rock compositions is discussed. Granitic compositions are considered in more detail as these are perhaps the most probable protolith to contain "sanidine hydrate" on metamorphism and are also the most extensively studied. The occurrence of "sanidine hydrate" may also be further restricted in metamorphosed granites by the presence of excess fluid or small amounts of melt.

8.2 Pressure-temperature stability field

From the results previously shown in Chapter 4 the lower pressure stability limit for "sanidine hydrate" has been determined and correspondingly the upper pressure stability limit for sanidine in the presence of water. In order to see whether "sanidine hydrate" is indeed a realistic reservoir for water in the upper mantle and lower crust, we need to know more about its stability field. In particular it would be interesting to know what the higher temperature stability limit for "sanidine hydrate" is, i.e. the temperature at which it melts in the presence of excess water. It would also be interesting to know how the addition of other components and phases affects the extent of the field in which "sanidine hydrate" is stable.

At higher temperatures "sanidine hydrate" should melt in the presence of excess water. At what temperatures this happens is not well known. However, the position of the wet melting curve of sanidine is known from the work of Goldsmith and Peterson (1990) (Fig. 8.1). The results of their experiments at high pressure were somewhat ambiguous. They discovered, at pressures in excess of 1.5 GPa, that melts do not quench to a coherent glass but to a fine grained granular brownish isotropic substance which they referred to as GIBIS (Granular Incoherent Brownish Isotropic Substance). Although identification of GIBIS was difficult as it was indistinguishable from the melt phase it was nevertheless thought to be a vapour quench. This situation could be caused by the critical behaviour of the fluid at these pressures and temperatures which would make the vapour phase and the melt indistinguishable. Goldsmith and Peterson postulated that the presence of GIBIS could be due to the incongruent solubility of the sanidine or microcline starting material in the vapour phase at high pressure, and hence the melting of sanidine would no longer be univariant and a melting interval would be detectable. This would explain the occurrence of GIBIS and hence a melting interval over a fairly broad temperature range of over 130°C at 2.5 GPa. Despite these problems they drew a line (shown in Fig. 8.1) which was their best approximation for the liquidus, i.e. the temperature at which crystals could no longer be seen within the GIBIS. Above 1.5 GPa none of their experiments were wholly crystalline and the solidus position could not be determined

In the synthesis and reversal experiments described in Chapter 4 carried out at similar pressures and temperatures to the experiments performed by Goldsmith and Peterson, there was no evidence for a phase which might have been GIBIS near the liquidus. However, all samples, from both synthesis and reversal experiments, contained material which was brownish and isotropic, but it was hard to tell if they were truly

isotropic as the birefringence in all of the crystals was extremely low and the crystal size in most runs was generally less than a micron. The brownish colour may simply have been the effect of an accumulation of crystals reducing the light transmitted. Even samples from the lowest temperature reversal experiments at 450°C contained this material and so it seems unlikely that this material is a product of melting. Investigation of some of the samples using scanning electron microscopy showed material which looked very much like Goldsmith and Peterson's GIBIS but again these were samples from well below the liquidus.

Goldsmith and Peterson's liquidus line would intersect the

"sanidine hydrate" = sanidine + water

$KAlSi_3O_8.nH_2O = KAlSi_3O_8 + H_2O$ (1)

reaction line at approximately 700°C and 2.8 GPa. This would obviously restrict the position of the reaction:

"sanidine hydrate" + water = liquid

$KAlSi_3O_8.nH_2O + H_2O = Liq$ (2)

to lying between the metastable extensions of the two reactions:

sanidine + water = liquid

$KAlSi_3O_8 + H_2O = Liq$ (3)

"sanidine hydrate" = sanidine + water

$KAlSi_3O_8.nH_2O = KAlSi_3O_8 + H_2O$ (4)

as shown by the dotted lines in Figure 8.1

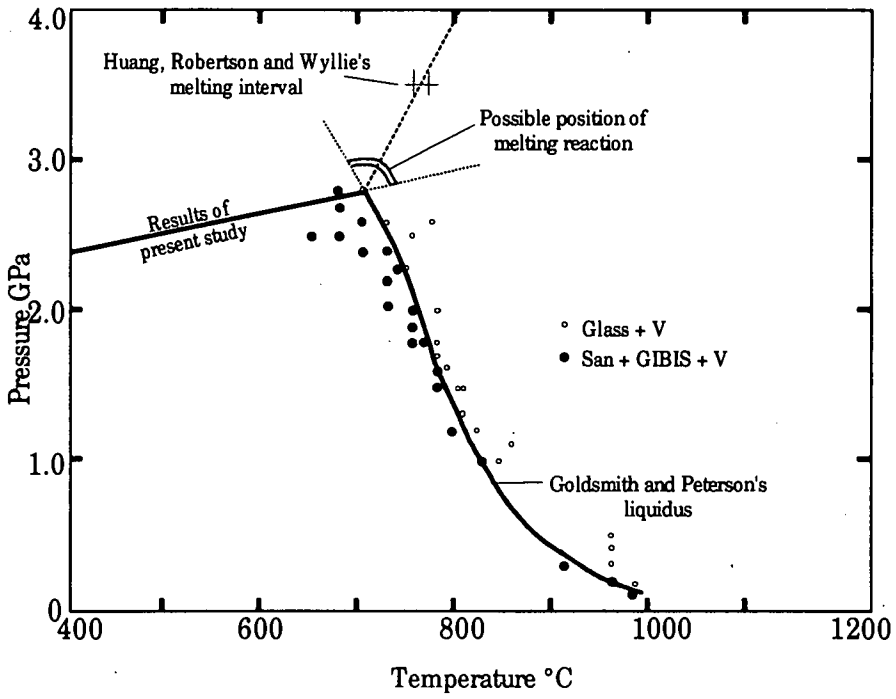

Fig. 8.1. A comparison of the results from the present study with the position of the liquidus as determined by Goldsmith and Peterson in 1990. Also shown is the position of the melting interval of Huang, Robertson and Wyllie (1973), although this is not a reversed reaction.

Huang, Robertson and Wyllie (1973) experimented with a synthetic sanidine and water at pressures up to 3.5 GPa in order to investigate the melting behaviour. They did not reverse these experiments. At pressures where "sanidine hydrate" should form they did two stage runs in which they held the sample at 600°C and 3.5 GPa for 5 hours to try to crystallise "sanidine hydrate" before changing the temperature to see if it melted. They obtained melting between 750 and 765°C at 3.5 GPa, but this was their only data point. If this is the stable melting temperature it would restrict the position of the wet melting curve of "sanidine hydrate" (reaction (2)) to lying approximately in the position shown by the dashed line at the top of Figure 8.1. Ryabinin et al. (1965) claimed to have found "sanidine hydrate" stable over the entire pressure-temperature range of their studies between 6.6 to 7.9 GPa and 500 to 2300°C. This would suggest a shallower gradient in the dashed line of Figure 8.1 than was suggested by Huang, Robertson and Wyllie (1973) but extrapolation from such high pressures and temperatures is probably unreliable. However, wherever this curve is placed, the stability field of "sanidine hydrate" is restricted to being at temperatures of less than the order of 700-1000°C in the pressure range of 3.0-4.0 GPa.

8.3 Geological setting

The geological environment where these pressure, temperature conditions required to form "sanidine hydrate" (shown by a shaded box in Figure 8.3) could exist would have to be at depths in excess of 60 km. The temperature required would have to be relatively low (possibly less than 700-1000°C), compared with an average geothermal gradient, for these depths. Pollack and Chapman (1977) calculated a series of geothermal gradients for oceanic and continental settings. Although these figures are unrealistic when extrapolated to great depths, theoretically, to reach the "sanidine hydrate" field would only be possible in a continental setting with a heat flow of less than 40 mWm^{-2} (approximately equal to 6.5°Ckm^{-1}). These conditions are probably abnormal, although calculated estimates from various provinces have shown that it is possible to achieve low heat flows. Pollack and Chapman show some examples of calculated mean heat flows. The Niger province has the lowest mean heat flow of 20 +/- 8 mWm^{-2} which should be low enough to form "sanidine hydrate" at depth given the right bulk composition. There are also other provinces with mean heat flows of 40 mWm^{-2} which would possibly be just on the boundary of producing "sanidine hydrate". For example:

Canadian shield	39 +/- 7 mWm^{-2},
Western Australia	39 +/- 8 mWm^{-2},
Sierra Nevada	39 +/- 12 mWm^{-2},
Baltic Shield	36 +/- 8 mWm^{-2}.

Very low geothermal gradients have also been calculated for some xenoliths in kimberlite pipes, for example lherzolite xenoliths in the Udachnaya kimberlite pipe from Siberia (Boyd 1984). Although these formed at much higher pressures and temperatures than those at which "sanidine hydrate" could form, they would lie on a geothermal gradient of about 40 mWm^{-2}. If xenoliths had been extracted from shallower levels in crust formed with the same geothermal gradient, they may well have contained "sanidine hydrate" if there was a sufficiently high water content.

Sanidine and coesite have also been found to occur in eclogite nodules in kimberlite pipes in the Roberts Victor mine in Kimberly, South Africa. These eclogite nodules are thought to have formed in pressure-temperature conditions in excess of 2.9 GPa and 900°C (Smyth and Hatton, 1977).

A more probable situation where these low temperature, high pressure conditions may exist would be in subduction zones rather than the continental shield areas

measured by Pollack and Chapman. Not only are low geothermal gradients more probable in subduction zones but there is more likelihood of there being a fluid or some hydrous minerals present, which could supply the water required for the reaction (1) to occur. Even in subduction zones a geothermal gradient of less than 6.5 $°Ckm^{-1}$ may be hard to produce. There are very few examples of such conditions found on the surface of the earth, although this is probably mostly due to the difficulty of bringing these rocks to the surface without severe retrogression which would overprint all of the original features. Schulze and Helmstead (1988) favoured the argument that the coesite-sanidine eclogite nodules from kimberlites were formed by subduction and prograde metamorphism of tholeiitic oceanic crust rather than by fractionation of basaltic magma. Green and Ringwood (1967) showed that, using experimental data, this metamorphism of basalts to produce sanidine and coesite was possible (see Section 8.5).

Relics of what may be ancient subduction zones, which show pressure temperature conditions almost sufficient to form "sanidine hydrate", have been found. The Dora Maira massif in the Western Alps was formed at very low geothermal gradients of possibly 7-8$°Ckm^{-1}$ (= 40 mWm^{-2}) at 2.8-3.5 GPa and 700-800°C (Schreyer, Massonne and Chopin 1987). This might be on the very edge of the stability field of "sanidine hydrate" (see hatched region in Figure 8.4). However, the bulk composition of the Dora Maira rocks (Fig. 8.2) would prevent sanidine, and hence "sanidine hydrate", from forming even if there were enough water present. Therefore it should be possible to subduct rocks into the "sanidine hydrate" stability field.

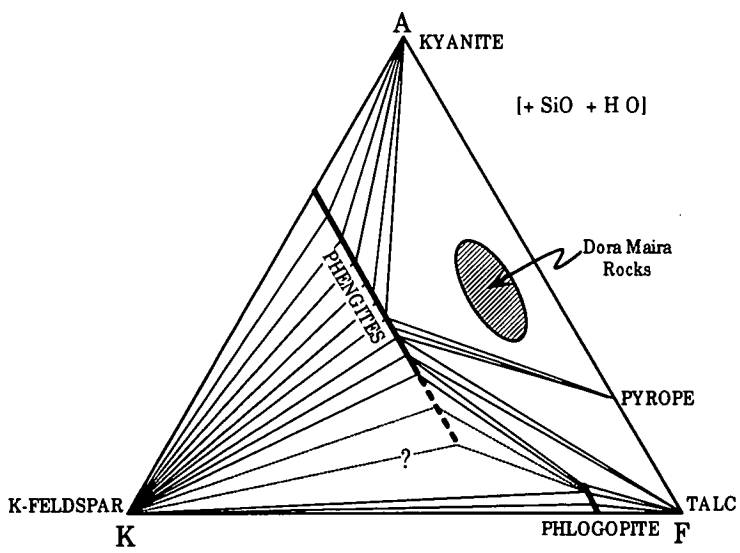

Fig. 8.2. An Al_2O_3-K_2O-FeO plot to show that the composition of the Dora Maira rocks cannot contain potassium feldspar as a stable phase. Redrawn from (Schreyer, Massonne and Chopin 1987)

Numerical simulations of subduction zone pressure-temperature-time paths can help constrain the occurrence of the pressure-temperature conditions required for the stability of "sanidine hydrate". Peacock (1991) conducted numerical experiments using a two dimensional finite difference model. The model simulates the heat transfer in a subduction zone with a dip of 26.6°. Oceanic geotherms were calculated using the conductive cooling of a mantle adiabat and an analytical solution describing induced convection was incorporated into the mantle wedge. Parameters were varied during the individual numerical experiments were (i) the initial age of the oceanic lithosphere, (ii) the convergence rate, (iii) the nature of the metamorphic dehydration reactions, (iv) the amount of shear heating and (v) the presence of induced mantle convection. Figure 8.3 shows some of the results of these experiments with the stability field of "sanidine hydrate" drawn in for comparison. The results of the numerical experiments show that the primary controls on a rock P-T-t path are (i) the initial thermal structure, (ii) the amount of previously subducted lithosphere (convergence rate x time), (iii) the position of the rock in the subduction zone and (iv) the vigour of induced mantle convection.

These numerical results demonstrate that the pressure-temperature conditions required for the formation of "sanidine hydrate" are more likely to occur in the subduction zone modelled, if (i) the subducting oceanic crust is at least 100 Ma old, (ii) the slab has subducted at least 600 km of material since its formation (iii) the rock is either in the base of the oceanic crust or in parts of the mantle wedge that do not get dragged down by the subducting slab, or (iv) in the top of the slab after a lot of crust has subducted if there is no convection in the mantle wedge.

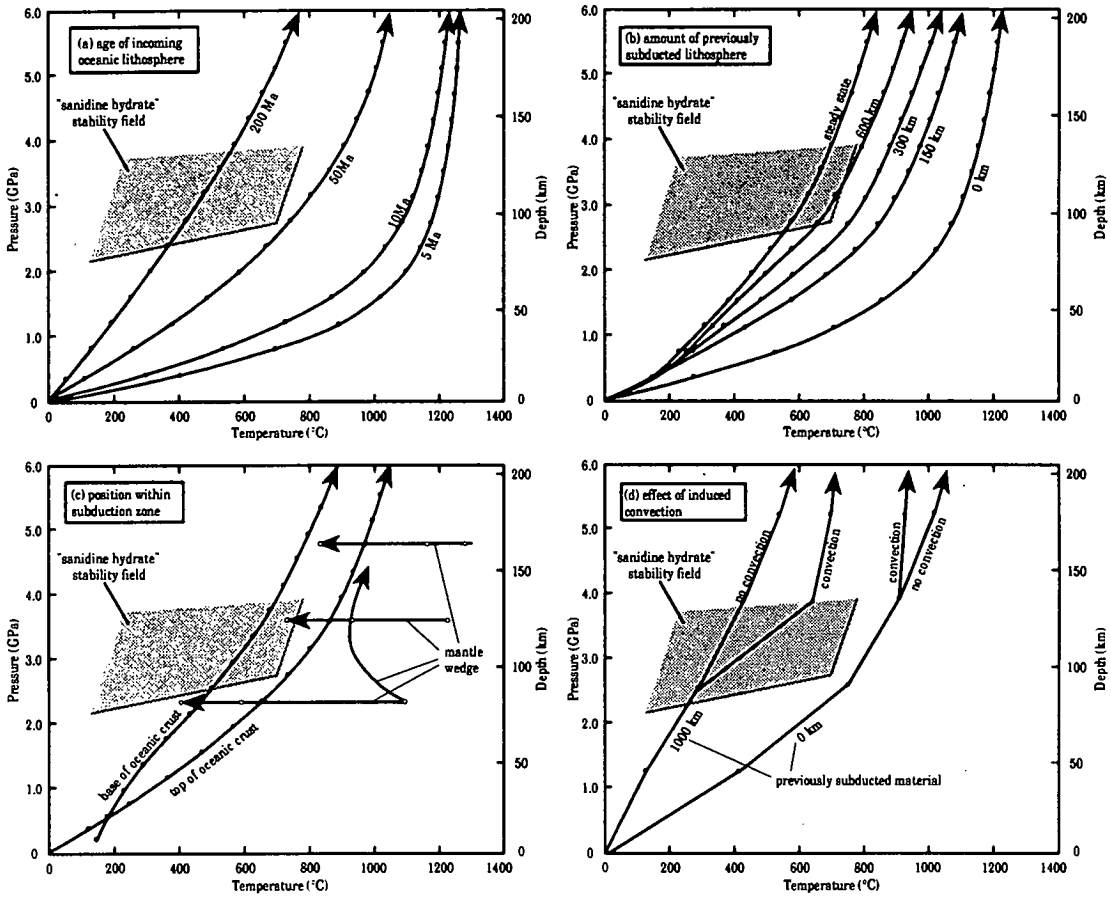

Fig. 8.3. Subduction zone P-T-t paths predicted by the two dimensional, heat transfer model and selected pressure-temperature constraints based on ancient subduction zones. The stability field of "sanidine hydrate" determined in this study is shown by the shaded region for comparison. Solid circles represent intervals of 1 Ma; open circles represent intervals of 10 Ma.
(a) Calculated P-T-t paths for the top of the subducted oceanic crust as a function of the age of the incoming oceanic lithosphere. Convergence rate is 3 cm Ma^{-1}.
(b) P-T-t paths followed by the top of the subducting oceanic crust as a function of the amount of previously subducted lithosphere (convergence rate x time). Convergence rate is 3 cm Ma^{-1}.
(c) P-T-t paths as a function of position in the subduction zone. Convergence rate is 3 cm Ma^{-1}.
(d) P-T-t paths followed by the top of the subducting slab as a function of the vigour of induced convection in the mantle wedge and the amount of previously subducted material. Convergence rate is 10 cm Ma^{-1}. Redrawn from Peacock (1991).

8.4 Compositional restrictions

The system K_2O-Al_2O_3-SiO_2-H_2O in which the present experiments have been performed is a simple one of only three phases in the pressure temperature range studied. Natural rocks are inevitably more complicated with many more phases and components. So the problem is, in order to find "sanidine hydrate" at high pressures, we firstly need to have a bulk composition which includes the components K_2O, Al_2O_3, SiO_2 and H_2O but without sufficient quantities of components that would favour the formation of other phases at the expense of "sanidine hydrate". Whether "sanidine hydrate" can be formed by reactions between phases other than either sanidine and vapour, or from crystallising a water rich sanidine melt, is not known. However, since it is known that if sanidine and vapour are stable up to pressures of 2.0 to 3.0 GPa, they will react to form "sanidine hydrate", it would be a useful starting point to look at the stability field of sanidine and vapour.

In most rock compositions sanidine is unlikely to ever form at high pressure as there are a large number of reactions which will remove any sanidine present at relatively low pressures. Figure 8.4 is a summary of many of the reactions which limit the stability of sanidine at high pressure. Figures 8.5, 8.6 and 8.7 show detail from Figure 8.4. The reactions shown are listed in the corresponding Tables 8.1, 8.2 and 8.3.

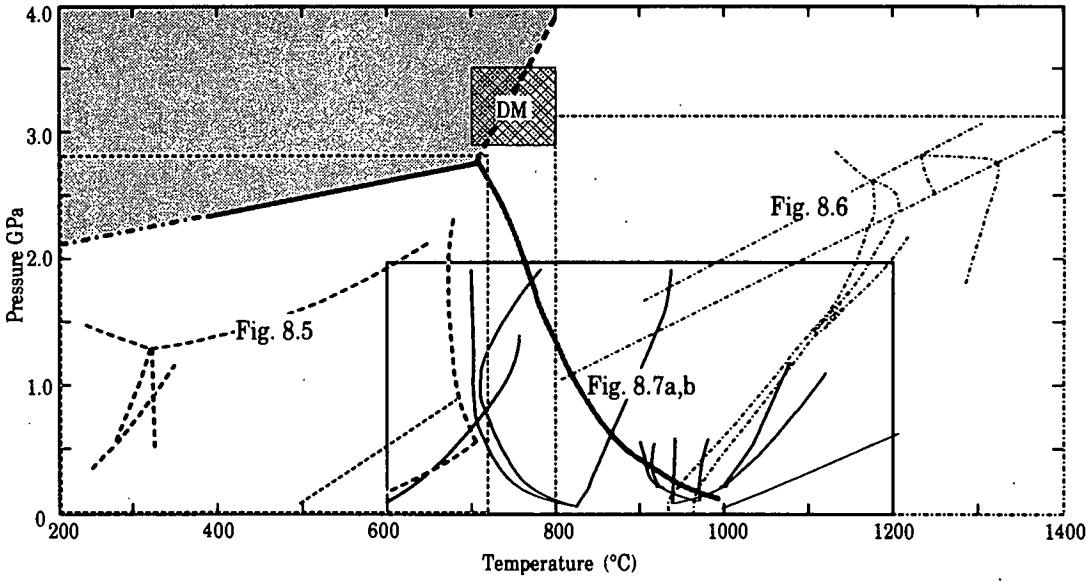

Fig. 8.4. A summary of the reactions which involve sanidine in the K_2O-MgO-CaO-SiO_2-H_2O-CO_2 system. The shaded area represents the stability field for "sanidine hydrate" The hatched box labelled DM are the pressure temperature conditions of the Dora Maira rocks. The heavy lines are taken from Figure 8.2. The three boxes refer to the enlargements shown in Figures 8.5, 8.6 and 8.7

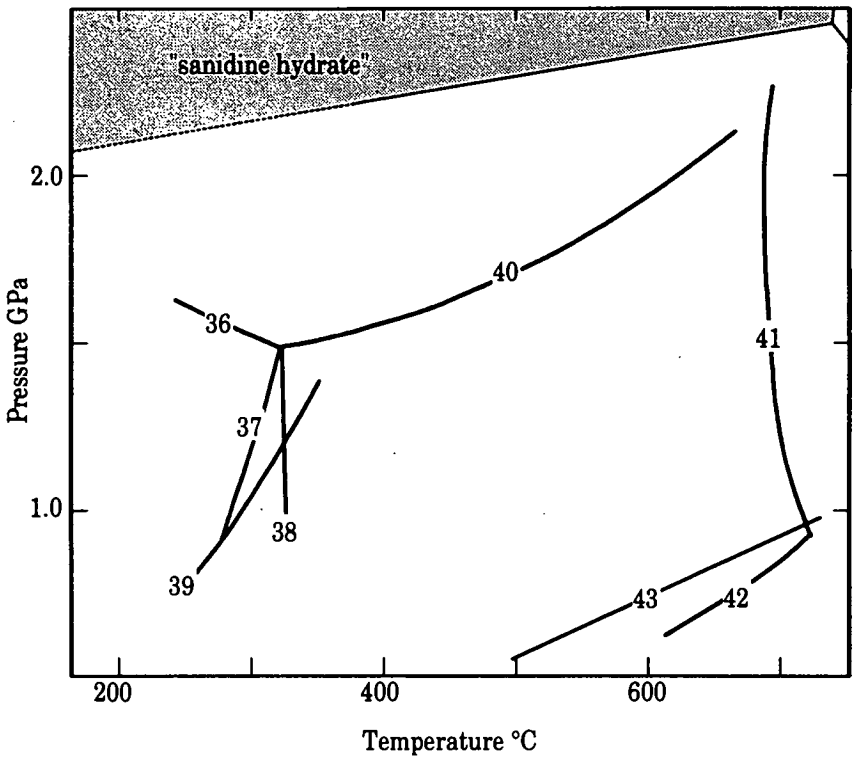

Fig. 8.5. Reactions involving sanidine enlarged from Figure 8.5. Symbols, reactions and references are listed in Table 8.1

Table 8.1, Reactions shown in Figure 8.5, (the high temperature side of the reaction is on the right)

Data from: ♠ Massonne and Schreyer (1987), ♣ Massonne (1992), ♦ Hewitt (1975)

Phl = phlogopite, Qz = quartz, Sa = potassium feldspar, Tc = talc, Phe = phengite, Cc = calcite, Cord = cordierite, Tr = tremolite, Chl = chlorite, L = melt, V = vapour, Fl = K, Mg rich fluid.

36	Tc + Sa + V = Phe + Qz + Fl (♣)	37	Tc + Phe + Sa = Phl + Qz + V (♣)
38	Tc + Sa + V = Phl + Qz + Fl (♣)	39	Chl + Sa = Phe + Phl + Qz + V (♠)
40	Phe +/- Qz + Fl = Sa + Phl V (♣)	41	Phe + Phl + Sa + Qz + V = L (♠)
42	Phe + Phl + Qz = Cord + Sa + V(♠)	43	Phl+Cc+Qz=Tr+Sa+V(CO_2 rich)(♦)

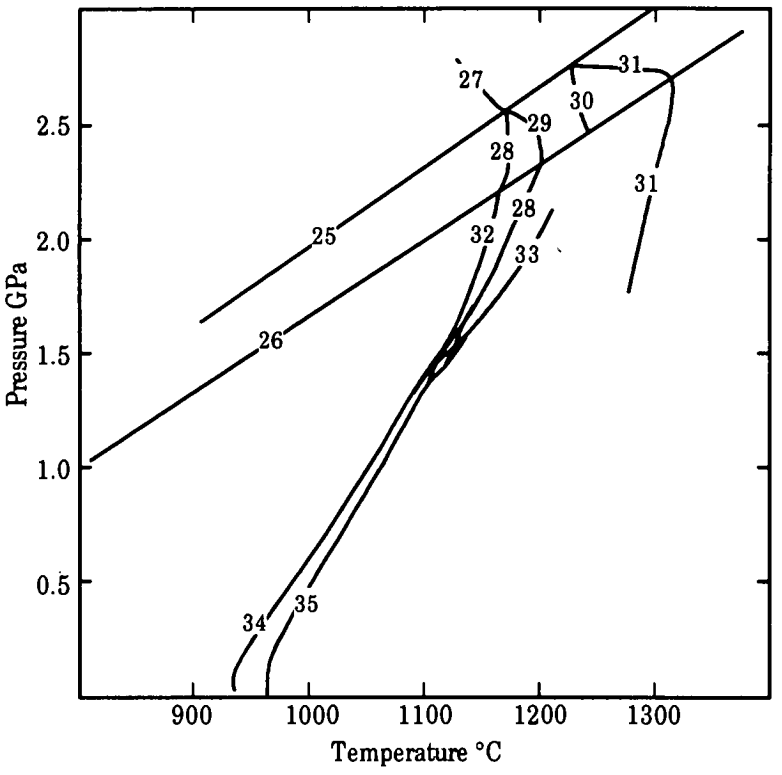

Fig. 8.6. Reactions involving sanidine enlarged from Figure 8.5. Symbols, reactions and references are listed in Table 8.2.

Table 8.2, Reactions shown in Figure 8.6, (the high temperature side of the reaction is on the right)

Redrawn from Hewitt and Wones (1984), data from Wendlandt and Eggler (1980)

Phl = phlogopite, Sa = potassium feldspar, En = enstatite, Fo = forsterite, Ks = kalsilite, Lc = leucite, L = melt, V = vapour.

25	Ks + En = Sa + Fo	26	Ks + Sa = Lc
27	Phl + Sa + Ks + V = En + L	28	Phl + Sa + Ks + V = Fo + L
29	Phl + Sa + Fo + V = En + L	30	Fo + Sa + Ks + CO_2 = L
31	Sa + Fo + CO_2 = En + L	32	Phl + Sa + Lc + V = Fo + L
33	Phl + Sa + V = En + L	34	Phl + En + Sa + V = Fo + L
35	Phl + Sa + V = Fo + Lc + L		

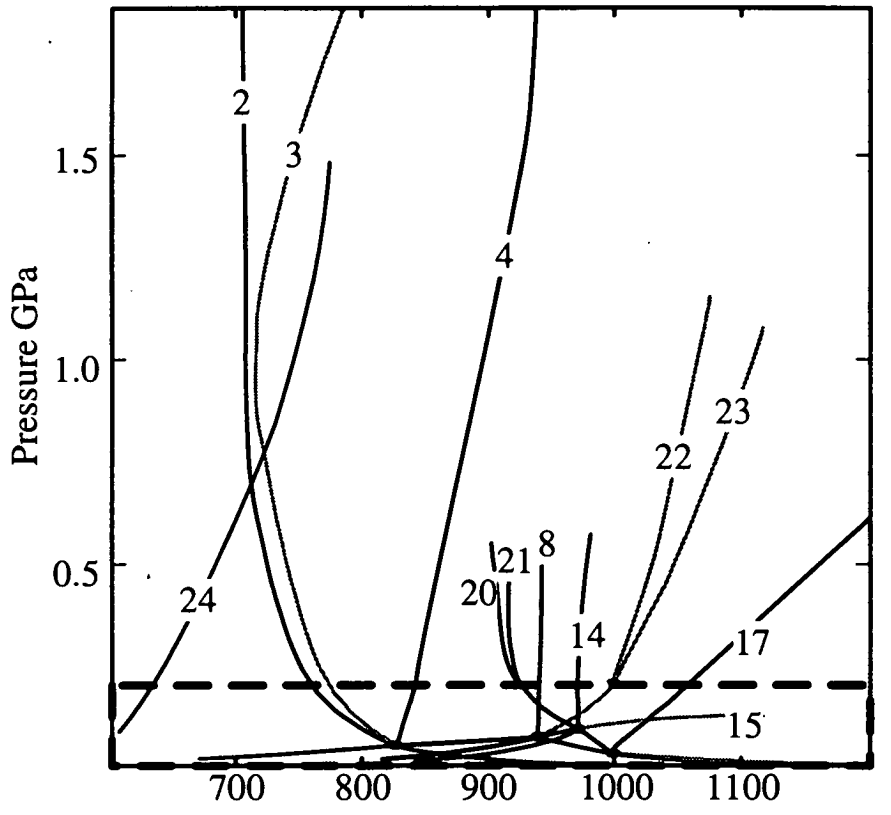

Fig. 8.6a, Reactions involving sanidine enlarged from Fig. 8.4
Symbols, reactions and references are explained in Table 8.3

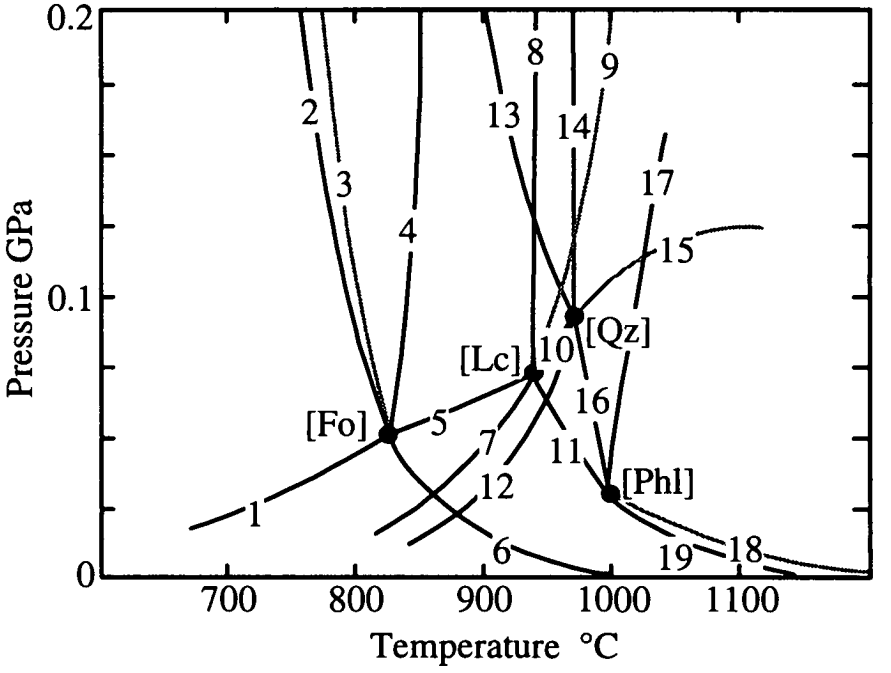

Fig, 8.6b, An enlarged view of the lower temperature part of Fig. 8.6a.
Symbols, reactions and references are explained in Table 8.3

Table 8.3, Reactions shown in Figure 8.7. , (the high temperature side of the reaction is on the right)

Redrawn from Hewitt and Wones (1984), data from: ♦ Luth (1967), ♠ Wendlandt and Eggler (1980), ♥ Wones and Dodge (1977), ♣ Wood (1976), ⊗ Bohlen et al (1983)

Phl = phlogopite, Qz = quartz, Sa = potassium feldspar, En = enstatite, Fo = forsterite, Lc = leucite, Phe = phengite, Si = sillimanite, Ky = kyanite, L = melt, V = vapour.

1	Phl + Qz = Sa + En + V (♣)	2	Qz + Sa + Phl + V = L (♥⊗)
3	Qz + Phl + V = En + L (♥⊗)	4	Qz + Phl = Sa + En + L (⊗)
5	Phl + L = Sa + En + V (♦)	6	Qz + Sa + En + V = L (♥)
7	Phl + En = Sa + Fo + V (♦)	8	Phl + Sa + En = Fo + L (♦)
9	Phl + En = Fo + L + V (♦)	10	Phl + L = Sa + Fo + V (♦)
11	Sa + En + V = Fo + L (♦)	12	Phl + Sa = Fo + Lc + L (♦)
13	Phl + Sa + V = Lc + L (♦)	14	Phl + Sa = Lc + Fo + L (♦)
15	Phl + L = Fo + Lc + V (♦)	16	Sa + Fo + V = Lc + L (♦)
17	Sa + Fo = Lc + En (♦, ♠)	18	Lc + En + V = Fo + L (♦)
19	Sa + En + V = Lc = L (♦)	20	Phl + Sa + Lc + V = L (♦)
21	Phl + Sa + V = L (♦)	22	Phl + En + V = Fo + L (♦)
23	Phl + En = Fo + L (♦)	24	Phe + Qz = Sa + Sill/Ky + V (♦)

These figures and tables show that under the pressures and temperature conditions of over 2.0-3.0 GPa and below 700-1000°C (the approximate stability field for "sanidine hydrate") , sanidine would not be stable with

	Reaction:
forsterite	25
talc + vapour	36, 35
phlogopite + vapour	40
cordierite + vapour	42
enstatite + vapour	1, 5
enstatite + liquid	4
forsterite + vapour	7, 10
tremolite + CO_2 rich vapour	43
silimanite/kyanite + vapour	24

Although the absence of sanidine does not forbid the occurrence of "sanidine hydrate", the reactions listed above would prevent the reaction:

"sanidine hydrate" = sanidine + water

$$KAlSi_3O_8.nH_2O = KAlSi_3O_8 + H_2O \quad (1)$$

from taking place and so reduce the likelihood of forming "sanidine hydrate".

Therefore, it would be interesting to find rocks which contain sanidine with either none or very small proportions of the above combinations of phases, so that these reactions will not remove sanidine from the rock altogether before reaching the pressure and temperature of interest.

8.5 Common bulk compositions:

In many sedimentary rocks potassium feldspar is not a common constituent. However, in the most common sedimentary rock types, siliciclastic sediments, potassium feldspar can be a large component. Siliciclastic sediments can have a diverse range of compositions. In sandstones the clasts are usually predominantly quartz and feldspar, with an average feldspar composition of 10-15% (Tucker 1981). The feldspar is usually predominantly potassium feldspar as it is chemically more stable than plagioclase feldspar and the continental basement has an average composition of granodiorite of which 25-30% of the feldspar is alkali feldspar, (Kearey and Vine, 1990). In arkoses the feldspar content can be as much as 50%. Immature greywackes can also contain large quantities of feldspar although the proportion of sodic plagioclase is normally higher than that of potassium feldspar. Mudrocks, which make up 45-55% of sedimentary lithologies (Tucker 1981), generally have almost no feldspar. Pure limestones contain very few or no silicate minerals.

The diverse compositions of these sediments inevitably result in a large variety of rocks when metamorphosed. Metamorphism of limestones would result in all of the silicate minerals transforming to calcsilicate minerals such as epidote, sphene or anorthite with no potassium feldspar. "True pelites", as described by Yardley (1989), contain no potassium feldspar. These are the ones that produce the characteristic zonation schemes (e.g. the Barrovian zones) and are the metamorphic equivalent of mudstones. However "true pelites" are relatively rare. More common are the metamorphosed greywackes. These can have a large range of compositions but they

frequently contain potassium feldspar. However, the proportion of potassium feldspar would have to exceed the proportions of all the phases with which it is unstable (see previous section for some examples) as the rock is buried. Therefore the quantity of sanidine remaining at high pressure may be greatly reduced or non-existent.

Basic igneous rocks contain little or no potassium feldspar. The only feldspar phase present is usually plagioclase which would be albite rich at low pressures and temperatures. When a basic igneous rock is metamorphosed the feldspar would become more anorthite rich at higher temperatures, and react to form jadeite at high pressures. Green and Ringwood (1967) showed experimentally that small quantities of sanidine can exist up to very high pressures. However, their experiments were conducted at high temperatures in the absence of water. If water were present amphiboles and micas may form instead. Some evolved igneous rocks can contain a large proportion of potassium feldspar. There may also be only relatively small proportions of the phases which would react with potassium feldspar when the rock is subjected to high pressure metamorphism. Hence it is possible that sanidine will be stable up to the sanidine - "sanidine hydrate" boundary in some evolved igneous rocks. The only rock types which have been studied fairly extensively at high pressure are synthetic granite compositions and even in these many of the reactions have not been reversed. Not much is known about the phase relations of other evolved igneous rock types which contain a large proportion of potassium feldspar, e.g. syenites. However, in comparison to granites, syenites are relatively rare.

8.6 Granites

Most granites are dominantly composed of potassium feldspar, albite rich plagioclase and quartz with smaller amounts of other phases. They are divided into two types according to the other phases present; biotite granites contain hornblende and biotite with the proportion of hornblende exceeding that of biotite; muscovite granites contain muscovite with only very small amounts of biotite.

The complicated phase relations of granites can be simplified by looking at experimental systems with a reduced number of components. These experiments have been carried out in many different systems, one of the most common being the haplogranitic system (albite-orthoclase-quartz-H_2O). However, it is convenient to compare these all on the same diagram even though the reactions do not lie in the same bulk compositional plane. Figure 8.8 is a summary of the phase relations

involving sanidine from the experimental systems which most closely approximate those for granites (Huang, Robertson and Wyllie (1973), Huang and Wyllie (1974) and Huang and Wyllie (1975)). The reactions shown are listed in Table 8.4. It shows some of the reactions which could occur in the KNASH (K_2O-Na_2O-Al_2O_3-SiO_2-H_2O) system involving the phases sanidine, "sanidine hydrate", muscovite, quartz, coesite, jadeite, albite, kyanite, sillimanite, corundum, water and melt. The system most closely approximates the muscovite bearing, S-type granite as reactions involving hornblende and biotite are not included.

Reactions (1), (2) and (14) show the relationships in the very simple situation involving only sanidine, "sanidine hydrate", water and melt. As other phases are added the melting temperature is reduced. The addition of muscovite lowers the melting temperature at high pressure only by a small degree (less than 30°C), as shown by reactions (3) and (4). At low pressures muscovite in this melting reaction is replaced by sanidine and corundum (reaction (5)). When quartz or coesite are added the melting temperature is reduced even further, by approximately 60°C, to give reactions (6) and (7). The addition of muscovite as well as quartz (reactions (8) and (9)) has little effect on the positions of reactions (6) and (7). Reactions (8) and (9) are almost coincident with reactions (6) and (7).

Reactions which include Na_2O as a component lower the melting temperature still further. Reactions (10), (11) and (12) include jadeite and albite in addition to sanidine/"sanidine hydrate" and quartz/coesite. These reactions must be the ones which most closely approximate an average granite as these are the major granite forming minerals. There are also reactions (e.g. 18, 19, 20 and 21) where sanidine would react with sillimanite/kyanite or corundum in the presence of melt or vapour, making it unstable in the high pressure, low temperature field. However, in granites, sanidine should always be a more abundant component than corundum or the aluminosilicates, and hence should never be removed altogether by these reactions.

Figure 8.9 shows how these reactions compare with the results from this work (Chapter 4) and the wet melting curve of Goldsmith and Peterson (1990) from Figure 8.1

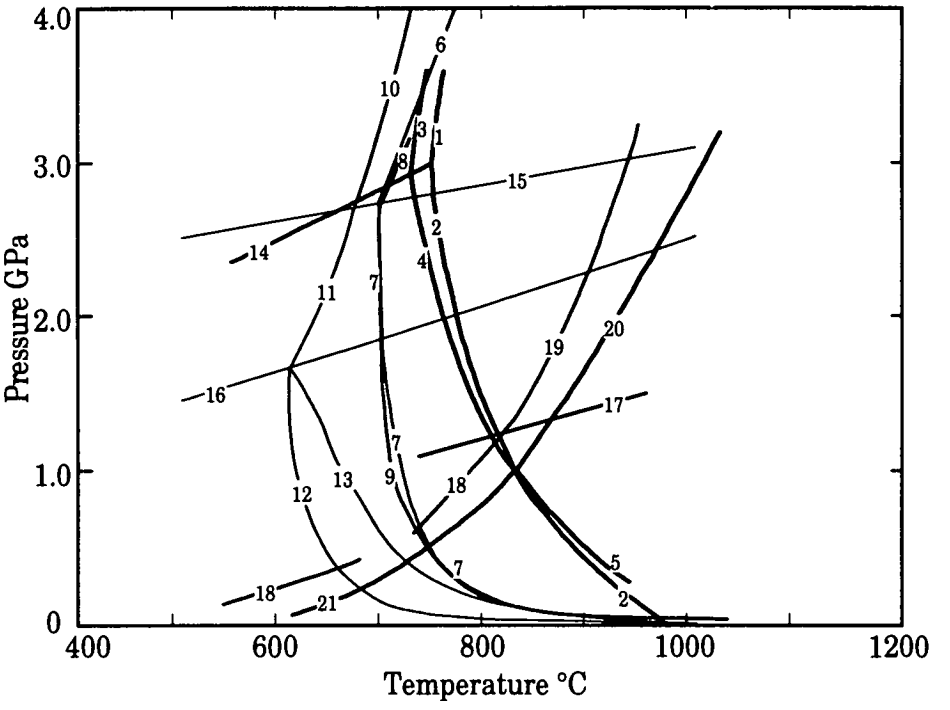

Fig. 8.8. A summary of the phase relations involving sanidine from the experimental systems which most closely approximate those for granites (Huang, Robertson and Wyllie (1973), Huang and Wyllie (1974) and Huang and Wyllie (1975)) in the KNASH (K_2O-Na_2O-Al_2O_3-SiO_2-H_2O) system. Reactions are listed in Table 8.4.

Table 8.4, Reactions shown in Figure 8.8. (the high temperature side of the reaction is on the right)

SH = "sanidine hydrate", Ms = muscovite, Sa = sanidine, Co = corundum, Qz = quartz, Ct = coesite, Jd = jadeite, Ab = albite, Si = sillimanite, Ky = kyanite, L = melt, V= vapour

1	SH + V = L	2	Sa + V = L
3	Ms + SH + V = L	4	Ms + Sa + V = L
5	Sa + Co + V = L	6	SH + Ct + V = L
7	Sa + Qz = V = L	8	Ms + SH + Ct + V = L
9	Ms + Sa + Qz + V = L	10	Jd + SH + Ct + V = L
11	Jd + Sa + Qz + V = L	12	Ab + Or + Qz + V = L
13	Ab + Sa + V = L	14	SH = Sa + V
15	Ct = Qz	16	Jd + Qz = Ab
17	Ky = Si	18	Ms + Qz = Sa + Si + V
19	Ms + Qz = Sa + Ky + V	20	Ms = Sa + Co + L
21	Ms = Sa + Co + V		

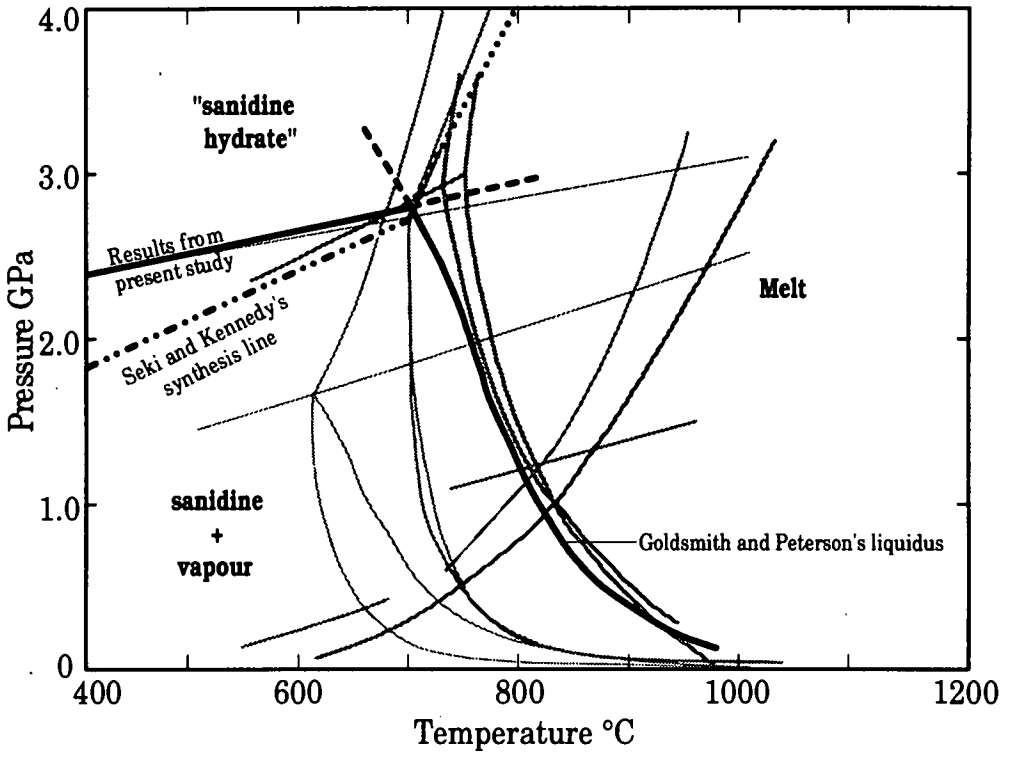

Fig. 8.9. A comparison of the present study (Fig. 8.1) with reactions relevant to granites (Fig. 8.8)

Figure 8.10 Shows how these reactions compare with the solidi and liquidi of natural granites from work performed on muscovite granites (Huang and Wyllie (1981)) and biotite granites (Stern and Wyllie (1981)). The dotted lines are the solidus and liquidus of a dry muscovite granite with all the water species held within the hydrous minerals (about 0.66 wt%) (vapour absent melting). The solid lines are for a muscovite granite with excess water and the dot-dash lines are for the melting of a biotite granite with excess water. The solidi for the wet muscovite and biotite granites both coincide closely with the position of the melting reactions involving jadeite/albite, "sanidine hydrate"/sanidine, coesite/quartz and vapour.

However these melting relations are for the conditions with excess water. If there is too much water present sanidine will react with the vapour to form muscovite. Figure 8.11 shows the stability field of sanidine with about 30wt% H_2O (Seki and Kennedy 1965). This is a large quantity of water but under these conditions all the potassium feldspar would disappear by about 1.0 GPa, by reacting to form muscovite. With less water potassium feldspar may be stable to higher pressures. Figure 8.12 shows the results for a natural granite from Stern and Wyllie (1981). The figure shows at what temperatures and percentage water content "sanidine hydrate" becomes unstable in the cases for 3.0 and 3.5 GPa.

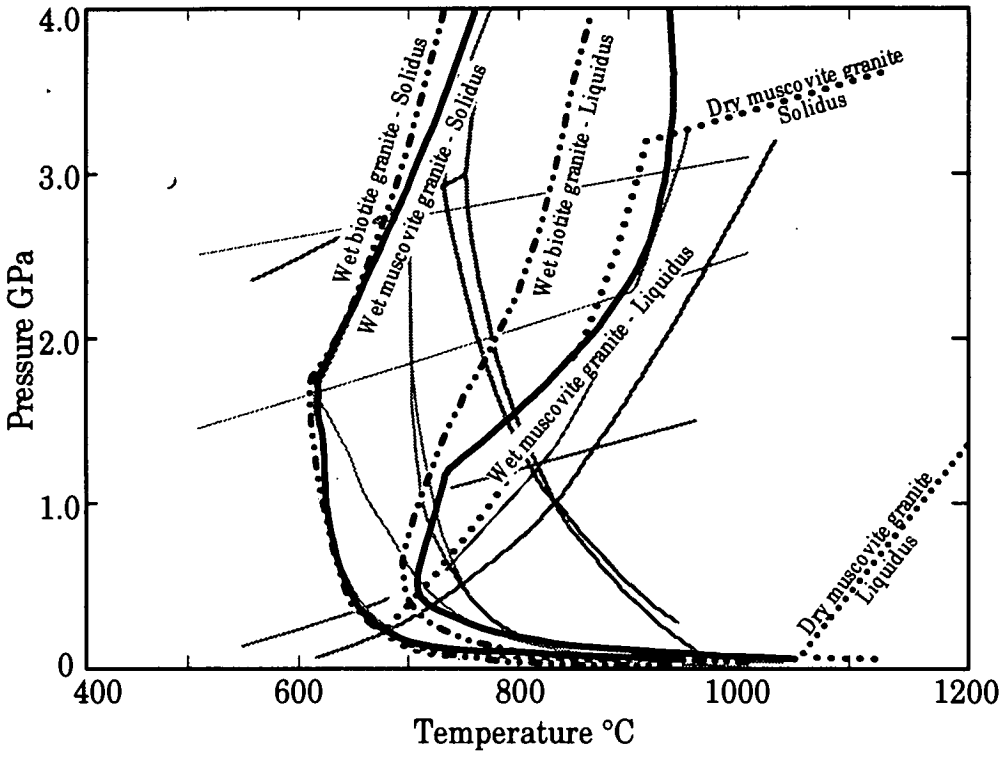

Fig. 8.10. A comparison of the granite reactions (Fig. 8.9) with the solidi and liquidi of dry muscovite granite, wet muscovite granite and wet biotite granite.(Huang and Wyllie (1981), Stern and Wyllie (1981)).

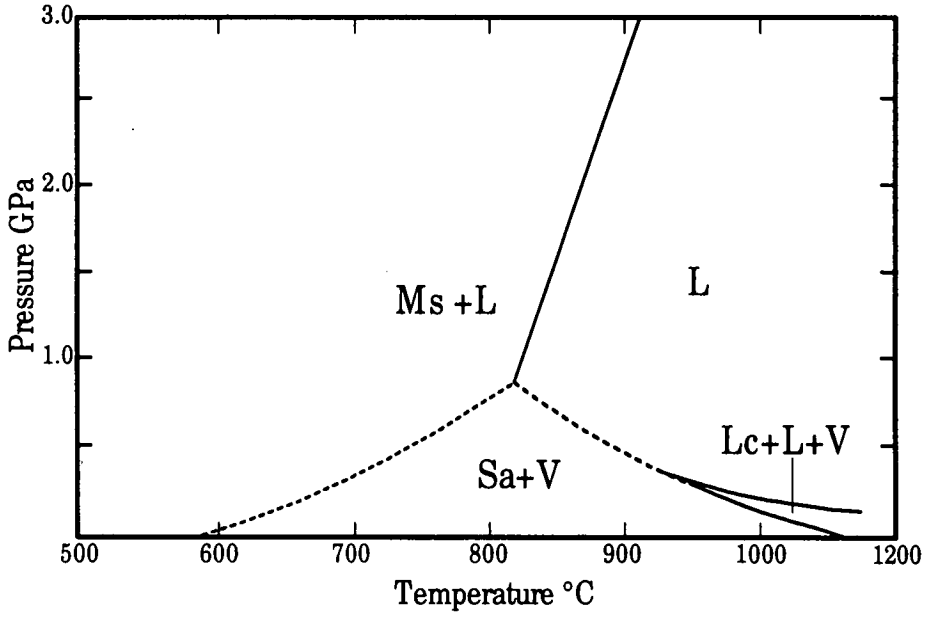

Fig. 8.11. The stability field of sanidine in the presence of approximately 30 wt% H_2O. (Seki and Kennedy 1965)

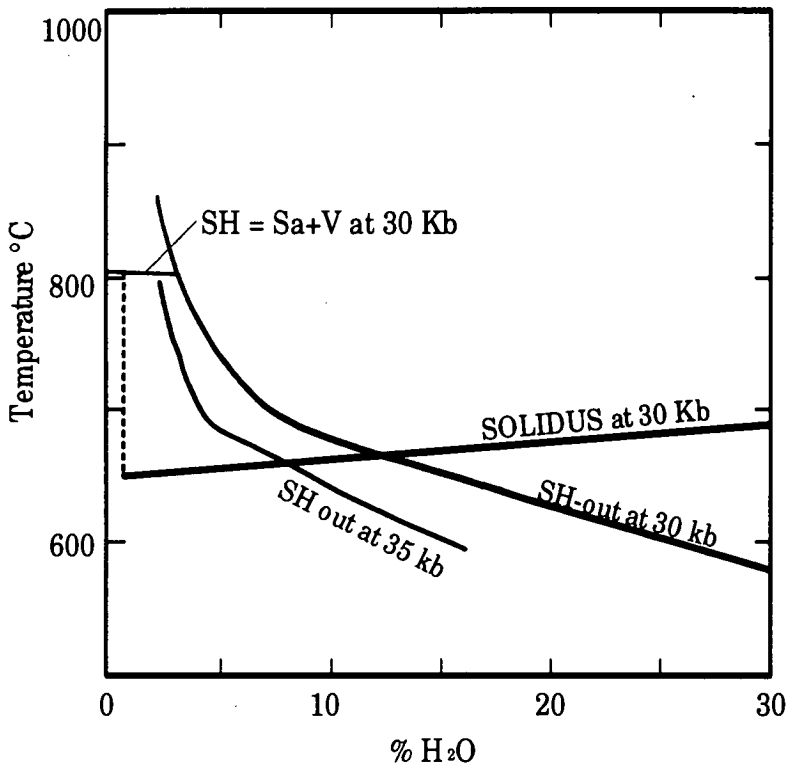

Fig. 8.12. The temperature and percentage water content at which "sanidine hydrate" dissolves in the vapour phase at 3.0 GPa. The line shown for 3.5 GPa is an extrapolation from the similar curve for sanidine at 2.5 GPa. (Stern and Wyllie (1981))

At 3.0 GPa they determined the percentage water content at which "sanidine hydrate" disappeared for a given temperature. This happens because, with increasing pressure, more rock will dissolve in the vapour phase. The vapour probably preferentially dissolves K_2O rather than Al_2O_3 or SiO_2. This may well help explain the increasing stability field of kyanite with increasing water content. The curve shown for 3.5 GPa is an extrapolation from the similar curve for the loss of sanidine at 2.5 GPa.

At high pressures water becomes very soluble in melt and so the melt will take up any water available. Huang and Wyllie (1975) found that melt became vapour saturated with 20wt% H_2O at 3.0 GPa. If "sanidine hydrate" could be formed by crystallisation from a melt it could only begin to form when there was very little melt remaining, as a free vapour phase would be unlikely in the presence of large quantities of melt.

Therefore, in order for "sanidine hydrate" to be stable, we need a composition in which there is just enough water to form "sanidine hydrate", but not so much that the sanidine dissolves or reacts to form muscovite, and a situation with little or no melt present.

8.7 Conclusions

In order for "sanidine hydrate" to form relatively low temperatures and yet high pressures are required in comparison to most geological conditions. It may only be possible to achieve these conditions in subduction zones and therefore evidence for the existence of "sanidine hydrate" at the surface will generally be overprinted by retrogression to lower pressure and higher temperature assemblies on uplift. It may not be possible to achieve these conditions in all subduction zones. Numerical modelling of a subduction zone suggests that situations where old oceanic crust is being subducted in a long standing subduction zone without induced convection in the mantle wedge may be more likely to produce the pressure-temperature conditions required. In addition the base of the oceanic crust or the mantle wedge would be colder than the upper part of the oceanic crust. The most probable bulk composition which could form "sanidine hydrate" from sanidine and water on metamorphism would be a granitic one. The subduction of granitic rocks is probably rather uncommon and they would probably never occur in the coldest parts of a subduction zone at the base of the oceanic crust or the mantle wedge. The water content of the rock must be sufficiently high to form "sanidine hydrate", or sanidine will persist until the reaction to form the wadeite type phase occurs as described by Kinomura et al. (1975). However, the water content must be only just sufficient to form "sanidine hydrate" as a large excess of water will begin to dissolve the components. In addition the presence of melt will inhibit the formation of "sanidine hydrate" as the melt will take up all of the available water.

Chapter 9
"Water" content of synthetic sanidines

9.1 Introduction

Potassium feldspar is nominally an anhydrous mineral with no stoichiometric water. In some naturally occurring examples, however, potassium feldspar has been found to contain structural OH groups or structural H_2O. These "water" species must lie within defect sites within the minerals. There are many defect sites which could accommodate structural OH, H_2O or H. Such defect sites can be formed by substitution of one species by another, or by creating or filling a vacancy in the structure. Any change in the charge caused by this defect must be coupled locally with another defect to maintain the overall charge balance. Although such defects have been proposed as "water" sites, determining which is in fact the correct type is not easy experimentally. Several substitution mechanisms have been proposed for hydrogen in feldspars and others have also been inferred by comparison with mechanisms of hydrogen substitution in quartz and other silicate minerals. Each substitution will show evidence for either structural OH or H_2O in an infrared spectrum. A few of the proposed substitutions in potassium feldspar are listed in Table 9.1.

Naturally occurring potassium feldspars appear to contain a variety of "water" species and hence several different types of defect sites (Kronenberg et al, in press). The general consensus of opinion from previous authors is that microcline generally contains structural H_2O whereas sanidine contains a larger proportion of structural OH. The defects responsible for these "water" species have not been absolutely identified.

In order to see whether the sanidines synthesised at high pressure during the present reversal experiments contained any structural "water" and to determine what type it is, infrared spectroscopy and thermogravimetric analysis have been used to investigate these high pressure sanidines. The methods used for these techniques were described in Chapter 3. The present chapter also describes the attempts to find a regular variation of structural "water" within sanidines synthesised under a number of different conditions. If sanidine is capable of dissolving more water at elevated pressures and temperatures, then it could be an important reservoir for water in lower crustal rocks. In slow cooled igneous rocks at low pressures and temperatures this water could exsolve. This may explain the occurrence of turbid feldspars containing micropores of fluid inclusions and deuteric alteration to form patch perthites as postulated by Worden et al. (1990). Bertelmann et al (1987) showed that annealing experiments on samples of Eifel sanidine caused fluid inclusions to form. Eifel sanidines contain a large proportion of structural "water" (0.017-0.036 wt%,

Hofmeister and Rossman, 1985b and Beran, 1986) and it could be the exsolution of this structural "water" which forms the fluid inclusions. If this were the case then it would imply that Eifel sanidines crystallised at pressures and temperatures where the structural "water" capacity of sanidine was greater. Evidence for exsolution of structural "water" has also been sought by looking at a suite of naturally occurring feldspars from the Klokken intrusion in South Greenland (see Chapter 10).

Table 9.1. Some proposed substitutions in potassium feldspar which could explain the occurrence of evidence for structural "water" observed in the infrared spectra.

Substitution	Description	Infrared observation
$\left[(H_2O)_K^{\cdot}\right]=\left[Ca_K^{\bullet}\right]or\left[Si_{Al}^{\bullet}\right]$	H_2O replaces K coupled with replacement of K by Ca or Al by Si (Kronenberg et al., in press)	H_2O
$\left[(H_2O)_{O_{A1,A2,B1,B2}}^{\bullet\bullet}\right]=2\left[Al_{Si}^{\cdot}\right]$	H_2O replaces O in four possible sites coupled perhaps with replacement of Si by Al (Kronenberg et al., in press)	H_2O
$\left[(H_2O)_{i_{1,2,3}}\right]$	H_2O fills one of three interstitial sites (Kronenberg et al., in press)	H_2O
$\left[H_i^{\bullet}\right]=\left[Al_{Si}^{\cdot}\right]$	H fills an interstitial site coupled with the replacement of Si by Al (Dennis, 1984)	OH or H_2O
Si-O-Si = Si-OH:HO-Si	The bridging O atom is replaced by two OH groups (Hobbs, 1984)	OH
$(4H)_{Si}or\left[3H_{Si}^{\cdot}\right]=\left[Ca_K^{\bullet}\right]$	Four H replace Si. If only three H can be fitted into the Si site a coupled replacement of K with Ca is also required (Hobbs, 1984)	OH

9.2 Previous work on "water" in potassium feldspar

Most studies on the water content of potassium feldspar have either been conducted on gem quality microclines or adularia, or on sanidine from the Eifel region of West Germany. Microclines and adularia seem to show similar patterns in their infrared spectra indicating a predominance of structural H_2O whereas sanidines seem to show more structural OH.

Hofmeister and Rossman (1985a) showed that the infrared spectrum of an amazonite changed considerably on freezing (Fig. 9.1b), and so that only a small quantity of the total water content was incorporated into the feldspar structure, the rest being held within fluid inclusions. White microcline from the Elisabeth R mine in Pala, California (Fig. 9.1a) contained two types of structural H_2O with no visible, microscopic fluid inclusion water. One type of structural H_2O, equivalent to Type I "water" of Aines and Rossman (1985) (see below), produced OH stretching absorption peaks at 3630 and 3550 cm^{-1} with a combination mode at 5130 cm^{-1}. The other type, equivalent to Type II "water" of Aines and Rossman (see below), produced absorption peaks at 3440, 3250 and 5620 cm^{-1} which were polarised in a different orientation to that of the first type. Hofmeister and Rossman (1985a) also saw two small peaks in the spectra indicative of liquid water at 3400 and 3050 cm^{-1}, which formed ice on freezing to liquid nitrogen temperatures. These spectral peaks may have been caused by sub-microscopic fluid inclusions. The quantities of structural "water" were calculated from the relative peak heights of the water peaks of the infrared spectra in comparison with a feldspar of known water composition measured by hydrogen extraction and manometry. The concentrations of structural "water" varied from 0 wt% in a sample of perthite from Amelia, Virginia to 0.1 wt% in a sample of the Elisabeth R mine white microcline, although most values were below 0.002 wt%.

Aines and Rossman (1985) obtained infrared spectra at high temperature in order to investigate the behaviour of trace hydrous components in silicate minerals. Microcline, also from the Elizabeth R mine, Pala, California, produced four absorption peaks in the OH stretching region of the spectrum (Fig. 9.2). These four peaks were attributed to two types of H_2O. Type I "water" had absorption peaks at 3620 and 3550 cm^{-1} and type II at 3440 and 3280 cm^{-1}, in close agreement with the white microcline from the Elisabeth R mine studied by Hofmeister and Rossman (1985a) described above. On heating, the Type II "water" disappeared by 400°C and so was thought to be contained in an open site or defect which could release its H_2O with ease. The Type I "water" persisted to 660°C and was presumed to occupy a

well-defined site in the feldspar structure. Above 550°C an almost isotropic band forms at 3690 cm^{-1}. It was not entirely clear whether this was a new component or one revealed by the Type I "water" band shifting to a lower energy. The formation of this peak was not reversed on cooling (Fig. 9.3). If this sample had crystallised at high temperatures the Type I "water" would not have been incorporated and instead the new species should have formed. Both Types I and II could have formed during the slow cooling and transition to maximum microcline.

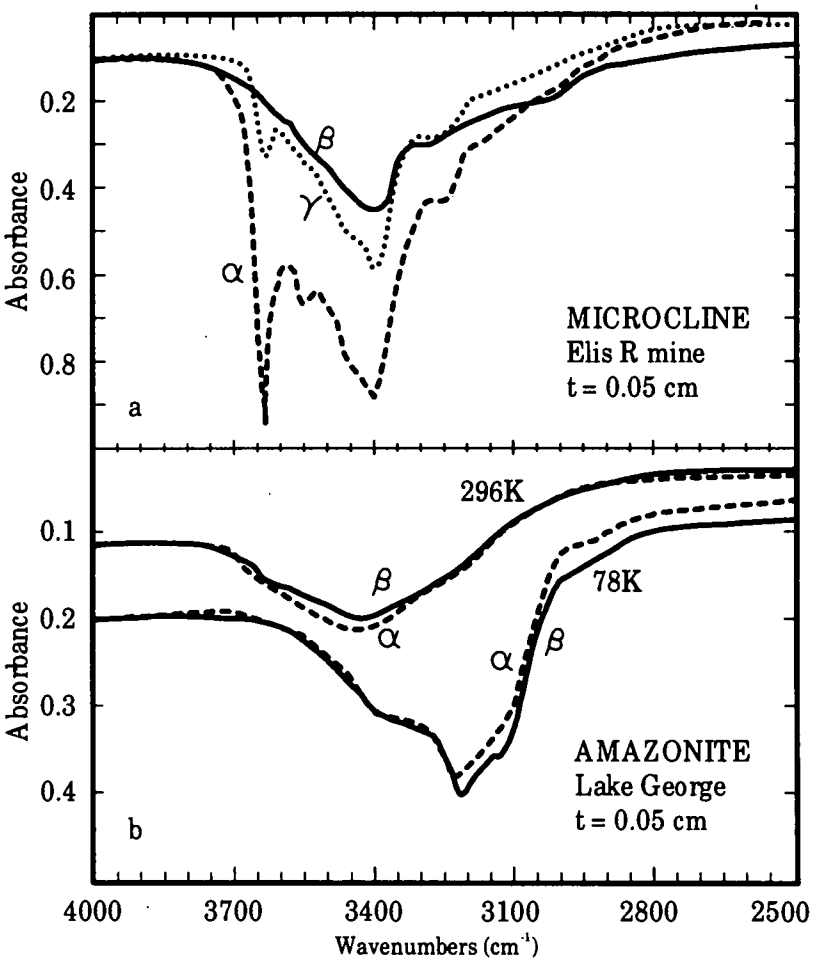

Fig. 9.1. Polarised infrared spectra of the OH stretching region of two feldspars a) a microcline from the Elisabeth R mine, Pala, California which shows four absorption peaks of structural H_2O, b) an amazonite from Lake George, Colorado composed mostly of water held within fluid inclusions shown by the formation of an ice band on freezing. (redrawn from Hofmeister and Rossman, 1985a)

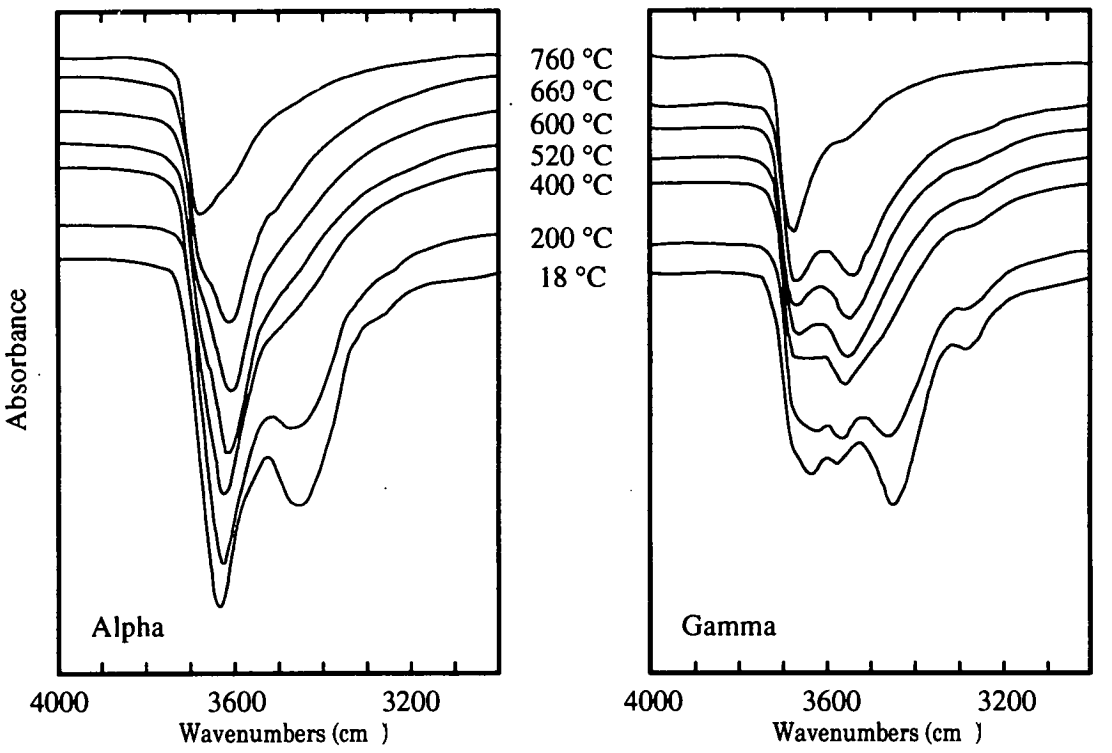

Fig. 9.2. The high temperature polarised spectra of a sample of microcline from the White Queen mine, Pala, California. (redrawn from Aines and Rossman, 1985)

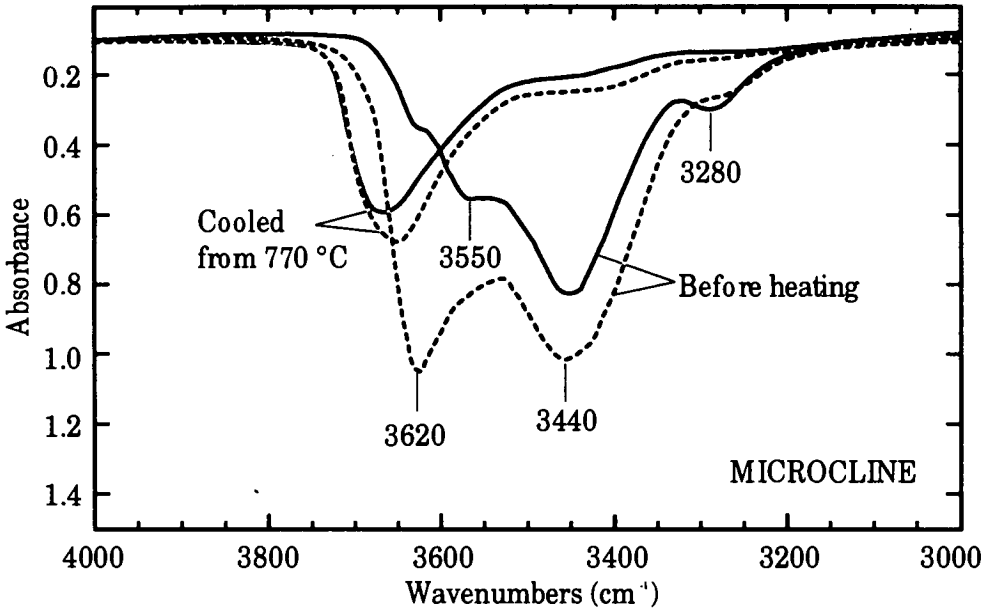

Fig. 9.3. A comparison of the spectrum of the cooled sample of Fig. 9.2 with the spectrum taken before heat treatment. Dashed lines = α, solid lines = γ. (redrawn from Aines and Rossman, 1985)

Kronenberg et al, (in press) studied a sample of Kristallina adularia from Switzerland using infrared spectroscopy. They found spectral peaks at 3620, 3455, 3280, 3090, 5250, 5130 and 4750 cm^{-1}. The peaks at 3620 and 3455 cm^{-1} were strongly aligned to crystallographic orientation and closely associated with two combination peaks of OH stretch and H_2O bend at 5250 and 5130 respectively. The peaks at 3280 and 3090 cm^{-1} were not so strongly aligned and the isotropic peak at 4750 cm^{-1} seemed to be related to the peak at 3090 cm^{-1}. The lack of OH stretching combination peaks below 4600 cm^{-1} implied that molecular water was the dominant species. All of these infrared OH stretching peaks did not change when subjected to liquid nitrogen temperatures, thus implying that they were all of structural rather than of fluid inclusion water. These results are comparable to the ones for microcline listed above.

The different polarisations of the four OH stretching peaks, found by Kronenberg et al., suggested the presence of multiple site defects. The two peaks that were highly aligned were non-zero for all orientations and were not parallel to any of the optical directions of the feldspar, and hence must be the result of several site defects closely aligned to each other. Kronenberg et al. investigated the rate at which these peaks were lost at high temperatures (see Fig. 9.4). They found that the peaks were lost in the same order as those in microcline (Aines and Rossman, 1985, see above) but that the rates suggested a single mechanism for diffusion which was too fast for volume diffusion. They therefore concluded that the H_2O molecules were held within stationary defect sites, but then other mobile sites were created when the H_2O diffused to the surface. For example hydrogen could be lost by proton diffusion leaving oxygen defects behind. The stationary sites could have been in a number of possible defect sites as shown by the first three types in Table 9.1. The potassium site was favoured by Hofmeister and Rossman (1985a) and Beran (1986) owing to its large size. However, Farver and Yund (1990) found that the interstitial sites in potassium feldspar were also large. It is also possible that the H_2O could substitute for oxygen atoms. Kronenberg et al. predicted the OH stretching frequencies for these potential defect sites by calculating the size of the defect assuming the structure for the feldspar of "sanidinized orthoclase" of Ribbe (1963). This method showed that the potassium site was the most probable as all the other possibilities would produce infrared peaks at lower wavenumbers. This substitution would have to be compensated for locally in order to maintain the overall charge balance, perhaps by calcium replacing potassium or silicon replacing aluminium.

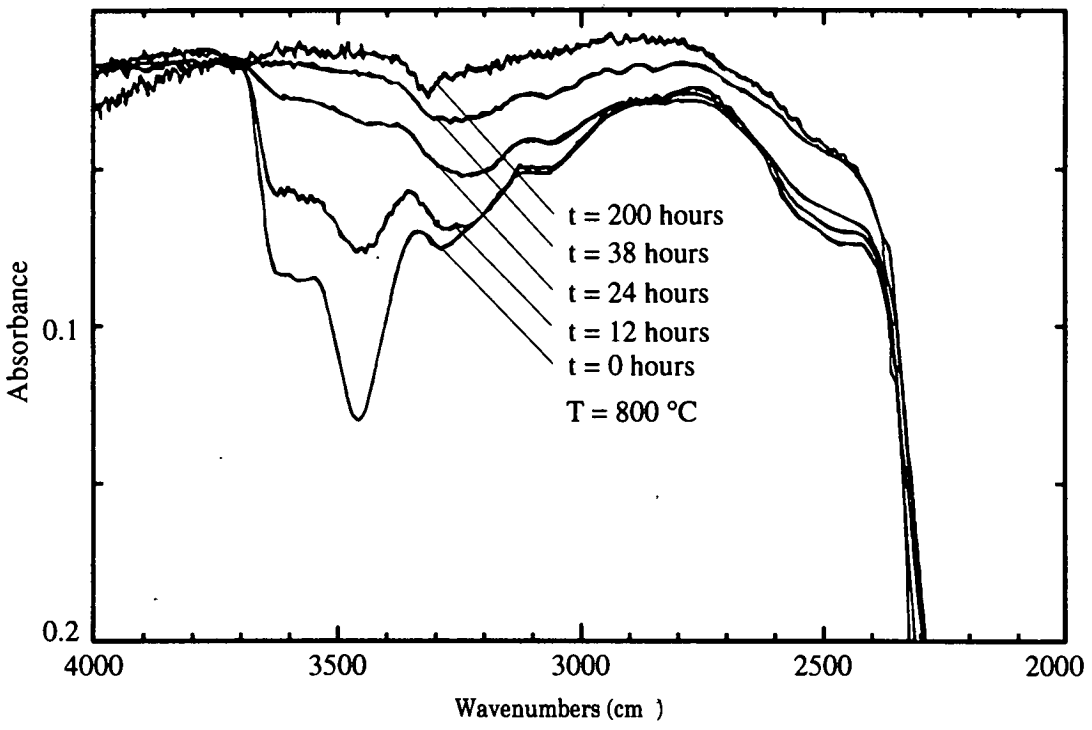

Fig. 9.4. Infrared spectra of (001) plates of adularia annealed in air at T = 800°C for time intervals t of 12 to 200 hours showing the systematic decline with increasing time of the bands at 3620 and 3455 cm^{-1} followed by the decline of the bands at 3280 and 3090 cm^{-1} (Redrawn from Kronenberg et al., in press).

Kronenberg et al also conducted experiments on the same sample of adularia at high partial pressures of water of up to 1 GPa in order to investigate rates of hydrogen gain. The rate of hydrogen gain was similar to that of hydrogen loss but produced new broad bands superimposed upon the original ones at 3455 and 3280 cm^{-1} (Fig. 9.5). The near infrared region of the spectrum still shows the presence of H_2O but the majority of the molecules must be held on different sites and in new orientations. However, it was not stated as to whether they checked that these peaks were structural ones by cooling the sample with liquid nitrogen whilst measuring the infrared spectra. These new peaks produce a spectrum similar to the one measured by Rossman and Smyth (1990) for a sanidine from a mantle eclogite (see below) but they are not in a similar position to those for Eifel sanidine (see below). The total water was estimated by measuring the integrated absorbance over the peaks between 3700 and 3000 cm^{-1} and the measurement then normalised to the sample thickness. The total water content prior to annealing experiments was 1360 ppm of hydrogen. On annealing the samples at high partial pressures of water the integrated absorbance rose, thus implying there was a larger concentration of water in the sample than at lower pressure conditions. After annealing at high partial pressures of water the total

water was difficult to measure owing to the change in shape of the spectra. However, an estimate of 2220 ppm of hydrogen was obtained after annealing at 900°C and 1 GPa of water pressure.

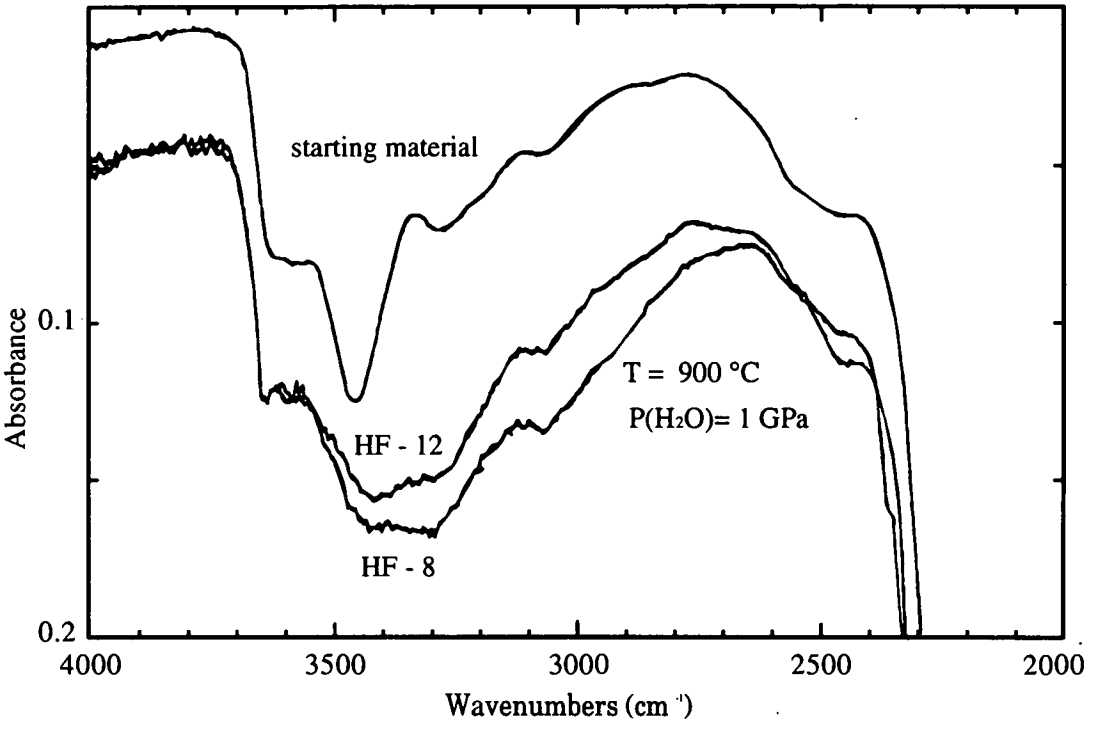

Fig. 9.5. Infrared spectra of (001) adularia plates annealed at T = 900°C and P(H_2O) = 1 GPa show new broad bands superposed upon the original bands displayed by the starting material. (Redrawn from Kronenberg et al., in press).

Most of the studies to date on sanidines have used the unusual sanidine megacrysts from the Eifel region of West Germany. These samples are clear, gem quality sanidines with extremely low dislocation densities (approximately 100/cm^3, Bertelmann, 1986) which can weigh several kilograms. The Al-Si order disorder rates and properties, summarised by Bertelmann et al. (1985) and studied by Bernotat-Wulf et al. (1988), are faster when they are away from crystal edges and dislocations. One hypothesis which may explain these fast-disordering properties is that the rate is enhanced by the presence of mobile "protons" in the structure. These "protons" may be preferentially lost in the region of grain boundaries and hence the rate of ordering is reduced. The source of these "protons" could well be structural "water".

Hofmeister and Rossman (1985b) showed that sanidine from Eifel in the Volkesfeld region of West Germany contained only a small proportion of the total water content as fluid inclusions, as there was no change in the infrared spectrum on freezing to

78K. They concluded that only 10 to 15% of the water held within the structure was of H_2O molecules, the remainder being structural OH groups. The evidence for this was the presence of a weak OH overtone in the spectra at 4550 cm^{-1} but any H_2O overtones at 5260 cm^{-1} were below noise level if they were present. If H_2O molecules were the more abundant species the 5260 cm^{-1} overtone should, in theory, be two to three times larger than the overtone at 4550 cm^{-1} and hence H_2O molecules were probably only a minor component of the total water. In addition, Hofmeister and Rossman determined the water content of the Eifel sanidine by hydrogen manometry as 0.017 wt%.

Beran (1986) also studied the water content of the Eifel sanidine. The quantity of water was found to be 0.036 wt% using an "elemental analyser". He found two bands in the OH stretching region of the spectrum (Fig. 9.6), a peak at 3400 cm^{-1} and a broader shoulder at 3050 cm^{-1}. A weaker band at 4550 cm^{-1} was attributed to a combination mode of OH stretching and implied the presence of some structural OH. In addition he noticed another absorption peak at 5150 cm^{-1} which he thought could be an overtone of H_2O. He thus concluded that there was both structural H_2O and OH groups present but that the larger component was perhaps structural H_2O. The sample of Eifel sanidine was then heated to see how the peaks changed. After three days at 700°C the broad shoulder in the spectrum at 3050 cm^{-1} increased slightly. On heating at 900°C for four days both of the OH stretching bands decreased slightly and then disappeared completely after a further three days at 1050°C.

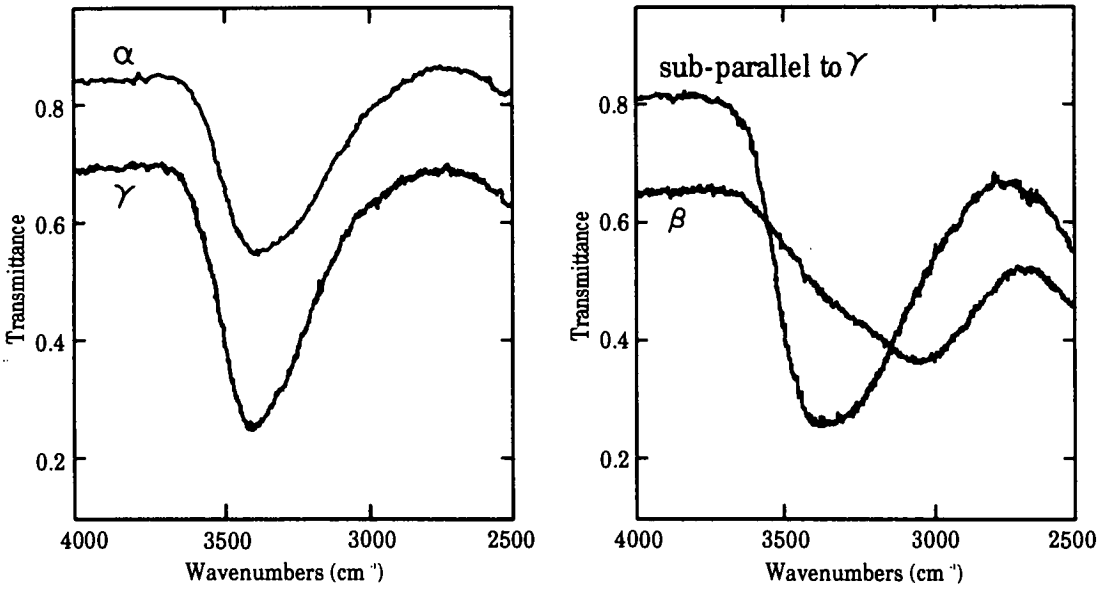

Fig. 9.6. The polarised infrared spectra of a sample of Eifel sanidine from the Volkesfeld area of West Germany. a) plate parallel to (010) b) plate perpendicular to the a axis (redrawn from Beran, 1986)

Behrens and Muller (1995) investigated the Eifel sanidines as part of a study of hydrogen feldspar. They found an absorption peak at 2485 cm^{-1} in hydrogen feldspar which he thought was an additional OH absorption band to the one at 3000 cm^{-1}. In order to check that this band was an OH band the hydrogen feldspar was exchanged with D_2O. This exchange shifted the peaks slightly in their position in good agreement with the theoretical shifts calculated from the frequency ratio ν_{OH}/ν_{OD} = 1.37, which led to the conclusion that the 2485 cm^{-1} infrared peak was due to an OH vibrational mode. Behrens and Muller also found an absorption peak at 2470 cm^{-1} in the Eifel sanidine. This peak decreased in size at the same time as the 3050 cm^{-1} on partial dehydration. They found that the OH combination mode at 4500 cm^{-1} was not well resolved but he did not find the evidence that Beran had found for structural H_2O in the region of 5150 cm^{-1}. Behrens and Muller concluded that the predominant water species in the Eifel sanidine were structural OH groups. The presence and identification of this peak at 2470 cm^{-1} was not mentioned by any of the other authors.

Detailed studies of structural "water" in other sanidines are rare. Rossman and Smyth (1990) investigated the water contents of minerals in mantle eclogite xenoliths from South African kimberlites. Figure 9.7 shows spectra from two of their sanidine samples. Most sanidine samples showed no infrared spectroscopic evidence, for the presence of water (e.g. sample 2). However, one turbid sample (1) showed a broad hump in the region of 3450 cm^{-1} which was attributed to fluid inclusion water. They did not explain the presence of the sharper shoulder at 3650 cm^{-1} or a possible slight shoulder on the trace at 3250 cm^{-1}. These peaks could be the result of structural "water" present but they do not appear to match the positions of the peaks in the Eifel sanidine

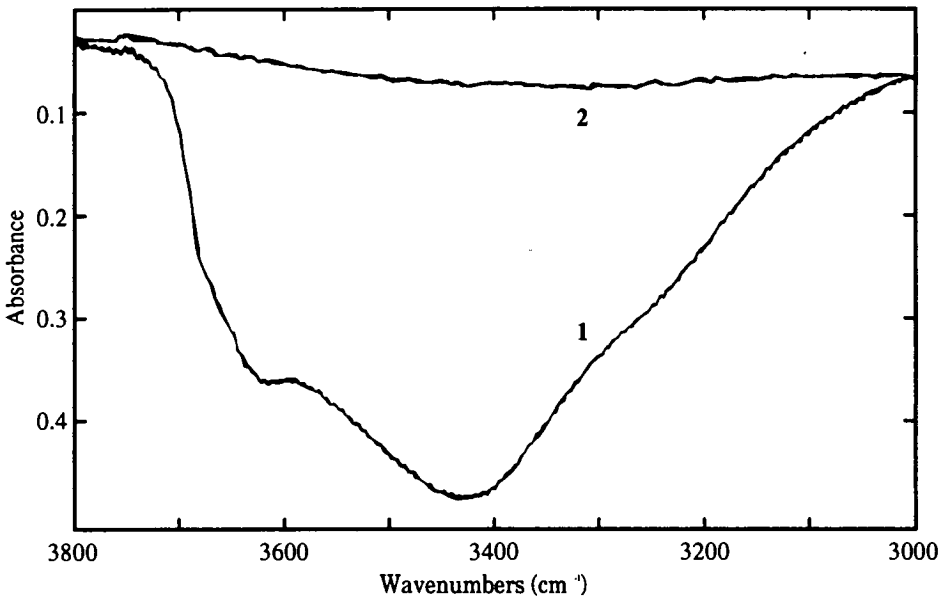

Fig. 9.7. Infrared spectra of two sanidines from grospydite SRV-1. One sample (1) was from a slightly turbid crystal and shows the presence of a broad hump of fluid inclusion water at approximately 3450 cm^{-1}. Rossman and Smyth did not explain the occurrence of the sharper shoulder at 3650 cm^{-1}, which could be structural "water", or a slight shoulder at 3250 cm^{-1}. The other sample (2) shows no evidence of "water" as either fluid inclusion water or as structural "water". (Redrawn from Rossman and Smyth, 1990)

9.3 Infrared spectroscopy of synthetic sanidines

In this present study the run products from synthesis experiments were fine powders with a grain size of approximately one micron. Hence these samples could not be studied using the infrared microscope and so a powder method of analysis was sought. Initially infrared spectra were measured with the samples mounted in potassium bromide discs. This is a widely used technique but is not ideal for studying small water contents of minerals, as the potassium bromide is hygroscopic, and therefore produces a broad hump on the spectrum from surface water. This broad hump may obscure some of the features of the mineral's spectrum. A second method using diffuse reflectance of the infrared radiation off the surface of the sample was employed for comparison. This reflectance method is not widely used but it should avoid the problems of masking by adsorbed surface water. Any remaining broad fluid water peaks will mostly be caused by fluid inclusion water.

9.3.1 *Potassium bromide disc method*

The two sanidines from runs 51 and 57 synthesised at high pressures as part of the reversal experiments were investigated by infrared spectroscopy using a potassium bromide disc method. Figure 9.8. is a trace of run 51 which shows the same features

as the trace of run 57. Both these spectra show no H_2O bending peak in the region of 1620 cm^{-1}. In the OH stretching region two spectral features can be seen; they are a small but fairly sharp peak at 3630 cm^{-1} and a broader hump at 3420 cm^{-1}. Both of these are probably not entirely of peaks for structural "water" as potassium bromide is hygroscopic and a peak for fluid surface water is inevitable. The peak at 3630 cm^{-1} probably represents structural OH but there could well be another structural OH peak hidden behind the surface water peak at 3420 cm^{-1}.

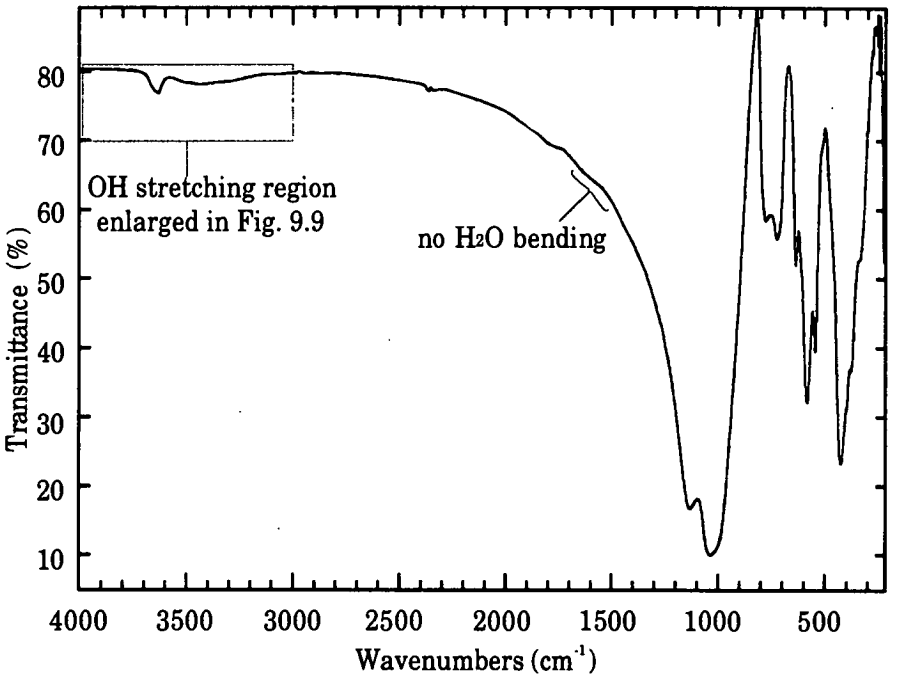

Fig. 9.8. Infrared spectrum of a sanidine synthesised at high pressure (run 51) showing a lack of a H_2O bending peak and two features in the OH stretching region.

These features can be seen more clearly by the black trace in Figure 9.9 which is an enlargement of the OH stretching region. For comparison another trace is shown in grey. This was the trace for run 45 which, after synthesis, was fired at 1100°C for 20 hours to see if this removed the traces of water. The fired run product had lost the sharp peak at 3630 cm^{-1} but whether the broad peak was entirely for surface water cannot be distinguished. When using a KBr disc it is almost impossible to avoid the adsorption of a small proportion of surface water as KBr is hygroscopic. The peak at 3420 cm^{-1} is probably due to surface water. In order to distinguish between fluid water on the surface of the sample or contained within fluid inclusions, and structural "water" peaks in the OH stretching region, the sample needs to be held at liquid nitrogen temperatures during analysis in order to observe the formation of ice peaks in the fluid. It was not possible to use liquid nitrogen on the equipment in the

National Museum of Scotland as the cooling facility was not available. The difference in the intensity of the two peaks is not of importance as it mostly reflects the different quantities of the sample used. The other feature of this part of the spectrum, the single sharp peak, must be due to the presence of structural OH groups within the sanidine crystals. The peaks in this trace are probably not the result of the presence of structural H_2O as there is no H_2O bending peak. There is another slight shoulder in the trace at 3280 cm^{-1} which could be part of an OH stretching peak hidden by the peak for surface water.

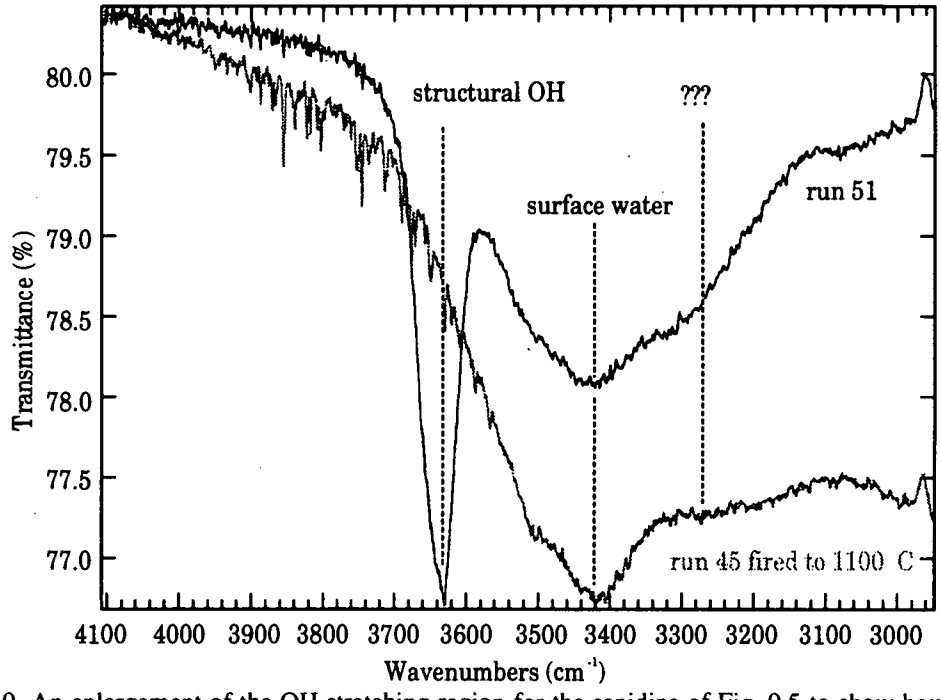

Fig. 9.9. An enlargement of the OH stretching region for the sanidine of Fig. 9.5 to show how run 51 (black trace) compares with run 45 (grey trace) which, after synthesis, was fired to 1100°C for 20 hours. The broad hump in both samples may be for adsorbed surface water and the sharp peak in run 51 must be caused by the presence of structural OH.

The OH stretching region appears similar to that described by Beran (1986) and is shown in Figure 9.6 but is displaced to higher wavenumbers. The peak found by Behrens and Muller (1995) in the 2400 to 2500 cm^{-1} range of the spectrum could not be seen in the spectra of runs 51 and 57. There were two peaks at slightly lower wavenumbers, between 2300 and 2400 cm^{-1}, which varied in height and bore no relation to the height of either of the OH stretching absorption peaks. These two peaks were also found in samples of "sanidine hydrate" and hence it was concluded that they were more likely to be the result of atmospheric CO_2. The overall shape of the spectra and the peak positions on it look more like that of adularia annealed at high partial pressures of water (Kronenberg et al., in press).

For comparison, a powdered sample of Eifel sanidine was made into a disc with potassium bromide. The OH stretching region is shown in Figure 9.10. The potassium bromide disc method shows no evidence for H_2O bending at approximately 1620 cm^{-1} and in the OH stretching region there is only a slight peak. Eifel sanidine has the highest structural "water" content of any known naturally occurring sanidine. Estimates of the quantity of water in Eifel sanidine vary from approximately 0.17 wt% (Hofmeister and Rossman, 1985b) to 0.36 wt% (Beran, 1986). A potassium bromide disc should contain randomly oriented crystals of the sample and therefore one would expect to see a spectrum which contains the peaks as seen in all orientations. Beran (1986) found two infrared peaks in Eifel sanidine at wavenumbers 3450 and 3050 cm^{-1}. The sample of Eifel sanidine, in the present study, mounted in potassium bromide, showed no evidence for two peaks in these positions and hence the slight peak seen must be caused by the surface water adsorbed by the potassium bromide. Since the quantity of sample of the synthetic sanidines and the Eifel sanidine used in the preparation of each potassium bromide disc for infrared spectroscopy was similar, the presence of peaks for the synthetic samples that were not in the Eifel sanidine would imply that the water content of the synthetic samples was greater. Attempts were made to quantify this water content of the synthetic samples using thermogravimetric analysis (see Section 9.4). The Eifel sanidine was also investigated in this respect using diffuse reflectance (see Fig. 9.10). This showed the presence of two small infrared peaks at 3450 and possibly 3050 cm^{-1} as described by Beran (1986).

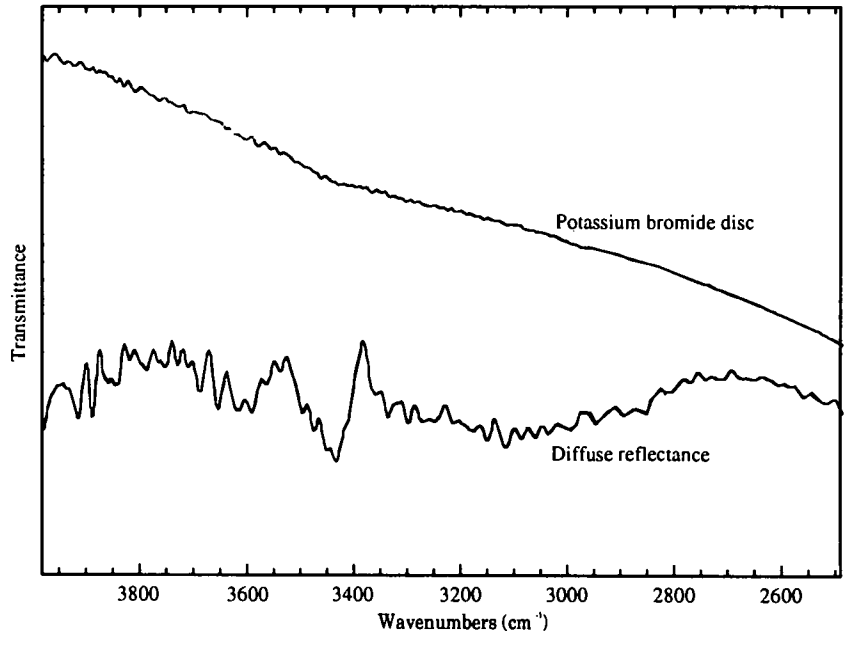

Fig. 9.10. Infrared spectra of powdered Eifel sanidine obtained using a potassium bromide disc method and a diffuse reflectance method. (spectra are not drawn to scale)

9.3.2 *Diffuse reflectance analysis*

The hygroscopic behaviour of potassium bromide made the investigation of small water contents difficult to observe as frequently the structural "water" peaks in the OH stretching region were obscured by the broad surface water peak. The grain size and powdered nature of the sample prohibited the use of the infrared microscope. Hence a less commonly used technique of diffuse reflectance was employed. This method should only show "water" peaks of the sample itself, although the spectra are usually poorer and contain additional peaks not found with other methods which are presumably the result of interference of some sort.

Spectra were measured for samples synthesised at a variety of pressures at approximately 700°C in order to see if the water content varied systematically with pressure and temperature of synthesis. In addition two different starting materials were compared. The original gel (DLH gel) starting material for the reversal experiments was made by D.L. Hamilton of Manchester University. Some gels were synthesised at the beginning of this study by the author (e.g. P3K100) but met with inexplicable problems in the low pressure runs (see Appendix A). These gels appeared to behave in the same manner as Hamilton's gel at higher pressures but at 0.1 GPa they contained slight additional impurities. A large proportion of the run product of these low pressure experiments was sanidine and so these samples were also studied. They should then at least be able to show whether the results of infrared spectroscopy were consistent or not.

The results of infrared spectroscopy on the samples synthesised with D.L. Hamilton's gel are shown in Figure 9.11. Those which used gel P3K100, as synthesised by the author, are shown in Figure 9.12. Tables 9.2 and 9.3 list the pressure, temperature and the weight percentage water content in the capsule for each experiment. The relative water content was estimated from each infrared spectra by measuring the peak area beneath the spectrum on a plot of absorbance against wavenumbers and normalising it to the area of a peak of the silicate structure (for method see Section 3.6.2b). The method may not be ideal but it is the best approximation available with powdered samples.

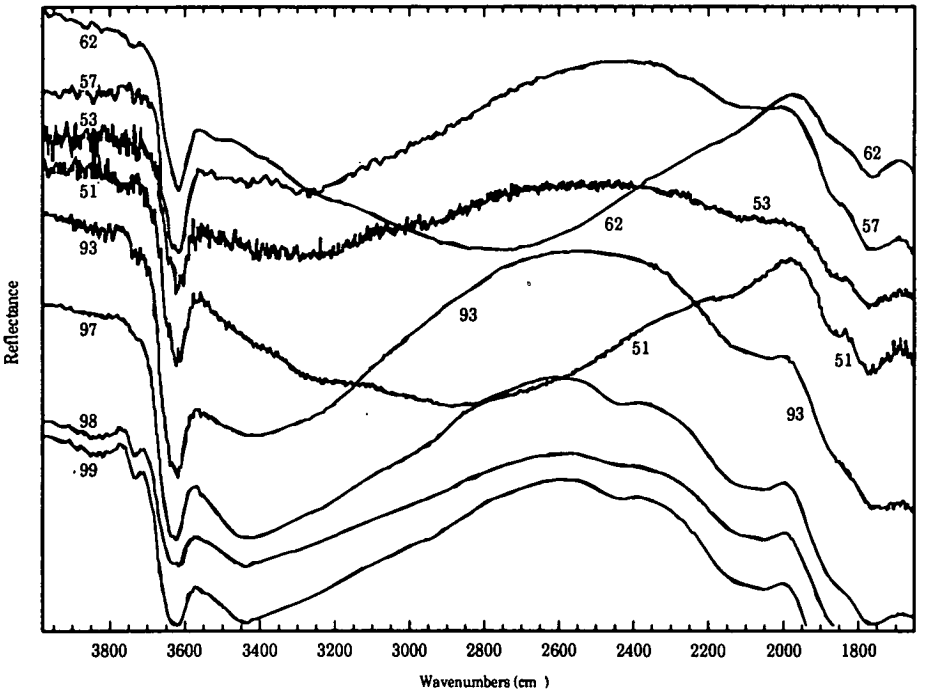

Fig. 9.11. Infrared spectra, from diffuse reflectance, of samples synthesised using D.L. Hamilton's gel. (spectra are not drawn to the same transmittance scale)

Table 9.2. Experimental conditions and normalised areas of OH peaks, measured on a plot of absorbance, of samples synthesised using D.L. Hamilton's gel. Infrared spectra are shown in Fig. 9.11.

Run No.	Pressure (GPa)	Temperature (°C)	Water in capsule (wt%)	Normalised area of OH peaks (3800-3000cm^{-1})	Normalised area of shoulder at (3690-3540 cm^{-1})
62	2.74	680	6.38	10.38	0.33
57	2.5	650	6.35	1.517	0.17
51	2.0	550	6.36	6.54	0.22
93	1.5	700	10.9	4.371	0.32
97	0.5	700	9.0	5.732	0.39
98	0.1	700	11.8	2.61	0.19
99	0.1	700	11.8	1.559	0.17

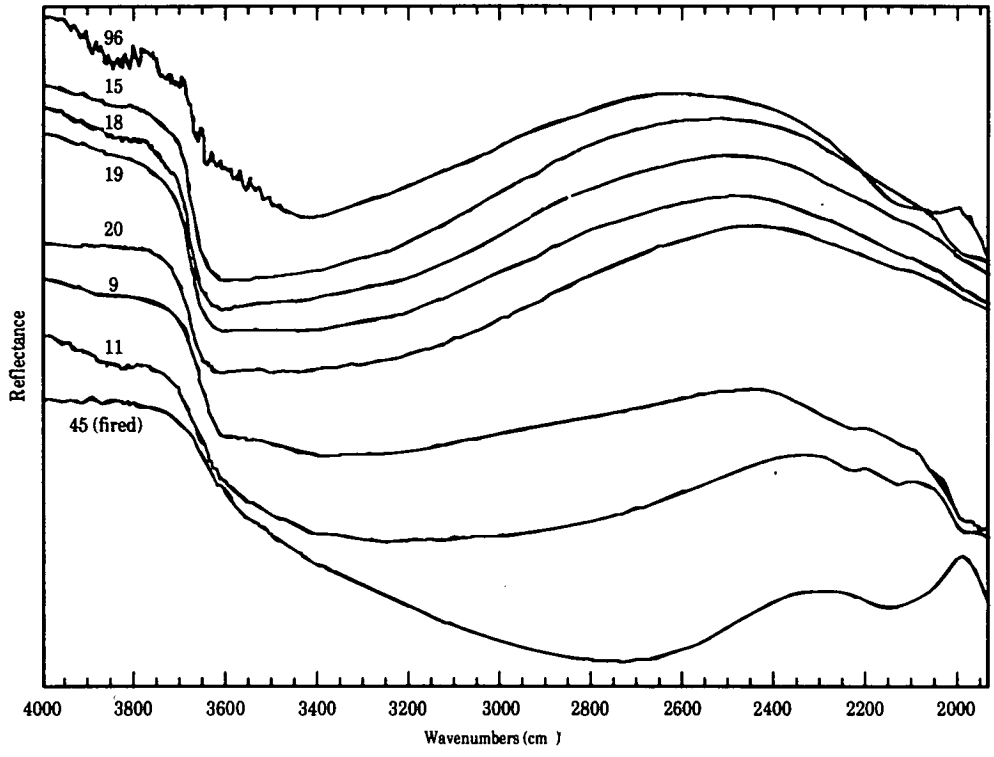

Fig. 9.12. Infrared spectra, from diffuse reflectance, of samples synthesised using gel P3K100. (spectra are not drawn to the same transmittance scale)

Table 9.3. Experimental conditions and normalised areas of OH peaks, measured on a plot of absorbance of samples synthesised using gel P3K100. Infrared spectra are shown in Fig. 9.12.

Run No.	Pressure (GPa)	Temperature (°C)	Water in capsule (wt%)	Normalised area of OH peaks (3800-3000cm^{-1})	Normalised area of shoulder at (3690-3540 cm^{-1})
96	0.5	700	10.4	2.11	0.09
18	0.1	750	1.87	13.37	0.82
20	0.1	750	2.01	11.33	0.79
11	0.1	750	2.63	2.40	0.09
19	0.1	750	2.03	10.47	0.45
15	0.1	750	5.9	6.72	0.57
9	0.1	750	2.73	2.08	0.08
45 (fired)	0.1	750	----	5.77	----

9.3.3 *Interpretation of diffuse reflectance analysis*

The spectra of feldspars crystallised from the two different gel starting materials appear to be quite different from each other. The spectra obtained from samples synthesised using D.L. Hamilton's gel all contain strong peaks in the region of 3620 cm^{-1} and 3400 cm^{-1}. In the samples synthesised using gel P3K100 the peak at 3620 cm^{-1} is less pronounced and sometimes absent. Samples 96 and 97 were both synthesised under the same experimental conditions, as they were run together in the same cold seal bomb, but with differing starting materials. The run products of these two experiments look substantially different to each other and yet similar to the other experiments that used the same gel starting material. In samples 51, 62 and the fired product of sample 45 there is a broad peak on the infrared spectrum in the region of 2900 cm^{-1}. The explanation for this peak at 2900 cm^{-1} is not obvious. The fired sample of run 45 did not contain an obvious peak in this region, using the potassium bromide disc method but does using this method. However, there are definitely some OH stretching peaks remaining even after firing and hence this shows that not all of the water had been lost by firing to 1150°C for only 12 hours. This would agree with the work of Kronenberg et al (in press) and Aines and Rossman (1985) who both stated that firing times of the order of 200 hours duration were required to remove all traces of structural "water".

Identification of these peaks as a particular type of water is not easy with infrared spectroscopy without the use of liquid nitrogen. This method of investigation was not possible on the equipment available. Evidence from the H_2O bending region was confused by the presence of additional peaks in the diffuse reflectance spectra which were not present with other techniques. The near infrared region of the spectrum showed no peaks for OH-OH and OH-H_2O combinations that were above the high noise level.

The attempts to calculate a relative quantity of water in these samples by normalising the peak areas were not successful (see Tables 9.2 and 9.3). The method of calculation is not as good as can be estimated with microscopic methods which involve normalising peak areas to sample thickness. Samples synthesised from gel P3K100 at 0.1 GPa and 750°C, which should be a similar material, do not all produce the same value. Also the variation is unrelated to the amount of water inserted into the capsule at the beginning of the synthesis experiments.

If these spectra are compared to spectra for the Eifel sanidines they appear to differ. The peaks are not in the same position as the peaks seen in Figure 9.10 or those

found by Beran (1986). In fact the spectra look more similar to those obtained by Kronenberg et al. (in press) for microclines annealed at high partial pressures of water (see Fig. 9.5) and also one spectrum for a sanidine from a mantle eclogite xenolith (number 2 in Fig. 9.7, Rossman and Smyth, 1990).

9.4 Thermogravimetric analysis of sanidines synthesised at high pressure

The sanidine synthesised at high pressure was observed by infrared spectroscopy and found to contain a component of structural OH (see previous section). Four samples of sanidine synthesised at high pressure (from runs 51, 57, 58 and 62) were examined using thermogravimetric analysis in order to see if the amount of the structural OH could be quantified and at what temperature the water was lost. Figure 9.13 shows a typical thermogravimetric trace of a sanidine synthesised at high pressure (from run 51).

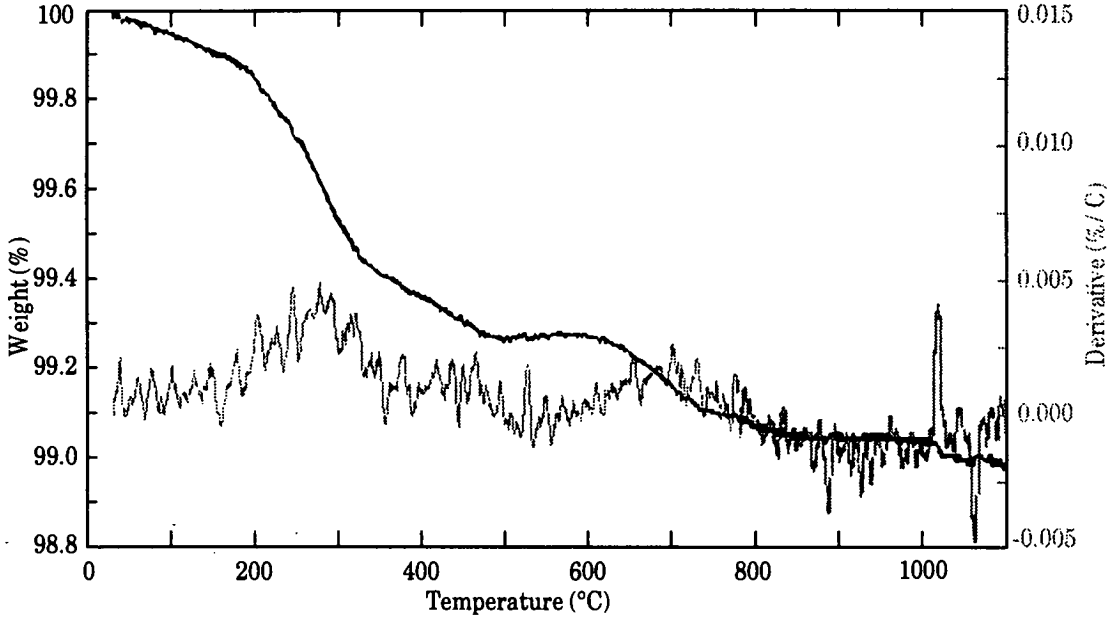

Fig. 9.13. A typical thermogravimetric result of a sanidine synthesised at high pressure (run 51) showing the weight loss (black line) and the derivative of the weight loss with respect to temperature (grey line) plotted against temperature. Weight loss could be caused by the loss of surface water, fluid inclusion water in micropores and structural OH groups, or a combination of these.

The thermogravimetric traces for runs 57 and 58 both showed a similar pattern to that of run 51 with only slight variations in the total weight loss. The trace for run 62 (Fig. 9.14) varied a little from those mentioned above.

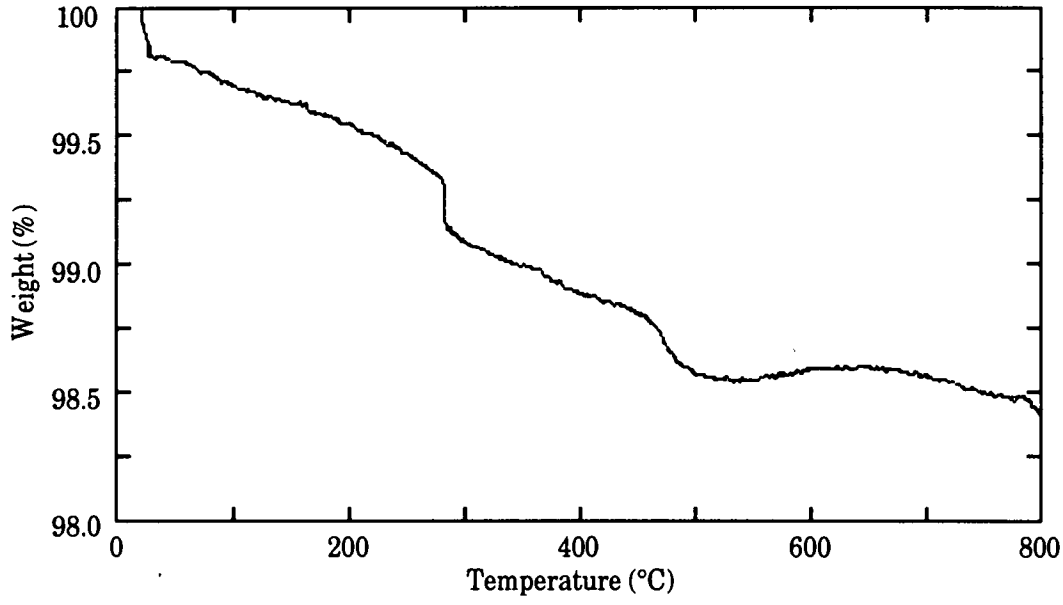

Fig. 9.14. The trace of the thermogravimetric result of a sanidine synthesised at high pressure (run 62) which varied from that of runs 51, 57 and 58 and had an increased total weight loss up to 800°C. Weight loss could be caused by the loss of surface water, fluid inclusion water in micropores and structural OH groups, or probably a combination of these.

Figure 9.13 displays the complex variable weight loss with temperature for run 51. There is an overall weight loss of approximately 1.0 wt%. However, this weight loss occurs in stages. Up to 250°C the weight loss is small (less than 0.1 wt%). From 250°C to 325°C a loss of approximately 0.45 wt% occurs. Between 325°C and 475°C the weight loss curve becomes shallower with a weight loss of only about 0.2 wt%. In the temperature range 475°C to 600°C no weight loss occurs and above 600°C the curve steepens again showing increased weight loss but flattens out again by 1150°C. All four samples studied were initially only taken up to 800°C. Attempts to run samples to higher temperatures were curtailed by the failure of the experimental equipment which prevented any more work being achieved for several months. Two samples were eventually run up to 1150°C to check for further weight loss above 800°C. Only a small loss of weight occurred between 800°C and 1150°C. The infrared traces in Figure 9.16 show that not all of the water had been lost by 1150°C and the weight loss curve shows slight change all the way up to 1150°C. Ideally the thermogravimetric analysis instrument should have been left at high temperature for

several hours until the weight loss reached a plateau. However, according to Kronenberg et al. (in press), this dehydration could take up to 200 hours which could have damaged the instrument.

It is more difficult to explain the results shown in Figure 9.13 at the higher temperatures. The potential sources of weight loss could be adsorbed surface water, water in fluid inclusions or structural OH or H_2O. Part of the weight loss might be from some of the structural OH of the 3620 cm^{-1} peak identified by infrared spectroscopy. It is probable that the loss of structural OH would be at higher temperatures than the temperatures for the loss of water within fluid inclusions.

It is interesting at this stage to compare the thermogravimetric trace in Figure 9.13 with that produced by a similar sample from run 45 (Fig. 9.15) which was fired at 1100°C for 20 hours to remove water. As was shown in the previous section this firing may not have been sufficient to remove all of the structural "water". However, the sample should have lost all of the water which it might have released in a short duration run up to 1150°C. Thus any water loss can be attributed to surface water being adsorbed by the sample after firing. This surface water must be the cause of that weight loss between 75°C and 300°C of approximately 0.1 wt%. The surface water loss, although at slightly higher temperatures than in the unfired runs, is probably an explanation of the initial weight loss in Figures 9.13 and 9.14. The small but steady increase in weight (0.25 wt%) of the fired sample (Fig. 9.15) over the entire temperature range measured is probably a result of measurement drift in the thermogravimetric analysis machine. If this effect is caused by the normal drift of the machine it would indicate that all measurements might be approximately 0.03 wt% below their true measurement for every 100°C increase in temperature.

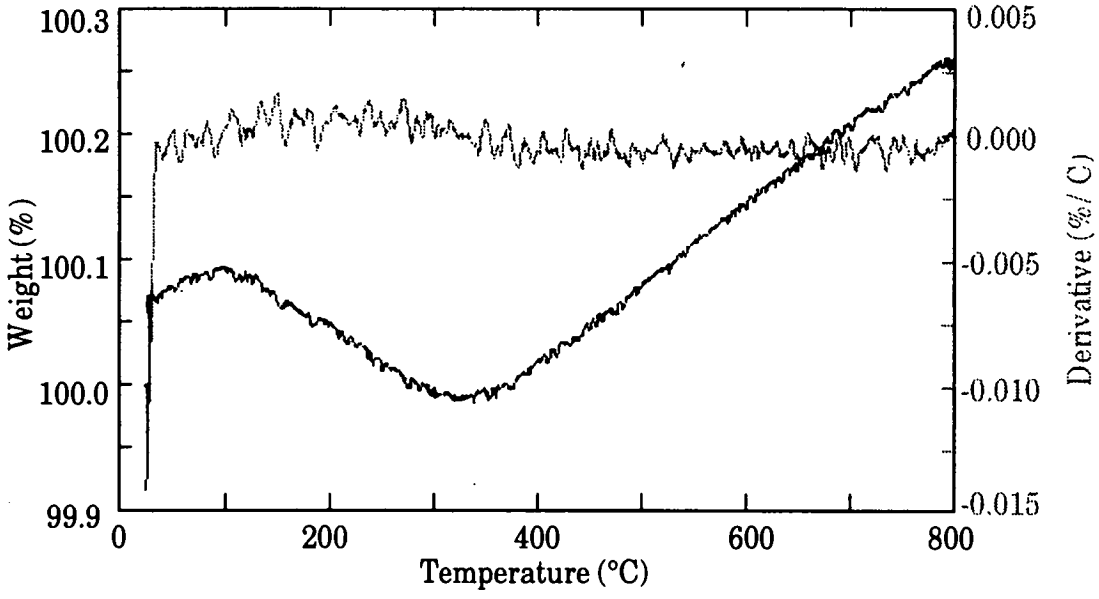

Fig. 9.15. A thermogravimetric result for a sanidine synthesised at high pressure (run 45) and then fired to 1100°C for 20 hours to remove any traces of structural OH over this temperature range (as identified by IR spectroscopy in Section 9.4.1). It shows the weight loss (black line) and the derivative of the weight loss with respect to temperature (grey line) plotted against temperature. Any weight loss should be the result of surface water adsorption. The gradual increase in weight over the entire temperature range measured is probably due to a slight measurement drift in the thermogravimetric analysis instrument.

9.4.1 *Infrared spectroscopy of the products of thermogravimetric analysis*

Samples of sanidine that had been subjected to thermogravimetric analysis were studied with infrared spectroscopy in order to see if all of their water had been removed. Some samples were run up to 800°C after which the water content was checked with infrared spectroscopy. The continuing presence of some remaining water meant that samples had to be run up to 1150°C, giving some idea of how the water content is affected by heating. All samples were checked with powder X-ray diffraction after thermogravimetric analysis to ensure that they remained as sanidine.

Infrared spectroscopy of the products of thermogravimetric analysis (Fig. 9.16) showed that at 800°C both water peaks were still present but perhaps the peak at 3620 cm^{-1} had slightly diminished in size relative to the peak at 3400 cm^{-1}. By 1150°C the peak at 3620 cm^{-1} had disappeared completely but the peak at 3400 cm^{-1} was still present. Kronenberg et al (in press) and Aines and Rossman (1985) found that the water in microcline and adularia only disappeared entirely when samples were annealed for 200 hours or more at high temperatures and that the peaks at lower wavenumbers took longer to disappear. The samples in this study were not held at

high enough temperatures for long enough to remove all of the water, leaving most of the water as a peak at approximately 3400 cm^{-1}.

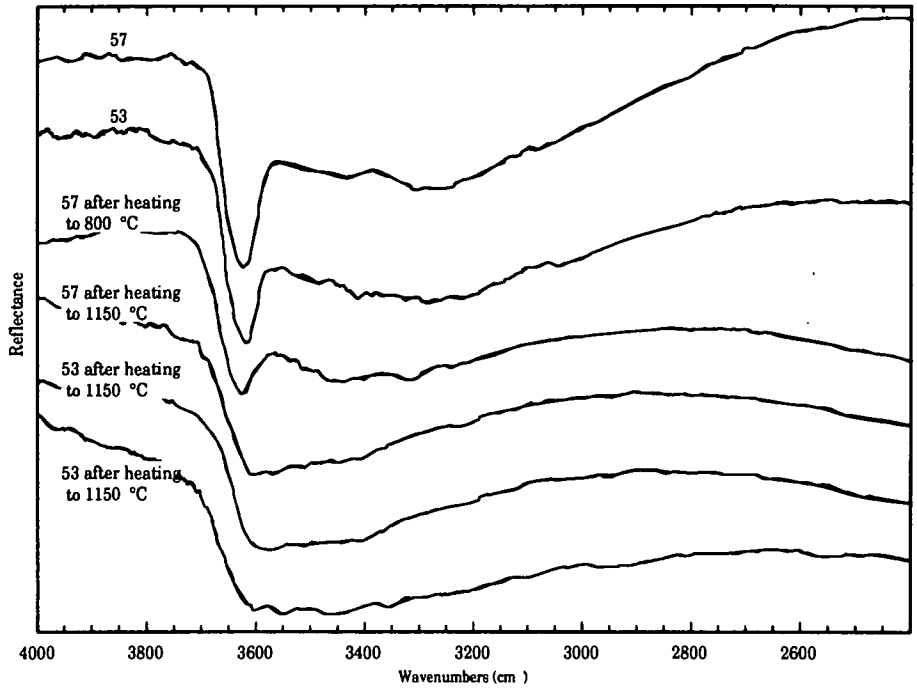

Fig. 9.16. Infrared spectra obtained by diffuse reflectance of samples subjected to thermogravimetric analysis up to different temperatures. (spectra not drawn to the same transmittance scale)

The normalised peak areas for samples subjected to thermogravimetric analysis were calculated and are listed in Table 9.4. The values calculated for the area of the shoulder at 3620 cm^{-1} decrease as would be expected on dehydration but do not appear to show the same values for the same degree of dehydration. It is probable that this decrease is not significant and that the normalisation method is not giving reasonable results, as was also shown in Tables 9.2 and 9.3. The anomalous values for the third sample of run 53 is caused by the spectrum being a different shape to any of the others. This sample was run in a thermogravimetric analysis instrument in Manchester and it is possible that it may have begun to melt which could result in the partially different shape of the spectrum at lower wavenumbers.

Table 9.4. Normalised areas of infrared OH stretching peaks in samples after heating during thermogravimetric analysis

Run description	Normalised area of OH peaks (3800-3000 cm^{-1})	Normalised area of shoulder (3690-3540 cm^{-1})
57	1.53	0.15
53	1.19	0.10
57 heated to 800°C	0.56	0.09
57 heated to 1150°C	0.98	0.09
53 heated to 1150°C	0.91	0.05
53 heated to 1150°C	28??	3??

9.5 Conclusions

Sanidines synthesised at high partial pressures of water in this study contain structural "water". The type of "water" is possibly structural OH contained within more than one defect site. The evidence for structural OH is not conclusive because of the lack of a liquid nitrogen cooling facility and the absence of any peaks above noise level in the near infrared spectrum. The only indication for structural OH is the lack of H_2O bending peaks when using the potassium bromide disc method. In three of the samples (from runs 62, 51 and the fired product of run 45) another peak appeared at 2900 cm^{-1} which was unusual and was not readily explained.

The general appearance of the spectra is more like that of adularia annealed at high partial pressures of water (Kronenberg et al., in press) or of a sanidine from a mantle eclogite xenolith (Rossman and Smyth, 1990) than that of Eifel sanidine. Eifel sanidines exhibit infrared peaks at lower wavenumbers (Beran, 1986). The method employing potassium bromide discs showed strong infrared peaks for the synthetic sanidines but not for a sample of Eifel sanidine run under the same conditions. Thus it is concluded that the water content of these synthetic sanidines is considerably greater than that of Eifel sanidine (0.018 wt% to 0.36 wt %, Hofmeister and Rossman, 1985b, and Beran, 1986, respectively) but by how much is not known.

The general shape of the infrared spectra did not vary with pressure of synthesis but looked substantially different for the two different starting materials used. Attempts to calculate relative water contents of these samples from the infrared spectra by measuring the peak area normalised to a peak from the silicate framework was inconclusive. The absolute water content could not be measured by these methods.

Thermogravimetric analysis showed that there were many stages to the weight loss with increase of temperature. Infrared spectroscopy of the residues from thermogravimetric analysis showed that not all the water had been lost by heating to 1150°C. The infrared peak at 3620 cm^{-1} had disappeared but the one at 3420 cm^{-1} still remained. This result is consistent with the outcome of the work of Kronenberg et al. (in press) and Aines and Rossman (1985) that it takes up to 200 hours at elevated temperatures to remove the water entirely.

Chapter 10
"Water" content of Klokken feldspars

10.1 Introduction

In Chapter 9 is described a study of the water contents of sanidines, synthesised at a variety of pressures and temperatures, and observed and measured by infrared spectroscopy and thermogravimetric analysis. It was anticipated that the study of sanidines synthesised under such conditions would show some systematic variation in their water contents, but the methods employed did not produce any useful results. If sanidine contains more structural "water" at high temperatures then, on slow cooling, it would presumably exsolve some of its structural "water". This exsolved water may contribute towards the fluid which causes low temperature deuteric alteration, which forms patch perthites and turbidity in most feldspars. Also, if pristine, unaltered feldspar retains the water content that it had on growth from the magma, it could, in principle, permit a quantitative estimate of magmatic water content which is a critical variable in igneous petrogenesis. Thus additional evidence for structural "water" variation was sought from naturally occurring feldspars.

Much work has been carried out on the water content of isolated samples of feldspar (e.g. Hofmeister and Rossman 1985a, Hofmeister and Rossman 1985b, Aines and Rossman 1985, Beran 1986, Behrens and Muller 1995 and Kronenberg et al., in press; see Section 9.2 for a review). However, variation in the water content of a suite of feldspars from a single pluton has not been investigated. The Klokken layered syenite of South Greenland (described in Section 10.2) is an ideal source of material for study as it contains rocks with over 80% by volume of alkali feldspars, and the various rock types are a well defined, evolving sequence, on the basis of Fe/(Fe+Mg) in mafic phases (Parsons, 1979 and Parsons and Becker, 1986a). The feldspars have been well characterised previously (Brown et al 1983, see also bibliography in Parsons and Becker, 1986a)). The central part of the pluton consists of two interleaved suites of rocks, the granular syenites and the laminated syenites. The feldspars in both these suites of rocks show a systematic variation in the periodicity of the exsolution lamellae with stratigraphic height in the intrusion, the periodicity increasing downwards away from the roof. The granular syenites increase in grain size from the top of the intrusion towards the bottom, and show a regular downward increase in Fe/(Fe+Mg) in pyroxenes and olivines. There is therefore good evidence that the granular syenites are an "upper border group" which congealed against the roof of the intrusion. It was suspected that a regular variation might also occur in the structural "water" content of these feldspars, perhaps increasing as the magma evolved. A set of rocks from the granular syenites was chosen for this study as these were the more pristine, fluid-inclusion-free samples. In addition an attempt was made to establish whether the structural "water" content of the granular and laminated

series differed at the same stratigraphic height in order to explain the variations in the exsolution micro-textures between the two suites (see Brown et al., 1983, Worden et al., 1990). As it turned out this measurement was not possible because of the large quantity of fluid inclusion water in the laminated syenites.

It was initially intended to apply both infrared spectroscopy and thermogravimetric analysis to the samples from the layered series of Klokken. Unfortunately, prior to the anticipated investigation, the Chemistry Department of St. Andrews University suffered a fire, followed by a flood which destroyed their thermogravimetric analysis machine. An alternative instrument was sought but none was found to have the precision required to study weight losses of less than 1% in a small sample of only a few milligrams. The machine in St. Andrews was not replaced in time and therefore the study of natural feldspars was restricted to infrared spectroscopy alone.

10.2 The Klokken intrusion (see bibliography of Parsons and Becker, 1986a))

The first stage in the formation of the Klokken intrusion was the crystallisation of gabbro, followed by unlaminated syenite around the wall of the intrusion. Then, possibly simultaneously, the granular syenites chilled from the roof downwards whilst the laminated syenites accumulated by settling at the base of the chamber (Fig. 10.1a). The dimensions of the magma chamber were calculated by Mason et al. (1985), which showed the minimum thickness of the total layered series to be 1370 - 3260 m, using trace elements in feldspars. As crystallisation proceeded the water content of the magma increased until the uppermost laminated syenites may have crystallised from an almost water-saturated magma. The lower part of the laminated syenites is not exposed. As the upper laminated syenites accumulated the lower granular syenites began to spall off, falling gently onto the pile of cumulate mush below (Fig. 10.1b). The granular syenites must have fallen slowly as they were not broken by the process. The density contrast between the crystallised granular syenites and the magma (consisting of a mixture of liquid and crystals) must have been small. The granular syenites fell while the laminated syenites were still at magmatic temperatures. The layered series of Klokken therefore consists of interleaved granular and laminated syenites. The granular syenites make up only 15% of the layered series and are more abundant near the top of the intrusion.

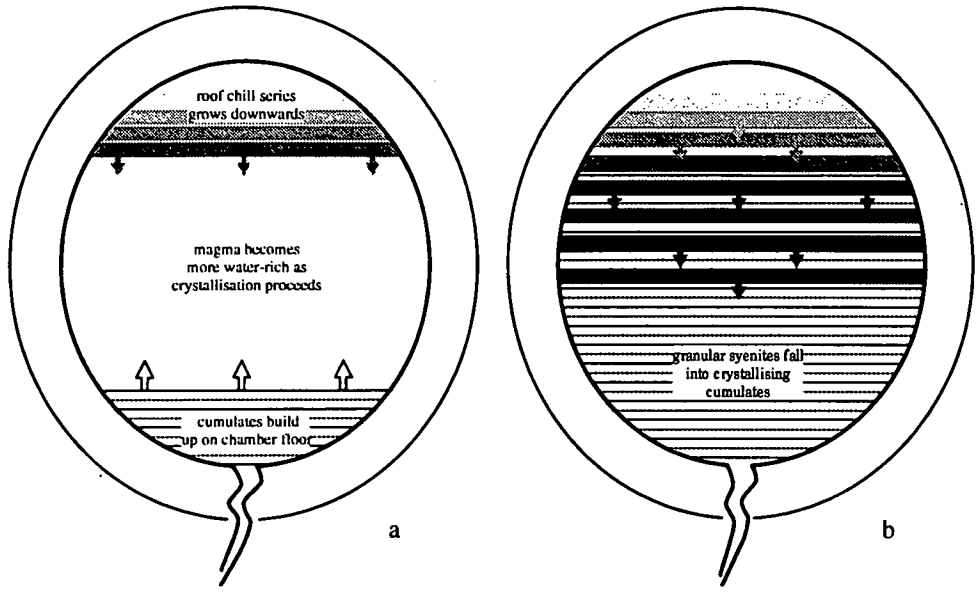

Fig. 10.1. Schematic sketch cross-section through the Klokken magma chamber in order to show how the two layered series may have formed. The outer part of the section represents the gabbro and unlaminated syenite that lines the outer wall of the intrusion (a) Granular syenites chill against the roof whilst the laminated syenites accumulate at the base of the magma chamber. (b) The granular syenites spall off onto the rising pile of cumulate mush. The true shape of the magma chamber is thought to be cylindrical with the layers forming a down pointing conical shape which may reflect the shape of the roof and floor of the chamber. The current exposure level means that approximately the lowermost third of the chamber is unexposed.

Textural observations of the two series are shown in Figure 10.2, which, for convenience, is drawn as if the granular syenites had not fallen into the laminated syenites. The textures of the granular syenites confirm the roof chill theory, with the grain size and periodicity of the primary exsolution lamellae increasing with distance from the roof of the chamber. The lamellar periodicities are not sufficiently coarse to fit the estimated cooling time but the coarsening process could well have been inhibited by ordering and twinning (Brown and Parsons, 1984). The Klokken cryptoperthites are by now fully ordered and the microcline is in the diagonal association in crypto- and micro-perthite "braid" intergrowths with low albite. The laminated syenites show a similar change with stratigraphic height but with a two-fold difference in the magnitude of the primary exsolution lamellar spacing. Brown et al (1983) suggested that this difference might be due to the water content of the magma from which the two series grew, since at the same stratigraphic height the feldspars in the granular and laminated syenites must have cooled at the same rate, and should therefore have similar lamellar periodicities

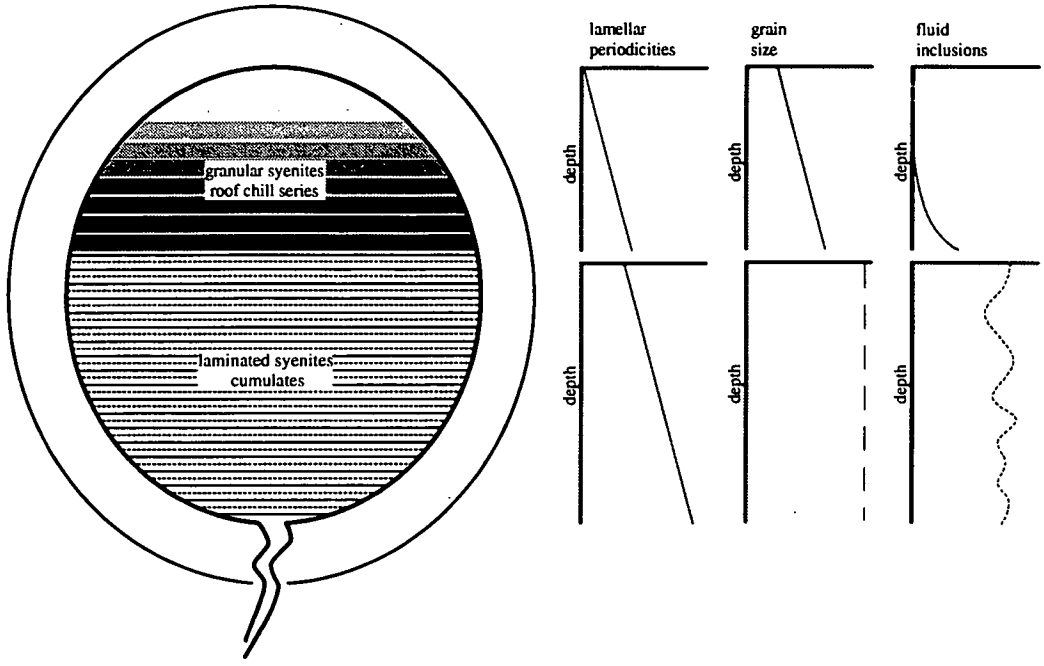

Fig. 10.2. Textural observations from the two syenite series. The magma chamber is sketched, for convenience, as if the granular syenites had not descended into the laminated syenites.

The lower granular and especially the laminated syenites show deuteric alteration forming patch perthites which cut across the primary texture and are turbid, containing myriads of tubular micropores (Worden et al., 1990). Burgess et al. (1992) showed these micropores contained fluid. The laminated syenites are more severely affected by this late stage alteration which again may indicate that a water rich magma formed these rocks. Only small patches of the feldspars in the laminated syenites were left unaltered. The deuteric alteration of the granular syenites also increases with depth from the roof of the chamber, being negligible near the top.

10.3 Models of formation of feldspar textures

The textural variation of the pristine feldspars and the deuteric alteration in the two syenites (Fig. 10.2) could have two explanations. Figure 10.3 sketches these two possible models for formation of the deuteric alteration by either late stage magmatic fluids or by exsolution of structural "water". The possibility for alteration by meteoric waters at low temperatures has been ruled out as the oxygen isotope signature of the fluid is an igneous one (Parsons et al., 1991).

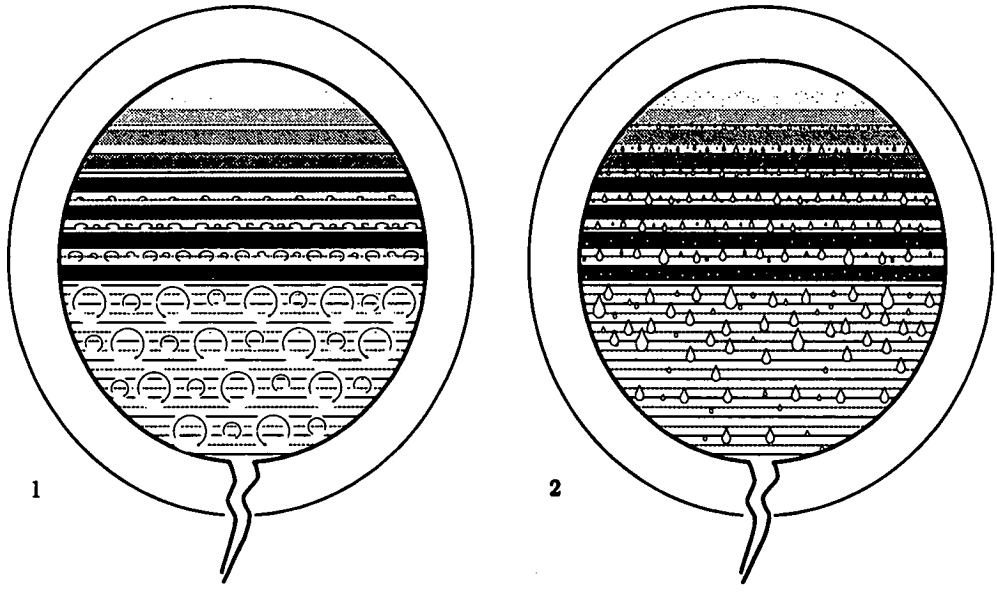

Fig. 10.3. Two models for the formation of the pattern of feldspar textures seen and as shown in Figure 10.2. Model 1 is that for the deuteric alteration is caused by low temperature magmatic fluids. Model 2 is that for exsolution of structural "water" incorporated at higher temperatures causes the deuteric alteration.

10.3.1 *Model 1: Alteration by late stage magmatic fluids*

As the magma crystallises both the granular syenites and the laminated syenites, it should become more water-rich because only a small proportion of the magmatic water can be incorporated into the cumulus crystals which are "anhydrous" (feldspar, clinopyroxene, olivine). The small amount of structural "water" incorporated into these "anhydrous" crystals will presumably increase as the water content of the magma increases. The last remaining magma to crystallise at the top of the laminated syenites could be water saturated. In fact much of the exposed, upper section of the laminated syenites could have crystallised from a magma close to water saturation. Parsons (1979) suggested that crystallisation from such a magma could explain the presence of the inversely graded layers seen in the laminated syenites in Klokken. In

each layer of the laminated syenites the quantity of iron-rich clinopyroxene and olivine increases upwards at the expense of the feldspar. The leucocratic part of the layer is usually more coarse grained, often drusy in comparison to the more mafic part of the layer. The variation in the vapour pressure will favour the crystallisation of first feldspar and then pyroxene as the degree of under-cooling changes with the depression of the melting curves. The drusy texture of the leucocratic parts of the laminated syenites, which also increases towards the top of the magma chamber, may indicate the presence of a free fluid released by a water saturated magma.

These magmatic fluids must have been stored within the magma chamber, perhaps in the drusy cavities, until temperatures below 400°C are attained, by which time the feldspars had become fully ordered but subsequently remained in coherent intergrowths. The magmatic fluids must have circulated through the relatively porous laminated syenites, thus causing catastrophic coarsening with the development of patch perthites and turbidity (Worden et al., 1990).

The granular syenites were unaltered by these late stage magmatic fluids because they were less permeable than the laminated syenites. The lower granular syenites are more altered, possibly because of their coarser grain size and as a result of the large volume of water-rich laminated syenite that surrounded them.

The pattern of granular syenites anticipated would therefore be as shown in Figure 10.4. The structural "water" of the feldspars may not show much variation with stratigraphic height but will probably increase as the water content of the magma increases. The structural "water" content of the feldspars would perhaps increase from the roof downwards in the granular syenites and from the floor upwards in the laminated syenites until some saturation level is achieved, either of the feldspar or the magma. After saturation the structural "water" component should be constant. The structural "water" component would probably be constant in the uppermost laminated syenites if the remaining pristine areas could be examined with infrared spectroscopy. The fluid inclusion water and deuteric alteration may increase slightly towards the base of the granular syenites, because of their proximity to large volumes of water rich laminated syenites, and would be relatively large and variable in the laminated syenites perhaps increasing towards the top of the chamber. The lower parts of the laminated syenites (beneath the current exposure level) may have formed before the magma became saturated and therefore may have fewer cavities and hence less fluid and deuteric alteration.

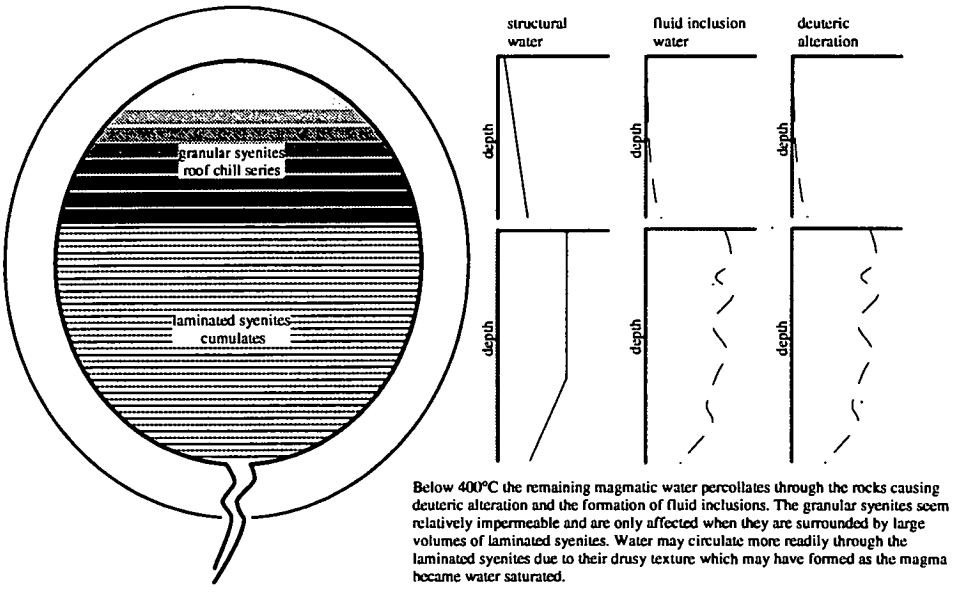

Fig. 10.4. The variation in water anticipated if low temperature magmatic fluids caused the deuteric alteration. (Model 1 in Fig. 10.3). The magma chamber is sketched, for convenience, as if the granular syenites had not descended into the laminated syenites.

10.3.2 *Model 2: Alteration by exsolved structural "water"*

At high temperatures, as the magma crystallises, a portion of the magmatic water becomes incorporated into the feldspars. However, feldspars cannot hold the same quantity of water as the magma and thus, as crystallisation proceeds, the magma water content increases and hence the structural "water" of the feldspars increases also. At some point the feldspar and the magma will become saturated with water. The two must reach saturation together, in an analogous manner to cordierite theory (Carrington and Harley (1996)), if the phase rule is obeyed. A three component system of vapour, liquid and potassium feldspar can be considered as the addition of any other phase will simply add another component (Fig. 10.5). Under vapour absent conditions, where there are only two phases present (e.g. point (1) on Figure 10.5), there are three degrees of freedom. Hence at fixed pressure and temperature the dissolved water content of the two phases is variable. As the magma crystallises the vapour component increases and the water contents of both the melt and the feldspar increase simultaneously in equilibrium with each other. The actual water content will be determined by the distribution coefficient of water between the feldspar and the melt. The melt and the feldspar must reach saturation together (point (2) on Figure 10.5) because as soon as the third vapour phase is present the degrees of freedom are limited to two. Hence at a fixed pressure and temperature the compositions of all three phases are fixed and can vary no longer. Addition of more vapour merely increases the proportion of the vapour phase without altering the composition of any

of the three phases. The pattern of variation in structural "water" would thus be as shown in Figure 10.6.

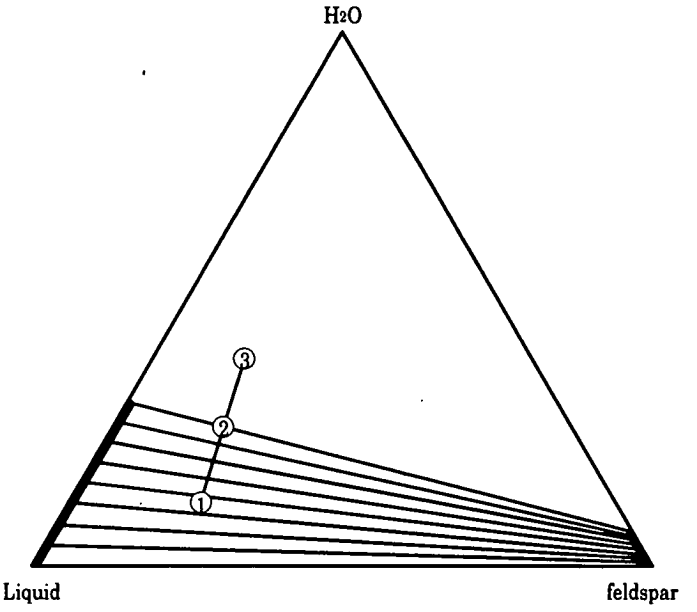

Fig. 10.5. A sketch to show that the melt and the feldspar crystals must reach saturation together at point (2) when the addition of more water brings the composition into a divariant field where the composition of the three phases is fixed if the pressure and temperature are constant.

In Chapter 9 it was anticipated that a variation of structural "water" in sanidine with pressure and temperature of synthesis would be apparent. The method used in the study of synthetic sanidine did not produce any useful results and so it was not possible to determine whether sanidine had a greater capacity for structural "water" at high temperatures or not. The model for exsolution of structural "water" forming the deuteric alteration in Klokken presumes that feldspars hold more structural "water" at elevated temperatures. There is some evidence, from the formation of fluid inclusions by Eifel sanidines during annealing experiments (Bertelmann et al., 1987), that sanidines can hold more structural "water" at the pressure-temperature conditions under which the Eifel sanidines crystallised. The conditions under which the Eifel sanidines formed are, however, unknown. Thus, if it is possible to show that this model is a plausible explanation for the textural observations seen at Klokken, then it would be a good indication that feldspars do have a larger capacity for water at higher temperatures. If feldspars crystallised at elevated temperatures incorporate water into their structure on crystallisation and are then slowly cooled, the maximum structural "water" content may decrease to a lower value at lower temperatures. The remaining water of the feldspars which contain more than this critical maximum

concentration will presumably be exsolved, perhaps below 450°C, to form a more localised fluid which causes the alteration.

The right hand side of Figure 10.6 shows the pattern of the variation of structural "water", fluid inclusion water and deuteric alteration expected after cooling if exsolved water was the main cause of alteration. The structural "water" should increase steadily in the pristine feldspars of the granular syenites until saturation is reached when the remaining water will exsolve to cause some deuteric alteration. If it could be shown that saturation of the structural "water" component of the feldspars occurred at the same level in the magma chamber as that where the fluid inclusions and the deuteric alteration just appear (i.e. in the lowermost two granular syenite samples) then this would not contradict the exsolution model for the formation of the deuteric alteration. The feldspars in the laminated syenites may be saturated over most of their range and therefore show a constant value for structural "water" in the small unaltered patches. The exsolved fluid inclusion water will increase in quantity from the bottom of the chamber until it reaches the level where the structural "water" in the high temperature feldspar became constant if the fluid released does not move far. As only the upper parts of the laminated syenites are exposed, it is probable that only that region is observed where the structural "water", fluid inclusion water and hence the deuteric alteration appear constant. Parsons and Becker (1986b) found that subsolidus fluids released by the laminated syenites circulated through the chamber causing irregular intra-layer variation. The circulation of fluid was thought to have formed the overall trend of the outer parts of the chamber being more evolved than the inner ones. This trend is shown by the zoning in pyroxenes which is reversed in high Mg samples near the centre, where pyroxenes have high Mg rims, but is normal in the more Na-rich samples nearer the outer parts of the intrusion, where the rims become richer in Na. The outer rocks can also contain almost pure acmite, usually with inter-cumulus quartz, and sometimes intensely coloured amphiboles. The fluids which caused these mineralogical differences may have done so at higher temperatures than those which caused the deuteric alteration of the feldspars (<450°C). There is little evidence that lower temperature fluids circulated as widely as the fluids at higher temperatures but if the pathways were still open then any exsolved fluids forming the deuteric alteration and fluid inclusions may not show the patterns described above.

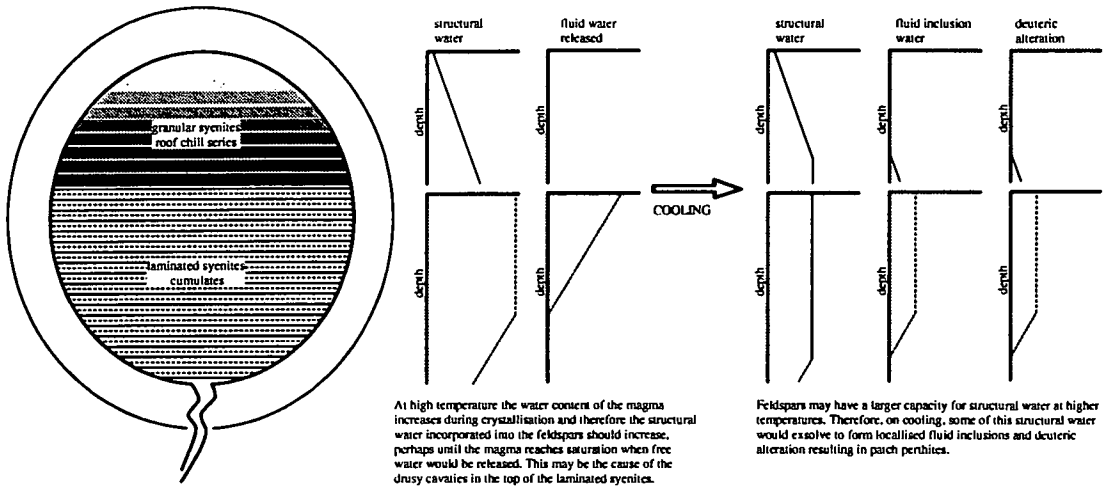

Fig. 10.6. The variation in water anticipated if exsolution of water incorporated into the feldspar structure at higher temperatures, caused the deuteric alteration. (Model 2 in Fig. 10.3). The magma chamber is sketched, for convenience, as if the granular syenites had not descended into the laminated syenites.

10.3.3 *Differentiating between the two different models*

If the theory of the exsolution of structural "water" were correct then the pattern of the structural "water" variation, in comparison to the fluid inclusion water and deuteric alteration, with depth should be examined. The increase in fluid inclusion water with distance from the roof of the chamber at the base of the granular syenites can be seen optically, but this observation would fit either hypothesis for the source of the water. If exsolution of structural "water" caused the deuteric alteration then one would expect the structural "water" component in the pristine areas of the feldspar to increase downwards until the fluid inclusions appear and from that point on remain constant. Hence the lower granular syenites and all the upper laminated syenites should have the same structural "water" content. In the presence of large amounts of fluid inclusion water an infrared spectrum would not show any evidence for structural "water", as any sharp structural "water" peaks would be obscured by the broad peak resulting from fluid water. The laminated syenites do contain small patches which are pristine but these were too small to permit measurement of their water content using the infrared microscope. The only evidence available must come from the less altered feldspars at the top of the intrusion in the granular syenites, in order to see whether the structural "water" component alters systematically. Hence five samples of the granular syenites were chosen for study by infrared spectroscopy. All the laminated syenites were too altered to identify structural "water" in their spectra (Walker 1991, figs 4.8p and 4.8q). The sample descriptions and compositions are given in Table 10.1 (Parsons et al, 1988)

Table 10.1. Chemistry and descriptions of samples from Klokken used in present study. Reproduced from Table 1 of Parsons et al (1988).

Sample No.	Height	General character and optical appearance	Bulk composition Or	Ab	An
GGU 140182	573 m from base	Featureless cryptoperthite. Glass clear crystals with rare trains of inclusions localised along fractures. Very simple grain boundaries. Grain size ≈ 1 mm	41.9	55.3	2.80
GGU 140175	550 m	As above. Grain size ≈ 1.5 mm	48.1	49.2	2.70
GGU 140115	318 m	Braid microperthite just visible in some areas. "Pleated" textures at grain boundaries. Glass clear crystals with rare trains of inclusions. ≈ 2 mm	41.5	56.5	2.00
GGU 140021	235 m	Braid microperthite universally visible. "Pleated" boundaries and slight suturing. Some areas with slight turbidity, particularly along grain edges, but glass clear material much predominant. Grain size ≈2-4mm	33.0	66.0	1.00
GGU 140092	55 m	As above. More areas of mild turbidity than 140021 but dominantly clear feldspar. Minor development of patch perthite in turbid areas. Grain size ≈ 4-10 mm	33.3	66.2	0.5

10.4 Methods of infrared spectroscopy used to determine the "water" content

The spectrometer and the techniques used for infrared spectroscopy were described in Chapter 3. The method of analysis used to study the natural feldspar was changed from that used for studying synthetic samples, owing to the differing nature of the samples. The synthetic samples were composed of a very fine grained powder and so the standard method of analysis was by the use of transmission of infrared radiation through a pressed disc of potassium bromide that had been mixed with the sample. This method had inherent problems due to the hygroscopic nature of the potassium bromide. If the water content of the sample was sufficiently large, as was perhaps found in the synthetic sanidine samples, then it would not be obscured by the broad, surface water peak. The potassium bromide method was initially used with ground samples of very pristine crystals of feldspar picked from each of the Klokken samples, but any water peaks were hidden by a broad surface water peak, and so the Klokken samples presumably have less structural "water" within them than the synthetic samples.

Another method for the analysis of the synthetic samples was of diffuse reflectance off finely powdered pristine samples. This method should result in an average spectrum for all orientations of the crystals. With the Klokken samples this reflectance method appeared to show peaks, not only in the 2800 cm^{-1} to 3600 cm^{-1}

region, but also at 3750 cm^{-1} and 3840 cm^{-1} (Fig. 10.7). Though not often used, this method provides an observation of an average spectrum. Transmission through a single crystal with the aid of an infrared microscope (see below) can produce an improved quality spectrum. Spectra measured using an infrared microscope (Fig. 10.8) did not have the peaks at 3750 cm^{-1} and 3840 cm^{-1}, and thus they were not pertaining to structural "water" peaks, but perhaps to interference from the diffuse reflectance method. The diffuse reflectance method was more useful for calculating the normalised peak areas in the OH stretching region, although the technique did not work well with the synthetic samples.

For comparison with the diffuse reflectance method and with previous work, spectra were also measured using a Nicolet Nicplan infrared microscope as described in Chapter 3. Rock samples were made into slabs of approximate thickness 0.2 to 0.3 mm, polished on both sides. The polish was not perfected in order to reduce the interference of reflected radiation which can reverberate between the two polished surfaces if they are parallel. The samples had to be of this thickness because the feldspar grain size was 1 mm in diameter in most of the samples and it was only possible to find a reasonable number of pristine crystals if the sections were thin. This thickness of sample gave strong peaks in the OH stretching region but was too thin to show any combination peaks, of OH stretching and H_2O bending, above noise level in the near infrared region of the spectrum above 4000 cm^{-1}.

10.5 Results of infrared spectroscopy

The diffuse reflectance (Fig. 10.7) gave five traces which appear very similar to the average of fifteen spectra obtained using the infrared microscope (Fig. 10.8) if the two peaks at 3750 and 3840 cm^{-1} are ignored. The shapes of these spectra do not appear to vary systematically with stratigraphic height in the pluton. The areas under the peaks between 3600 and 2800 cm^{-1} were measured and normalised to the area of a peak between 1190 and 1050 cm^{-1}, which is one of the peaks produced by the sanidine framework, i.e. it represents either an Al-O bond or an Si-O bond, the size of which should not change between similar feldspars. The normalised areas for all the peaks in this range and also the shoulder at 3560 cm^{-1} are listed in Table 10.2. Normalising the area under the peaks was only possible with the drift method, as the microscope method was saturated in the region of the spectrum which contained the reference peak and no other suitable peaks were available. The area of the shoulder at 3560 cm^{-1} was measured by drawing a tangent which approximated the edge of a broad hump at 3400 cm^{-1}. This normalisation process is not strictly valid as the peak

used as a reference is partly outside the linear range of the spectra which lies between 100% and 20% transmittance (Brian Jackson, *pers. comm.*). However, there is also no systematic variation when using the drift method, in the area under the peaks prior to normalisation. These should be roughly proportional to the quantity of water, with stratigraphic height, if the grain size of the samples are all similar.

Table 10.2. Normalised areas beneath OH stretching peaks on a plot of absorbance against wavenumbers obtained using a diffuse reflectance method. All values were normalised to a peak between 1190 and 1050 cm^{-1}.

Sample number (in order of stratigraphic height in the magma chamber)	All OH stretching peaks Area 3740 - 2800 cm^{-1}	Main shoulder at 3560 cm^{-1} Area 3690 - 3540 cm^{-1}
140182	330	1.60
140175	88.7	4.70
140115	24.5	2.23
140021	37.4	1.14
140092	30	0.83

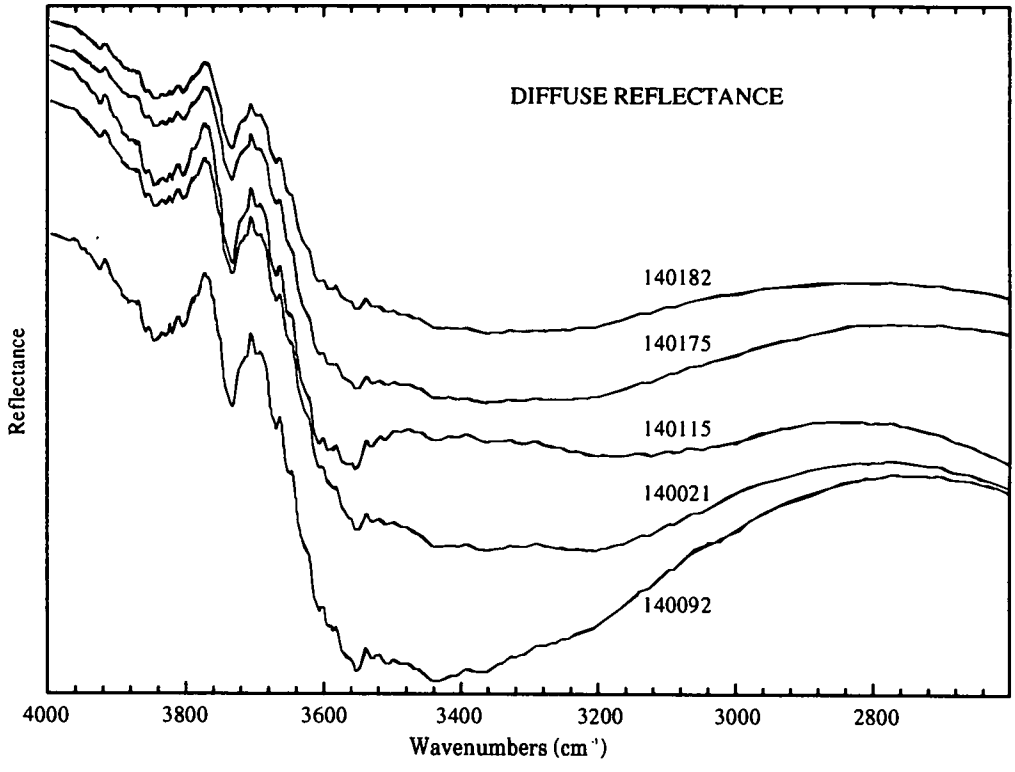

Fig. 10.7. Analysis of powdered samples of pristine, fluid inclusion free feldspars from the Klokken granular syenites using a diffuse reflectance method. Spectra are not drawn to the same reflectance scale.

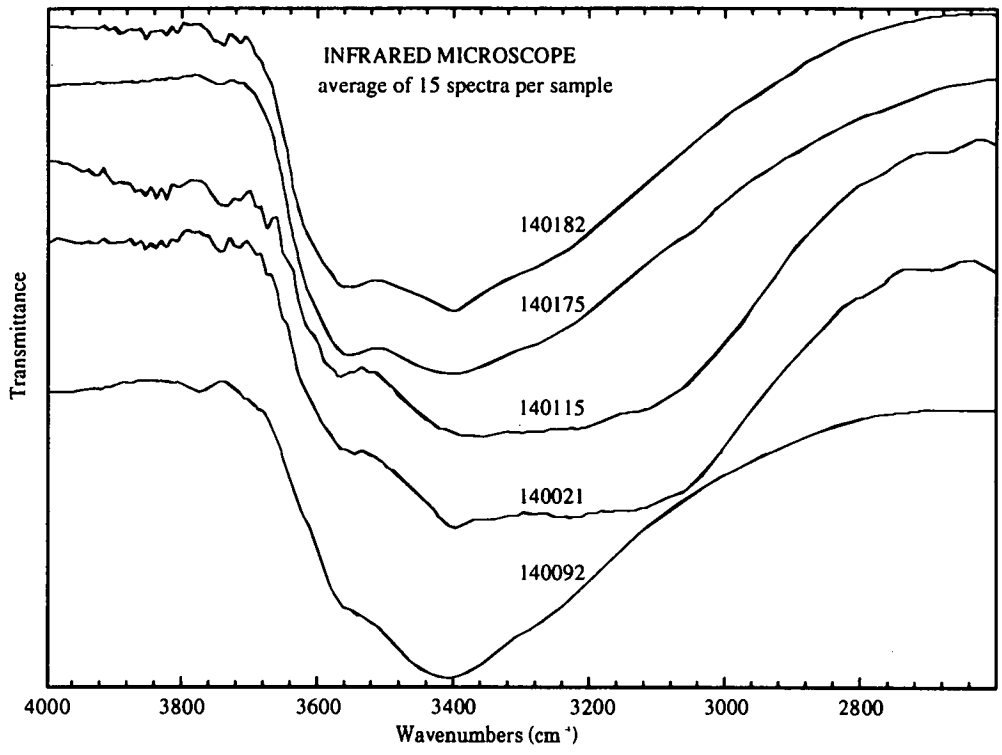

Fig. 10.8. Spectra from five samples of the Klokken granular syenites measured using an infrared microscope and taking an average of 15 spectra per sample. Spectra are not drawn to the same transmittance scale.

The fifteen separate spectra from each sample show that the variation between crystals is large. Various authors (e.g. Hofmeister and Rossman, 1985a) have shown that structural "water" in feldspars can occur in a fixed orientation within the lattice. When polarised radiation interacts with an H_2O molecule it causes the symmetric stretching and bending vibrations to be excited when the incident radiation is parallel to the two-fold symmetry axis of the H_2O molecule. The asymmetric vibration is excited when the incident radiation is perpendicular to this direction but in the plane of the molecule. Although polarised incident radiation was not used in this study the peaks should still show some variation with the orientation of the crystal. With these thick sections and the lack of a high power optical objective on the infrared microscope, it was not possible to acquire good interference figures to fully orientate each crystal. However, some idea of the orientation of each crystal could be gathered from the pattern of the exsolution lamellae. In these coherent crypto- and microperthites the lamellae always exsolve either along the planes $\{\overline{6}6\overline{1}\}$ or parallel to b*. Therefore, if two sets of lamellae can be seen optically forming a sharp crossed "braid" pattern, the plane of the crystal must be near (001). If only one set of sharp lamellae is seen the crystal is probably perpendicular to (001). As each of the spectra were measured the texture of the crystal was noted and photographed in order to

estimate the orientation of the crystal. Commonly no texture was visible in all of the samples, especially in the cryptoperthites 140182, 140175 and 140115, and sometimes the crystals appeared patchy. The patchiness may have been localised patch perthite development, but was often the result of the poor polish on the section or the presence of an abundance of apatite inclusions. Tables 10.3, 10.4, 10.5, 10.6 and 10.7 list the descriptions of each crystal and the peaks present in each of the spectra measured for the samples 140182, 140175, 140115, 140021 and 140092 respectively. The corresponding spectra are shown in Figs 10.9, 10.10, 10.11, 10.12 and 10.13.

The peak positions observed in these five samples were at:

3560 cm^{-1}	sharp
3400 cm^{-1}	broad
3400 cm^{-1}	sharp
3280 cm^{-1}	sharp
3230 cm^{-1}	broad
3060 cm^{-1}	broad

There does not seem to be any systematic variation in these spectra with the orientation of the crystal. In fact six of the spectra from sample 140021 were taken using different portions of the same crystal which should therefore have the same orientation. The crystal used was one with a very strong crossed pattern of exsolution lamellae and so was in the plane of (001). Figure 10.14 shows the large variation in these six spectra. Four of the spectra look very similar but two are quite different with an extra sharp peak at 3400 cm^{-1}. The parts of the crystal sampled with the infrared beam all looked similar under the microscope.

Table 10.3. Peaks observed in 15 spectra (Fig. 10.9) of different crystals of sample 140182 using an infrared microscope.

Sample 140182 Scan No.	Description of exsolution textures	Peaks present				
1	not observed	3560s	3400b	3400s		
2	not observed	3560s	3400b		3230b	
3	not observed	3560s	3400b		3230b	
4	not observed	3560s	3400b		3230b	
5	not observed	3560s	3400b	3400s	3230b	
6	not observed	3560s	3400b	3400s?		
7	not observed	3560s	3400b		3230b	
8	no obvious texture	3560s	3400b			
9	no obvious texture	3560s	3400b		3230b?	
10	no obvious texture	3560s	3400b			3280s
11	very weak crossed lamellae	3560s	3400b			3280s
12	weak crossed lamellae	3560s	3400b			3280s
13	weak straight lamellae	3560s	3400b		3230b	
14	very weak crossed lamellae	3560s	3400b		3230b	
15	weak straight lamellae	3560s	3400b		3230b	

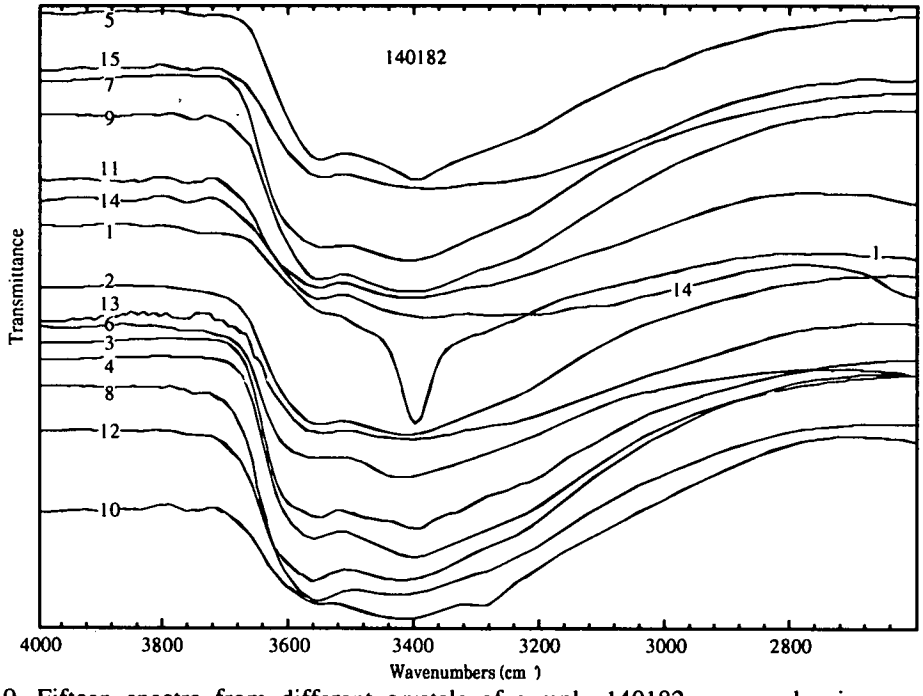

Fig. 10.9. Fifteen spectra from different crystals of sample 140182 measured using an infrared microscope. Spectra are not drawn to the same transmittance scale. Peaks are listed in Table 10.3.

Table 10.4. Peaks observed in 15 spectra (Fig. 10.10) of different crystals of sample 140175 using an infrared microscope.

Sample 140175 Scan No.	Description of exsolution textures	Peaks present			
1	no obvious texture, patchy	3560s	3400b	3230b	
2	no obvious texture, patchy	3560s	3400b	3230b	
3	no obvious texture	3560s	3400b	3230b	
4	no obvious texture	3560s	3400b	3230b	
5	very weak straight lamellae, patchy	?	?	3230b	3060b
6	strong straight lamellae	3560s	3400b	3230b	
7	no obvious texture	3560s	3400b	3230b	
8	no obvious texture, patchy	3560s	3400b	3230b	
9	weak straight lamellae	3560s	3400b	3230b	
10	weak straight lamellae	3560s	3400b	3230b	
11	no obvious texture	?	?	3230b	3060b
12	no obvious texture	3560s	3400b	3230b	
13	no obvious texture	3560s	3400b	3230b	
14	no obvious texture	3560s	3400b	3230b	
15	no obvious texture	3560s	3400b	3230b	

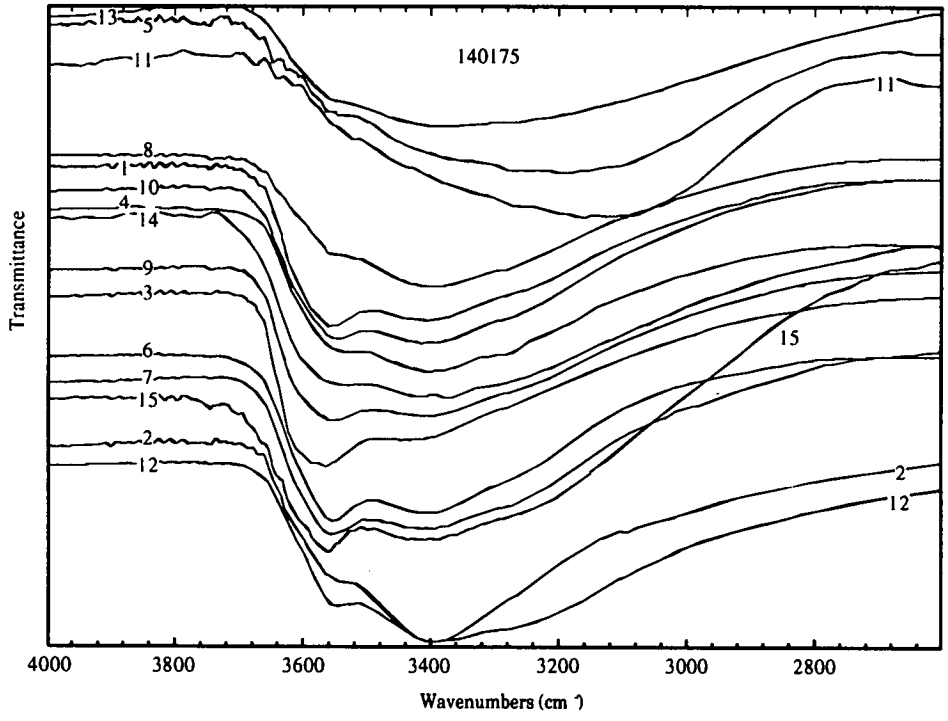

Fig. 10.10. Fifteen spectra from different crystals of sample 140175 measured using an infrared microscope. Spectra are not drawn to the same transmittance scale. Peaks are listed in Table 10.4.

Table 10.5. Peaks observed in 15 spectra (Fig. 10.11) of different crystals of sample 140115 using an infrared microscope.

Sample 140115 Scan No.	Description of exsolution textures	Peaks present			
1	not observed	3560s	3400b	3230b	
2	not observed		?		3060b
3	not observed		?	?	3060b
4	not observed	3560s	3400b		
5	not observed	?		?	3060b
6	weak crossed lamellae	3560s	3400b		
7	weak crossed lamellae	3560s	3400b	3230b	3060b
8	no obvious texture		3400b		3060b
9	no obvious texture	3560s	3400b	?	
10	weak straight lamellae		3400b		3060b
11	weak straight lamellae	3560s	3400b	3230b	
12	no obvious texture	3560s	3400b	3230b	
13	strong straight lamellae	3560s	3400b	3230b	
14	no obvious texture		?		3060b

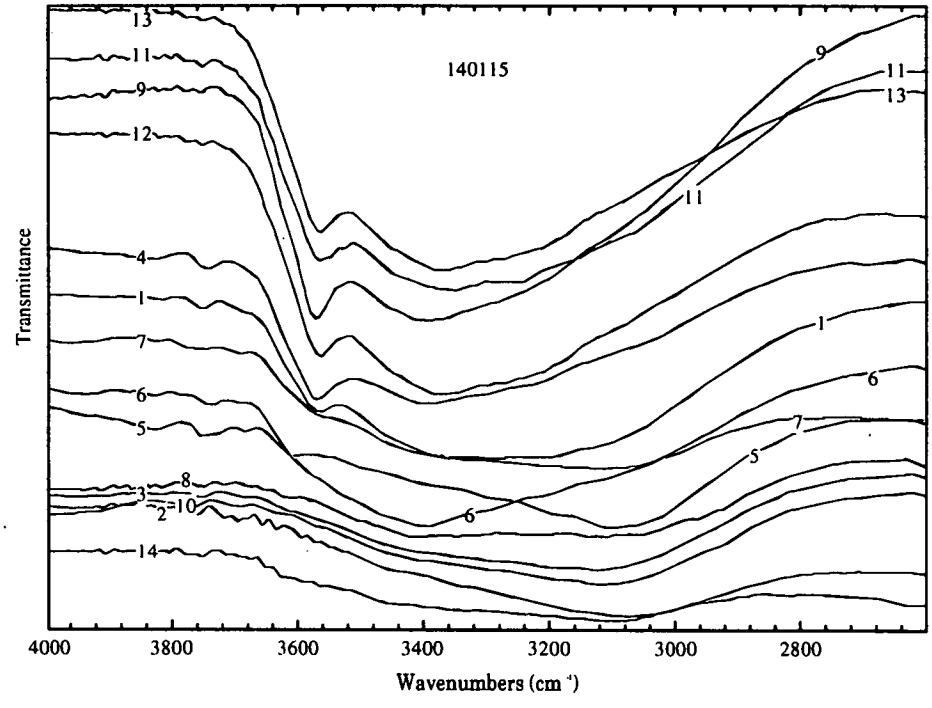

Fig. 10.11. Fourteen spectra from different crystals of sample 140115 measured using an infrared microscope. Spectra are not drawn to the same transmittance scale. Peaks are listed in Table 10.5.

Table 10.6. Peaks observed in 15 spectra (Fig. 10.12) of different crystals of sample 140021 using an infrared microscope.

Sample 140021 Scan No.	Description of exsolution textures	Peaks present				
1	not observed		3400b			3060b
2	weak crossed lamellae		3400b			3060b
3	weak crossed lamellae	3560s			3230b	
4	strong straight lamellae		3400b			3060b
5	strong straight lamellae	3560s	3400b			
6	no obvious texture		?	3400s		3060b
7	strong straight lamellae		3400b			3060b
8	no obvious texture		3400b			3060b
9	no obvious texture		3400b			3060b
10	strong crossed lamellae		3400b			3060b
11	strong crossed lamellae	3560s	?	3400s	3230s?	
12	strong crossed lamellae		3400b			3060b
13	strong crossed lamellae		3400b			3060b
14	strong crossed lamellae	3560s	3400b	?	3230b	
15	strong crossed lamellae		3400b			3060b

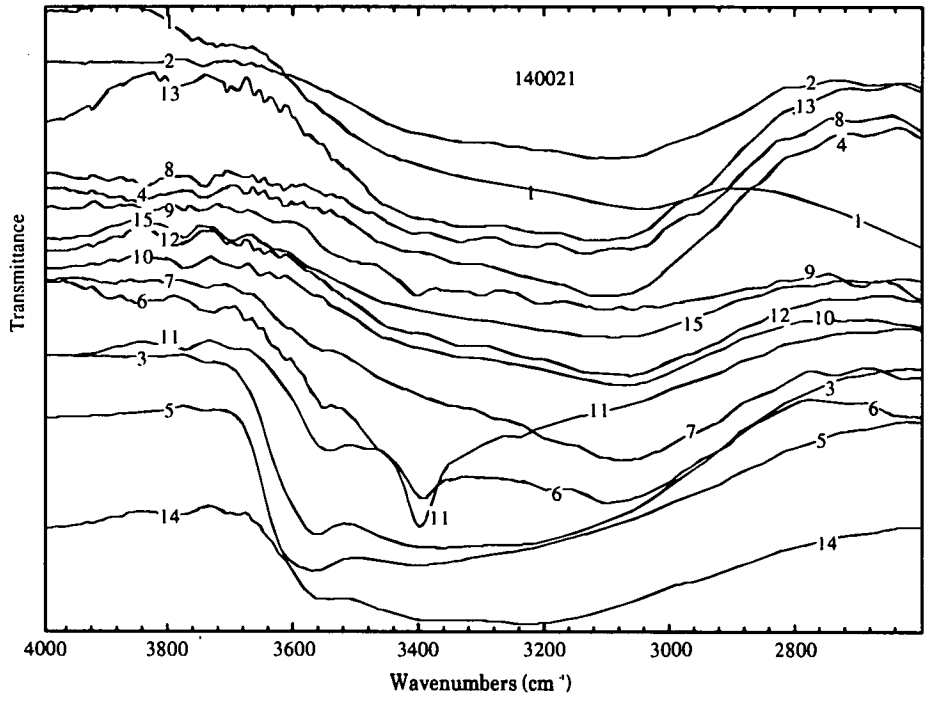

Fig. 10.12. Fifteen spectra from different crystals of sample 140021 measured using an infrared microscope. Spectra are not drawn to the same transmittance scale. Peaks are listed in Table 10.6.

Table 10.7. Peaks observed in 15 spectra (Fig. 10.13) of different crystals of sample 140092 using an infrared microscope.

Sample 140092 Scan No.	Description of exsolution textures	Peaks present		
1	strong straight lamellae		3400b	3230b
2	strong straight lamellae	3570s	3400b	3230b
3	strong crossed lamellae		3400b	3230b
4	strong crossed lamellae	3570s	3400b	3230b
5	strong straight lamellae		3400b	3230b
6	no obvious texture		3400b	3230b
7	strong straight lamellae	3570s	3400b	3230b
8	no obvious texture	3570s	3400b	3230b
9	no obvious texture	3570s	3400b	3230b
10	weak straight lamellae, patchy	3570s	3400b	3230b
11	no obvious texture, patchy	3570s	3400b	3230b
12	no obvious texture, patchy	3570s	3400b	3230b
13	strong crossed lamellae	3570s	3400b	3230b
14	strong crossed lamellae	3570s	3400b	3230b
15	strong crossed lamellae	3570s	3400b	3230b

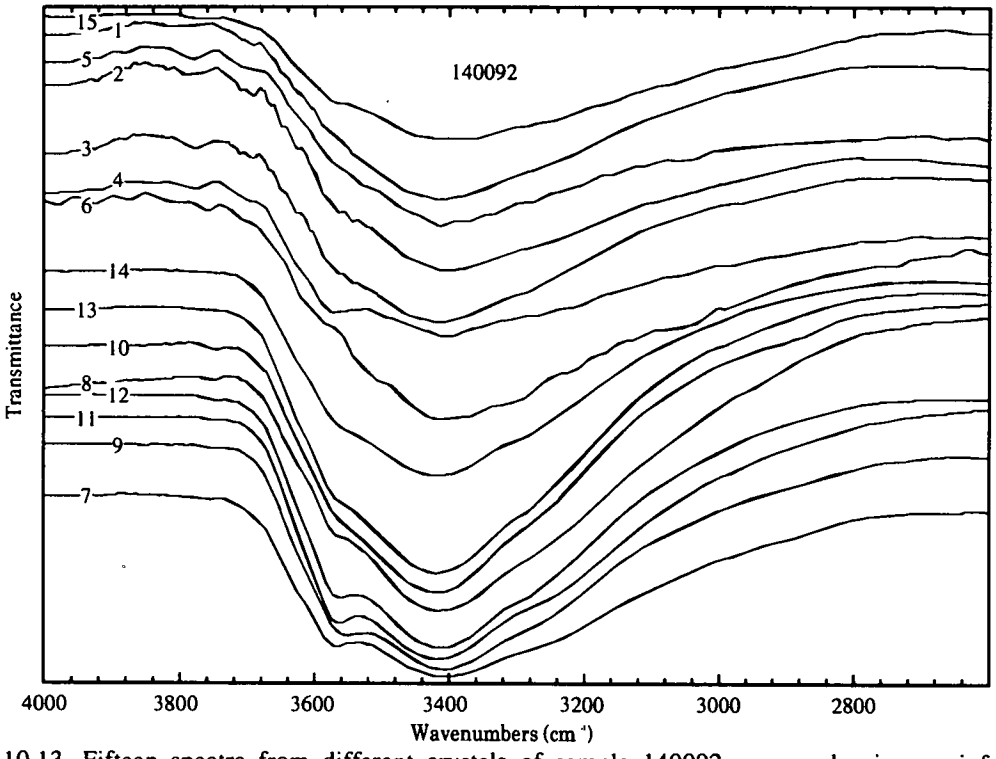

Fig. 10.13. Fifteen spectra from different crystals of sample 140092 measured using an infrared microscope. Spectra are not drawn to the same transmittance scale. Peaks are listed in Table 10.7.

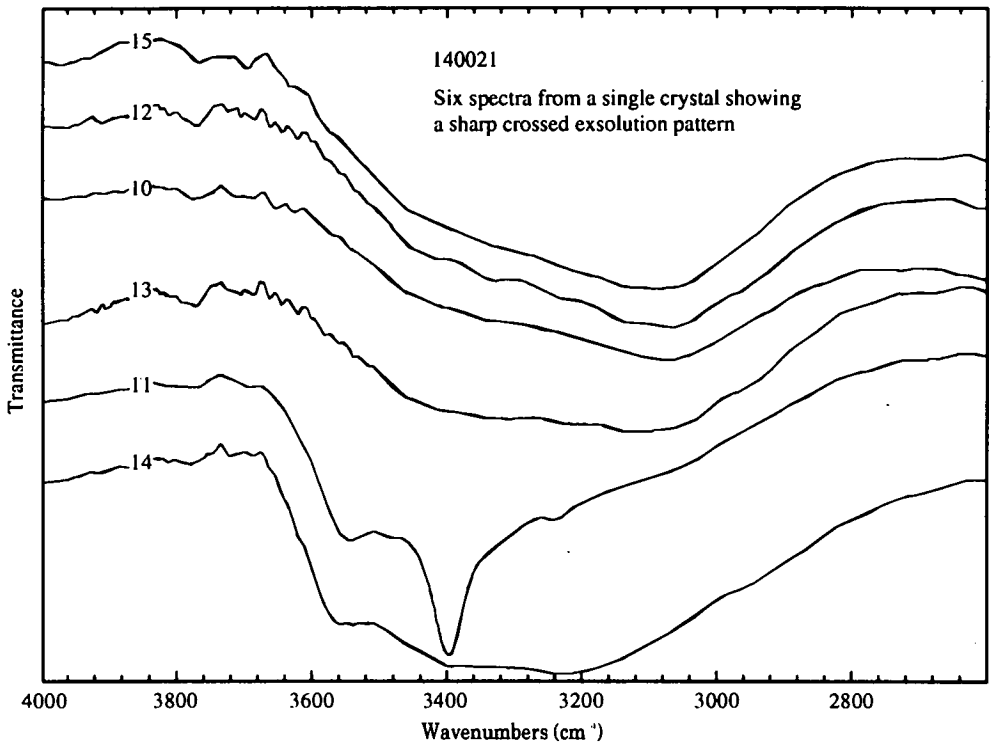

Fig. 10.14. Six spectra, measured using an infrared microscope, from a single crystal from sample 140021 showing the large variation in shape of the spectra for a single optic orientation. Spectra are not drawn to the same transmittance scale

10.6 Discussion

The lack of any systematic variation of the infrared spectra in the OH stretching region with stratigraphic height in the Klokken syenites, as predicted by the model for the exsolution of structural "water" (Fig. 10.6), may indicate that the water which caused the deuteric alteration of the feldspars to form patch perthites and fluid inclusions was caused mainly by magmatic fluids percolating through the rocks. It is possible that the exsolution of structural "water" from the high temperature feldspars may be a component of these fluids which caused the alteration but it is not the dominant one.

The lack of systematic variation with orientation of the crystal is not understood. Taking the spectra at face value the variation of the water content even within one crystal is so large that any interpretation based on these results appears to be doubtful.

It is, however, interesting to note how these traces compare with those of previous authors. The feldspars from Klokken are composed of approximately half potassium feldspar, as microcline, and half a sodium-rich plagioclase. Previous workers have

only studied end member feldspars of gem quality. The combination of two feldspars in a perthite may cause additional confusion in the behaviour of structural "water".

The evidence for structural "water" in potassium feldspar was summarised in Chapter 9. The general consensus of opinion is that sanidines show evidence of predominantly structural OH and microclines of structural H_2O, probably held in two, or perhaps more, sites. Plagioclase feldspars seem to show evidence for structural OH (Hofmeister and Rossman, 1986).

Two of these studies of potassium feldspar used white microcline from the Elisabeth R mine in Pala, California (Aines and Rossman, 1985 and Hofmeister and Rossman, 1985a). Aines and Rossman (1985) showed the microcline contained two types of H_2O which were lost on heating at different temperatures. Type I produced peaks at 3620 cm^{-1} and 3550 cm^{-1} which persisted on heating up to 660°C, whereas the peaks for Type II at 3440 cm^{-1} and 3280 cm^{-1} only remained until 400°C. Hofmeister and Rossman (1985a) found that the peaks at 3620 and 3550 cm^{-1} were strongly polarised in different directions as would be expected for symmetric and asymmetric stretching of a water molecule held in one site in the crystal structure in a fixed orientation. The Type II water was not strongly polarised. Hofmeister and Rossman also saw peaks at 3400 and 3050 cm^{-1}. When they looked at these spectra at liquid nitrogen temperatures only the peaks at 3400 and 3050 cm^{-1} formed additional peaks as a result of the formation of ice (see Section 3.6.1) showing that these two peaks were due to free fluid water. They did not attempt to explain the reason for the presence of two peaks for fluid water. Fluid water either in fluid inclusions or on grain boundaries and fractures should produce one broad peak in the OH stretching region at lower wavenumbers than structural OH peaks (Aines and Rossman, 1984). A separate fluid peak at higher wavenumbers might result from fluid contained within a population of very small pores where the degree of hydrogen bonding is less. The other four OH peaks were therefore structural peaks. Kronenberg et al (in press) conducted a similar study on Kristallina adularia from Switzerland. They too found peaks in similar positions at 3620, 3455, 3280 and 3090 cm^{-1} which agreed well with the work of Hofmeister and Rossman (1985a) and Aines and Rossman (1985). All three of these studies found two peaks in the near infrared around 5200 cm^{-1} but none at 4500 cm^{-1} which also indicated that the predominant water species in microcline is molecular H_2O.

In plagioclase of oligoclase composition, however, Hofmeister and Rossman (1986) found three broad bands at 3600, 3450 and 3170 cm^{-1} at ambient temperatures. They claimed that these represented structural OH rather than structural H_2O as there were no peaks in the 5200 cm^{-1} region, but they did not mention the presence of a

combination band at 4500 cm^{-1} either, as would be expected from structural OH. The water content of this plagioclase, measured by integrated area of OH peaks normalised to sample thickness, was considerably smaller, by approximately an order of magnitude, than microcline in their previous study. They also did not state any evidence for all three of these bands being structural "water", for example by the formation of ice peaks at liquid nitrogen temperatures. One or more of these three peaks may in fact be due to fluid inclusion water. Despite this uncertainty the spectrum for plagioclase does appear to be considerably different to that for microcline.

In the present study the spectra appeared in general more like the spectra for microcline than plagioclase. It was not possible to study the change in the peaks at liquid nitrogen temperatures, as the microscope was not equipped with the facility to do so, and so the presence of fluid water was not confirmed. Two large, broad peaks, which may have been fluid water, were observed in the same location as the fluid water of Hofmeister and Rossman (1985a) at 3400 and 3050 cm^{-1}. There was commonly a strong sharp peak at 3570 cm^{-1} which may well have been of the same origin as the one observed at 3550 cm^{-1} in all the previous work on microclines. However, if this was evidence of structural Type I "water" as described by Aines and Rossman (1985) the partner to this peak at 3620 cm^{-1} appears to be missing. If Type II "water" occurs it is often hard to observe on the spectra owing to the presence of the two broader peaks. Occasionally there was a sharper peak at 3400 cm^{-1} on top of the broader one and more rarely a sharp peak 3280 cm^{-1}. These could be indicative of Type II "water". Often here there was a further broad peak at 3230 cm^{-1} which had not been noted by any of the above authors.

Clearly the spectra of the samples from Klokken show some similarities with microcline but are not identical. The water peaks in the 2800 to 3600 cm^{-1} region require the use of a liquid nitrogen cooling stage in order to identify whether these are fluid water peaks. However, a full understanding of the structural "water" peaks is probably impossible due to the nature of the samples. Additional evidence from the near infrared was unobtainable with this thickness of sample as any peaks were below noise level. Thicker samples, producing larger peaks, would contain very few, if any, entirely pristine feldspars. By usual standards in plutonic igneous rocks these Klokken feldspars are exceptionally pristine and fluid inclusion free in comparison with most feldspars from other localities and yet even in these samples most of the structural "water" component peaks are not easy to observe behind the broader fluid inclusion peaks. Hence it is not envisaged that this method of identifying the structural "water" components can be of much use elsewhere with poorer quality

specimens. In particular the structural "water" content of the laminated syenites was almost entirely obscured by the fluid inclusion water and therefore it would not be possible to study differences between the laminated and granular syenites.

10.7 Conclusions

No obvious systematic changes of structural "water" with stratigraphic height within the granular syenites of the intrusion may indicate that exsolution of structural "water" is not the dominant cause of deuteric alteration. However, the diffuse reflectance method may not be suitable for calculating relative water contents (see Section 9.3.2). Microscopic methods of observation should be more reliable when normalised to sample thickness but, since the variation in the infrared peaks with orientation of the crystal was irregular, any comparison between samples was difficult. It was not possible to fully identify the OH stretching peaks. Klokken contains pristine, fluid inclusion free feldspars and yet the quality of the samples was not sufficiently good to permit a complete study of the water content using infrared spectroscopy. The presence of both microcline and albite in the perthites may be the cause of further confusion to the spectra. This technique seems to be of little use except for the study of the large gem quality feldspars used in previous investigations.

Chapter 11
Conclusions and possibilities for further work

11.1 Conclusions and implications of this research

Potassium feldspar has been studied using a variety of techniques with the aim of achieving a fuller understanding of its behaviour at high partial pressures of water. High pressure experiments with the piston cylinder apparatus have been used to determine the position of the reaction defining the upper pressure stability limit of potassium feldspar with water to form a hydrated phase, "sanidine hydrate", and to synthesise both sanidine and "sanidine hydrate" for investigation of the solubility of water in these minerals. The variation of the structural "water" contents of "sanidine hydrate" was examined using infrared spectroscopy and thermogravimetric analysis. X-ray diffraction techniques were also used to investigate the variation of the cell parameters of "sanidine hydrate" with the quantity of structural "water". Infrared spectroscopy was used as a method of calculating the relative amounts of structural "water" in synthetic and natural sanidines in order to establish whether the structural "water" of these also varied with pressure-temperature conditions of crystallisation.

The main conclusions of these studies are summarised below:

1) The position of the reaction between sanidine and water to form "sanidine hydrate" lies between the four brackets of 2.35 and 2.5 GPa at 450°C, 2.4 and 2.59 GPa at 550°C, 2.67 and 2.74 GPa at 650°C and 2.70 and 2.72 GPa at 680°C.

2) The predominant water species in "sanidine hydrate" is structural H_2O molecules held within one site in the crystalline structure.

3) The apparent quantity of this structural H_2O varied between 4.42 and 5.85 wt% over the pressure range of 2.7 to 3.2 GPa and temperature range of 450 to 680°C. These apparent values for structural H_2O may be low as the samples were contaminated with platinum when they were extracted from the capsule in the piston cylinder experiment.

4) This variation in the structural "water" content in "sanidine hydrate" was not a regular variation with the pressure and temperature of synthesis, perhaps implying that the platinum contamination was obscuring any of the systematic behaviour. However, it was shown that the water could be removed entirely from "sanidine hydrate" by dehydration to create an anhydrous hexagonal phase, "hexasanidine". The measured water content of "sanidine hydrate" did not exceed one molecule of H_2O per formula unit. Therefore it is probable that a solid solution exists between $KAlSi_3O_8.H_2O$

and hexagonal $KAlSi_3O_8$ in a similar manner to that found in cymrite (Graham et al., 1992, Viswanathan et al., 1992).

5) The unit cell parameters of "sanidine hydrate" were a = 0.5337 (±0.0003) nm and c = 0.7714 (±0.0009) nm and were not found to vary over the pressure-temperature range of synthesis studied. The unit cell parameters of "hexasanidine" were a = 0.5288 (±0.001) nm and c = 0.7818 (±0.0005) nm. Thus the a cell parameter of "sanidine hydrate" decreases whereas the c cell parameter increases on dehydration. This behaviour is very similar in manner and magnitude to that found by Viswanathan et al. (1992) for the cell parameters of cymrite and hexacelsian.

6) The data from the reversal experiments, the unit cell parameters and the water content of "sanidine hydrate" were used to calculate thermodynamic data on the reaction. Attempts to evaluate thermodynamic data on the dehydration of "sanidine hydrate", using the measured structural "water" contents, showed that the variation was not systematic with pressure and temperature. Hence the calculated variation in the composition of "sanidine hydrate" as a function of pressure and temperature was not used in further calculations on the reaction between sanidine and water to form "sanidine hydrate". The use of constant values for the water contents gave values similar to each other if either the average, of 0.83 molecules per formula unit, or 1 molecule of H_2O per formula unit was used. A method of calculation, as described by Chatterjee (1991), gave values for the average enthalpy $\Delta H^{\circ}_{(r)<T>}$ over the pressure-temperature range studied of 18000 (±5000) $Jmol^{-1}$ and average entropy $\Delta S^{\circ}_{(r)<T>}$ of 92.75 (±5.80) $JK^{-1}mol^{-1}$ if n = 0.83 in the formula $KAlSi_3O_8.nH_2O$.

7) Sanidines synthesised in experiments over a pressure range from 0.1 to 2.5 GPa and a temperature range of 550 to 750°C contain structural "water" perhaps occurring as OH groups. The quantity of this water may be greater than that found in natural sanidines from the Eifel region of West Germany, that have high water contents of between 0.036 and 0.018 wt%. The structural "water" in these synthetic sanidines absorbs infrared radiation at lower wavenumbers in the OH stretching region than the structural "water" in Eifel sanidine but otherwise the spectra are similar in shape.

8) Attempts to show the systematic variation of the structural "water" component of these synthetic sanidines with pressure and temperature of

synthesis was not successful. In fact the spectra appeared to differ more depending on the starting material used rather than the pressure-temperature conditions.

9) Within the OH stretching region, infrared spectra from feldspars in the Klokken layered syenites, from South Greenland, appear more like microcline annealed at high partial pressures of water than plagioclase but they do not exhibit a peak at 3620 cm^{-1} as would the microclines studied by previous authors. The type of structural water species could not be fully identified but may be a combination of H_2O and OH. There was also probably some fluid inclusion water present, causing broad peaks even in the most pristine samples. These OH stretching peaks did not appear to show any clear pattern dependent on the orientation of the crystal as would be expected.

10) Evidence for systematic variation in the quantity of structural "water" was not found in the Klokken layered syenites. This may indicate that there was no systematic variation in the feldspars examined but it probably implies that the method of calculating the normalised areas of peaks, as an indication of relative concentration, is not a good one. However, this result does not provide any positive evidence for a magma with an evolving fluid composition or that potassium feldspar is capable of containing more structural "water" at higher temperatures. Hence the dominant cause of the widespread deuteric alteration seen in parts of this intrusion could not be determined.

The stability of "sanidine hydrate" at high partial pressures of water could provide a reservoir for water in rocks subjected to high partial pressures of water but low temperatures, as "sanidine hydrate" is capable of dissolving up to approximately 6.0 wt% of water in its structure. It may be possible to attain these conditions in some subduction zones. Numerical modelling of a subduction zone suggests that situations where old oceanic crust is being subducted in a long standing subduction zone without induced convection in the mantle wedge may be more likely to produce the pressure-temperature conditions required. However, the bulk composition of the rocks may restrict the occurrence of "sanidine hydrate". The most probable bulk composition which would be likely to form "sanidine hydrate" at these pressures and temperatures would be that of a granite. The occurrence of granitic rocks in this type of environment may also be rather rare. The stability of "sanidine hydrate" would also be reduced if the water content were too high as it may then dissolve. If there were melt present most of the water would be taken up by in the melt and sanidine

might crystallise in its place and thus the stability of "sanidine hydrate" would be further reduced.

Evidence for the water solubility of potassium feldspar was not obtainable either from synthetic sanidines or from natural perthites from Klokken. Hence the capacity for potassium feldspar to act as a reservoir for water under different geological conditions was not determined.

11.2 Possibilities for future work

a) Experiments with natural sanidine as a starting material

The problems encountered calculating the relative proportions of water in the synthetic sanidines may be a result of the method of calculation from diffuse reflectance infrared spectra that was used for the study. Normalising the infrared peak areas in the OH stretching region to those which should be caused by vibrations in part of the silicate framework structure may not be successful when the reference peak is in part below 10 - 15 % transmittance. Previous work has calculated the quantity of water in natural feldspars by normalising the peak area to the thickness of the sample and then comparing the area with that of a feldspar or a silicate with a known water content measured by hydrogen manometry. These measurements, however, can only be obtained with the use of an infrared microscope. Synthetic feldspars have a grain size which is too small to use a microscopic method because of difficulties in the preparation and mounting of the samples. An epoxy resin mount could not be used as it would produce peaks that caused interference in the OH stretching region and the thickness of the sample would then not be known.

These problems may be surmountable by using thin slabs of natural sanidine as a starting material in the high pressure runs. This technique would make the sample thickness measurable but would introduce other difficulties. For example the structural "water" in feldspars is usually held in some fixed orientation within the crystal structure and therefore, in order to fully quantify the structural "water", several orientations through each crystal must be inspected at each of the experimental conditions. It would not be possible to fit a crystal of natural feldspar in a piston cylinder experiment that would be large enough to slice into many different orientations. Therefore several experiments would be required on slabs pre-cut into different orientations at each pressure and temperature of interest.

This work presumes that the water in feldspars would diffuse in and out of the structure at rates fast enough to reproduce in the laboratory. Kronenberg et al. suggested that this would not be a problem. However, experiments would need to be performed in order to check that the water content measured was in fact the equilibrium water content.

The peaks would require to be identified properly with the aid of a liquid nitrogen cooled stage in order to determine whether any of the peaks in the OH stretching region were due to fluid inclusion water. In addition some experiments would need to be carried out on samples with a thickness of roughly 1 mm. Such thick crystals would produce more information from the near infrared region of the spectrum where combination modes can be seen which may help to distinguish between structural H_2O and OH.

For this work a large crystal of natural feldspar of pristine quality and free of fluid inclusions would need to be used. An obvious choice would be a sample of Eifel sanidine which is renowned for its perfection. However, Eifel sanidine may have an unusual infrared water signature in comparison to the synthetic sanidines investigated in this project and may thus not be representative.

b) Formation of fluid inclusions and deuteric alteration

The behaviour of potassium feldspar at high partial pressures of water would be more complete if the formation of fluid filled micropores and deuteric alteration were better understood. These textures appear able to form in slowly cooled igneous rocks (e.g. the Klokken intrusion described in Chapter 10) at temperatures below 450°C as the surrounding feldspars seem to have fully ordered prior to this event. Since much of the upper crust is composed of feldspar (≈60%) these micropores could act as a large reservoir for fluids. In addition, if these textures are restricted to the lower pressure-temperature conditions, they may lead to profound differences in both the chemical and physical behaviour of rocks in the upper and lower crust. The formation of these microtextures during cooling is well understood but their stability during burial and metamorphism is not known. A series of experiments on feldspars with a variety of microtextures from well-understood geological environments formed under a range of conditions would help to establish the stability of these structures. In addition, the composition of the fluid may have a strong effect on the textures and a number of differing fluid compositions could be investigated

APPENDIX A GELS

Initially it was intended to synthesise the gel starting materials, for use in the pressure, temperature experiments described in Chapter 4. However many problems were encountered and after five attempts the starting material finally used for the majority of the experiments was one provided by D.L. Hamilton of Manchester University. Some of the early experiments with the gels synthesised here (e.g. P3K100) were used for analysis by infrared spectroscopy and thermogravimetric analysis and showed identical behaviour to the ones which used D.L. Hamilton's gel. The methods used and the problems encountered during gel making are outlined below.

Methods of gel making

The method used for making gels should produce a very fine, homogeneous mixture of oxides in the correct proportions to give the required mineral composition of $KAlSi_3O_8$, to an accuracy which, in theory, should be better than it is possible to analyse. The first two batches were made using the "Edinburgh" method which was similar to that described by Biggar and O'Hara (1969) apart from the initial phase of the dehydration stage. The third, fourth and fifth batches used a simpler method, called here the "Manchester" method, described by Hamilton and Henderson (1968), which avoids the more complex titration stages of the "Edinburgh" method

The "Edinburgh" method

The general procedure for making these gels was to dissolve K_2CO_3 and Al metal powder separately in nitric acid and then to make up the solutions in a volumetric flask to known concentrations. The solutions were titrated together into a PTFE beaker, in the correct proportions, to give 10g of gel. The solution was then dehydrated down and diluted again with water a further two times, to reduce the excess of nitric acid and hence the quantity of ammonium nitrate needed to be removed later on in the process. This dilution also thickened the gel. Ethanol was added to allow the next additive, tetraethylorthosilicate (TEOS, $Si(OC_2H_5)_4$ 98%), to mix properly. Then the correct weight of TEOS was added and thoroughly mixed. An excess of NH_3 solution was quickly added to give, in theory, a thick gel of $Al(OH)_3$ which should trap all of the other elements in an even distribution. The gel was then left covered overnight, to enable complete hydrolysis of the TEOS. The gels were dried in the oven for up to four days at about 70°C, that is below the ignition point of ethanol, and then transferred to a 250 cm^3 glass beaker. This was slowly heated up in an isomantle and later an oven, to a temperature of 150°C, until all of the ammonium nitrate had been expelled. This could take several days, but once complete the residue

was transferred to a PalAu basin and fired in the furnace from 200°C up to 900°C gradually over a period of five or six days. In theory the weight of the yield after this procedure should be about 10 ± 0.03 g

The "Manchester" method

To check that errors were not appearing in the complicated titration process of the "Edinburgh" method a simpler method was adopted which avoided this for the batches three, four and five. This method involved accurate weighing of the required amounts of the starting materials straight into a PTFE beaker and then dissolving the K and Al altogether in nitric acid on a water bath, after which the TEOS was added in the same way as previously, and the method continued as described above.

Results and problems of gel making

The problems with the making of gels were never fully understood. Apart from the initial batch all the four subsequent batches produced remarkably consistent results with good yields indicating that there were no faults associated with their manufacture. The yield is the best indication that the composition is correct as all of the analysis methods which can be used to test the composition have large errors and the composition needs to be known more accurately than this.

When the gels were analysed using X-ray fluorescence they appeared to have the correct composition within the margins of error. It was not possible to get useful results by attempting to glass the gel on a melting stage microscope in order to obtain its composition from the electron probe. The melt produced was too viscous and inhomogeneous and produced streaky glasses whose compositions varied by up to 10% in each element within an individual bead. The melt produced at even higher temperatures using an iridium strip heater was prone to volatile loss of potassium and remained inhomogeneous. High pressure experiments, at 0.5 GPa in the gas bombs and 30 GPa in the solid media apparatus that used these gels, produced the same results as other gels, for example that made by D.L. Hamilton. However, at low pressures of 0.1 GPa in the cold seal apparatus, the gels produced mostly sanidine which was to be expected but also there were a few extra small peaks in the powder X-ray diffraction trace. These peaks were difficult to identify but they could have been traces of leucite and kalsilite. Why they occurred in these gels and not in the gel made by D.L. Hamilton is not clear, though the mere presence of these further peaks precluded the use of these gels in the reversal experiments on the reaction between sanidine and water to form "sanidine hydrate". The successful synthesis of sanidine using these gels in the gas bombs had not been attempted prior to the reversal experiments

APPENDIX B

Diagramatic summary of thesis

please lift

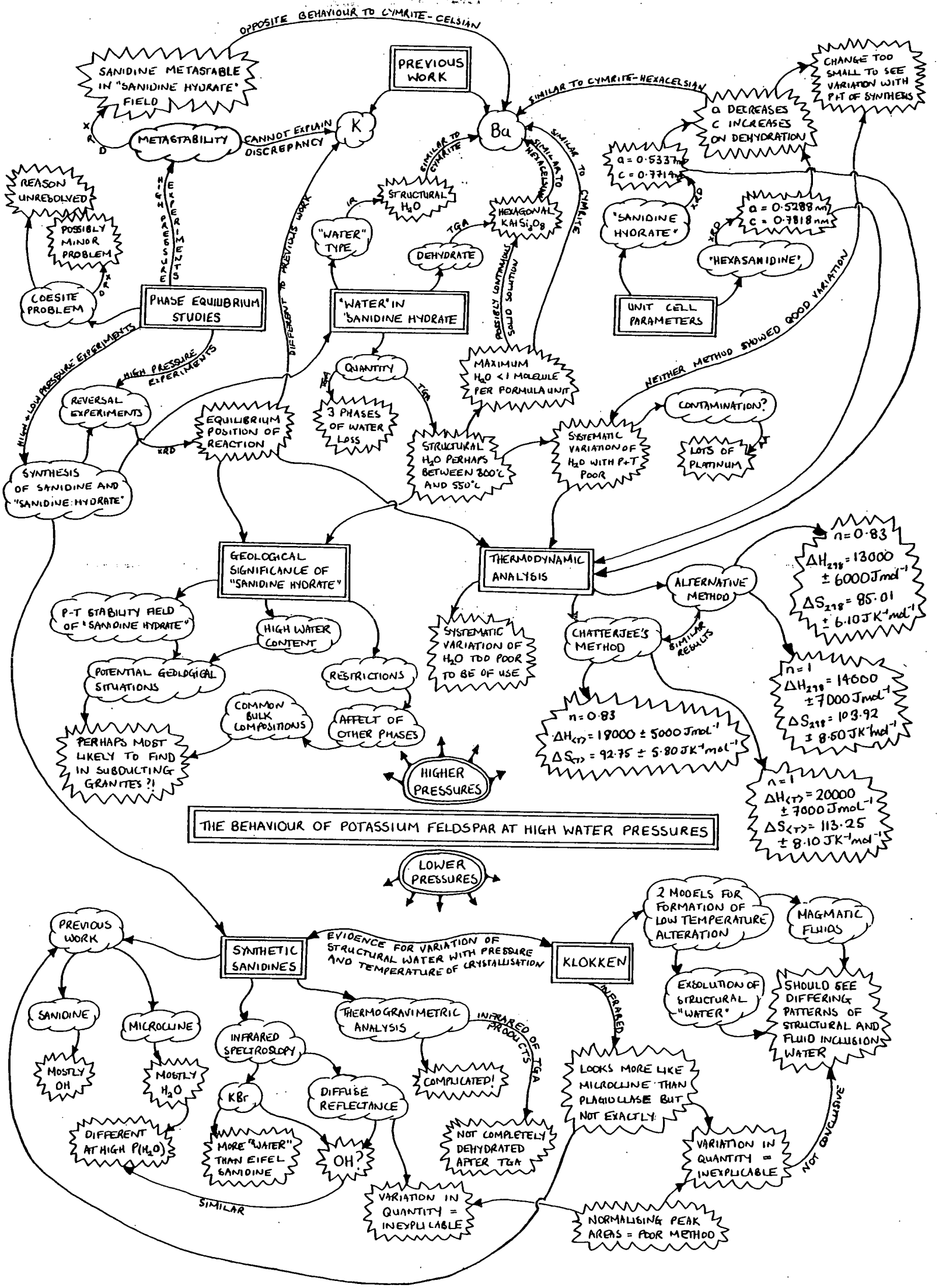
PREVIOUS WORK
OPPOSITE BEHAVIOUR TO CYMRITE-CELSIAN
SIMILAR TO CYMRITE-HEXACELSIAN
SANIDINE METASTABLE IN "SANIDINE HYDRATE" FIELD
METASTABILITY
CANNOT EXPLAIN DISCREPANCY
K
Ba
XRD
HIGH PRESSURE EXPERIMENTS
REASON UNRESOLVED
POSSIBLY MINOR PROBLEM
XRD
COESITE PROBLEM
PHASE EQUILIBRIUM STUDIES
DIFFERENT TO PREVIOUS WORK
SIMILAR TO CYMRITE
SIMILAR TO HEXACELSIAN
IR
STRUCTURAL H_2O
"WATER" TYPE
TGA
DEHYDRATE
HEXAGONAL $KAlSi_2O_8$
POSSIBLY CONTINUOUS SOLID SOLUTION
"WATER" IN "SANIDINE HYDRATE"
a DECREASES c INCREASES ON DEHYDRATION
CHANGE TOO SMALL TO SEE VARIATION WITH P&T OF SYNTHESIS
a = 0·5337 nm
c = 0·7719 nm
XRD
"SANIDINE HYDRATE"
a = 0·5288 nm
c = 0·7818 nm
XRD
"HEXASANIDINE"
UNIT CELL PARAMETERS
NEITHER METHOD SHOWED GOOD VARIATION
HIGH & LOW PRESSURE EXPERIMENTS
HIGH PRESSURE EXPERIMENTS
REVERSAL EXPERIMENTS
XRD
EQUILIBRIUM POSITION OF REACTION
SYNTHESIS OF SANIDINE AND "SANIDINE HYDRATE"
QUANTITY
TGA
3 PHASES OF WATER LOSS
MAXIMUM H_2O < 1 MOLECULE PER FORMULA UNIT
STRUCTURAL H_2O PERHAPS BETWEEN 300°C AND 550°C
SYSTEMATIC VARIATION OF H_2O WITH P+T POOR
CONTAMINATION?
LOTS OF PLATINUM
GEOLOGICAL SIGNIFICANCE OF "SANIDINE HYDRATE"
THERMODYNAMIC ANALYSIS
ALTERNATIVE METHOD
n = 0·83
ΔH_{298} = 13000 ± 6000 J mol^{-1}
ΔS_{298} = 85·01 ± 6·10 J K^{-1} mol^{-1}
P-T STABILITY FIELD OF "SANIDINE HYDRATE"
HIGH WATER CONTENT
POTENTIAL GEOLOGICAL SITUATIONS
RESTRICTIONS
COMMON BULK COMPOSITIONS
AFFECT OF OTHER PHASES
PERHAPS MOST LIKELY TO FIND IN SUBDUCTING GRANITES?!
SYSTEMATIC VARIATION OF H_2O TOO POOR TO BE OF USE
CHATTERJEE'S METHOD
SIMILAR RESULTS
n = 0·83
$\Delta H_{\langle T \rangle}$ = 19000 ± 5000 J mol^{-1}
$\Delta S_{\langle T \rangle}$ = 92·75 ± 5·80 J K^{-1} mol^{-1}
n = 1
ΔH_{298} = 14000 ± 7000 J mol^{-1}
ΔS_{298} = 103·92 ± 8·50 J K^{-1} mol^{-1}
n = 1
$\Delta H_{\langle T \rangle}$ = 20000 ± 7000 J mol^{-1}
$\Delta S_{\langle T \rangle}$ = 113·25 ± 8·10 J K^{-1} mol^{-1}
HIGHER PRESSURES
THE BEHAVIOUR OF POTASSIUM FELDSPAR AT HIGH WATER PRESSURES
LOWER PRESSURES
SYNTHETIC SANIDINES
EVIDENCE FOR VARIATION OF STRUCTURAL WATER WITH PRESSURE AND TEMPERATURE OF CRYSTALLISATION
KLOKKEN
PREVIOUS WORK
SANIDINE
MICROCLINE
MOSTLY OH
MOSTLY H_2O
DIFFERENT AT HIGH $P(H_2O)$
SIMILAR
INFRARED SPECTROSCOPY
KBr
MORE "WATER" THAN EIFEL SANIDINE
DIFFUSE REFLECTANCE
OH?
THERMOGRAVIMETRIC ANALYSIS
INFRARED OF TGA PRODUCTS
COMPLICATED!
NOT COMPLETELY DEHYDRATED AFTER TGA
VARIATION IN QUANTITY = INEXPLICABLE
INFRARED
2 MODELS FOR FORMATION OF LOW TEMPERATURE ALTERATION
MAGMATIC FLUIDS
EXSOLUTION OF STRUCTURAL "WATER"
SHOULD SEE DIFFERING PATTERNS OF STRUCTURAL AND FLUID INCLUSION WATER
LOOKS MORE LIKE MICROCLINE THAN PLAGIOCLASE BUT NOT EXACTLY
VARIATION IN QUANTITY = INEXPLICABLE
NOT CONCLUSIVE
NORMALISING PEAK AREAS = POOR METHOD

BIBLIOGRAPHY

Aines, R.D., G.R. Rossman, 1985: The high temperature behaviour of trace hydrous components in silicate minerals: *American Mineralogist,* Vol. 20: 1196-1179

Aines, R.D., G.R. Rossman, 1984: Water in minerals? A peak in the infrared: *Journal of Geophysical Research,* Vol. 89, No B6, 4059-4017

Anderson, G.M., C.W. Burnham, 1983: Feldspar solubility and the transport of aluminium under metamorphic conditions: *American Journal Of Science*, Vol. 283A: 283-297

Behrens, H., G. Muller, 1995: An infrared spectroscopic study of hydrogen feldspar ($HAlSi_3O_8$): *Mineralogical Magazine,* Vol. 59: 15-24

Bell, P., H. Mayo, J. England, 1971: A discussion of pressure distribution in modern solid-pressure-media apparatus: *Carnegie Institute of Washington Yearbook,* Vol. 70: 277-281

Beran, A., 1986: A model of water allocation in Alkali Feldspars, derived from Infrared-spectroscopic investigations. *Physics and Chemistry of Minerals,* Vol. 13: 306-310

Bernotat-Wulf H., D. Bertelmann, H. Wondratschek, 1988: The annealing behaviour of Eifel Sanidine (Volkesfeld) III The influence of the sample surface size on the order-disorder transformation rate. *Neues Jahrburch fur Mineralogie Monashefte*. 503-515

Bertelmann, E. Fortsch, D. H. Wondratschek, 1985: On the annealing behaviour of sanidines: the exceptional case of the Eifel sanidine megacrysts: *Neues Jahrburch fur Mineralogie Abteilungen* Vol. 152: 123-141

Bertelmann, D., J. Walther, H. Wondratschek, 1987: Annealing-induced inclusions and transformation behaviour of Eifel sanidines: *Terra Cognita*, Vol. 7: 257-258

Bertelmann, D., 1982: Untersuchungen der Al/Si-Ordnungsanderung und der Baufehler am Sanidin von Volkesfeld/Eifel. - Dissertation, Universitat Karlsruhe

Biggar, G.M., M.J. O'Hara, 1969: A Comparison of gel and glass starting materials for phase equilibrium studies: *Mineralogical Magazine,* Vol. 37: 286.

Bohlen, S. R., A. L. Boettcher, 1982: The quartz-coesite transformation: A precise determination and the effects of other components: *Journal of Geophysical Research*, Vol. 87: 7073-7078

Bohlen, S.R., A.L. Boettcher, V.J. Wall, J.D. Clemens, 1983: Stability of phlogopite-quartz and sanidine-quartz: a model for melting in the lower crust: *Contributions to Mineralogy and Petrology*, Vol. 83: 270-277

Bohlen, S.R., 1984: Equilibria for precise pressure calibration and a frictionless furnace assembly for the piston-cylinder apparatus: *Neues Jahrburch fur Mineralogie Monashefte*, Vol. 9: 404-412

Bose, K., J. Ganguly, 1995: Quartz-coesite transition revisited: Reversed experimental determination at 500-1200°C and retrieved thermochemical properties: *American Mineralogist*, Vol. 80: 231-238

Boyd, F. R., 1984: Siberian geotherm based on lherzolite xenoliths from the Udachnaya kimberlite, USSR: *Geology*, Vol. 12: 528-530

Braithwaite, R.S.W., 1990: Infrared spectroscopy as a technique for the investigation of minerals: *J. Russell Soc.*, Vol. 3(2): 71-79

Brown, W.L., S.M. Becker, I. Parsons, 1983: Cryptoperthites and cooling rate in a layered syenite pluton: A chemical and TEM study: *Contributions to Mineralogy and Petrology*, Vol. 82: 13-25

Brown, W.L., I. Parsons, 1984: Exsolution and coarsening mechanisms and kinetics in an ordered cryptoperthite series: *Contributions to Mineralogy and Petrology*, Vol. 86: 3-18

Burgess, R., S.P. Kelley, I. Parsons, F.D.L. Walker, R.H. Worden, 1992: ^{40}Ar-^{39}Ar analysis of perthite microtextures and fluid inclusions in alkali feldspars from the Klokken syenite, South Greenland: Earth and Planetary Science Letters, Vol. 109: 147-167

Burnham, C.W., J.R. Holloway, N.F. Davis, 1969: Thermodynamic properties of water to 1000°C and 10,000 bars: *Geological Society of America Special Paper*, Vol. 132

Carrington, D.P., 1994: Partial melting and phase relations in metapelitic granites: *Unpublished PhD thesis*: University of Edinburgh

Carrington, D.P., S.L. Harley: 1996: Cordierite as a monitor of fluid and melt water contents in the lower crust: an experimental calibration: *Geology*, in review.

Carron, M.K., M.E. Mrose, H.N. Reiser, 1964: New data on cymrite, a hydrated silicate of barium and aluminium (abstr): *Geological Society of America Special Paper*, Vol. 82: 26

Chatterjee, N.D., 1991: Applied Mineralogical Thermodynamics: Springer Verlag: Berlin, Heidelberg, New York

Clark, S.P., 1959: Effect of pressure on the melting points of eight alkali halides: *Journal of Chemical Physics*, Vol. 31: 1526-1531

Dennis, P.F., 1984: Oxygen self-diffusion in quartz under hydrothermal conditions: *Journal of Geophysical Research*, Vol. 89: 4047-4057

Drits, V.A., A.A. Kashaev, 1969: The Origin of Satellites in the Reciprocal Lattice of Cymrite: *Kristallografiya*, Vol. 13: 700

Drits, V.A., A.A. Kashaev, G.V. Sokolova, 1975: Crystal structure of cymrite: *Kristallografiya*, Vol. 20: 280-286

Essene, E.J., 1967: An occurrence of cymrite in the Franciscan formation, California: *American Mineralogist*, Vol. 52: 1885-1890

Farver, J.R., R.A. Yund, 1990: The effect of hydrogen, oxygen and water fugacity on oxygen diffusion in alkali feldspar: *Geochimica et Cosmochimica Acta*, Vol. 54: 2953-2964

Ford, C.E., 1972: Temperature distribution and measurement in "Tuttle" hydrothermal pressure vessels: Progress in Experimental Petrology, Natural Environment Research Council (Great Britain), Series d, No. 2: 87-88

Goldman, D.S., G.R. Rossman, 1977: Channel constituents in cordierite: *American Mineralogist*, Vol. 62: 1144-1157

Goldsmith, J.R., 1981: The join $CaAl_2Si_2O_8$-H_2O (anorthite-water) at elevated pressures and temperatures: *American Mineralogist*, Vol. 66: 1183-1188

Goldsmith, J.R., J.W. Peterson, 1990: Hydrothermal melting behaviour of $KAlSi_3O_8$ as microcline and sanidine. *American Mineralogist*, Vol. 75: 1362-1369.

Graham C.M., J.A.K. Tareen, P.F. Macmillan, B.M. Lowe, 1992: An experimental and thermodynamic study of cymrite and celsian stability in the system BaO-Al_2O_3-SiO_2-H_2O: European Journal of Mineralogy. Vol. 4: 251-269

Green, D.H., A.E. Ringwood, 1967: An experimental investigation of the gabbro-to-eclogite transformation and its petrological applications: *Geochimica et Cosmochimica Acta*, Vol. 31: 767-833

Griggs, D.T., G.C. Kennedy, 1956: A simple apparatus for high pressures and temperatures: *American Journal of Science*, Vol. 254: 722-735

Hamilton, D.L., C.M.B. Henderson, 1968: The preparation of silicate compositions by a gelling method: *Mineralogical Magazine*, Vol. 36: 832-838

Hewitt, D.A., D.R. Wones, 1984: Experimental phase relations of the micas, in: S.W. Bailey, ed., Micas: *Reviews in Mineralogy*, Vol. 13, Mineralogical Society of America: 201-247

Hewitt, D.A., 1975: Stability of the assemblage phlogopite-calcite-quartz: *American Mineralogist*, Vol. 60: 391-397

Hobbs, B., 1984: Point defect chemistry of minerals under a hydrothermal environment: *Journal of Geophysical Research*, Vol. 89: 4026-4038

Hofmeister, A.M., G.R. Rossman, 1985a: A spectroscopic study of irradiation colouring of amazonite: structurally hydrous, Pb bearing feldspar: *American Mineralogist*, Vol. 70: 794-804

Hofmeister, A.M., G. R. Rossman, 1985b: A Model for the Irradiative Coloration of Smoky Feldspar and the Inhibiting Influence of Water: *Physics and Chemistry of Minerals*: Vol. 12: 324-332

Holland, T.J.B., 1980: The reaction albite=jadeite+quartz determined experimentally in the range 600-1200°C: *American Mineralogist*, Vol. 65: 129-134

Holland, T.J.B., R. Powell, 1985: An internally consistent thermodynamic data set with uncertainties and correlations: 2. Data and results: *Journal of Metamorphic Geology*, Vol. 3, 343-370

Huang, W.L., Robertson, P.J. Wyllie, 1973: Melting relations of muscovite to 30 kbrs in the system $KAlSi_3O_8$-Al_2O_3-H_2O: *American Journal of Science* Vol. 273: 415-427.

Huang W.L., P.J. Wyllie, 1974: Melting relations of muscovite with quartz and sanidine in the K_2O-Al_2O_3-SiO_2-H_2O system to 30 kbrs and an outline of paragonite melting relations: *American Journal of Science*. Vol. 274: 378-395.

Huang W.L., P.J. Wyllie, 1975: Melting reactions in the system $NaAlSi_3O_8$-$KAlSi_3O_8$-SiO_2 to 35 kbrs, dry and with excess water: *Journal of Geology*, Vol. 83: 737-748.

Huang, W. L., P. J. Wyllie, 1981: Phase relations of S-type with H_2O to 35 kb: Muscovite granite from Harney Peak, South Dakota: *Journal of Geophysical Research*: Vol. 86, No. B11: 10515-10529

Hsu, L.C., 1994: Cymrite: new occurrence and stability: *Contributions to Mineralogy and Petrology*, Vol. 118: 314-320

Kearey, P., F.J. Vine, 1990: Global Tectonics: Blackwell Scientific Publications, Oxford

Kinomura, N., S. Kume, M. Koizumi, 1975: Synthesis of $K_2SiSi_3O_9$ with silicon in 4- and 6- co-ordination: *Mineralogical Magazine*, Vol. 40: 401-404

Kronenberg, A.K., R.A. Yund, G.R. Rossman, in press: Stationary and mobile hydrogen defects in potassium feldspar: submitted to *Geochimica et Cosmochimica Acta*

Larsen, E., G. Berman, 1965: Opredeleniye prozrachnykh mineralov pod microskopom (Determination of transparent minerals under the microscope): Izd. Nedra

Luth, W.C., 1967: Studies in the system $KAlSiO_4$-Mg_2SiO_4-SiO_2-H_2O: I, Inferred phase relations and petrologic applications: *Journal of Petrology*, Vol. 8: 372-416

Mason, R.A., I. Parsons, J.V.P. Lang, 1985: Trace and minor element chemistry of alkali feldspars in the Klokken layered syenite series: *Journal of Petrology*, Vol. 26: 952-970

Massonne, H. J., W. Schreyer, 1987: Phengite geobarometry based on the limiting assemblage with K-feldspar, phlogopite and quartz: *Contributions to Mineralogy and Petrology*, Vol. 96: 212-224

Massonne, H. J., 1992: Evidence for low temperature ultrapotassic siliceous fluids in the subduction zone environments from experiments in the system K_2O-MgO-Al_2O_3-SiO_2-H_2O (KMASH): *Lithos* Vol. 28: 421-434

Mirwald, P.W., I.C. Getting, G.C. Kennedy, 1975: Low friction cell for piston cylinder high temperature apparatus: *Journal of Geophysical Research*, Vol. 80: 1519-1525

Moles, N., 1985: Metamorphic conditions and uplift history in central Perthshire: evidence from mineral equilibria in the Foss celsian-barite-sulphide deposit, Aberfeldy: *Journal of the Geological Society of London*, Vol. 142: 39-52

Nitsch, K.H., Reaktion von Barium feldspat (Celsian) mit H_2O zu Cymrite unter metamorphen Bendigungen. *Fortschr. Mineral.*: 58 Beih.: 98-100.

Parsons, I., 1979: The Klokken gabbro-syenite complex South Greenland: cryptic variation and origin of inversely graded layering: *Journal of Petrology*, Vol. 20: 653-694

Parsons, I., S.M. Becker, 1986a: Layering, compaction and post-magmatic processes in the Klokken intrusion: in I. Parsons Ed. Origins of Igneous Layering: NATO ASI series, Series C, Vol. 196: Reidel, Dordrecht, Holland: 29-92

Parsons, I., S.M. Becker, 1986b: High-temperature fluid-rock interaction in a layered syenite pluton: *Nature*, Vol. 321: 764-769

Parsons, I., D.C. Rex, P. Guise, A.N. Halliday, 1988: Argon loss by alkali feldspars: *Geochimica et Cosmochimica Acta*, Vol. 52: 1097-1112

Parsons, I., R.A. Mason, S.M. Becker, A.A. Finch, 1991: Biotite equilibria and fluid circulation in the Klokken intrusion: *Journal of Petrology*, Vol. 32: 1299-1333

Peacock, S.M., 1991: Numerical simulation of subduction zone pressure-temperature-time paths: constraints on fluid production and arc magmatism: *Philosophical Transactions of the Royal Society of London*, Vol. 335: 341-353

Pentinghaus, H., K.H. Nitsch, 1986: Charakterisierung synthetischer Cymrite $Ba(Al_2Si_2O_8.H_2O)$. *Fortschr. Mineral.*, Vol. 64, Beih. 1: 143

Pollack, H. N., D. S. Chapman, 1977: On the regional variation of heat flow, geotherms, and lithospheric thickness: *Tectonophysics*: Vol. 38: 279-296

Powell, R., T.J.B. Holland, 1985: An internally consistent thermodynamic data set with uncertainties and correlations: 1. Methods and a worked example: *Journal of Metamorphic Geology*, Vol. 3: 327-342

Press, W.H., S.A. Teukolsky, W.T. Vetterling, B.P. Flannery, 1992: Numerical Recipes in Fortran: The Art Of Scientific Computing, 2nd Edition: Cambridge University Press: Cambridge, New York

Randle, H.A., 1994: Experimental element-partitioning and phase-equilibrium studies relevant to subduction zones: *Unpublished PhD thesis*: University of Edinburgh

Ribbe, P.H., 1963: A refinement of the crystal structure of sanidinized orthoclase: *Acta Crystallographica*, Vol. 16: 426-427

Rossman G.R., J.R. Smyth, 1990: Hydroxyl contents of accessory minerals in mantle eclogites and related rocks: American Mineralogist, Vol. 75: 775-780.

Ryabinin Y.N., V.K. Markov, V.P. Petrov, I.S. Delitsin, 1965: Transformations of natural sanidine at high pressures and temperatures: *Geochemistry International* 2: 1105-1111

Scheel, H.J., 1971: Lead feldspar: *Zeitschrift fur Kristallographie*, Vol. 133: 264-272

Schreyer W., H.J. Massonne, C. Chopin, 1987: Continental crust subducted to depths near 100 km : Implications for magma and fluid genesis in collision zones: Magmatic Processes: Physiochemical Principles. The Geochemical Society Special Publication No. 1.

Schulze D.J., H. Helmsteadt, 1988: Coesite-sanidine eclogites from kimberlites: Products of mantle fractionation or subduction?: *Journal of Geology* 96 435-443.

Seki Y., G.C. Kennedy, 1964a: The breakdown of potassium feldspar $KAlSi_3O_8$ at high temperatures and high pressures: *American Mineralogist,* Vol. 19: 1688-1708

Seki Y., G.C. Kennedy, 1964b: Phase relations between cymrite, $BaAlSi_3O_8(OH)$, and celsian, $BaAlSi_3O_8$: *American Mineralogist,* Vol. 49: 1407-1426.

Seki, Y., G. C. Kennedy, 1965: Muscovite and its melting relations in the system $KAlSi_3O_8$-H_2O: *Geochimica et Cosmochimica Acta* Vol. 29: 1077-1083

Smith, C.W., F.A. Bannister, M.H. Hey, 1949: Cymrite, a new barium mineral from the Benallt manganese mine, Rhiw, Caernarfonshire: *Mineralogical Magazine,* Vol. 28: 676-681

Smith J.V., W.L. Brown, 1987: Feldspar Minerals Vol. I 2nd edition. Springer-Verlag.

Smyth J.R., C.J. Hatton, 1977: A coesite-sanidine grospydite from the Roberts Victor kimberlite: *Earth and Planetary Science Letters,* Vol. 34: 284- 290

Spear, F.S., 1993: Metamorphic Phase Equilibria and Pressure-Temperature-Time Paths: Mineralogical Society of America Monograph, Washington

Stern, P. J. Wyllie, 1981: Phase relationships of I-type granite: *Journal of Geophysical Research,* Vol. 86: 10412-422

Tucker, M.E., 1981: Sedimentary Petrology: Blackwell Scientific Publications, Oxford

Viswanathan K., O. Harniet, M. Epple, 1992: Hydrated barium aluminosilicates, $BaAl_2Si_2O_8.nH_2O$, and their relations to cymrite and hexacelsian: *European Journal of Mineralogy*: Vol. 4: 271-278.

Walker, F. D. L., 1991: Micropores in alkali feldspars: *Unpublished PhD thesis:* University of Edinburgh

Welch, M.D., 1987: Experimental studies of selected amphiboles in the system Na_2O-CaO-MgO-Al_2O_3-SiO_2-H_2O-F_2 and its subsystems: *Unpublished PhD thesis*: University of Edinburgh

Wendlandt, R.F., D.H. Eggler, 1980: The origin of potassic magmas 2: Stability of phlogopite in natural spinel lherzolite and in the system $KAlSiO_4$-MgO-SiO_2-H_2O-CO_2 at high pressures and temperatures: *American Journal of Science*, Vol. 280: 421-458

Wones, D.R., F.C.W. Dodge, 1977: The stability of phlogopite in the presence of quartz and diopside, in: D.G. Fraser, ed., Thermodynamics in Geology. Dordrecht, Holland: D. Reidel Publishing Co.: 229-247

Wood, B.J., 1976: The reaction phlogopite + quartz = enstatite + sanidine + H_2O, in G.M. Biggar Ed., Progress in Experimental Petrology, Natural Environment Research Council (Great Britain), Series D

Worden, R. H., F. D. L. Walker, I. Parsons, W. L. Brown, 1990: Development of microporosity, diffusion channels and deuteric coarsening in perthitic alkali feldspars: *Contributions to Mineralogy and Petrology*, Vol. 104: 507-515

Yardley, B.W.D., 1989: An introduction to Metamorphic Petrology: Longman Earth Science Series: Longman Scientific and Technical, New York

Yoshiki, B., K. Matsumoto, 1951: High temperature modification of Barium Feldspar: *Journal of the American Ceramic Society*, Vol. 34, No. 9: 333-336